AD_____

Award Number: DAMD17-03-1-0094

TITLE: Integrating Molecular Imaging Approaches to Monitor Prostate Targeted Suicide and Anti-angiogenic Gene Therapy

PRINCIPAL INVESTIGATOR: Makoto Sato, Ph.D

CONTRACTING ORGANIZATION: University of California
Los Angeles, California 90024

REPORT DATE: February 2005

TYPE OF REPORT: Annual Summary

PREPARED FOR: U.S. Army Medical Research and Materiel Command
Fort Detrick, Maryland 21702-5012

REPORT DOCUMENTATION PAGE

Form Approved
OMB No. 0704-0188

1. REPORT DATE *(DD-MM-YYYY)*	**2. REPORT TYPE**	**3. DATES COVERED** *(From - To)*
01-02-2005	Annual Summary	1 Feb 2003 – 31 Jan 2005

4. TITLE AND SUBTITLE

Integrating Molecular Imaging Approaches to Monitor Prostate Targeted Suicide and Anti-angiogenic Gene Therapy

5a. CONTRACT NUMBER

5b. GRANT NUMBER
DAMD17-03-1-0094

5c. PROGRAM ELEMENT NUMBER

6. AUTHOR(S)

Makoto Sato, Ph.D

E-Mail:

5d. PROJECT NUMBER

5e. TASK NUMBER

5f. WORK UNIT NUMBER

7. PERFORMING ORGANIZATION NAME(S) AND ADDRESS(ES)

University of California
Los Angeles, California 90024

8. PERFORMING ORGANIZATION REPORT NUMBER

9. SPONSORING / MONITORING AGENCY NAME(S) AND ADDRESS(ES)
U.S. Army Medical Research and Materiel Command
Fort Detrick, Maryland 21702-5012

10. SPONSOR/MONITOR'S ACRONYM(S)

11. SPONSOR/MONITOR'S REPORT NUMBER(S)

12. DISTRIBUTION / AVAILABILITY STATEMENT
Approved for Public Release; Distribution Unlimited

13. SUPPLEMENTARY NOTES

14. ABSTRACT

To develop safe and efficient gene therapy protocol for advanced stages of prostate cancer, we aimed to combinethe selective suicide and anti-angiogenic gene therapy approaches into an effective targeted treatment forprostate cancer. We propose to incorporate a strong and tissue-specific two-step transcriptional amplification(TSTA) system to mediate prostate-targeted thymidine kinase (sr39tk) gene expression in prostate cancer cells. This targeted vector can be also utilized as a positron emission tomography (PET) reporter. We have shown thatthe TSTA-sr39tk adenoviral vector, in combination with prodrug ganciclovir, efficiently killed tumor cellswhereas it exhibited minimal liver toxicity compared to CMV-sr39tk vector in human prostate tumor xenograftedmice model. In addition, the anti-angiogenic adenoviral vectors expressing TSP1 and ADAMTS1 exhibited a stronginhibitory effect on the initial development of hormone refractory prostate cancer CWR22Rv1 cell lines in nudemice. We foresee that anti-angiogenic adenoviral vectors, in combination with the prostate targeted TSTAvector, will be an excellent therapeutic option for advanced stages of prostate cancer.

15. SUBJECT TERMS
No subject terms provided

16. SECURITY CLASSIFICATION OF:			**17. LIMITATION OF ABSTRACT**	**18. NUMBER OF PAGES**	**19a. NAME OF RESPONSIBLE PERSON**
a. REPORT	**b. ABSTRACT**	**c. THIS PAGE**			USAMRMC
U	U	U	UU	76	**19b. TELEPHONE NUMBER** *(include area code)*

Standard Form 298 (Rev. 8-98)
Prescribed by ANSI Std. Z39.18

Table of Contents

Introduction

The objective of this project is to combine the selective suicide and anti-angiogenic gene therapy approaches into an effective targeted treatment for prostate cancer. We propose to incorporate a highly potent and specific two-step transcriptional amplification (TSTA) system to mediate prostate-targeted thymidine kinase (tk) gene expression in prostate cancer cells. In diagnostic applications, this targeted vector will be utilized as a PET reporter gene. The hypotheses are: 1) this PET imaging reporter virus could be useful to illuminate prostate metastatic cells in living animals, 2) this selective tk virus could also be an efficient therapeutic vector in the suicide gene therapy approach, and 3) a combinatorial approach using this suicide gene therapy and anti-angiogenesis could be more efficient to eradicate prostate cancer.

Body

Task 1a. Amplify and propagate the adenovirus vectors up to large scale.

The recombinant adenoviruses (Ad), AdCMV-TSP1, AdCMV-METH1, and AdTSTA-sr39tk, were propagated to make higher titer stocks in 293 cells. The titer of these Ads usually falls between 1 and 5 x 10^{10} /ml by plaque formation assay in 293 cells. We regularly obtain approximately 10^{11} pfu virus per preparation by utilizing suspension cultures of 293 cells.

During the process of viral propagation, we encountered a problem. We could not detect the expression from AdCMV-METH1, which was probably due to an unexpected mutation in the viral genome and the outgrowth of the mutant form. Therefore, we picked a clone from the earlier mixed clones of the AdCMV-METH1 and then propagated it to a large scale. All vectors propagated up to a large scale were plaque tittered and the expression of the transgenes was confirmed. We also examined the androgen regulation of transgene expression in AdTSTA-sr39tk.

Although the TSTA vector exhibited robust and specific activity, we found some potential problems of the TSTA adenoviral vectors which might arise in clinical settings. 1) Due to the limitation of the cloning site in the AdEasy adenoviral construction system, we located two expression cassettes side by side in the E1 region of the adenovirus. Although the TSTA vectors exhibited superior prostate cell specificity, this might cause non-specific transgene expression due to the feed-forward loop in the single TSTA system that could eventually lead to unwanted side effects [1]. 2) Due to the usage of the two identical polyadenylation signals for both expression cassettes in the head-to-head TSTA vector, potential homologous recombination was predicted to occur during the process of viral propagation. In fact, we observed a low level of the homologous recombination in 293 by polymerase chain reaction (Figure 1, unpublished data).

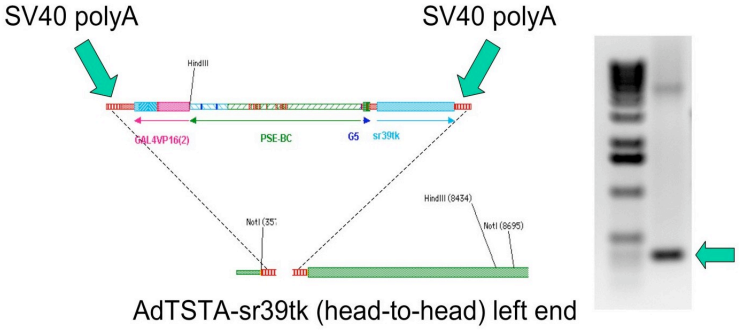

Figure 1. Potential recombina-tion problem in AdTSTA-sr39tk. Head-to-head configuration of AdTSTA-sr39tk contains two identical polyA sequence (green arrows). In fact, we were able to detect recombined viral DNA by polymerase chain reaction using primers flanking expression cassettes outside of the E1 region (green arrow at the right).

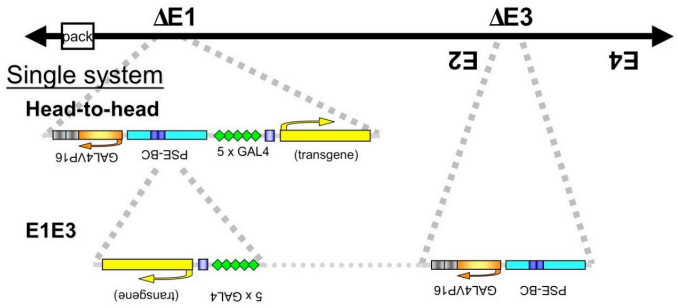

Figure 2. New configuration of the TSTA adenoviral vector. In order to overcome potential drawback of the old head-to-head vector, we developed E1E3 configuration of the TSTA vector. In the E1E3 configuration, two components of the TSTA system, PSE-BC driving Gal4VP16 activator and 5 repeats of GAL4 binding sites controlling transgene, are located in E3 and E1 region, respectively.

Since we are moving forward with the application of AdTSTA-sr39tk to future clinical trials, overcoming these potential problems is essential. With this in mind, we developed a new configuration of the TSTA system in adenovirus, which has the modified PSA promoter driving Gal4VP16 (activator component) in the E3 region of the adenovirus and the five GAL4 binding sites driving the reporter/therapeutic component in the E1 region (Figure 2). We hypothesized that physical separation of the two components would circumvent any interference between them. This promised to be the case, as the regulation of the expression was tremendously improved. Figure 3 shows the comparative study of different configurations of the TSTA vector. Human prostate cancer cells of the LNCaP cell line were infected with either the head-to-head or E1E3 vector as well as the separate system of the TSTA vectors (co-infection of the activator virus and the reporter virus) for comparison. Absolute activity of the E1E3 vector with 10nM R1881 (synthetic androgen) was only 1.3-fold lower than that of the head-to-head vector. However, the baseline activity of the E1E3 vector with 10μM Casodex (anti-androgen) was 34-fold lower compared to that of the head-to-head vector. Taken together, the overall androgen induction of the E1E3 vector was approximately 26-fold larger than that of the head-to-head vector. Furthermore, the E1E3 vector does not carry the sequence, which may cause the potential homologous recombination, which is particularly important when clinical grade vector production starts. Currently, the manuscript is in preparation for the comparison study of different configurations of the TSTA system. In addition to the E1E3 configuration of AdTSTA-firefly luciferase (Fluc), the adenoviral vector mentioned above, we also constructed an E1E3 configuration TSTA adenovirus vector carrying sr39tk as a transgene. As anticipated, the E1E3 configuration of AdTSTA-sr39tk exhibited similar levels of sr39tk expression as the head-to-head configuration of the vector (Figure 4).

Recently, our lab's PI, Dr. Lily Wu, was awarded the support of the National Cancer Institute - Rapid Access to Interventional Development (RAID) Pilot program (attached document). The purpose of the RAID program is to assist the translation to the clinic of novel anticancer therapeutic interventions arising in the academic community. The clinical trial will utilize the TSTA vector to detect disseminated prostate cancer cells in regional lymph nodes. Due to our preliminary data, we decided to use this E1E3 configuration of the TSTA-sr39tk vector instead

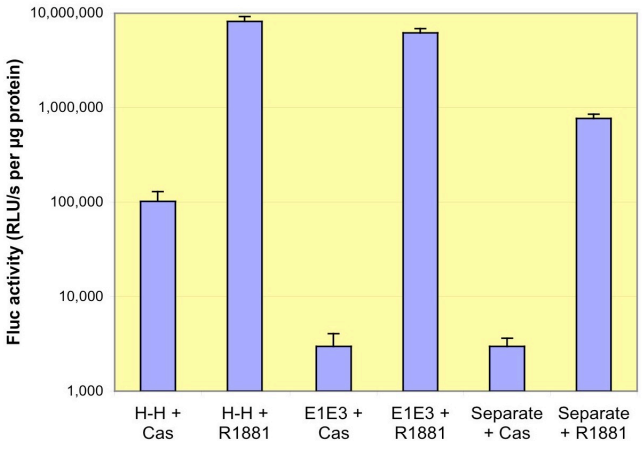

Figure 3. Comparison of the activity of different configurations of the TSTA system in adenovirus. LNCaP cells were infected either with the head-to-head (H-H), E1E3 or separate (co-infection of two distinct virus) form of TSTA adenovirus. Each infection was performed in the presence of anti-androgen (Cas, Casodex) or synthetic androgen (R1881) to examine the baseline or induced level of expression, respectively.
The H-H and E1E3 exhibited comparable activity in the presence of R1881. However, background activity in the presence of Casodex was more than 30 times lower by the E1E3 and separate form.

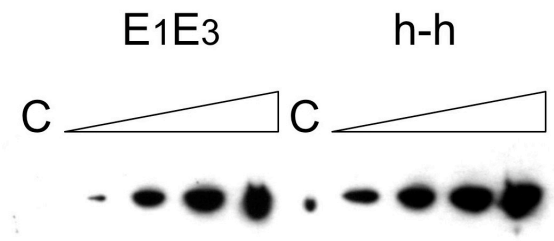

Figure 4. CWR22Rv1 cells were infected at MOI=5 either with the E1E3 or head-to-head TSTA adenorial vectors. Cells were incubated either with 10μM Casodex (C) or 10nM R1881. Two days post infection, cells were harvested and subjected to SDS-PAGE. Using the anti-HSV-tk polyclonal antibody, HRP-conjugated secondary antibody and chemiluminescence, TK is visualized. The bands with the triangle denote the serial (3x) dilution from one sample with 10nM R1881.

of the head-to-head version for any possible clinical trial.

Task 1b. Perform both imaging modalities for naïve animals.

A previously published article [1] reports that the potency of the prostate-specific TSTA adenoviral vector exceeds that of the strong constitutive CMV driven vector. However, significant androgen responsive and prostate-specific activity of this vector is retained. Intravenously or intraperitonealy injected 10^7 pfu of head-to-head AdTSTA-Fluc exhibited a low signal from the lungs. However, the intensity of the signal was more than two-orders lower than the signal seen in the tumors [1]. When the AdTSTA-Fluc vector with the E1E3 configuration was injected systemically, no higher than background activity was observed in the lung areas of the animals (Figure 5, unpublished data). This suggests that the signal we observed with the head-to-head configuration of the TSTA-Fluc vector from the lung area is due to the non-specific expression of the virus in these areas.

To explore the androgen regulation of the TSTA virus *in vivo*, we injected 10^7 pfu of the adenoviral vectors into the prostate of naïve SCID mice and followed the expression by optical imaging. Robust expression was observed from the lower abdomen from day 7 to 26, and it decreased approximately 50 to 60 % after castration on day 28. This suggests that expression from the TSTA vectors in the prostate is well regulated by androgen. Moreover, to explore biodistribution and transduction of the organs by adenoviral vector administered by different routes, we combined real-time polymerase chain reaction with in vivo optical imaging to monitor gene expression from the vectors. This study demonstrated that each tissue retains various amounts of adenoviral vector, depending on the route of injection. Intravenous and intraperitoneal injections resulted in the greatest gene expression and viral DNA in the liver, whereas intraperitoneal injections led to greater gene delivery to the prostate, for example [2].

We used the adenoviral vector carrying Fluc as a transgene to investigate the activity of the TSTA system because optical imaging is 100 to 1000 times more sensitive compared to micro positron emission tomography (mPET) imaging. Since we observed only faint signals from the naïve animals injected with AdTSTA-FL, we decided to halt mPET imaging with AdTSTA-sr39tk in naïve animals.

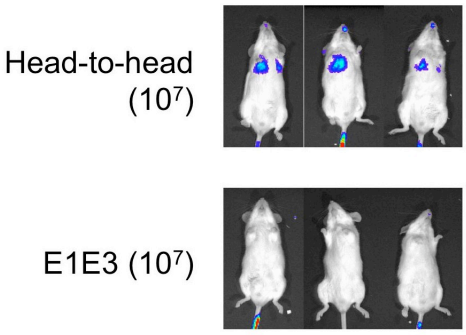

Figure 5. Systemic injection of two different configurations of the TSTA adenoviral vectors. 10^7 pfu of either head-to-head or E1E3 TSTA adenoviral vector was injected to SCID mice via tail vein. Optical imaging was performed periodically to monitor luciferase expression from the vectors. Three representative animals of 36 days post infection are shown. No detectable signal was seen in the lung area of the mice with E1E3 configuration.

Task 1c. Perform both imaging modalities for tumor bearing mice.

The experiments performed in the context of this task are reported in the following manuscripts [1, 3].

[1] Sato M, Johnson M, Zhang L, Zhang B, Le K, Gambhir SS, Carey M and Wu L.

Optimization of Adenoviral Vectors to Direct Highly Amplified Prostate-Specific Gene Expression for Imaging and Gene Therapy. *2003, Molecular Therapy, 8: 726-737*.

[3] Sato M, Johnson M, Zhang L, Gambhir SS, Carey M and Wu L.
Functionality of Androgen Receptor-based Gene Expression Imaging in Hormone Refractory Prostate Cancer. *2005, Clinical Cancer Research, 11: 3743-3749*.

In the first article [1], we showed strong expression of the TSTA adenoviral vector in human prostate tumor xenografts in mice, which was comparable to the CMV driven vector. The TSTA vector exhibited strong signal in the tumor while the CMV vector showed a strong signal in the liver as well. In addition, we compared the single and separate configurations of the TSTA system, looking for the optimum regulation. Based on the finding of better androgen regulation by the separate system, we designed the E1E3 TSTA vector.

In the second report [3], we focused on the relationship between the activity of the TSTA system and androgen receptor (AR). In order to induce expression by the PSA promoter, the ligand must bind to the AR first, then the complex enters the nucleus and binds to the androgen responsive elements in the PSA promoter. Therefore, the activity of the TSTA system, that utilizes the PSA promoter, suggests the functional status of endogenous AR. Since the TSTA system is active in the hormone refractory prostate cancer (HRCaP) cell lines that we tested, as well as in androgen dependent prostate cancer, the AR is suggested to be functionally active in both stages of prostate cancer. To confirm that mPET imaging is feasible utilizing the TSTA system, four x 10^9 of AdTSTA-sr39tk was injected into LAPC-9 human prostate cancer xenografts in SCID mice (Ref. i). The animals were then used for mPET imaging (Figure 6). MicroPET images were successfully obtained using the reporter probe [^{18}F]-FHBG (9-(4-^{18}F-fluoro-3-[hydroxy-methyl]butyl)guanine) in both androgen dependent and HRCaP LAPC-9 tumors. To our knowledge, this is the first report of PET imaging achieved by a prostate-specific promoter driving expression system in both androgen dependent and androgen independent prostate cancer (HRCaP). Together with the fact that the majority of recurrent prostate cancers express AR (and they are functional to express PSA, the serum marker for prostate cancer), we foresee that the TSTA approach can be a promising gene therapy or diagnostic strategy for the advanced stages of prostate cancer.

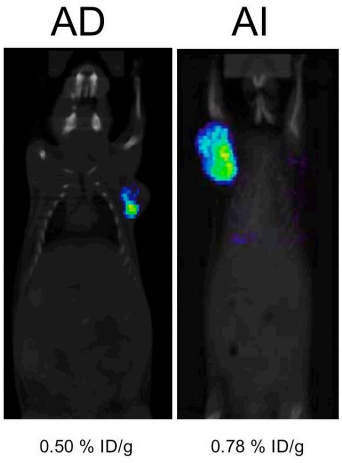

Figure 6. Combined microPET and microCT of LAPC-4 AD and AI tumor. 4 x 10^9 infectious units of AdTSTA-tk was injected to AD and AI LAPC-4 tumors. One week later, [^{18}F]-FHBG injected animals were anesthetized and scanned for microPET and microCT sequentially. The signal in the tumor was measured by % injected dose of substrate per gram of tissue (%ID/g), listed below the image. Background signals from the gastro-intestinal tract are removed for the sake of convenience.

Task 2a. Evaluate anti-angiogenic effect of Ad with anti-angiogenic factors.

Angiogenesis has had people interested in developing agents with effective tumor growth inhibitory effects for the past two decades. This is based on the rationale that development and growth of tumors requires angiogenesis. Therefore, anti-angiogenic therapy using an adenoviral vector, which can efficiently transduce cells, to express such a factor sounds attractive.

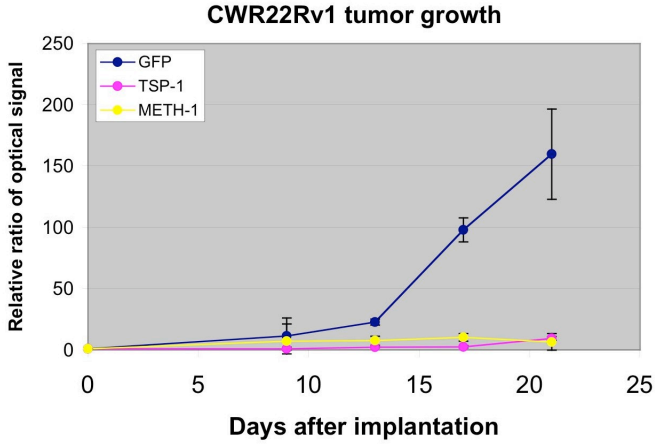

Figure 7. The effect of anti-angiogenic adenovirus vectors on the development of tumor with CWR22Rv1 human prostate cancer cells. Cells were infected with respective adenovirus vectors as well as lenti CMV-Fluc (firefly luciferase) to track tumor growth by optical imaging before implantation. Ten to the sixth cells were implanted into the flanks of SCID mice. The animals were imaged every four starting on the ninth day post implantation. Relative ratio of optical signals are shown as a growth of the tumors.

Thrombospondin-1 (TSP1) (Ref. ii) is one of the endogenous anti-angiogenic factors that associates with the extracellular martix. TSP1 exhibits significant angiostatic activity, and has been shown to inhibit endothelial cell chemotaxis and proliferation. METH-1 (metalloprotease and thrombospondin-1, preferably called ADAMTS1 currently, a disintegrin-like and metalloprotease with thrombospondin) is another anti-angiogenic factor that was shown to have more potent anti-angiogenic activity than the TSP1 protein. Both TSP1 and METH-1 were more active than endostatin (Ref. iii), an older anti-angiogenic factor.

Ad vectors, expressing each anti-angiogenic factor, were propagated as described in Task 1a. To investigate the effect of these vectors on the initial development of prostate cancer, we performed *ex vivo* infections on the human prostate cancer cell line CWR22Rv1 (Ref. iv). We selected this cell line because CWR22Rv1 exhibited a rapid tumor forming ability within 14 to 21 days compared to over one month with LAPC-4 cells. Since our focus on this study was to look at the ability to inhibit rapid initial tumor development, we chose CWR22Rv1 cells to examine the activity of the anti-angiogenic factors on faster cell growth. More importantly, CWR22Rv1 is an AR positive HRCaP cell line, implying that the prostate-specific TSTA is active in this cell line [3]. CWR22Rv1 cells were infected either with an MOI=3 of AdCMV-TSP1, AdCMV-ADAMTS1, or AdCMV-GFP. AdCMV-GFP was used as a negative control. Importantly, the cells were marked with lentivirus carrying CMV-Fluc to track tumor growth after implantation by noninvasive optical imaging. After *ex vivo* infection, 10^6 cells per mouse were implanted subcutaneously into the flanks of male nude mice. The animals were subjected to optical imaging every four days starting on the ninth day post implantation. As shown in Figure 7, AdCMV-TSP1 and AdCMV-ADAMTS1 exhibited strong inhibitory effects on the development of CWR22Rv1 tumors in nude mice. There was no clear difference between these two anti-angiogenic factors. Consequently, both anti-angiogenic factors have similar inhibitory effects on the onset of CWR22Rv1 tumor development.

Recently, in the collarorative project with Dr. Iruela-Arispe's group in the Molecular Biology Institute at UCLA, we demonstrated that TSP1 is a substrate for ADAMTS1 (Figure 8) [4]. We infected 293T cells with AdCMV-ADAMTS1 and harvested conditioned medium. The incubation of purified TSP1 and conditioned medium exhibited site specific cleavage of TSP1. The controversial fate of the TSP1 *in vivo*, whether it stimulates or inhibits angiogenesis, could be explained by the function of ADAMTS1. The result suggested that the matrix bound TSP1, forming homotrimer, may function to stimulate angiogenesis, while monomer TSP1 fragments, cleaved by ADAMTS1, may exhibit an anti-angiogenic effect.

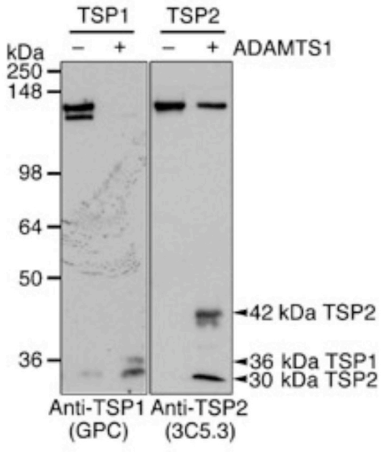

Figure 8. In vitro cleavage activity of ADAMTS1. Purified human TSP1 and TSP2 were incubated with either control media (-) or the conditioned medium derived from 293T expressing ADAMTS1 (+). 36kDa and 42+30kDa fragments were obtained in the presence of ADAMTS1 activity from TSP1 and TSP2, respectively [4].

Therefore, the tumor growth inhibitory effect we observed above suggests that the TSP1 expressed by AdCMV-TSP1 might not form homotrimer in vivo. Since we did not observe better anti-angiogenic effects by AdCMV-TSP1 and the anti-angiogenic effect of endogenous TSP1 would be induced by ADAMTS1 from AdCMV-ADAMTS1, it may be more reasonable to use ADAMTS1 only or ADAMTS1 and TSP1 together.

Task 2b. Evaluate cytotoxic effect of AdTSTA-tk-mediated suicide gene therapy.

Findings relevant to these tasks were reported in the following manuscript [5].

[5] Johnson M, Sato M, Burton J, Gambhir SS, Carey M and Wu L.
In Vivo Molecular Imaging to Monitor Prostate Cancer-directed Suicide Gene Therapy. 2005, Molecular Imaging, *4: 463-472*.

Previously, we reported that the TSTA-sr39tk adenoviral vector exhibited robust tumor cell killing equivalent to that of the non-specific, constitutively active construct, AdCMV-sr39tk, while the liver toxicity was more than 2.5-fold lower with the TSTA vector compared to the CMV vector (Figure 9). However, in the collaborative study between our group and the NCI-RAID program team, we encountered potential homologous recombination problems. This was the main reason why we began to shift the vector configuration from head-to-head to E1E3. We confirmed that the expression levels from those vectors are comparable.

Besides the suicide gene therapy study, we performed quantitative real-time PCR to examine the distribution of the vectors in tumors and livers because we observed solid signals from the livers of mice injected with AdCMV-sr39tk but not with AdTSTA-sr39tk. The PCR data indicated that tumor-directed vector administration did not preclude gene delivery to non-targeted vital organs such as the liver. Our results led us to hypothesize that a tissue-specific vector provides added safety over a constitutively active vector. Indeed, imaging studies clearly showed that the prostate-specific TSTA vector remained transcriptionally silent in the liver while robustly active in the tumor.

Task 3. Generate combined AdTSTA-tk/TSP1(METH1) and evaluate combinatorial therapeutic effect of suicide and anti-angiogenic gene therapy.

Strong suppression of tumor growth has been suggested by the combination of an anti-angiogenic therapy approach and some other therapies (Ref. v-vii). Integrating anti-angiogenic therapy with suicide gene therapy controlled by the prostate-specific TSTA system will allow us to evaluate the maximum possible cytotoxic effects and minimum side effects. An anti-

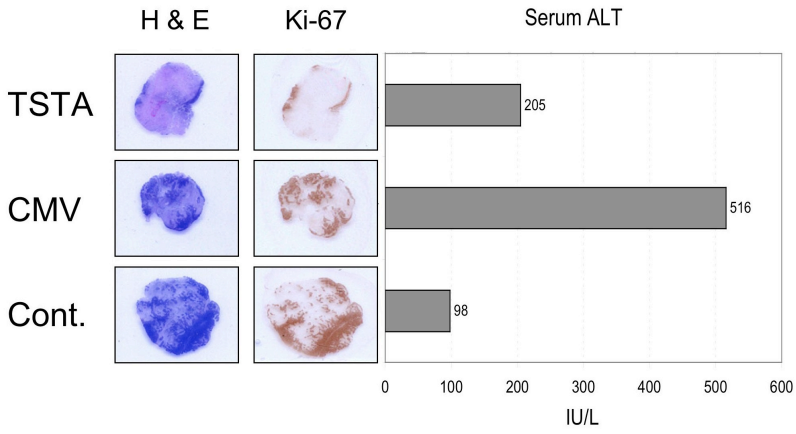

Figure 9. Suicide gene therapy study by CMV- and TSTA- sr39tk adenoviral vectors [5]. Four times 10^9 pfu of the virus was injected into human prostate cancer LAPC-4 xenografts on mice followed by ganciclovir treatment for one week. Serum ALT was also measured in each group on day 22. Sections of tumors were stained with hematoxylin and eosin (H & E) or immunostained by cell proliferation marker, Ki-67 antibody. The histology indicated tumor cell killing in the CMV and TSTA injected tumor with at the similar level of residual proliferating tumor cells (Ki67+). However, the levels of serum ALT exhibited 2.5 times higher liver toxicity with AdCMV-sr39tk.

angiogenic treatment would be an excellent option not just for gene therapy but for a variety of approaches to cancer as a combination therapy partner. In addition to this combined approach, bioluminescence imaging and microPET imaging technologies to monitor gene transduction and cytotoxicity will provide a new gene therapy protocol to fight the advanced stages of prostate cancer.

Due to shifting the sr39tk expressing TSTA adenoviral vector from head-to-head to the E1E3 configuration, we have not been able to accomplish a combined therapeutic approach to date. Currently, we are planning a combined approach of ADAMTS1 anti-angiogenic and TSTA-sr39tk or ADAMTS1 and TSTA-oncolytic gene therapy in the bone metastasis model of LAPC-9 human prostate cancer cells in mice (Ref. viii). The TSTA-oncolytic adenoviral vector is an oncolytic adenovirus that has been developed based on the outcomes of previous research funded by the DOD. Essential proteins for viral replication, E1A and E1B, are expressed by the TSTA system in the TSTA-oncolytic adenoviral vector. That means prostate specific modified PSA promoter drives a strong artificial transactivator, GAL4VP16, which in turn binds to centrally located four repeats of the GAL4 binding site located between bidirectional E1A and E1B genes. The TSTA-oncolytic adenoviral vector has shown prostate specific E1 expression and viral replication *in vitro*.

In this model, bone metastasis derived human prostate cancer LAPC-9 tumor cell suspensions (Ref. i) will be injected to the tibias of SCID mice. Bones and lymph nodes are the major metastasis sites of human prostate cancer. Approximately 10^5 LAPC-9 cells per animal will be transduced with lenti-CMV-Renella luciferase prior to injection to monitor the tumor size after implantation by optical imaging. The ADAMTS1 vector will be co-injected into the lesion with either the E1E3 TSTA-sr39tk or the TSTA-oncolytic adenoviral vectors. Prodrug treatment will follow the TSTA-sr39tk injection. Efficacy of the treatment will be assessed by radiographs, optical and mPET imaging and serum PSA measurements.

Key Research Accomplishments

- Adenoviral vectors carrying TSTA-sr39tk, CMV-TSP1 and CMV-ADAMTS1 were constructed and prepared as viral stocks. Expression of the transgenes was confirmed by western analysis. Also, androgen regulation of the TSTA vector was confirmed by in vitro infection study with prostate cancer cell lines.
- Robust transcriptional activity of AdTSTA-sr39tk and AdTSTA-Fluc enabled us to monitor gene expression in tumors, but they were silent when injected into naïve animals. Particularly, the achievement in mPET imaging with AdTSTA-sr39tk is remarkable, since it has been hampered to perform PET imaging due to lower sensitivity of PET imaging and relatively lower activity of tissue specific promoter driven expression systems.
- AdTSTA-tk and AdTSTA-Fluc were shown to be dependent on the functionality of androgen receptor, meaning the TSTA system should be active in the majority of prostate tumors.
- Due to the potential homologous recombination in the head-to-head configuration of the TSTA vector, an E1E3 configuration of the TSTA vector was developed. Superior androgen induction (regulation) and equivalent levels of transgene expression have been shown. Therefore, the E1E3 configuration of the TSTA-sr39tk vector will be used instead of the head-to-head version for the future clinical trials funded by National Cancer Institute.
- AdCMV-TSP1 and AdCMV-ADAMTS1 exhibited a strong inhibitory effect on the CWR22Rv1 tumor development. Ex vivo infected tumor cell lines were implanted to mice and tumor growth was monitored by Renilla luciferase activity. Since TSP1 is a substrate for ADAMTS1, co-infection of both or sole infection of ADAMTS1 vector may be more reasonable. In addition, effect of TSP1 on angiogenesis is controversial.
- Suicide gene therapy study employing AdTSTA-sr39tk showed safeguard ability against liver toxicity compared to AdCMV-sr39tk while exhibiting similar tumor cell killing. Combination of the suicide gene therapy and anti-angiogenic gene therapy has not been accomplished mostly due to the change of the suicide gene therapy vector (from the head-to-head to the E1E3 configuration). An animal study with intratibial implantation of human prostate cancer cells is currently planned for the combinatorial gene therapy approaches.

Reportable Outcomes

Manuscripts:

1) Sato M, Johnson M, Zhang L, Zhang B, Le K, Gambhir SS, Carey M and Wu L. Optimization of Adenoviral Vectors to Direct Highly Amplified Prostate-Specific Gene Expression for Imaging and Gene Therapy. *Molecular Therapy, 8: 726-737 (2003).* (**Enclosed in appendix**)
2) Johnson M, Huyn S, Burton J, Sato M and Wu L. Differential Biodistribution of Adenoviral Vector In Vivo as Monitored by Bioluminescence Imaging and Quantitative Polymerase Reaction. *Human Gene Therapy, 17(12): 1262-1269 (2006).* (**Enclosed in appendix**)
3) Sato M, Johnson M, Zhang L, Gambhir SS, Carey M and Wu L. Functionality of Androgen Receptor-based Gene Expression Imaging in Hormone Refractory Prostate Cancer. *Clinical Cancer Research, 11: 3743-3749 (2005).* (**Enclosed in appendix**)
4) Lee NV, Sato M, Annis DS, Loo JA, Wu L, Mosher DF and Iruela-Arispe ML. ADAMTS1 mediates the release of antiangiogenic polypeptide from TSP1 and 2. *EMBO J, 25(22): 5270-5283 (2006).* (**Enclosed in appendix**)
5) Sato M*, Johnson M*, Burton J, Gambhir SS, Carey M and Wu L. In Vivo Molecular Imaging to Monitor Prostate Cancer-directed Suicide Gene Therapy. *Molecular Imaging, 4(4): 463-472 (2005).* (*=equally contributed) (**Enclosed in appendix**)
6) Figueiredo M, Sato M, Johnson M, Wu L. Specific targeting of gene therapy to prostate cancer using a

two-step transcriptional amplification system (Review). *Future Oncol, 2: 391-406 (2006).*
7) Iyer M, Sato M, Johnson M, Gambhir SS, Wu L. Applications of molecular imaging in cancer gene therapy (Review). *Curr Gene Ther, 5: 607-618 (2005).*

Abstracts:

a) Sato M, Johnson M, Zhang L, Gambhir SS, Carey M and Wu L. Prostate-Specific Oncolytic Adenovirus Based on Bidirectional TSTA System. American Society of Gene Therapy (ASGT) annual meeting at St. Louis. 6/2005.
b) Sato M, Johnson M, Zhang L, Gambhir SS, Carey M and Wu L. Enhanced Tissue-Targeting Vector Mediated Multi-Modality Gene Expression Imaging in Hormone Refractory Prostate Cancer. American Association of Cancer Research (AACR) annual meeting at Anaheim. 4/2005.
c) Sato M, Johnson M, Zhang L, Gambhir SS, Carey M and Wu L. Development of Prostate Specific Oncolytic Adenovirus Utilizing Bidirectional TSTA System. Academy of Molecular Imaging annual meeting at Florida. 3/2005.
d) Sato M, Johnson M, Zhang L, Gambhir SS, Carey M and Wu L. Development of Prostate Specific Oncolytic Adenovirus Utilizing Bidirectional TSTA System. American Association of Cancer Research (AACR) special meeting-Basic, Translational, and Clinical Advances in Prostate Cancer at Florida. 11/2004.
e) Sato M, Johnson M, Gambhir SS, Carey M and Wu L. TSTA mediated multi-modality gene-expression imaging in hormone refractory prostate cancer. ASGT annual meeting at Minneapolis. 6/2004.

Conclusions

We have shown that the TSTA system, a robust and prostate targeted gene expression system, is a useful tool for an efficient and safer suicide gene therapy vector as well as bioluminescence and microPET imaging reporter vector in human prostate tumor xenografted mice model. In addition to the strong tumor killing activity of AdTSTA-sr39tk in combination with ganciclovir, the anti-angiogenic adenoviral vectors exhibited a strong inhibitory effect on the initial development of hormone refractory prostate cancer CWR22Rv1 cell lines in nude mice. We foresee that anti-angiogenic adenoviral vectors, in combination with the prostate targeted TSTA vector, will be an excellent therapeutic option for advanced stages of prostate cancer.

References

i. Klein KA, Reiter RE, Redula J, Moradi H, Zhu XL, Brothman AR, Lamb DJ, Marcelli M, Belldegrun A, Witte ON, Sawyers CL. Progression of metastatic human prostate cancer to androgen independence in immunodeficient SCID mice. *Nature Medicine, 3: 402-408 (1997).*
ii. Good DJ, Polverini PJ, Rastinejad F, Le Beau MM, Lemons RS, Frazier WA, Bouck NP. A tumor suppressor-dependent inhibitor of angiogenesis is immunologically and functionally indistinguishable from a fragment of thrombospondin. *Proc Natl Acad Sci U S A, 7: 6624-6628 (1990).*
iii. Vazquez F, Hastings G, Ortega MA, Lane TF, Oikemus S, Lombardo M, Iruela-Arispe ML. METH-1, a human ortholog of ADAMTS-1, and METH-2 are members of a new family of proteins with angio-inhibitory activity. *J Biol Chem, 274: 23349-23357 (1999).*
iv. Sramkoski RM, Pretlow TG 2nd, Giaconia JM, Pretlow TP, Schwartz S, Sy MS, Marengo SR, Rhim JS, Zhang D, Jacobberger JW. A new human prostate carcinoma cell line, 22Rv1. *In Vitro Cell Dev Biol Anim, 35: 403-409 (1999).*

v. Griscelli F, Li H, Cheong C, Opolon P, Bennaceur-Griscelli A, Vassal G, Soria J, Soria C, Lu H, Perricaudet M, and Yeh P. Combined effects of radiotherapy and angiostatin gene therapy in glioma tumor model. *Proc Natl Acad Sci U S A, 97: 6698-6703 (2000)*.
vi. Isayeva T, Kumar S, Ponnazhagan S. Anti-angiogenic gene therapy for cancer. *Int J Oncol. 25: 335-343 (2004)*.
vii. Thorpe PE. Vascular targeting agents as cancer therapeutics. *Clin Cancer Res. 10: 415-427 (2004)*.
viii. Lee Y, Schwarz E, Davies M, Jo M, Gates J, Wu J, Zhang X, Lieberman JR. Differences in the cytokine profiles associated with prostate cancer cell induced osteoblastic and osteolytic lesions in bone. *J Orthop Res. 21: 62-72 (2003)*.

ARTICLE

doi:10.1016/j.ymthe.2003.08.016

Optimization of Adenoviral Vectors to Direct Highly Amplified Prostate-Specific Expression for Imaging and Gene Therapy

Makoto Sato,[1] Mai Johnson,[1] Liqun Zhang,[2] Baohui Zhang,[1] Kim Le,[2] Sanjiv S. Gambhir,[3]* Michael Carey,[2,3] and Lily Wu[1,3,†]

[1]*Department of Urology,* [3]*Crump Institute of Molecular Imaging and Department of Molecular and Medical Pharmacology, and* [2]*Department of Biological Chemistry, University of California at Los Angeles School of Medicine, Los Angeles, California 90095*

**Present address: Department of Radiology and Bio-X Program, Stanford University, Stanford, CA.*

[†]*To whom correspondence and reprint requests should be addressed. Fax: (310) 206-5343. E-mail: LWu@mednet.ucla.edu.*

Gene expression-based imaging coupled to gene therapy will permit the prediction of therapeutic outcome. A significant challenge for successful gene therapy is to achieve a high-level of specific gene expression; however, tissue-specific promoters are weak. We postulate that if the weak activity of tissue-specific promoters can be amplified to the levels of strong viral promoters, which have been successful in preclinical scenarios, while retaining specificity, the therapeutic index of gene therapy can be greatly augmented. With this in mind, we developed a two-step transcriptional activation (TSTA) system. In this two-tiered system, a modified prostate-specific antigen promoter was employed to drive a potent synthetic transcriptional activator, GAL4-VP2. This, in turn, activated the expression of a GAL4-dependent reporter or therapeutic gene. Here we demonstrate that recombinant adenoviral vectors (Ads) in which we have incorporated prostate-targeted TSTA expression cassettes retain cell specificity and androgen responsiveness in cell culture and in animal models, as measured by noninvasive optical bioluminescence imaging. We investigated the mechanism of TSTA in different adenoviral configurations. In one configuration, both the activator and the reporter components are inserted into a single Ad (AdTSTA-FL). The activity of AdTSTA-FL exceeds that of a cytomegalovirus promoter-driven vector (AdCMV-FL), while maintaining tissue specificity. When the activator and reporter components are placed in two separate Ads, androgen induction is more robust than for the single AdTSTA-FL. Based on these findings, we hope to refine the TSTA Ads further to improve the efficacy and safety of prostate cancer gene therapy.

Key Words: prostate-specific expression, two-tiered amplification, androgen regulation, adenoviral vector, optical imaging

INTRODUCTION

Metastatic and recurrent hormonal refractory prostate cancer (HRPC) account for an estimated loss of one life every 17 minutes in the United States [1]. Androgen ablation is the main treatment for advanced disease and can induce an initial remission and achieve symptomatic improvement in 80–90% of patients [2–4]. However, progression to HRPC is inevitable even in the absence of circulating androgen. Currently, there is no effective treatment for HRPC, and median survival is approximately 12 months. Gene-based therapy is a promising possibility for HRPC [5,6]. However, an important prerequisite for developing a safe and effective therapy is to achieve high levels of prostate-specific gene expression *in vivo* [6].

The use of tissue-specific promoters to express transgenes is an attractive approach that is particularly suitable for prostatic tissue, because it is one of the organs other than the pancreas and breast that expresses an unusually high number of unique genes. A survey of the Cancer Genome Anatomy Project database published by the National Cancer Institute (http://www.ncbi.nlm.nih.gov/ncicgap/) lists more than 2000 prostate-specific genes, although the majority of them are not fully characterized at this time. Many prostate-specific genes, including pros-

1525-0016/03 $30.00

tate-specific antigen (PSA) and prostate-specific membrane antigen, are well characterized [7–12]. The PSA gene is regulated by testosterone (T) and dihydrotestosterone (DHT), which bind androgen receptor (AR). The ligand-bound AR binds directly to sites within the PSA promoter and enhancer, thus activating PSA gene expression [7,10,11]. Clinical findings indicate that AR and PSA are expressed in all stages of prostate cancer and in distant metastases, even after androgen-deprivation therapy [13–16]. Currently, serum PSA measurements remain the most reliable means to detect recurrent HRPC [17]. Numerous studies support the likelihood that the AR pathway is still functioning in HRPC at castrated levels of DHT and T. Several mechanisms have been proposed to facilitate AR function under androgen-deprived conditions [6,18], such as AR overexpression [19]; increased expression of the nuclear receptor transcriptional coactivators, SRC-1 and SRC-2 [20]; AR mutations that confer expanded ligand specificity [21]; or cross talk between other signaling cascades and AR pathways [22].

We were interested in generating systems for delivery of therapeutic and imaging genes to prostate cancer. We designed our systems around the PSA promoter because of its ability to function in early androgen-dependent prostate cancer and in advanced-stage HRPC [23] and metastasis. Although the native PSA regulatory elements confer tissue selectivity, their activity is too weak to mediate efficient vector-based gene expression *in vivo* [6]. Therefore, we have undertaken two strategies to augment the activity of the PSA promoter/enhancer, while maintaining its specificity. First, the upstream enhancer core of PSA was duplicated in a construct designated PSE-BC, which achieved 20-fold enhancement of activity compared to the native PSA enhancer and promoter construct [24,25]. An adenoviral vector (Ad) bearing this PSE-BC promoter-driven firefly luciferase (FL) gene was able to achieve targeted expression in distant metastatic prostate cancer cells in living mice [26]. In a second approach, we employed a two-step transcriptional amplification (TSTA) system both to elevate and to modulate the activity of the PSA enhancer/promoter over a 1000-fold range [27,28]. In this two-tiered system illustrated in Fig. 1a, the PSA regulatory region was employed to express the potent synthetic transcription activator, GAL4-VP2, which in turn activates a GAL4-responsive reporter. In tissue culture transfection studies, optimal TSTA constructs displayed levels of activity significantly higher than the cytomegalovirus immediate early promoter (CMV), while maintaining prostate cell specificity and ligand responsiveness [27,28].

Imaging of vector-mediated transgene expression provides a critical assessment of the *in vivo* capabilities of targeted gene transfer. Rapid advances in imaging technology have allowed repetitive monitoring of the location, magnitude, and kinetics of reporter gene expression in small living animals [29–31]. Optical bioluminescence imaging (BLI) is particularly suitable for small animal studies, with the distinct advantage of low background signal, rapid scanning time, and low cost in comparison to radionuclide imaging. The *in vivo* expression of the popular FL reporter gene can be monitored by a highly sensitive cooled charge-coupled device (CCD) camera after the administration of the relatively nontoxic d-luciferin substrate in living animals [32,33]. Because imaging can provide real-time information on *in vivo* biological processes, the BLI technology was used to monitor estro-

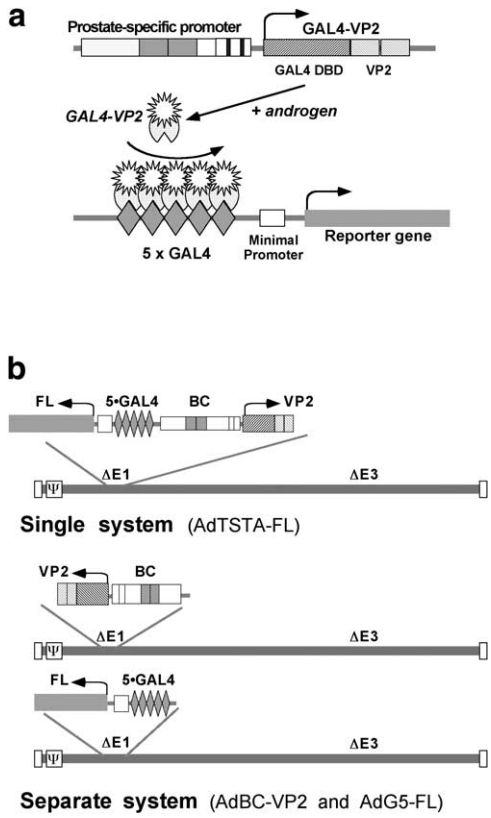

FIG. 1. Schematic representation of TSTA system. (a) Illustration of the two-step transcriptional activation process. In the first step, GAL4-VP2 activator proteins (fusion of GAL4 DNA binding domain and two copies of the VP16 transactivation domain) are expressed under the control of a prostate-specific promoter (an augmented PSA promoter, PSE-BC), which is activated by androgen. In the second step, GAL4-VP2 binds to a GAL4-responsive promoter and activates the expression of the FL reporter gene. (b) The two different TSTA configurations in Ad. In the single TSTA Ad (AdTSTA-FL), both activator and reporter are inserted into the E1 region of the same Ad in a head-to-head orientation. In the separate TSTA Ads (AdBC-VP2 and AdG5-FL), activator and reporter components are incorporated into the E1 region of two separate Ads with the transcription oriented toward the left end of the viral genome. BC is the abbreviation of the PSE-BC prostate-specific promoter [25]. ψ denotes the packaging signal of adenovirus and open rectangles at both termini denote inverted terminal repeats of the viral genome.

doi:10.1016/j.ymthe.2003.08.016

gen receptor function under physiological conditions and during pharmacological intervention [34].

To assess the potential of the TSTA system in gene therapy applications, we incorporated the system into an Ad, which is an efficient *in vivo* gene delivery vehicle. The purpose of this study was to investigate the *in vivo* specificity of and the parameters necessary to achieve optimal regulation of the TSTA system in different Ad configurations. In the AdTSTA-FL construct, the activator and reporter component were inserted into the Ad in a divergently linked head-to-head configuration. Alternatively, two Ads that separately express the GAL4-responsive FL and the PSE-BC-regulated GAL4-VP2 activator were also generated. We analyzed the prostate-specific expression and androgen regulation of the separate TSTA Ads in comparison to the single AdTSTA-FL *in vitro* and *in vivo*. We found that separate Ads elicited a more robust response to androgen versus the single Ad.

RESULTS

Generation of Adenovirus Vectors Containing the TSTA System

The TSTA system is schematically represented in Fig. 1a. We previously determined the combination of activator and reporter plasmid TSTA constructs that achieves the highest levels of activity in prostate cancer cells using transfection studies [28]. Based on these results, we generated TSTA Ads, utilizing the bacterial recombination AdEasy methodology [35]. The activator is composed of an augmented prostate-specific PSE-BC promoter/enhancer [25] controlling the expression of the chimeric activator protein, GAL4-VP2 (the GAL4 DNA-binding domain fused to two tandem repeats of the herpes simplex virus VP16 activation domain) [28]. The reporter component consists of five repeats of the 17-bp GAL4 binding sites positioned upstream of a minimal promoter containing the adenovirus E4 gene TATA box driving FL. We inserted the activator (BC-VP2) and reporter (G5-FL) components linked in a divergent head-to-head orientation into the E1 region of the Ad, resulting in the AdTSTA-FL vector (Fig. 1b). We also constructed two Ads, designated AdBC-VP2 and AdG5-FL, which harbor the BC-VP2 activator and the G5-FL reporter, respectively (Fig. 1b).

Specificity of the TSTA Vectors

We evaluated the capability of AdTSTA-FL to direct prostate-specific expression by infecting a variety of cell lines derived from different tissues. Human serotype 5 Ad exhibits wide cell-type viral tropism. However, the susceptibility of a cell line to Ad infection is modulated by the cell surface expression of coxsackievirus and adenovirus receptor (CAR) [36,37] and αv integrins [38]. Thus, a measurement of infectivity in different cell lines is needed to assess the activity of AdTSTA-FL. Initially, we determined relative infectivity of different cells by normalization to the activity of AdCMV-FL, in which the FL expression is driven by the constitutively active CMV promoter. Our view was that similar pfu (plaque-forming unit) amounts of AdTSTA-FL and AdCMV-FL should display similar infectivity. Thus, differences in the activity of AdCMV-FL in different lines would represent a standard for normalizing infectivity of AdTSTA-FL. However, two findings alerted us to the potential inaccuracy of this measurement: (1) a 3- to 4-fold androgen induction was noted in the AdCMV-FL-infected prostate cell lines (data not shown) and (2) a greater than 30-fold difference in activity was observed between the most and the least active cell lines infected with equivalent doses of AdCMV-FL (data not shown). Discrepancy between luciferase activity and physical viral DNA measurement mediated by AdCMV-luc in different cell types has been reported [39]. An ideal assay to measure infectivity is not available.

In this study we elected to use the viral DNA uptake in the cells as a measurement of infectivity. We harvested the internalized viral DNA from infected cells and quantified the FL DNA by real-time PCR. We determined the infectivities of LNCaP and LAPC-4 (prostate carcinoma), H157 and A549 (lung cancer), MCF-7 (breast carcinoma), HepG2 (liver cancer), and HeLa (cervical carcinoma) cell lines by this viral DNA uptake approach. Among the panel of cell lines that we tested, HeLa cells were the least susceptible to infection and their infectivity was designated as 1. The infectivities of LNCaP, H157, A549, MCF7, LAPC-4, and HepG2 cells were 1.7-, 1.6-, 1.5-, 1.3-, 1.1-, and 1.1-fold higher than that of HeLa cells, respectively. Differential CAR expression in different stages of prostate carcinoma [40] might contribute to the enhanced infection in LNCaP cells.

We evaluated the activity of AdTSTA-FL in several prostate cancer cell lines, including two androgen-responsive cell lines (LNCaP and LAPC-4 [41]) and two AR-negative lines (DU145 and PC-3). Infection was carried out at a calculated AdTSTA-FL dosage of 1 infectious unit (pfu) per cell (m.o.i. 1). The normalized FL activity in LAPC-4 was 4.4-fold lower than LNCaP (see Fig. 5b and data not shown). Conversely, the FL activity in AR-negative prostate cancer lines was negligible (nearly 500-fold lower than in LNCaP cells, data not shown). For simplicity, we compared the normalized FL activities to that of the LNCaP cell line, set at 100% (Fig. 2a). The activity in A549, H157, HepG2, HeLa, and MCF7 cells was 290-, 1200-, 4500-, 6000-, and 20,000-fold lower than in LNCaP cells, respectively (Fig. 2a). The FL activity in nonprostate cell lines and AR-negative prostate cancer lines was not induced by androgen (data not shown). We also observed consistent diminished cell-specific expression in infections. At higher m.o.i. the cell specificity became less apparent due to higher androgen-independent or basal activity, an effect that we do not completely understand (data not shown). For example, AdTSTA-FL-mediated activity in HeLa cells at m.o.i. 10 was 660-fold lower than in

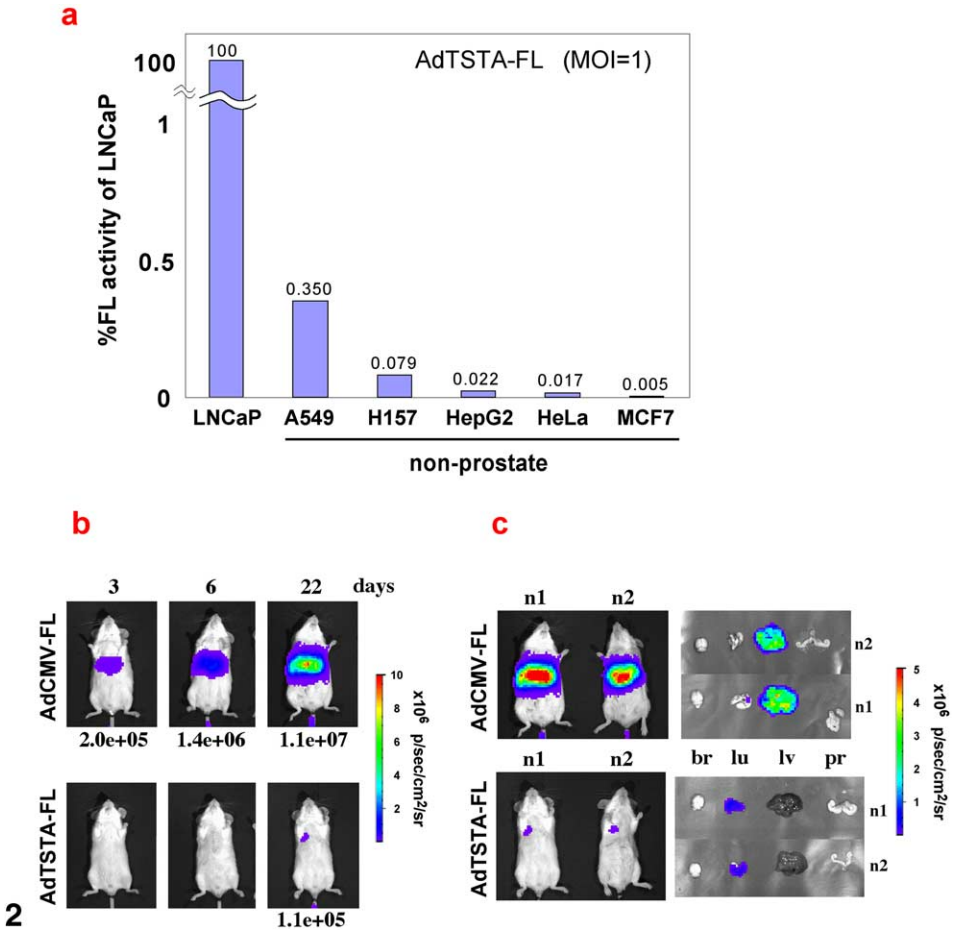

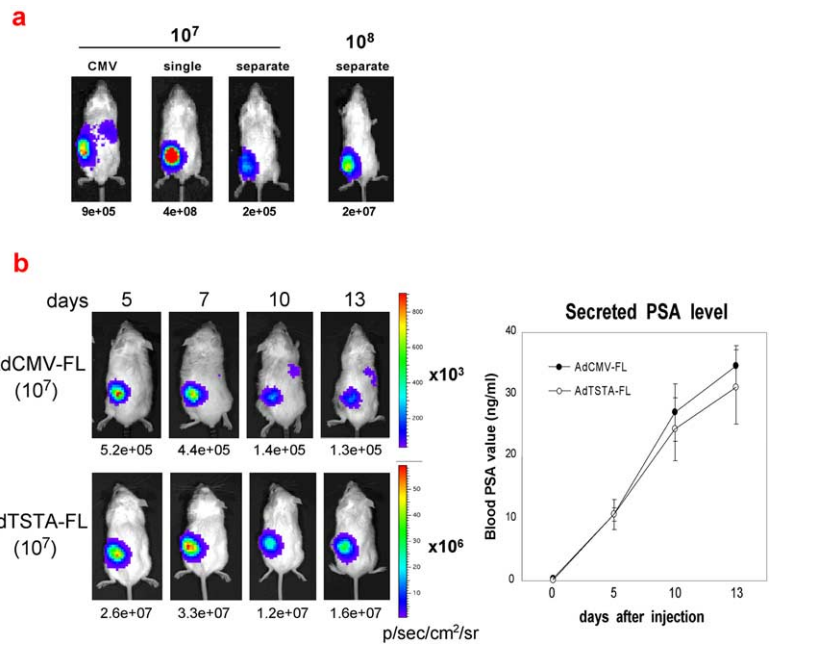

doi:10.1016/j.ymthe.2003.08.016

LNCaP cells, compared to 6000-fold at m.o.i. 1 (data not shown; see Discussion).

We next investigated the specificity of the single AdTSTA-FL *in vivo*. We compared its activity to that of AdCMV-FL, because vector DNA quantitation studies in animals are less well controlled. We employed CCD imaging to monitor *in vivo* expression over a 22-day period. Fig. 2b illustrates the optical imaging profiles of animals that received systemic administration of AdTSTA-FL or AdCMV-FL. A robust signal emanating from the midsection of mice injected with AdCMV-FL via the tail vein was seen as early as 3 days postinjection, which we determined was due to efficient liver transduction as assessed by imaging of isolated organs (Figs. 2b and 2c). In contrast, the AdTSTA-FL-injected animals did not have detectable signals until a late time point (day 22), which signals then appeared in the lung (Figs. 2b and 2c); however, this signal is more than 3 orders of magnitude lower than tumor-directed expression (see Fig. 3). The absence of optical signal in the prostate after tail vein injection of AdTSTA-FL is unclear at this time. However, limitations of *in vivo* Ad distribution that result in low gene transfer to organs other than mouse liver have been well documented [42]. We expand on these issues under Discussion.

We next evaluated intratumoral activity mediated by both single and separate TSTA Ads in LAPC-4 xenografts, which were derived from a lymph node metastatic lesion from a patient [41]. LAPC-4 expresses PSA and AR and exhibits androgen-responsive gene expression and growth. Fig. 3a shows that intratumoral injection of 10^7 pfu of the single AdTSTA-FL resulted in a robust signal at 4 days postinjection, compared to AdCMV-FL. In a cohort of four animals, the average activity of AdTSTA-FL was 110-fold higher than that seen with AdCMV-FL ($P = 0.06$).

Cancer-specific gene therapy based on activation of a toxic gene by the Cre/lox recombination system delivered by separate two Ads has been reported to work in animals [43,44]. However, *in vivo* transduction of the two paired TSTA Ads, AdBC-VP2 and AdG5-FL, into the same cell, is anticipated to be less effective than delivery of a single vector containing both elements. Thus, it is not surprising that injection of 10^7 pfu of each of the two Ads resulted in lower optical signal (2×10^5 photons/s/cm^2/sr) versus single Ad (4×10^8 photons/s/cm^2/sr). When the dose of the two paired TSTA Ads was increased to 10^8 pfu each, expression level (2×10^7 photons/s/cm^2/sr) higher than that of 10^7 pfu of AdCMV-FL (9×10^5 photons/s/cm^2/sr) was achieved (Fig. 3a). However, this magnitude of activity is still lower than can be achieved by 10^7 pfu of AdTSTA-FL (4×10^8 photons/s/cm^2/sr).

We examined the kinetics of expression after intratumoral delivery of 10^7 pfu of AdCMV-FL and AdTSTA-FL into LAPC-9 tumors. The LAPC-9 xenograft expresses AR and PSA and was derived from a bone metastasis [41]. Sequential optical images between 5 and 13 days postviral injection were recorded (Fig. 3b). The TSTA vector displayed 50- to 100-fold higher levels of FL activity than the AdCMV-FL during this period (Fig. 3b). The increasing serum PSA levels in both groups likely reflect the increase in tumor mass over the duration of the time course (Fig. 3b, right). However, despite the consistent increase in serum PSA levels the intratumoral FL signals gradually decayed after day 7 in both the AdCMV and the AdTSTA cohorts (Fig. 3b) due to the transient nature of Ad-mediated gene expression. The LAPC-9 tumors, like the LAPC-4 tumors, show a propensity for vector leakage into systemic circulation. However, we consistently observed a greater magnitude of leakage in LAPC-4 tumors, which was manifested as prominent signals in the liver after intratumoral injection of AdCMV-FL [26]. Because both vectors (TSTA and CMV) are serotype 5 adenovirus with the same deletion of the E1 and E3 genes, their biodistribution in mice should not differ. Intratumoral injection of AdTSTA-FL should result in the same extent of vector leakage as AdCMV-FL. However, no detectable liver signal was observed after intratumoral injection of AdTSTA-FL.

FIG. 2. Cell specificity of the TSTA Ad. (a) *In vitro* cell specificity of AdTSTA-FL. The prostate cell line LNCaP and nonprostate cell lines were infected with AdTSTA-FL at m.o.i. 1. Cells were harvested and subjected to an FL assay 48 h after infection. FL activity was normalized to cell numbers and infectivity of each cell line as assayed by real-time PCR (see Materials and Methods). FL activity was plotted for each cell line using LNCaP (an androgen-responsive prostate carcinoma line) as a normalization standard, set at 100%. The activities in nonprostate cell lines are more than 290-fold lower than in LNCaP. (b) *In vivo* tissue specificity of AdTSTA-FL. 10^7 pfu (plaque-forming units = infectious units) of Ad was injected into naïve mice via the tail vein and FL expression was sequentially monitored by optical imaging at days 3, 6, and 22. Robust liver signals were noted in the AdCMV-FL-injected animals starting at day 3 and increasing from that point onward. The AdTSTA-FL-injected animals remained transcriptionally silent until day 22, when a weak signal was noted in the lung. Numbers below the images are the maximal activities in the region of interest as photons (p) acquired per second per square centimeter per steridan (sr). (c) Optical activities in the isolated organs. Two additional animals (n1 and n2) from the AdCMV-FL- or AdTSTA-FL-injected group were sacrificed at day 22, and the isolated organs were reimaged. The liver is the predominant site of expression in AdCMV-FL-injected animals. Low level of expression in the lung was observed in the AdTSTA-FL-injected animals (br, brain; lu, lung; lv, liver; and pr, prostate).

FIG. 3. *In vivo* FL expression mediated by single and separate TSTA Ads in LAPC-4 xenografts and prostates. (a) Optical signals after injections of the respective Ads in LAPC-4 tumors. 10^7 or 10^8 pfu of Ads (as specified) was injected. The injection of separate Ads denotes the coadministration of both AdBC-VP2 and AdG5-FL at the specified dosage. CCD images of representative animals analyzed at 4 days postinjection were shown. (b) Kinetics of FL expression in LAPC-9 tumors. 10^7 pfu of AdCMV-FL or AdTSTA-FL was injected intratumorally. Optical signals were monitored on the specified days after viral injection. The number below each image represents the maximal signal over the tumor. The graph on the right represents the averaged serum PSA level measured in the animals at the specified days post-viral injection.

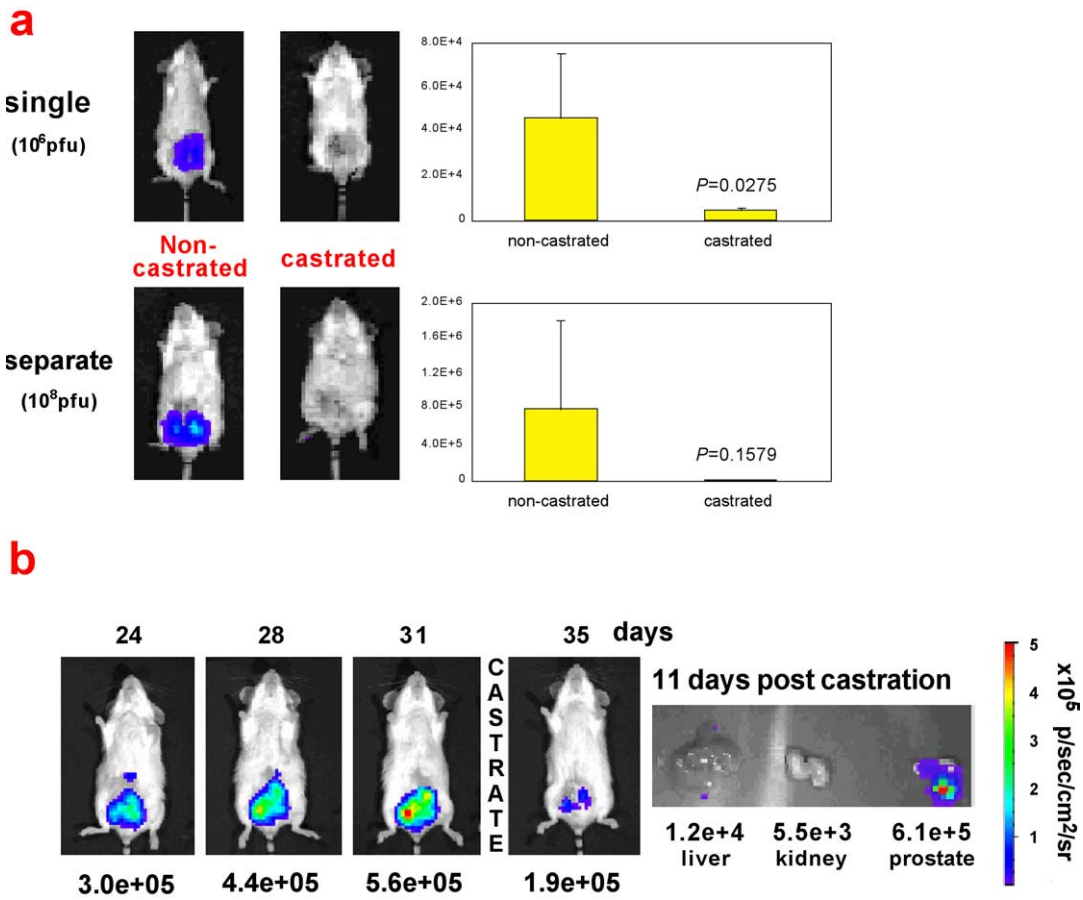

FIG. 4. Intraprostatic signals in intact and castrated animals. (a) AdTSTA-FL (10^6 pfu) or AdBC-VP2 and AdG5-FL (10^8 pfu each) were injected into the prostate of intact and castrated male SCID (7-days postcastration). The images were taken 4 days after viral injection. In each group, n is ≥ 3 animals. The averages and standard errors are plotted on the right. The FL signals in the castrated animals were 4.7×10^3 and 9.6×10^3 with single and separate TSTA Ad, respectively. The significance between intact and castrated animals is denoted in each graph as the P value. (b) The FL signal mediated by AdTSTA-FL in the same animal before and after castration. 10^7 pfu of AdTSTA-FL was injected into prostate in intact SCID mice. Days post-intraprostatic viral injection are indicated above the mouse images. The animal was castrated at day 31 and reimaged at day 35 (4 days postcastration). The animal was sacrificed at 11 days postcastration (day 42). The prostate gland was the predominant site of expression. The optical activity is specified below each image.

This finding supports our view that the prostate specificity of TSTA is able to prevent expression of FL in the liver.

Androgen Regulation of the TSTA Ads

To determine if TSTA Ads respond to androgen regulation *in vivo* we assessed FL expression in the prostates of intact and castrated male SCID mice (Fig. 4). We injected 10^6 pfu of AdTSTA-FL or 10^8 pfu each of AdBC-VP2 and AdG5-FL into the prostate glands of cohorts of either intact male mice or mice castrated 7 days prior to injection (androgen-deprived group). The intact males infected with the single- or two-virus TSTA vectors displayed significant optical signals compared to the castrated mice. We conclude that both vector systems are responding to androgen depletion *in vivo* (Fig. 4a). The FL expression level of a 100-fold higher dose of the separate TSTA Ads was 20-fold greater than that of the single AdTSTA-FL (Fig. 4a, graphs). We also observed androgen regulation of AdTSTA-FL in the prostate gland when castration was performed 30 days postinjection, after FL expression had stabilized. In this case a 3-fold drop in expression was observed 3 days after castration (Fig. 4b).

To investigate androgen regulation of the TSTA Ads in more detail, we employed cell culture infection studies, in which the concentration of androgen and its antagonists could be carefully manipulated. We infected two androgen-dependent prostate cancer cell lines, LNCaP and LAPC-4, with TSTA Ads at different m.o.i. and androgen concentrations. Androgen levels in the medium were manipulated by adding R1881 (methylenetrienolone), a synthetic androgen that is more stable than DHT under culture conditions. The antagonist Casodex was used to minimize residual androgen activity in the charcoal-

doi:10.1016/j.ymthe.2003.08.016

stripped serum because even low androgen levels activate the highly sensitive TSTA system. Both the activator and the reporter TSTA components are required to generate detectable FL in the two-virus system (Fig. 5a). Additionally, androgen stimulated the FL activity for both the separate and the single TSTA Ads, with the highest activity observed between 1 and 10 nM R1881. In Fig. 5b, AdTSTA-FL demonstrates a clear m.o.i.- and R1881-dependent increase in FL activity. In the presence of 1 nM R1881, activity increased 27-fold from m.o.i. 0.1 to m.o.i. 1 in LNCaP cells and 96-fold from m.o.i. 1 to m.o.i. 10 in LAPC-4 cells.

We also quantitated the androgen response of TSTA Ads by calculating the fold induction, based on the ratio of the highest activity at 10 nM R1881 over the basal activity in the presence of Casodex. Both separate and single TSTA Ads exhibited high levels of androgen induction in LNCaP and LAPC-4 cells. The androgen induction observed in infections at m.o.i. 1 and 5 of separate Ads were 672- and 915-fold, respectively, in LNCaP cells, and 52- and 67-fold, respectively, in LAPC-4 cells. The androgen induction mediated by the single AdTSTA-FL was 117- and 101-fold at m.o.i. 1 and 5 in LNCaP cells, respectively, and 35- and 24-fold in LAPC-4 cells at m.o.i. 1 and 5, respectively. The single AdTSTA-FL displayed diminished androgen inducibility compared to separate TSTA Ads. This point is illustrated in Fig. 5c by a plot of the relative induction ratio of separate Ads to single AdTSTA-FL in LNCaP and LAPC-4 cells at the two different m.o.i. The lower inducibility of AdTSTA-FL is not due to a lower maximal activity, but to a higher basal activity (in the presence of Casodex). Because this higher basal activity could potentially contribute to reduced specificity, we investigated the activation mechanism of TSTA Ads in more detail.

Investigating the Activation Mechanism in Single and Separate TSTA Ads

To investigate the mechanism responsible for differences in androgen induction, we analyzed FL activity and activator protein expression profiles over a wide range of infection ratios. LNCaP cells were infected with AdTSTA-FL at m.o.i. of 50, 16.7, 5.6, 1.9, 0.62, and 0.21 (threefold serial dilutions). For the separate system, we added AdBC-VP2 and AdG5-FL at the indicated m.o.i. to generate levels of activator and reporter gene delivery equivalent to those in the single AdTSTA-FL infections. We demonstrated by Southern blotting that equal m.o.i. of AdTSTA-FL and AdBC-VP2 led to equivalent amounts of vector delivery (data not shown). We then examined FL activity and activator expression 48 h postinfection, as shown in Fig. 6. It is difficult to compare directly the levels of FL activity of single and separate Ad infections, especially at low m.o.i., due to the limited codelivery. However, both systems exhibited m.o.i.-dependent increases in activity as indicated in earlier figures. We observed a saturation of activity in both single and separate TSTA vectors. Overall, the magnitude of FL activity corresponded very well with the level of GAL4-VP2 expression measured by Western blotting. In the single AdTSTA-FL infections, the GAL4-VP2 expression reached a maximum at m.o.i. 16.7. We did not observe a plateau of activator expression in the separate TSTA infections at the range of m.o.i. tested. A surprising finding was that at each m.o.i., the activator expression in the single AdTSTA-FL was considerably higher than that mediated by the AdBC-VP2 in the separate system, despite comparable levels of activator (BC-VP2) gene delivery (data not shown). Given the fact that the same PSE-BC promoter-driven GAL4-VP2 expression cassette was inserted into both the single and the separate TSTA Ads, the different protein levels observed imply that a property of the vector genome context or design is influencing GAL4-VP2 expression. We propose in the Discussion that a self-perpetuating feedforward loop may be activated by the head-to-head orientation of AdTSTA-FL. A positive feedback loop could explain the higher basal activity observed for the single virus AdTSTA-FL even in the presence of Casodex (Fig. 5).

DISCUSSION

The key objectives of this study were to investigate the regulation of the TSTA system in different Ad configurations and to define the dynamic range of this system in different *in vivo* settings. Published and ongoing studies by our groups have demonstrated that TSTA technology is an effective approach to augment the activity of a weak tissue-specific promoter [27, 28]. Our goal is to develop these targeted gene expression systems for diagnostic and therapeutic applications in clinical settings. Thus, we have incorporated our PSA promoter-based TSTA system into an adenoviral gene delivery vector. Inserting the two components of TSTA, the activator and the reporter component, into a single vector does improve the functional efficiency of this system *in vivo*. In fact, the activity of the first single vector we generated, AdTSTA-FL, is quite impressive, as its activity consistently exceeded AdCMV-FL in all AR-expressing prostate cancer cell lines and tumors tested ([23] and this study), and it also displayed significant prostate specificity in cell culture studies, achieving 290-fold or higher levels of tissue discrimination (Fig. 2a). AR-mediated expression is a critical component of the PSA-based promoter in the TSTA system. We utilized the optical signal produced by AdTSTA-FL in tumors to monitor the dynamics of AR function during prostate cancer progression [23].

To understand the mechanism of activation of TSTA in adenoviral vectors better, we examined and compared the activity of single and separate TSTA configured Ads. The activity of this TSTA system is fully dependent on the GAL4-VP2 activator (Fig. 6). A second interesting finding is that despite equivalent promoter (PSE-BC) and gene

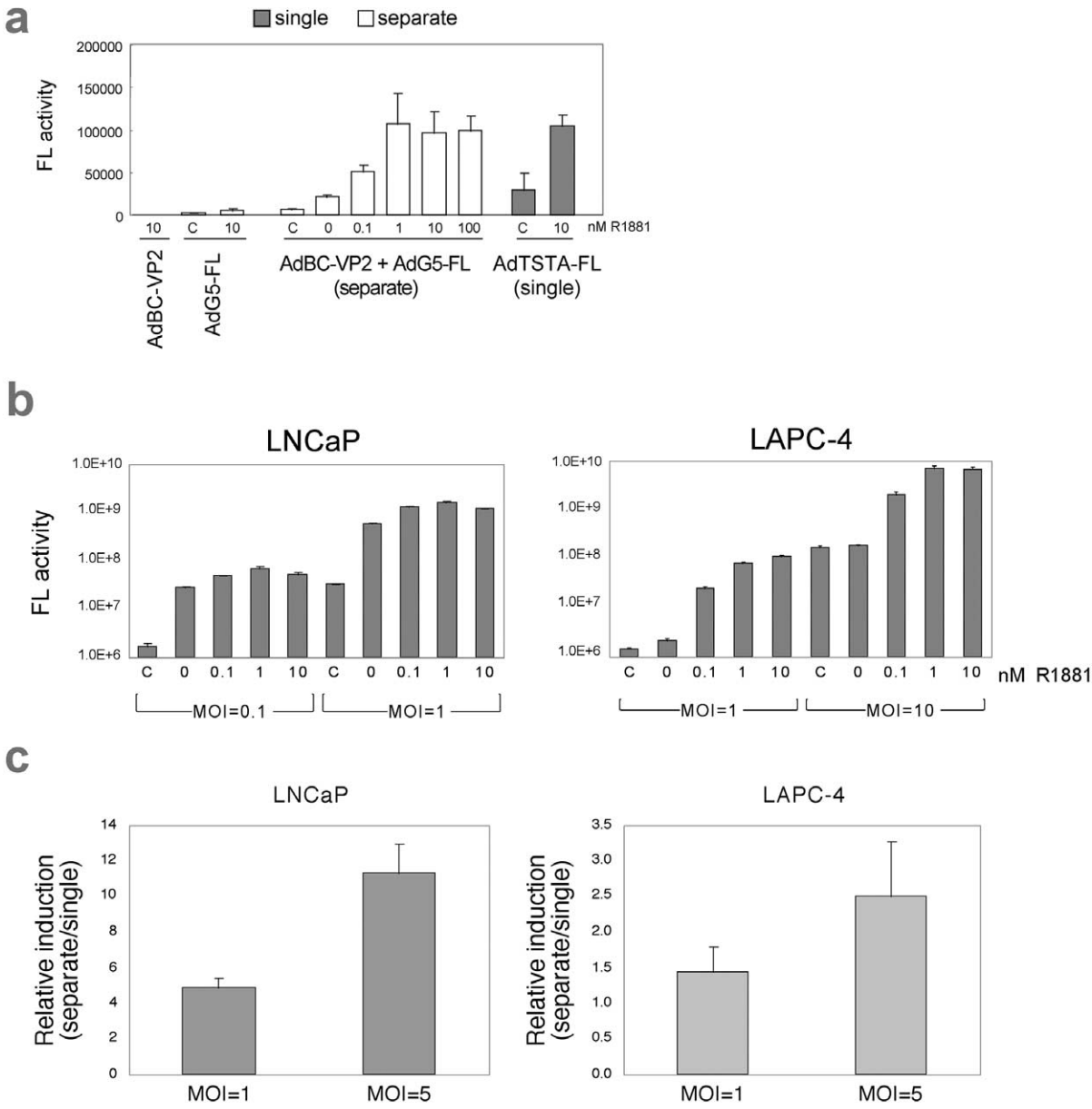

FIG. 5. *In vitro* expression and regulation of the single and separate TSTA Ads. (a) Expression of TSTA Ads in LAPC-4. LAPC-4 cells were infected with Ad at m.o.i. 10. 48 h postinfection the cells were harvested and assayed. Infections with AdBC-VP2 or AdG5-FL exhibited minimal activity. The FL activities of co-infection of separate TSTA Ads increased with increasing amount of synthetic androgen (R1881, nM). C denotes the addition of 10 μM Casodex (anti-androgen). (b) Androgen regulation of AdTSTA-FL. LNCaP and LAPC-4, two androgen-dependent prostate cell lines, were infected with AdTSTA-FL at the indicated m.o.i. in the presence of Casodex or R1881. The FL activities assayed at 48 h postinfection are shown. (c) Relative androgen induction ratio of the separate to the single TSTA Ads. The cells were infected at m.o.i. 1 or 5. Fold induction of activity was calculated based on the ratio of the peak activity (in 10 nM R1881) to the basal activity (in 10 μM Casodex). The relative induction ratio was calculated by dividing the androgen induction in the separate TSTA Ads infection by the induction in the single-AdTSTA-FL-infected cells. The ratio shows that separate TSTA Ads exhibit higher androgen induction than the single Ad.

delivery of the activator in the single and separate TSTA Ads, the single AdTSTA-FL consistently expressed an elevated level of GAL4-VP2 activator. This finding indicates that the head-to-head configuration in the single Ad promotes an increase in GAL4-VP2 and, hence, FL expression. This result could also contribute to the slightly elevated basal activity mediated by AdTSTA-FL in androgen-depleted cell culture medium. We hypothesize that a feedforward loop might be at play in the single AdTSTA-FL. A schematic illustration of this idea is shown in

doi:10.1016/j.ymthe.2003.08.016

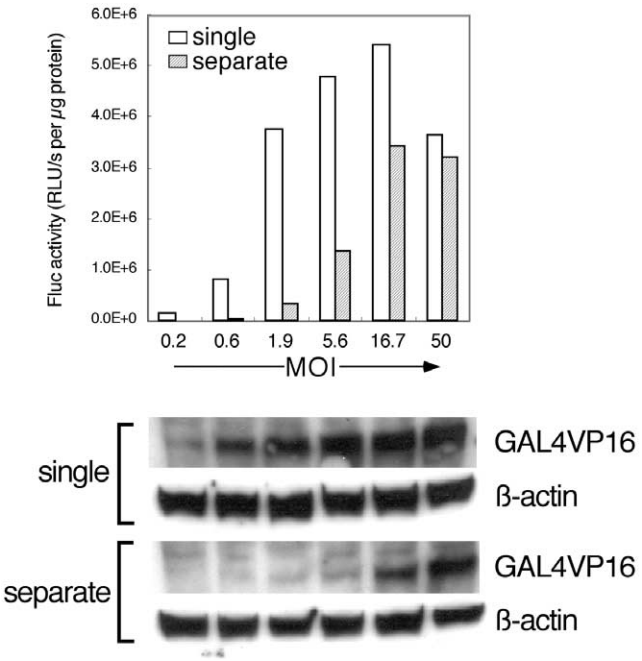

FIG. 6. The activation mechanism in TSTA Ads. LNCaP cells were infected with AdTSTA-FL at specified m.o.i. For the separate system, both AdBC-VP2 and AdG5-FL were infected at the denoted m.o.i. The FL activities and GAL4-VP2 activator expression were examined at 48 h postinfection. Western blot analysis is shown at the bottom. The GAL4-VP2 activator was probed with anti-GAL4 polyclonal antibody (see Materials and Methods). β-Actin is shown as a control.

Fig. 7. The initial expression of GAL4-VP2 (step 1) is regulated by the PSE-BC promoter. In step 2, GAL4-VP2 binds to the GAL4 sites and activates FL gene expression. However, in the head-to-head configuration, the multiple GAL4-VP2 activators could also stimulate transcription in the direction of the PSE-BC promoter in an enhancer-like manner (step 3), further enhancing the synthesis of GAL4-VP2 (step 4). The feedforward loop leads to a perpetuating cycle of activator production that exceeds the natural capability of the PSE-BC promoter. This phenomenon could also contribute to "leaky" expression in nonprostate cells when the TSTA vector is administered at high m.o.i. From these results, we would postulate that functional separation of the activator and reporter components in a single vector might achieve tighter regulation of the TSTA system.

A transcriptionally targeted gene expression approach [reviewed in 45] could reduce the potential side effects of Ad-mediated cytotoxic cancer gene therapy such as that mediated by the herpes simplex virus thymidine kinase (HSV-TK) gene [46]. After intratumoral injection of Ad constitutively expressing luciferase or other reporter gene, leakage of the vector into systemic circulation resulted in transgene expression in the liver [26,47]. From this finding liver toxicity can be anticipated after intratumoral injection of CMV-driven HSV-TK Ad following administration of the prodrug ganciclovir. When a tissue- or cancer-specific promoter is employed to drive HSV-TK, the same extent of vector delivery to the liver is expected to occur. However, HSV-TK expression in the liver will be restricted by the tissue-specific promoter and therefore transgene-mediated liver toxicity should be reduced.

The gene-expression targeting approach employed in this study will not alter the *in vivo* liver distribution observed of Ad5 [26,48]. This preferential Ad transduction has contributed to liver toxicity [48–50] due to the innate immune response to viral capsid proteins [51] and cell-mediated immunity against viral gene products [52,53]. Utilization of a specific promoter to drive transgene expression was shown to reduce both the immune response against the Ad and the associated liver toxicity [54]. In addition, the potent gene expression mediated by the TSTA system could potentially reduce the amount of vector needed to transduce cancer cells *in vivo* compared to nonamplified tissue-specific vectors. Reducing the input dosage of Ad has been documented to reduce liver toxicity [49–52]. A second consequence of Ad sequestration in the liver [48,49] is that viral distribution to other organs such as kidney and intestine was nearly 1000-fold lower [55]. To improve *in vivo* gene transduction to other organs or tumors, many studies are under way to divert the natural adenovirus tropism away from the liver by ablation of CAR- and integrin-mediated interactions [48,55,56].

The inability to detect prostatic expression after tail vein administration of 10^7 pfu of AdTSTA-FL (Figs. 2b and 2c) could be due to liver sequestration. We have detected FL expression in the prostate after intravenous administration of 1.8×10^9 pfu of AdPSE-BC-FL [25]. The AdTSTA-FL is estimated to be about 50-fold more active than AdPSE-BC-FL [23,28]. However, the 180-fold lower dosage of AdTSTA-FL used in this study compared to AdPSE-BC-FL [25] might be below the threshold of detection for

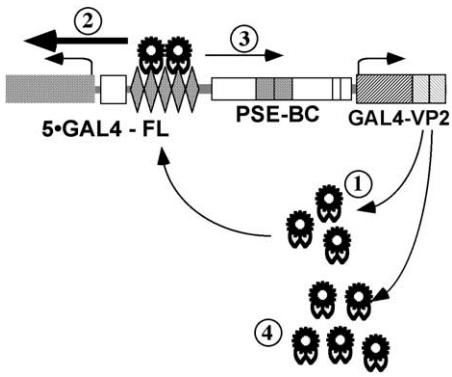

FIG. 7. Schematic representation of the activation mechanism. The feedforward loop mechanism postulates that GAL4-VP2 expression is upregulated by the activator's binding to the designed GAL4 sites in a self-activated manner.

optical imaging. Moreover, by an intraperitoneal route of vector delivery we have been able to detect specific optical signals in the prostate (M. Johnson and L. Wu, unpublished data).

The mechanism for the low level of expression observed in lung tissue is unclear (Figs. 2b and 2c). We speculate that there could be transcription factors common to both lung and prostate that partially contribute to the regulation of the PSA promoter. For example, GATA zinc finger transcription factors have been shown to bind to the PSA promoter [57], and they are involved in lung development [58] and transcription of lung-specific promoters [59]. A large family of Ets transcription factors could also participate in epithelial-specific expression in the lung and prostate [60–62]. Investigating these intriguing possibilities might lead to a better understanding of tissue-specific gene regulation.

It is quite evident that the TSTA approach can amplify the activity of many other weak tissue-specific promoters. Dr. Gambhir's group has demonstrated that the activity of the hypoxia-inducible VEGF promoter can be amplified [63]. A similar approach has been employed to amplify the carcinoembryonic antigen promoter in a binary adenovirus system [64]. This approach exhibited increased therapeutic index compared to constitutive viral RSV-driven HSV-TK suicide gene therapy [64]. To adapt the TSTA system to other promoters, it will be necessary to adjust the various components of TSTA (i.e., the potency of the specific promoter, the strength of the activator, and the number of GAL4 sites) to achieve optimal regulation and expression dictated by the specific applications.

The modular and titratable nature of the TSTA system also makes it particularly attractive for a variety of gene therapy applications [28]. Transgene levels needed to achieve therapeutic efficacy in different gene therapy strategies might vary greatly; for example, p53 tumor suppressor expression in genetic corrective strategies might need to be higher than cytokine expression in immune-mediated tumor rejection. The various adjustable constituents of TSTA can be fine-tuned to achieve the most effective and least toxic therapeutic result. We have shown that transcriptionally targeted Ad (AdPSE-BC-luc) can achieve cell-specific expression to localize metastatic prostate cancer lesions in living mice, using optical CCD imaging [26]. To translate this finding to clinical diagnostic settings, a higher energy imaging modality will be needed to circumvent the loss of optical signal observed with increased tissue depth. Positron emission tomography (PET) is a radionuclide imaging modality widely used in clinical settings. Our institution has acquired substantial experience in adapting this modality to gene-based imaging in small animals, using the HSV-TK or the dopamine type 2 receptor reporter genes [29,30,65]. Compared to optical imaging, PET has the distinct advantage of providing tomographic quantitative image signals and adaptability for human imaging. However, optical imaging is several orders of magnitude higher in sensitivity than PET in small animal applications [66]. Thus, the highly amplified and prostate-specific expression mediated by TSTA will likely permit the development and successful implementation of gene-based PET imaging to detect metastasis *in vivo*.

Many of our studies have demonstrated that the TSTA system is a promising tool to create future targeted gene-based diagnostic and therapeutic applications. With an in-depth understanding of its functional properties and fine-tuning of various components of TSTA, a truly safe, effective, and specific treatment can be developed for metastatic or hormone-refractory prostate cancer.

MATERIALS AND METHODS

Adenovirus constructs. AdCMV-FL was constructed as previously described [25,33]. The single AdTSTA-FL and separate TSTA Ads, AdBC-VP2 and AdG5-FL, were constructed with the AdEasy system [35]. The head-to-head fragment of activator and reporter in the single virus was derived from PBCVP2G5-L [28]. The construction of AdTSTA-FL has been previously described [23]. A *Not*I fragment containing the PSE-BC-driven GAL4-VP2 expression cassette was cloned into the *Not*I site of pShuttle to generate AdBC-VP2. For the construction of AdG5-FL, an *Asp*718–*Sal*I fragment with five GAL4 binding sites upstream of the minimal adenovirus E4 and FL genes was blunted and ligated into the *Eco*RV site of pShuttle. All the pShuttle expression plasmids were used for recombination with pAdEasy-1 in the BJ5183 rec^+ bacteria strain to generate the full-length recombinant virus-containing plasmid. The viruses were propagated in 293 cells, purified on a CsCl gradient, and titered by plaque assays on 293 monolayers. Viruses are stored in 10 mM Tris–HCl, 1 mM $MgCl_2$, and 10% glycerol at −80°C until use.

Cell culture and infection studies. The human prostate cancer cell lines, LNCaP and LAPC-4, were grown in RPMI 1640 and Iscove's modified DMEM, respectively, and supplemented with 10% fetal bovine serum (FBS) and 1% penicillin/streptomycin solution. PC-3, Du145, HeLa, MCF7, HepG2, A549, and H157 cells were cultured in RPMI 1640 (Mediatech, Herndon, VA) with 10% FBS and 1% penicillin/streptomycin. For FL assays, the cultured cells were plated onto 24-well plates at 5×10^4 cells per well, and cells were counted at the day of infection to calculate m.o.i. For prostate cell lines, medium was replaced with 10% charcoal-stripped serum for 2 days prior to infection. The cells were infected with AdTSTA-FL or co-infected with AdBC-VP2 and AdG5-FL at certain m.o.i. Following infection, the synthetic androgen methylenetrienolone (R1881; NEN Life Science Products, Boston, MA) or anti-androgen bicalutamide (Casodex) was added to samples as indicated. At 48 h postinfection, the cells were harvested and lysed, using passive lysis buffer (Promega, Madison, WI). Levels of FL activity were measured according to the manufacturer's instructions (Promega), using a luminometer (Berthold Detection Systems, Pforzheim, Germany) with a 10-s integration time. Each value was calculated as the average of triplicate samples.

Real-time PCR was performed to quantify the amount of intracellular viral DNA. HeLa, MCF7, HepG2, H157, A549, and LNCaP cells were infected with AdG5-FL at m.o.i. 0.1 or 1 36 h after plating. After 12 h, cells were harvested and lysed. The total DNA was prepared with the DNeasy Tissue Kit (Qiagen, Valencia, CA). Opticon2 (MJ Research, Boston, MA) real-time PCR was performed, using these DNAs as template and the DyNAmo SYBR Green qPCR Kit (Finnzymes, Espoo, Finland). The viral FL sequences were detected by the following primer set: FL-a (5′-GAGATACGCCCTGGTTCCTG-3′) and FL-b (5′-GCATACGACGATTCTGTGATTTG-3′). Infectivity was calculated based on the copy number of internalized viral DNA divided by cell number. The relative infectivities of all cells are in reference to HeLa cells, which were set as 1, as they are the least susceptible to infection among the cell lines we tested.

doi:10.1016/j.ymthe.2003.08.016

Animal experiments with CCD imaging. Animal care and procedures were performed in accordance with the University of California Animal Research Committee guidelines. Eight- to ten-week-old male SCID mice (ICRSC-M, ~25 g, Taconic Farms, Germantown, NY) were used in these studies. Human prostate tumor xenografts were generated in SCID mice as previously described [41]. The LAPC-4 xenograft was originally provided by Dr. Charles Sawyers at UCLA. We passaged the tumor by implanting small tumor fragments mixed 1:1 with Matrigel (Collaborative Research, Bedford, MA) subcutaneously into the flanks of male SCID mice.

For the naïve mouse experiments, 10^7 pfu of Ad was injected via the tail vein ($n = 3$). *In vivo* expression was monitored sequentially over time. For the LAPC-4 xenografts, tumors were allowed to grow for 3 weeks prior to injection and reached a diameter of approximately 1 cm. AdBC-VP2 and AdG5-FL (10^8 pfu each) or AdTSTA-FL (10^7 pfu) was injected at three sites on each tumor at 10 μl per site ($n = 3$). Optical CCD imaging was performed at the indicated days postinjection. Intraprostatic injections were performed 7 days after castration. Both castrated and noncastrated animals received injection of 10^8 infectious units each of the paired TSTA Ads or 10^6 infectious units of the single TSTA Ad in both posterior lobes of the prostate ($n = 4$ per group). For each imaging session, the mice were anesthetized with ketamine/xylazine (4:1), and the d-luciferin substrate (150 mg/kg in PBS, Xenogen) was given intraperitoneally at a volume of 200 μl, with a 20-min incubation period prior to imaging. CCD images were obtained using a cooled IVIS CCD camera (Xenogen, Alameda, CA), and images were analyzed with IGOR-PRO Living Image Software, as described [26,28], in units of photons acquired per second per square centimeter per steridan.

Western blot analysis of GAL4-VP2 expression. LNCaP cells were grown in 60-mm dishes and infected with AdTSTA-FL or co-infected with AdBC-VP2 and AdG5-FL at m.o.i. 0.21, 0.62, 1.9, 5.6, 16.7, or 50 (threefold serial dilution). For co-infection, each Ad was administered at the m.o.i. listed above. Forty-eight hours later, the cells were harvested and lysed with RIPA buffer (1% NP-40, 0.1% sodium deoxycholate, 150 mM NaCl, and 50 mM Tris–HCl (pH 7.5), protease inhibitor cocktail (Sigma, St. Louis, MO)). The samples were fractionated on 8–16% gradient acrylamide gels (Gradipore, Frenchs Forest, Australia) and subjected to immunoblot analysis with rabbit polyclonal antibodies generated against intact GAL4-VP2 or β-actin A5316 (Sigma). Detection was done by visualization of bands with HRP-labeled secondary antibody and ECL (Amersham Pharmacia Biotech, Piscataway, NJ).

ACKNOWLEDGMENTS

We appreciate the technical support of Erika Billick, the assistance of Wendy Aft on manuscript preparation, and helpful discussions with Drs. Harvey Herschman and Helen Brown. This work is supported by Department of Defense (DOD) CDMRP PC020536 (to L.W.), California Cancer Research Program 3NI0226 (to L.W.), NIH R01 CA101904 (to L.W.), CapCURE (to M.C., S.S.G.), DOD PC 991019 (to Charles Sawyers and M.C.), DOD PC020177 (to M.C.), an interdisciplinary seed grant from the JCCC (to M.C., L.W., and S.S.G.), R01 CA82214 (to S.S.G.), SAIRP R24 CA92865 (to S.S.G.), and Department of Energy Contract DE-FC03-87ER60615 (to S.S.G.). M.S. is supported by a DOD CDMRP postdoctoral fellowship (PC020531).

RECEIVED FOR PUBLICATION JUNE 16, 2003; ACCEPTED AUGUST 20, 2003.

REFERENCES

1. American Cancer Society (2002). Cancer Facts & Figures 2002. Am. Cancer Soc., Atlanta, pp. 3–15.
2. Denis, L., and Murphy, G. P. (1993). Overview of phase III trials on combined androgen treatment in patients with metastatic prostate cancer. *Cancer* **72:** 3888–3895.
3. Hellerstedt, B. A., and Pienta, K. J. (2002). The current state of hormonal therapy for prostate cancer. *CA Cancer J. Clin.* **52:** 154–179.
4. Labrie, F. (2002). Androgen blockade in prostate cancer in 2002: major benefits on survival in localized disease. *Mol. Cell. Endocrinol.* **198:** 77–87.
5. Mabjeesh, N. J., Zhong, H., and Simons, J. W. (2002). Gene therapy of prostate cancer: current and future directions. *Endocr. Relat. Cancer* **9:** 115–139.
6. Wu, L. and Sato, M. (2003). Integrated, molecular engineering approaches to develop prostate cancer gene therapy. *Curr. Gene Ther.* **3:** 452–467.
7. Cleutjens, K. B., van der Korput, H. A., van Eekelen, C. C., van Rooij, H. C., Faber, P. W., and Trapman, J. (1997). An androgen response element in a far upstream enhancer region is essential for high, androgen-regulated activity of the prostate-specific antigen promoter. *Mol. Endocrinol.* **11:** 148–161.
8. Noss, K. R., Wolfe, S. A., and Grimes, S. R. (2002). Upregulation of prostate specific membrane antigen/folate hydrolase transcription by an enhancer. *Gene* **285:** 247–256.
9. O'Keefe, D. S., *et al.* (1998). Mapping, genomic organization and promoter analysis of the human prostate-specific membrane antigen gene. *Biochim. Biophys. Acta* **1443:** 113–127.
10. Pang, S., *et al.* (1997). Identification of a positive regulatory element responsible for tissue-specific expression of prostate-specific antigen. *Cancer Res.* **57:** 495–499.
11. Schuur, E. R., Henderson, G. A., Kmetec, L. A., Miller, J. D., Lamparski, H. G., and Henderson, D. R. (1996). Prostate-specific antigen expression is regulated by an upstream enhancer. *J. Biol. Chem.* **271:** 7043–7051.
12. Watt, F., *et al.* (2001). A tissue-specific enhancer of the prostate-specific membrane antigen gene, FOLH1. *Genomics* **73:** 243–254.
13. Hobisch, A., Culig, Z., Radmayr, C., Bartsch, G., Klocker, H., and Hittmair, A. (1995). Distant metastases from prostatic carcinoma express androgen receptor protein. *Cancer Res.* **55:** 3068–3072.
14. Koivisto, P. A., and Helin, H. J. (1999). Androgen receptor gene amplification increases tissue PSA protein expression in hormone-refractory prostate carcinoma. *J. Pathol.* **189:** 219–223.
15. Sweat, S. D., Pacelli, A., Bergstralh, E. J., Slezak, J. M., Cheng, L., and Bostwick, D. G. (1999). Androgen receptor expression in prostate cancer lymph node metastases is predictive of outcome after surgery. *J. Urol.* **161:** 1233–1237.
16. van der Kwast, T. H., and Tetu, B. (1996). Androgen receptors in untreated and treated prostatic intraepithelial neoplasia. *Eur. Urol.* **30:** 265–268.
17. Bok, R. A., and Small, E. J. (2002). Bloodborne biomolecular markers in prostate cancer development and progression. *Nat. Rev. Cancer* **2:** 918–926.
18. Feldman, B. J., and Feldman, D. (2001). The development of androgen-independent prostate cancer. *Nat. Rev. Cancer* **1:** 34–45.
19. Visakorpi, T., *et al.* (1995). In vivo amplification of the androgen receptor gene and progression of human prostate cancer. *Nat. Genet.* **9:** 401–406.
20. Gregory, C. W., *et al.* (2001). A mechanism for androgen receptor-mediated prostate cancer recurrence after androgen deprivation therapy. *Cancer Res.* **61:** 4315–4319.
21. Zhou, Z. X., Lane, M. V., Kemppainen, J. A., French, F. S., and Wilson, E. M. (1995). Specificity of ligand-dependent androgen receptor stabilization: receptor domain interactions influence ligand dissociation and receptor stability. *Mol. Endocrinol.* **9:** 208–218.
22. Abreu-Martin, M. T., Chari, A., Palladino, A. A., Craft, N. A., and Sawyers, C. L. (1999). Mitogen-activated protein kinase kinase kinase 1 activates androgen receptor-dependent transcription and apoptosis in prostate cancer. *Mol. Cell. Biol.* **19:** 5143–5154.
23. Zhang, L., *et al.* (2003). Interrogating androgen receptor function in recurrent prostate cancer. *Cancer Res.* **63:** 4552–4560.
24. Latham, J. P., Searle, P. F., Mautner, V., and James, N. D. (2000). Prostate-specific antigen promoter/enhancer driven gene therapy for prostate cancer: construction and testing of a tissue-specific adenovirus vector. *Cancer Res.* **60:** 334–341.
25. Wu, L., *et al.* (2001). Chimeric PSA enhancers exhibit augmented activity in prostate cancer gene therapy vectors. *Gene Ther.* **8:** 1416–1426.
26. Adams, J. Y., *et al.* (2002). Visualization of advanced human prostate cancer lesions in living mice by a targeted gene transfer vector and optical imaging. *Nat. Med.* **8:** 891–897.
27. Iyer, M., Wu, L., Carey, M., Wang, Y., Smallwood, A., and Gambhir, S. S. (2001). Two-step transcriptional amplification as a method for imaging reporter gene expression using weak promoters. *Proc. Natl. Acad. Sci. USA* **98:** 14595–14600.
28. Zhang, L., *et al.* (2002). Molecular engineering of a two-step transcription amplification (TSTA) system for transgene delivery in prostate cancer. *Mol. Ther.* **5:** 223–232.
29. Blasberg, R. G., and Tjuvajev, J. G. (1999). Herpes simplex virus thymidine kinase as a marker/reporter gene for PET imaging of gene therapy. *Q. J. Nucl. Med.* **43:** 163–169.
30. Gambhir, S. S. (2002). Molecular imaging of cancer with positron emission tomography. *Nat. Rev. Cancer* **2:** 683–693.
31. Massoud, T., and Gambhir, S. S. (2003). Molecular imaging in living subjects: seeing fundamental biological processes in a new light. *Genes Dev.* **17:** 545–580.
32. Rehemtulla, A., *et al.* (2000). Rapid and quantitative assessment of cancer treatment response using in vivo bioluminescence imaging. *Neoplasia* **2:** 491–495.
33. Wu, J. C., Sundaresan, G., Iyer, M., and Gambhir, S. S. (2001). Noninvasive optical imaging of firefly luciferase reporter gene expression in skeletal muscles of living mice. *Mol. Ther.* **4:** 297–306.
34. Ciana, P., *et al.* (2003). In vivo imaging of transcriptionally active estrogen receptors. *Nat. Med.* **9:** 82–86.
35. He, T. C., Zhou, S., da Costa, L. T., Yu, J., Kinzler, K. W., and Vogelstein, B. (1998). A simplified system for generating recombinant adenoviruses. *Proc. Natl. Acad. Sci. USA* **95:** 2509–2514.
36. Bergelson, J. M., *et al.* (1997). Isolation of a common receptor for coxsackie B viruses and adenoviruses 2 and 5. *Science* **275:** 1320–1323.
37. Roelvink, P. W., Mi Lee, G., Einfeld, D. A., Kovesdi, I., and Wickham, T. J. (1999).

Identification of a conserved receptor-binding site on the fiber proteins of CAR-recognizing adenoviridae. *Science* **286:** 1568–1571.
38. Wickham, T. J., Mathias, P., Cheresh, D. A., and Nemerow, G. R. (1993). Integrins alpha v beta 3 and alpha v beta 5 promote adenovirus internalization but not virus attachment. *Cell* **73:** 309–319.
39. Fechner, H., *et al.* (2000). Trans-complementation of vector replication versus coxsackie–adenovirus-receptor overexpression to improve transgene expression in poorly permissive cancer cells. *Gene Ther.* **7:** 1954–1968.
40. Rauen, K. A., *et al.* (2002). Expression of the coxsackie adenovirus receptor in normal prostate and in primary and metastatic prostate carcinoma: potential relevance to gene therapy. *Cancer Res.* **62:** 3812–3818.
41. Klein, K. A., *et al.* (1997). Progression of metastatic human prostate cancer to androgen independence in immunodeficient SCID mice. *Nat. Med.* **3:** 402–408.
42. Fechner, H., *et al.* (1999). Expression of coxsackie adenovirus receptor and alphav-integrin does not correlate with adenovector targeting in vivo indicating anatomical vector barriers. *Gene Ther.* **6:** 1520–1535.
43. Kijima, T., *et al.* (1999). Application of the Cre recombinase/loxP system further enhances antitumor effects in cell type-specific gene therapy against carcinoembryonic antigen-producing cancer. *Cancer Res.* **59:** 4906–4911.
44. Ueda, K., *et al.* (2001). Carcinoembryonic antigen-specific suicide gene therapy of cytosine deaminase/5-fluorocytosine enhanced by the Cre/loxP system in the orthotopic gastric carcinoma model. *Cancer Res.* **61:** 6158–6162.
45. Wu, L., Johnson, M. and Sato, M. (2003). Transcriptionally-targeted gene therapy to detect and treat cancer. *Trends Mol. Med.* **9:** 421–429.
46. Shalev, M., *et al.* (2000). Suicide gene therapy toxicity after multiple and repeat injections in patients with localized prostate cancer. *J. Urol.* **163:** 1747–1750.
47. Lohr, F., Huang, Q., Hu, K., Dewhirst, M. W., and Li, C. Y. (2001). Systemic vector leakage and transgene expression by intratumorally injected recombinant adenovirus vectors. *Clin. Cancer Res.* **7:** 3625–3628.
48. Alemany, R., and Curiel, D. T. (2001). CAR-binding ablation does not change biodistribution and toxicity of adenoviral vectors. *Gene Ther.* **8:** 1347–1353.
49. Tao, N., *et al.* (2001). Sequestration of adenoviral vector by Kupffer cells leads to a nonlinear dose response of transduction in liver. *Mol. Ther.* **3:** 28–35.
50. Morral, N., *et al.* (2002). Lethal toxicity, severe endothelial injury, and a threshold effect with high doses of an adenoviral vector in baboons. *Hum. Gene Ther.* **13:** 143–154.
51. Zhang, Y., *et al.* (2001). Acute cytokine response to systemic adenoviral vectors in mice is mediated by dendritic cells and macrophages. *Mol. Ther.* **3:** 697–707.
52. Yang, Y., Su, Q., and Wilson, J. M. (1996). Role of viral antigens in destructive cellular immune responses to adenovirus vector-transduced cells in mouse lungs. *J. Virol.* **70:** 7209–7212.
53. Jooss, K., Yang, Y., Fisher, K. J., and Wilson, J. M. (1998). Transduction of dendritic cells by DNA viral vectors directs the immune response to transgene products in muscle fibers. *J. Virol.* **72:** 4212–4223.
54. Pastore, L., *et al.* (1999). Use of a liver-specific promoter reduces immune response to the transgene in Ads. *Hum. Gene Ther.* **10:** 1773–1781.
55. Nakamura, T., Sato, K., and Hamada, H. (2003). Reduction of natural adenovirus tropism to the liver by both ablation of fiber-coxsackievirus and adenovirus receptor interaction and use of replaceable short fiber. *J. Virol.* **77:** 2512–2521.
56. Einfeld, D. A., *et al.* (2001). Reducing the native tropism of adenovirus vectors requires removal of both CAR and integrin interactions. *J. Virol.* **75:** 11284–11291.
57. Perez-Stable, C. M., Pozas, A., and Roos, B. A. (2000). A role for GATA transcription factors in the androgen regulation of the prostate-specific antigen gene enhancer. *Mol. Cell. Endocrinol.* **167:** 43–53.
58. Laverriere, A. C., MacNeill, C., Mueller, C., Poelmann, R. E., Burch, J. B., and Evans, T. (1994). GATA-4/5/6, a subfamily of three transcription factors transcribed in developing heart and gut. *J. Biol. Chem.* **269:** 23177–23184.
59. Bruno, M. D., Korfhagen, T. R., Liu, C., Morrisey, E. E., and Whitsett, J. A. (2000). GATA-6 activates transcription of surfactant protein A. *J. Biol. Chem.* **275:** 1043–1049.
60. Neve, R., *et al.* (1998). The epithelium-specific ets transcription factor ESX is associated with mammary gland development and involution. *FASEB J.* **12:** 1541–1550.
61. Oettgen, P., *et al.* (2000). PDEF, a novel prostate epithelium-specific ets transcription factor, interacts with the androgen receptor and activates prostate-specific antigen gene expression. *J. Biol. Chem.* **275:** 1216–1225.
62. Tymms, M. J., *et al.* (1997). A novel epithelial-expressed ETS gene, ELF3: human and murine cDNA sequences, murine genomic organization, human mapping to 1q32.2 and expression in tissues and cancer. *Oncogene* **15:** 2449–2462.
63. Wang, Y., Iyer, M., Wu, L., Carey, M., and Gambhir, S. S. (2002). A two-step transcriptional approach for imaging of vascular endothelial growth factor (VEGF) gene expression using a bioluminescent reporter gene. *Mol. Imaging Biol.* **4:** S42.
64. Qiao, J., *et al.* (2002). Tumor-specific transcriptional targeting of suicide gene therapy. *Gene Ther.* **9:** 168–175.
65. Gambhir, S. S., *et al.* (2000). Imaging transgene expression with radionuclide imaging technologies. *Neoplasia* **2:** 118–138.
66. Ray, P., Wu, A. M., and Gambhir, S. S. (2003). Optical bioluminescence and positron emission tomography imaging of a novel fusion reporter gene in tumor xenografts of living mice. *Cancer Res.* **63:** 1160–1165.

HUMAN GENE THERAPY 17:1262–1269 (December 2006)

Brief Report

Differential Biodistribution of Adenoviral Vector *In Vivo* as Monitored by Bioluminescence Imaging and Quantitative Polymerase Chain Reaction

MAI JOHNSON,[1,*] STEVE HUYN,[2,*] JEREMY BURTON,[2] MAKOTO SATO,[3] and LILY WU[1–3]

ABSTRACT

A better understanding of the *in vivo* biodistribution of adenoviral vectors would enable the researcher to anticipate potential side effects due to off-targeted site of transduction, and aid in the strategic design of gene therapy. We combined real-time polymerase chain reaction with *in vivo* optical imaging to examine viral transduction in liver, lung, spleen, kidney, prostate, and lymph nodes. A replication-deficient serotype 5 adenoviral vector expressing the firefly luciferase gene under the control of a constitutive cytomegalovirus promoter was administered *in vivo* via different routes. Intravenous and intraperitoneal injections resulted in greatest gene expression and viral DNA in the liver, whereas intraperitoneal injections led to a greater extent of gene delivery to the prostate. Although prostate-directed injection resulted in dominant gene expression in the targeted site, leakage of the vector to other organs was also observed. Vector injection into the lymphatic-rich paw tissue or the subcutaneous tissue of shoulder or chest followed the expected lymphatic drainage pattern, resulting in the accumulation of viral vector in ipsilateral brachial and axillary lymph nodes. Collectively, this study demonstrates that each tissue retains various amounts of adenoviral vector, depending on the route of administration. This knowledge is useful in the strategic design and implementation of adenovirus-mediated gene therapies.

INTRODUCTION

ACCORDING TO THE *Journal of Gene Medicine*, a total of 1145 gene therapy clinical trials were conducted worldwide in 2006, with the majority (67%) designed to treat cancer (see www.wiley.co.uk/genmed/clinical/). Of the numerous vectors being investigated, adenovirus (Ad) is the most commonly used vector, making up 25% of gene therapy clinical trials. The advantages of using adenovirus are severalfold: (1) ease of genetic manipulation (Chartier *et al*., 1996; Kanerva *et al*., 2002; Lozier *et al*., 2002; Plante *et al*., 2004), (2) efficiency in transducing an array of cell types, (3) ability to grow recombinant viruses to high titers (Wilson, 1996), and (4) its stability in storage (Croyle *et al*., 1998). However, in clinical applications, the success of gene therapy relies on vector selectivity, high transgene expression, and transduction efficacy. In addition to these factors, determination of the optimal route of viral delivery could aid in maximizing transduction efficiency to the tissue of interest while minimizing potential toxicity to nontargeted organs. Hence, a better understanding of the *in vivo* trafficking of adenoviral vectors could guide us in determining the most effective route of injection for gene therapy preclinical and clinical trials.

To date several biodistribution studies that have used adenoviral vectors, have been published (see review by Gonin and Gaillard, 2004). The majority of these studies were carried out via the intravenous route of administration (Wood *et al*., 1999; Alemany *et al*., 2000; Tao *et al*., 2001; Bernt *et al*., 2003). In addition, other groups have evaluated local region-directed injection routes such as the intravesicular (Wood *et al*., 1999) or intratumoral injection route (Wang *et al*., 2005). Although these studies are informative, they give limited insight into the full

[1]Department of Molecular, Cellular, and Integrative Physiology, [2]Department of Molecular and Medical Pharmacology, and [3]Department of Urology, University of California Los Angeles, Los Angeles, CA 90095.
*M.J. and S.H. contributed equally.

extent of adenoviral trafficking and transgene expression. Several factors can greatly influence the adenoviral vector-mediated gene transduction process to various tissue *in vivo*. They include (1) the quantity of vector delivered to different sites by the circulatory system, (2) the susceptibility of different tissues to adenoviral infection, and (3) the transcriptional activity of the promoter used to drive expression of the transgene. Cellular binding and infection mediated by serotype 2 and 5 adenovirus are critically dependent on several interactions: the penton base with α_v integrins (Wickham *et al*., 1993); the viral fiber knob domain of the coxsackie and adenovirus receptor (CAR) (Bergelson *et al*., 1997), and fiber interaction with heparan sulfate glycosaminoglycans (Dechecchi *et al*., 2001). The murine homolog of CAR (mCAR) is highly expressed in murine liver (Bergelson *et al*., 1998). Because of these factors, intravenous adenoviral administration invariantly resulted in dominant expression in the liver (Alemany *et al*., 2000; Lozier *et al*., 2002; Bernt *et al*., 2003). Despite different attempts to alter viral tropism through ablation of CAR-interacting motifs on the fiber knob, liver-dominant transduction persisted (Alemany and Curiel, 2001; Leissner *et al*., 2001). Hence, an unresolved issue in adenoviral gene delivery concerns determining how to circumvent the liver-dominated distribution to reach other target sites.

Use of different routes of vector administration can likely alter the amount of vector delivery to different organs. In this study we examine and compare the differential tissue accumulation of adenoviral vector after intravenous, intraperitoneal, intraprostatic, subcutaneous, and footpad injections. We employed a quantitative real-time polymerase chain reaction (PCR) method (Higuchi *et al*., 1992; Morrison *et al*., 1998; Livak and Schmittgen, 2001) to assess the magnitude of viral DNA accumulated in lung, liver, spleen, kidney, and prostate tissue. In addition, we used bioluminescence imaging (BLI), a modality based on the expression of luciferase reporter genes, to monitor *in vivo* gene expression. This modality is advantageous in its ability to dynamically, and noninvasively, monitor transgene expression at various time points in small animals. Although strong viral promoters, such as that derived from cytomegalovirus (CMV), have frequently been applied to express reporter genes *in vivo* (Boshart *et al*., 1985), the transcriptional activity of this promoter is clearly not uniform in various infected tissues (Zarrin *et al*., 1999), and is also subject to transcriptional silencing *in vivo* (Al-Dosari *et al*., 2006). Hence, in this study, quantitative real-time PCR analysis of viral DNA distribution served as a cross-reference for the luciferase activity mediated by CMV promoter-driven adenovirus.

MATERIALS AND METHODS

Adenovirus administration and optical imaging

Animal care and procedures were performed in accordance with the University of California Animal Research Committee guidelines. Male severe combined immunodeficient (SCID) mice used in this study were obtained from Taconic Farms (Germantown, NY). AdCMV-fl (1×10^8 or specified plaque-forming units [PFU]) or saline was injected into the tail vein (for intravenous administration), peritoneum, prostate, or forepaw. Before imaging, mice were anesthetized with ketamine–xylazine (4:1) and D-luciferin substrate (150 mg/kg in phosphate-buffered saline [PBS]; Xenogen, Alameda, CA) was given intraperitoneally at a volume of 200 μl. After a 20-min incubation period, mice were imaged for luciferase expression with a cooled IVIS CCD camera (Xenogen). At the end point, each organ was harvested, using sterile instruments in a fume hood. This was done to prevent cross-contamination of tissue samples. Isolated organs were placed in a 6-well petri dish and imaged for gene expression. After imaging, all organs were snap frozen in liquid nitrogen, and immediately stored at −80°C until genomic DNA could be extracted.

Luciferase assay

Lymph nodes were homogenized in 200 μl of passive lysis buffer (Promega, Madison, WI) and vortexed for 15 min at room temperature to allow complete lysis. Lysate (10 μl) from each lymph node was assayed with a firefly luciferase assay kit (Promega) according to standard protocol. Luciferase activity was measured with a Sirius luminometer (Berthold Detection Systems, Pforzheim, Germany) and readings were normalized to total protein concentration as determined by Bradford assay (Pierce Biotechnology, Rockford, IL).

Real-time PCR

To extract genomic DNA, whole organs were thawed, and mechanically homogenized with a sterile scalpel. Twenty-five to 30 mg of homogenate was then processed with a DNeasy kit (Qiagen, Valencia, CA). Each sample was treated with RNase (20 mg/ml) to prevent RNA contamination in the PCR. Real-time PCR was carried out with 100 ng of genomic DNA as the template for each reaction. Primers were designed with the Integrated DNA Technologies (Coralville, IA) primer design application, and were used to amplify 150 bases of the E2 region in the adenoviral backbone (forward primer, 5′-GGGCGAGATCTTCCAACATA-3′; reverse primer, 5′-GCTCTCCTTTTGCACGGTAG-3′). The β-actin gene was used as an endogenous/internal loading control (forward primer, 5′-TCAAGATCATTGCTCCTCCTGAGC-3′; reverse primer, 5′-TACTCCTGCTTGCTGATCCACATC-3′). Standard curve analysis, with serial dilutions of each template, demonstrated that amplification of both the E2 and β-actin genes, using the preceding primer sets, was efficient. The correlation coefficient r^2 was 0.998 and 0.995 for actin and E2, respectively. Real-time PCRs were carried out in a Chromo4 thermal cycler (Bio-Rad, Hercules, CA) using SYBR green master mix (Applied Biosystems, Foster City, CA), which contains SYBR green I dye, AmpliTaq Gold DNA polymerase, dNTPs, and optimized buffer components. To minimize variation between the samples and to improve reproducibility, all reactions were carried out with a master mix consisting of Applied Biosystems SYBR green PCR mix, genomic DNA, and sterile nuclease-free water. All target and control PCRs were done in triplicate.

Data analyses

Optical images were analyzed with Living Image software (Xenogen) overlaid on IGOR-Pro software (WaveMetrics, Lake Oswego, OR) in units of photons (P) acquired per second (sec) per cm^2 per steradian (sr). All values represent an average in

the group and error bars indicate the standard error of the mean (SEM). For real-time PCR data analysis, we opted to use the comparative or relative threshold cycle (C_t) method for quantitation of gene dosage (Winer *et al*., 1999; Schmittgen *et al*., 2000; Livak and Schmittgen, 2001). In the comparative method of analysis, we analyzed the change in magnitude of the target gene (adenovirus E2 gene), delivered into treated animals, relative to a noninjected control group. Quantitative data obtained by this method can be significantly impacted by variation in the actual viral dose delivered into the animal. For example, tissue extravasations at the injection site could contribute to variation in the total amount of virus administered. To account for this variation, viral copy number is also expressed as a percentage relative to viral copy number in the liver.

RESULTS AND DISCUSSION

Intravenous and intraperitoneal injection results in greatest accumulation of adenoviral vectors and gene expression in the liver

Extensive studies have documented that intravenous injection results in viral accumulation in the liver (Vrancken Peeters *et al*., 1996; Nunes *et al*., 1999; Alemany *et al*., 2000; Lozier *et al*., 2002; Bernt *et al*., 2003). Here, we examined the extent of adenovirus accumulation in other organs in addition to the liver, after systemic administration. To investigate the biodistribution, a serotype 5 E1/E3-deleted replication-deficient adenovirus vector, expressing the firefly luciferase reporter gene (fl), in the presence of a strong constitutive cytomegalovirus (CMV) promoter was used. After tail vein injection of 1×10^8 PFU of Ad-CMV-fl vector, luciferase transgene expression was observed in the liver starting 2 days postinjection, which increased over time (Fig. 1A). Because of the dominant liver signal masking the weaker signal from other tissues, we opted to excise individual organs in order to measure gene expression more accurately. After whole body imaging on day 14, the isolated liver exhibited transgene activity that was two orders of magnitude greater than that seen in lung, kidney, or prostate tissue, and the spleen exhibited the lowest expression among the organs examined (Fig. 1B). Quantitative real-time PCR displayed the highest viral DNA copy number in the liver followed by spleen, kidney, lung, and prostate (Table 1). Although there is strong correlation between optical imaging signal and real-time PCR in the liver, variations were observed in the other organs. The spleen, for example, presented a relatively high viral copy number, but appears to exhibit low transgene expression by optical imaging. The appar-

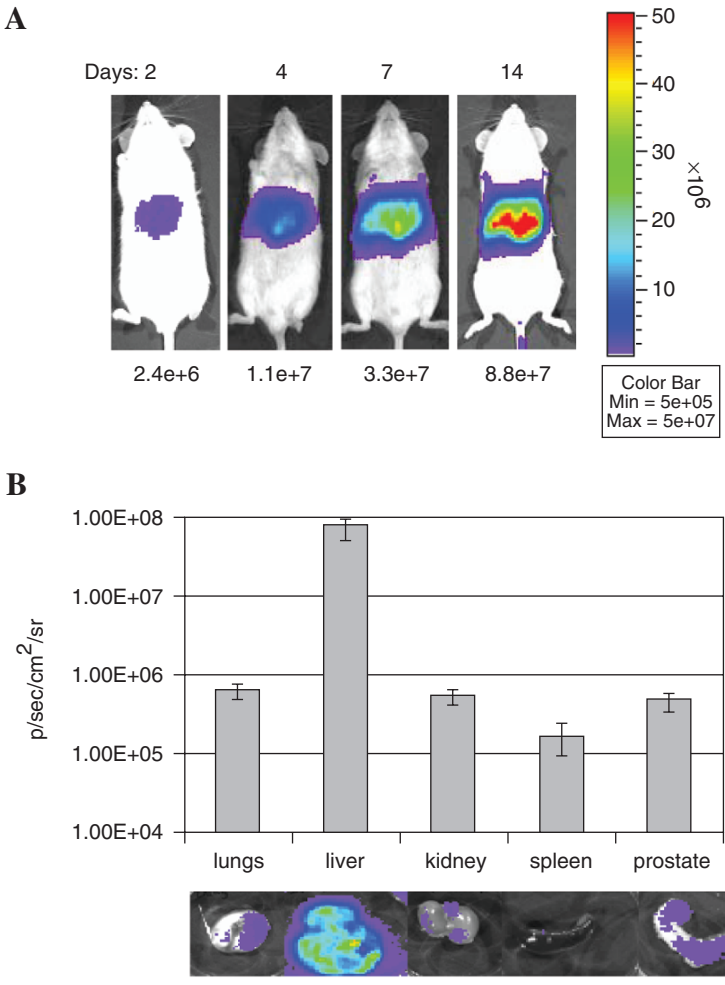

FIG. 1. Intravenous delivery of 1×10^8 Ad-CMV-fl via the tail vein. (**A**) Luciferase gene expression continued to increase from day 2 to day 14. (**B**) Isolated organs on day 14 revealed the highest level of gene expression in the liver, followed by lungs, kidneys, and prostate, with spleen showing the lowest. (Error bars represent the SEM; $n = 4$.)

TABLE 1. SUMMARY OF VIRAL COPY NUMBER AND LUCIFERASE EXPRESSION RELATIVE TO LIVER

	Liver	*Lung*	*Kidney*	*Spleen*	*Prostate*
Percent Viral Copy Number Relative to Liver					
Intravenous	100	1.5	2	42.4	0.1
Intraperitoneal	100	0.1	12.9	7.8	10.4
Intraprostatic	100	2.7	1	5.5	1189.2
Percent Luciferase Relative to Liver					
Intravenous	100	0.8	0.7	0.2	0.6
Intraperitoneal	100	1.3	20.7	10.2	2.0
Intraprostatic	100	1.4	0.7	0.3	156.5

ent low light emission in the spleen could be attributed to the high level of hemoglobin, a major absorber of visible light (Weissleder, 2001). Other contributing factors could be that the resident immune cells in the spleen are less susceptible to adenoviral transduction, or that the CMV promoter is less active in immune cells compared with liver cells (Schmidt *et al*., 1990; Leon *et al*., 1998). Consequently, although there seems to be low transgene expression, the actual viral particles are comparable to that observed in the liver. Intraperitoneal injection is yet another route that is used in targeting studies, and has shown clinical relevance for ovarian cancer (Kanerva *et al*., 2002). A question of interest to our group is whether the intraperitoneal injection route can improve targeting to the prostate (as would be necessary in the treatment or diagnosis of prostate cancer), a site that is difficult to reach through intravenous administration. Intraperitoneal administration of AdCMV-fl resulted in increased transgene expression in the peritoneal area of the animals over the course of 14 days (Fig. 2A). By day 14, a signal from the liver of the animals was discernible. The isolated organs showed highest luciferase expression in the liver, followed by kidneys, spleen, and prostate, with lowest expression seen in the lungs (Fig. 2B). Although real-time PCR findings were con-

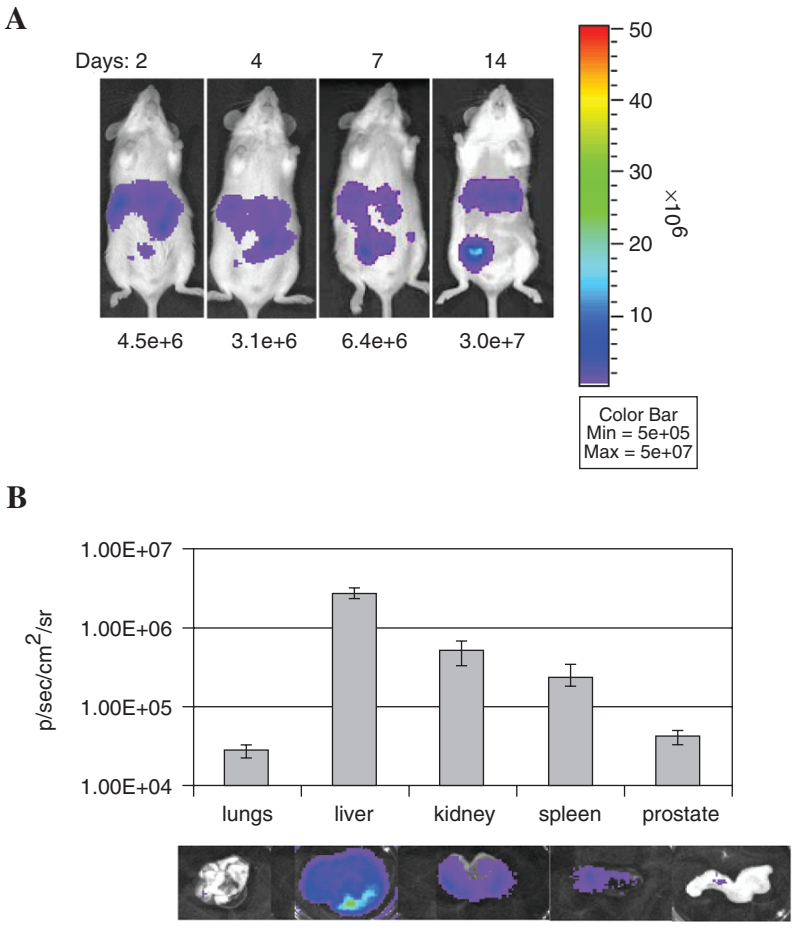

FIG. 2. Intraperitoneal delivery resulted in viral dissemination to the prostate. (**A**) Luciferase gene expression continued to increase from day 2 to day 14, with distinguishable liver signal by day 14. (**B**) Optical imaging of isolated organs on day 14 revealed the highest level of gene expression in the liver, followed by kidneys, spleen, prostate, and lungs. (Error bars represent the SEM; $n = 5$.)

sistent with the optical imaging results, they indicated that a higher proportion of viral vector (DNA) was delivered to both the prostate and kidney relative to liver, when compared with intravenously injected animals (Table 1).

Intraprostatic injection results in greatest accumulation of adenoviral vectors in the prostate

Intraprostatic injection is a local administration route that has been applied in the treatment of benign prostatic hyperplasia (Plante *et al*., 2004) and prostate cancer (Herman *et al*., 1999). We evaluated the pattern of adenoviral dissemination by injecting 1×10^8 PFU of AdCMV-fl virus into the dorsal lobes of the prostate. Regions of interest were drawn around the prostate and the chest area to analyze transgene expression. We observed an increase in both prostate and liver signal in the animals over a period of 14 days (Fig. 3A). Extracted organs on day 14 showed comparable transgene expression in the liver and the prostate (Fig. 3B). However, there was more than 10-fold higher viral DNA in the prostate compared with the liver (Table 1). Thus, by direct injection, one can limit the spread of the virus to distant sites, thereby decreasing potential toxic side effects (Timme *et al*., 1998). Nevertheless, the dissemination of virus to nontargeted organs is likely unavoidable regardless of the injection route. Therefore, restricting gene expression to the tissue of interest, through incorporation of tissue-specific promoters, could potentially limit expression in nontarget tissue such as the liver. For example, a highly amplified prostate-specific gene expression (two-step transcriptional activation [TSTA]) system has been developed and incorporated in adenoviral gene therapy vectors. These vectors (termed AdTSTA-fl and AdTSTA-sr39tk) are prostate cell selective and androgen regulated (Sato *et al*., 2003; Wu *et al*., 2003; Zhang *et al*., 2003; Ilagan *et al*., 2005). Intraprostatic and tumor-directed injection of these vectors resulted in prostate-targeted gene expression. The specificity of these viral vectors for prostate tissue acted as a safeguard against inadvertent expression in the liver (Adams *et al*., 2002; Sato *et al*., 2003; Johnson *et al*., 2005).

Paw and subcutaneous injection resulted in virus dissemination to the lymph nodes

Lymphatic capillaries in the dermal layers of skin drain accumulated interstitial fluids, proteins, and immune cells. These

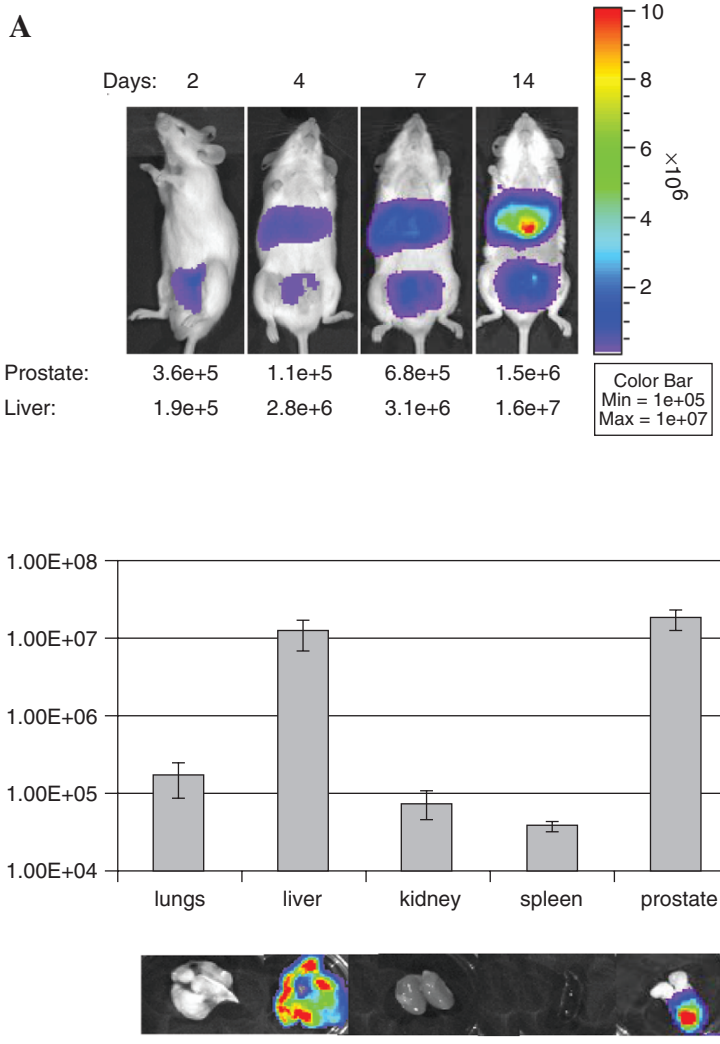

FIG. 3. Retention of viral DNA in the prostate via intraprostatic injection. (**A**) Luciferase expression was seen in the prostate 2 days postinjection, with observable signal in the liver on day 4. Signal from both the prostate and liver increased over time. (**B**) Liver and prostate possess comparable levels of gene expression as observed by optical imaging, followed by lungs, kidneys, and spleen. (Error bars represent the SEM; $n = 4$.)

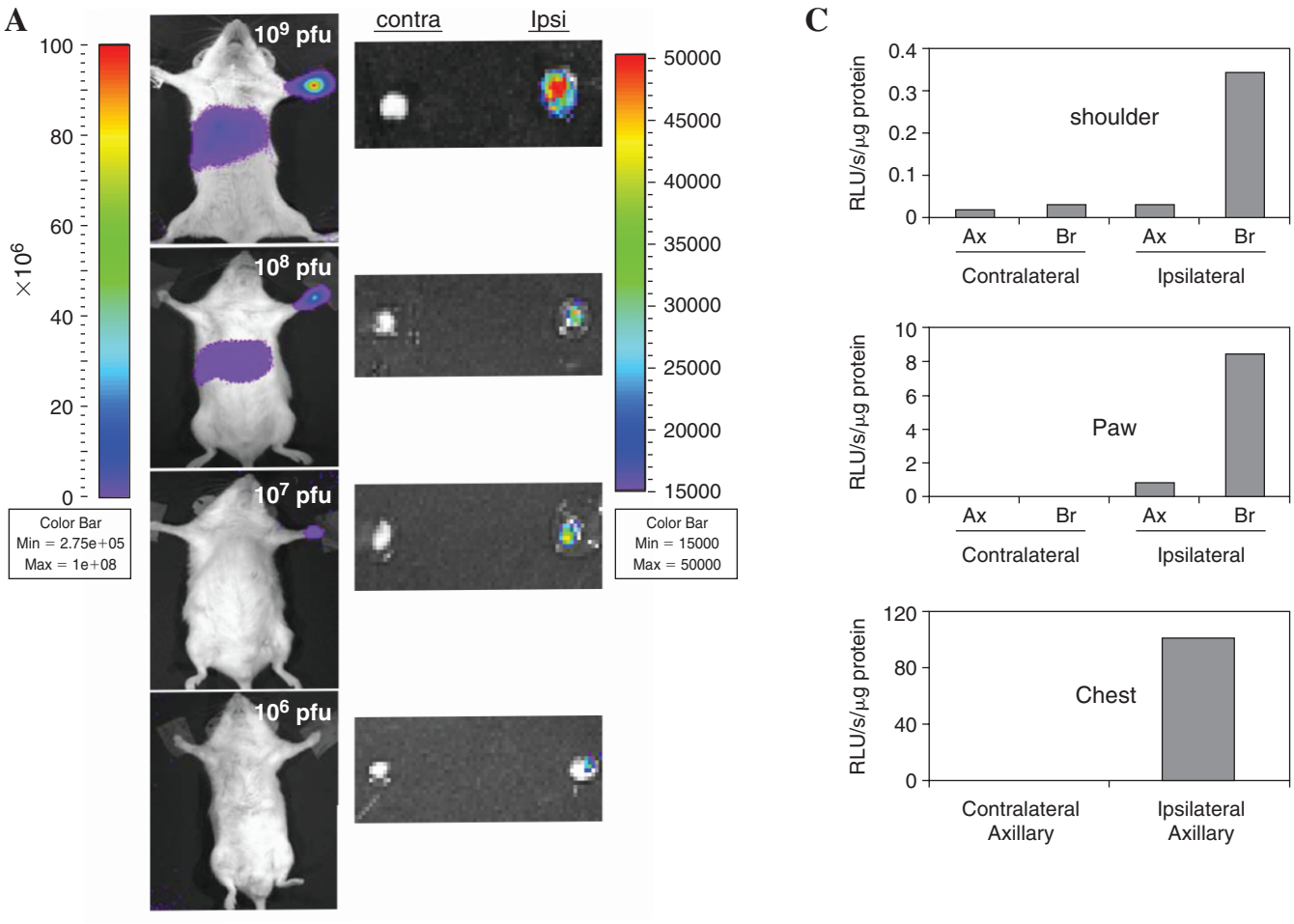

FIG. 4. Lymphatic distribution of adenoviral vector. (**A**) Injection of adenovirus into the left paw leads to bioluminescence at the injection site (imaged 3 days postinjection). At 10^8 and 10^9 PFU detectable signal is emitted from the liver. *Ex vivo* analysis reveals that signals could be readily detected in ipsilateral but not contralateral brachial nodes. (**B**) Ipsilateral brachial and axillary nodes exhibited significantly higher DNA levels than the contralateral side as examined by quantitative PCR. (**C**) AdCMV-fl (10^8 PFU) injected subcutaneously into the shoulder, paw, or chest displays the highest bioluminescence activity in extracts derived from proximal lymph nodes. (Error bars represent the SEM; $n = 3$.)

capillaries converge to form lymphatic vessels in the subcutis, which carry the fluid to lymph nodes for filtration before reentering the blood circulation (Tilney, 1971). We were interested in examining whether the adenovirus could be effectively directed to the lymphatic circulation. Because the density of lymphatic capillaries is particularly high in the extremities of the animal, we injected AdCMV-fl into the subcutaneous tissue of the left forepaw and measured bioluminescence and DNA lev-

els in draining ipsilateral and contralateral lymph nodes. Signal detected at the site of forepaw injection correlated with the amount of virus (Fig. 4A). At higher concentrations (10^8 and 10^9 PFU), expression could be detected in the liver, indicating that some of the virus had entered the blood circulation. Although signals in the lymph nodes were too low to be visible on *in vivo* imaging of entire animals, *ex vivo* analysis of luminescence revealed that brachial lymph node signals could be detected with signals proportional to the injected dose. PCR analysis confirmed that the level of DNA was significantly higher (about three to five orders of magnitude) in ipsilateral lymph nodes compared with contralateral counterparts (Fig. 4B).

Previous studies of lymphatic drainage patterns in rodents have shown that colloidal carbon, injected in various regions of the subcutis, drains in a predictable manner to the proximal lymph nodes (Tilney, 1971). For example, when injected in the shoulder and paw, colloids drain primarily via the brachial plexus whereas injection in the chest/mammary pad results in drainage through the axillary plexus. To examine whether adenovirus also follows this drainage pattern, AdCMV-fl (1×10^8 PFU) was administered subcutaneously into the shoulder, paw, or chest area. Measurements of firefly luciferase activities in tissue extracts of isolated lymph nodes confirmed the expected drainage pattern (Fig. 4C). Whereas injection of virus into the paw and shoulder drained primarily to brachial lymph nodes, chest-directed injection led to dominant axillary lymph node signals. In all cases, the signal was found in ipsilateral but not contralateral nodes. Our findings indicate that adenovirus is taken up into the lymphatic circulation and accumulates within regional lymph nodes.

CONCLUSION

Through these studies, we observed differential dissemination of adenovirus to lung, liver, prostate, spleen, kidney, and regional lymph nodes, based on the initial route of administration. A greater understanding of viral dissemination would be important for delineating the limitations of these vectors, and for assessing the feasibility of targeting a particular site as would be desired in the treatment of metastatic disease. Furthermore, a better understanding of adenoviral biodistribution could aid in the anticipation, and prevention, of unwanted side effects due to the presence of dominant sites of transduction. Collectively, this information could help elucidate the most efficient route to administer adenoviral vectors, and aid in the strategy, design, and implementation of adenovirus-mediated therapies.

ACKNOWLEDGMENTS

The authors deeply appreciate Dee Bojanic for providing excellent technical assistance in this study. This work is supported by NIH R01 CA101904, DAMD17-03-1-0095, and the California Cancer Research Program 3NI0226 (to L.W.). S.H. is supported by UCLA Tumor Immunology training grant 5-T32-CA009120-29 and J.B. is supported by UCLA RTPS training program T32-GM008652.

REFERENCES

ADAMS, J.Y., JOHNSON, M., SATO, M., BERGER, F., GAMBHIR, S.S., CAREY, M., IRUELA-ARISPE, M.L., and WU, L. (2002). Visualization of advanced human prostate cancer lesions in living mice by a targeted gene transfer vector and optical imaging. Nat. Med. **8,** 891–897.

AL-DOSARI, M., ZHANG, G., KNAPP, J.E., and LIU, D. (2006). Evaluation of viral and mammalian promoters for driving transgene expression in mouse liver. Biochem. Biophys. Res. Commun. **339,** 673–678.

ALEMANY, R., and CURIEL, D.T. (2001). CAR-binding ablation does not change biodistribution and toxicity of adenoviral vectors. Gene Ther. **8,** 1347–1353.

ALEMANY, R., SUZUKI, K., and CURIEL, D.T. (2000). Blood clearance rates of adenovirus type 5 in mice. J. Gen. Virol. **81,** 2605–2609.

BERGELSON, J.M., CUNNINGHAM, J.A., DROGUETT, G., KURT-JONES, E.A., KRITHIVAS, A., HONG, J.S., HORWITZ, M.S., CROWELL, R.L., and FINBERG, R.W. (1997). Isolation of a common receptor for coxsackie B viruses and adenoviruses 2 and 5. Science **275,** 1320–1323.

BERGELSON, J.M., KRITHIVAS, A., CELI, L., DROGUETT, G., HORWITZ, M.S., WICKHAM, T., CROWELL, R.L., and FINBERG, R.W. (1998). The murine CAR homolog is a receptor for coxsackie B viruses and adenoviruses. J. Virol. **72,** 415–419.

BERNT, K.M., NI, S., GAGGAR, A., LI, Z.Y., SHAYAKHMETOV, D.M., and LIEBER, A. (2003). The effect of sequestration by nontarget tissues on anti-tumor efficacy of systemically applied, conditionally replicating adenovirus vectors. Mol. Ther. **8,** 746–755.

BOSHART, M., WEBER, F., JAHN, G., DORSCH-HASLER, K., FLECKENSTEIN, B., and SCHAFFNER, W. (1985). A very strong enhancer is located upstream of an immediate early gene of human cytomegalovirus. Cell **41,** 521–530.

CHARTIER, C., DEGRYSE, E., GANTZER, M., DIETERLE, A., PAVIRANI, A., and MEHTALI, M. (1996). Efficient generation of recombinant adenovirus vectors by homologous recombination in *Escherichia coli*. J. Virol. **70,** 4805–4810.

CROYLE, M.A., ROESSLER, B.J., DAVIDSON, B.L., HILFINGER, J.M., and AMIDON, G.L. (1998). Factors that influence stability of recombinant adenoviral preparations for human gene therapy. Pharm. Dev. Technol. **3,** 373–383.

DECHECCHI, M.C., MELOTTI, P., BONIZZATO, A., SANTA-CATTERINA, M., CHILOSI, M., and CABRINI, G. (2001). Heparan sulfate glycosaminoglycans are receptors sufficient to mediate the initial binding of adenovirus types 2 and 5. J. Virol. **75,** 8772–8780.

GONIN, P., and GAILLARD, C. (2004). Gene transfer vector biodistribution: Pivotal safety studies in clinical gene therapy development. Gene Ther. **11**(Suppl. 1)**,** S98–S108.

HERMAN, J.R., ADLER, H.L., AGUILAR-CORDOVA, E., ROJAS-MARTINEZ, A., WOO, S., TIMME, T.L., WHEELER, T.M., THOMPSON, T.C., and SCARDINO, P.T. (1999). *In situ* gene therapy for adenocarcinoma of the prostate: A phase I clinical trial. Hum. Gene Ther. **10,** 1239–1249.

HIGUCHI, R., DOLLINGER, G., WALSH, P.S., and GRIFFITH, R. (1992). Simultaneous amplification and detection of specific DNA sequences. Biotechnology **10,** 413–417.

ILAGAN, R., ZHANG, L.J., POTTRATZ, J., LE, K., SALAS, S., IYER, M., WU, L., GAMBHIR, S.S., and CAREY, M. (2005). Imaging androgen receptor function during flutamide treatment in the LAPC9 xenograft model. Mol. Cancer Ther. **4,** 1662–1669.

JOHNSON, M., SATO, M., BURTON, J., GAMBHIR, S.S., CAREY, M., and WU, L. (2005). Micro-PET/CT monitoring of herpes thymidine kinase suicide gene therapy in a prostate cancer xenograft: The advantage of a cell-specific transcriptional targeting approach. Mol. Imaging **4,** 463–472.

KANERVA, A., WANG, M., BAUERSCHMITZ, G.J., LAM, J.T., DESMOND, R.A., BHOOLA, S.M., BARNES, M.N., ALVAREZ, R.D., SIEGAL, G.P., CURIEL, D.T., and HEMMINKI, A. (2002). Gene transfer to ovarian cancer versus normal tissues with fiber-modified adenoviruses. Mol. Ther. **5,** 695–704.

LEISSNER, P., LEGRAND, V., SCHLESINGER, Y., HADJI, D.A., VAN RAAIJ, M., CUSACK, S., PAVIRANI, A., and MEHTALI, M. (2001). Influence of adenoviral fiber mutations on viral encapsidation, infectivity and *in vivo* tropism. Gene Ther. **8,** 49–57.

LEON, R.P., HEDLUND, T., MEECH, S.J., LI, S., SCHAACK, J., HUNGER, S.P., DUKE, R.C., and DEGREGORI, J. (1998). Adenoviral-mediated gene transfer in lymphocytes. Proc. Natl. Acad. Sci. U.S.A. **95,** 13159–13164.

LIVAK, K.J., and SCHMITTGEN, T.D. (2001). Analysis of relative gene expression data using real-time quantitative PCR and the $2^{-\Delta\Delta CT}$ method. Methods **25,** 402–408.

LOZIER, J.N., CSAKO, G., MONDORO, T.H., KRIZEK, D.M., METZGER, M.E., COSTELLO, R., VOSTAL, J.G., RICK, M.E., DONAHUE, R.E., and MORGAN, R.A. (2002). Toxicity of a first-generation adenoviral vector in rhesus macaques. Hum. Gene Ther. **13,** 113–124.

MORRISON, T.B., WEIS, J.J., and WITTWER, C.T. (1998). Quantification of low-copy transcripts by continuous SYBR green I monitoring during amplification. Biotechniques **24,** 954–958, 960, 962.

NUNES, F.A., FURTH, E.E., WILSON, J.M., and RAPER, S.E. (1999). Gene transfer into the liver of nonhuman primates with E1-deleted recombinant adenoviral vectors: Safety of readministration. Hum. Gene Ther. **10,** 2515–2526.

PLANTE, M.K., FOLSOM, J.B., and ZVARA, P. (2004). Prostatic tissue ablation by injection: A literature review. J. Urol. **172,** 20–26.

SATO, M., JOHNSON, M., ZHANG, L., ZHANG, B., LE, K., GAMBHIR, S.S., CAREY, M., and WU, L. (2003). Optimization of adenoviral vectors to direct highly amplified prostate-specific expression for imaging and gene therapy. Mol. Ther. **8,** 726–737.

SCHMIDT, E.V., CHRISTOPH, G., ZELLER, R., and LEDER, P. (1990). The cytomegalovirus enhancer: A pan-active control element in transgenic mice. Mol. Cell. Biol. **10,** 4406–4411.

SCHMITTGEN, T.D., ZAKRAJSEK, B.A., MILLS, A.G., GORN, V., SINGER, M.J., and REED, M.W. (2000). Quantitative reverse transcription-polymerase chain reaction to study mRNA decay: Comparison of endpoint and real-time methods. Anal. Biochem. **285,** 194–204.

TAO, N., GAO, G.P., PARR, M., JOHNSTON, J., BARADET, T., WILSON, J.M., BARSOUM, J., and FAWELL, S.E. (2001). Sequestration of adenoviral vector by Kupffer cells leads to a nonlinear dose response of transduction in liver. Mol. Ther. **3,** 28–35.

TILNEY, N.L. (1971). Patterns of lymphatic drainage in the adult laboratory rat. J. Anat. **109,** 369–383.

TIMME, T.L., HALL, S.J., BARRIOS, R., WOO, S.L., AGUILAR-CORDOVA, E., and THOMPSON, T.C. (1998). Local inflammatory response and vector spread after direct intraprostatic injection of a recombinant adenovirus containing the herpes simplex virus thymidine kinase gene and ganciclovir therapy in mice. Cancer Gene Ther. **5,** 74–82.

VRANCKEN PEETERS, M.J., PERKINS, A.L., and KAY, M.A. (1996). Method for multiple portal vein infusions in mice: Quantitation of adenovirus-mediated hepatic gene transfer. Biotechniques **20,** 278–285.

WANG, Y., YANG, Z., LIU, S., KON, T., KROL, A., LI, C.Y., and YUAN, F. (2005). Characterisation of systemic dissemination of non-replicating adenoviral vectors from tumours in local gene delivery. Br. J. Cancer **92,** 1414–1420.

WEISSLEDER, R. (2001). A clearer vision for *in vivo* imaging. Nat. Biotechnol. **19,** 316–317.

WICKHAM, T.J., MATHIAS, P., CHERESH, D.A., and NEMEROW, G.R. (1993). Integrins $\alpha_v\beta_3$ and $\alpha_v\beta_5$ promote adenovirus internalization but not virus attachment. Cell **73,** 309–319.

WILSON, J.M. (1996). Adenoviruses as gene-delivery vehicles. N. Engl. J. Med. **334,** 1185–1187.

WINER, J., JUNG, C.K., SHACKEL, I., and WILLIAMS, P.M. (1999). Development and validation of real-time quantitative reverse transcriptase-polymerase chain reaction for monitoring gene expression in cardiac myocytes *in vitro*. Anal. Biochem. **270,** 41–49.

WOOD, M., PERROTTE, P., ONISHI, E., HARPER, M.E., DINNEY, C., PAGLIARO, L., and WILSON, D.R. (1999). Biodistribution of an adenoviral vector carrying the luciferase reporter gene following intravesical or intravenous administration to a mouse. Cancer Gene Ther. **6,** 367–372.

WU, L., JOHNSON, M., and SATO, M. (2003). Transcriptionally targeted gene therapy to detect and treat cancer. Trends Mol. Med. **9,** 421–429.

ZARRIN, A.A., MALKIN, L., FONG, I., LUK, K.D., GHOSE, A., and BERINSTEIN, N.L. (1999). Comparison of CMV, RSV, SV40 viral and Vλ1 cellular promoters in B and T lymphoid and non-lymphoid cell lines. Biochim. Biophys. Acta **1446,** 135–139.

ZHANG, L., JOHNSON, M., LE, K.H., SATO, M., ILAGAN, R., IYER, M., GAMBHIR, S.S., WU, L., and CAREY, M. (2003). Interrogating androgen receptor function in recurrent prostate cancer. Cancer Res. **63,** 4552–4560.

Address reprint requests to:
Dr. Lily Wu
Department of Urology
University of California, Los Angeles
675 Charles Young Drive South
Los Angeles, CA 90095-1738

E-mail: lwu@mednet.ucla.edu

Received for publication May 17, 2006; accepted after revision October 18, 2006.

Published online: November 15, 2006.

Functionality of Androgen Receptor–Based Gene Expression Imaging in Hormone Refractory Prostate Cancer

Makoto Sato,[1] Mai Johnson,[1,2] Liqun Zhang,[3] Sanjiv S. Gambhir,[4,5,6,7] Michael Carey,[3,5,6] and Lily Wu[1,4,5,6]

Abstract

Purpose: A highly augmented, prostate-specific two-step transcriptional amplification (TSTA) method was developed with the ultimate goal of delivering an effective and safe gene-based treatment to prostate cancer patients. Because very limited treatment options are available for recurrent hormone refractory prostate cancer (HRPC), it is imperative to assess whether the prostate-specific antigen (PSA) promoter-based TSTA gene therapy will be functional in HRPC.

Experimental Design: We tested the TSTA-driven adenovirus vector on three androgen-dependent and six HRPC models. Real-time gene expression was monitored by both optical imaging and the combined modality of positron emission tomography (PET) and computed tomography.

Results: The TSTA-driven firefly luciferase expressing adenoviral vector was active in all androgen receptor (AR)–expressing HRPC models, but inactive in AR- and PSA-negative lines. Interestingly, the TSTA-mediated gene expression was induced by hydrocortisone in MDA PCa 2b, a cell line with mutated AR that possesses altered ligand specificity. In animal models, the TSTA-mediated optical signal was more robust in the HRPC than androgen-dependent tumors. In a parallel trend, a TSTA vector that expresses the herpes simplex virus thymidine kinase PET reporter gene also displayed more robust PET signal in the HRPC tumor.

Conclusions: The activity of TSTA system is AR dependent and it recapitulates the functional status of endogenous AR. These data support the conclusion that AR function is activated in HRPC despite castrated levels of androgen. Together with the fact that majority of recurrent prostate cancers express AR and PSA, we foresee that the TSTA approach can be a promising gene therapy strategy for the advanced stages of prostate cancer.

Although recent data suggest that the death rate from prostate cancer is decreasing by 4% per year since 1994, it is still the second leading cause of cancer death in men, with an estimated 230,110 new cases and 29,900 deaths in the United States in 2004 (1). About one third of men with prostate cancer believed to have localized disease will already have micrometastasis at the time of therapy (2). Despite treatment with surgery, 20% to 30% of the patients will suffer from disease recurrence as defined by serum prostate-specific antigen (PSA) elevation (3, 4). In the aggressive, high-grade (Gleason 8-10) disease, majority of PSA recurrence is detected within 2 years after surgery with median survival of <3 years (3). Hormone therapy blocking androgen function can induce short-term remission, but the refractory disease eventually recurs (2). At this stage, the disease is defined as androgen-independent (AI) or hormone refractory prostate cancer (HRPC). The median survival for patients with metastatic HRPC is ~18 months, and systemic chemotherapy provides only a palliation of symptoms (5).

Androgen receptor (AR), the mediator of the physiologic effects of androgen (6), regulates the growth of normal and malignant prostate epithelial cells. Following the binding of the activating ligand dihydrotestosterone, AR translocates from the cytoplasm into the nucleus, binds directly to DNA recognition sites, and induces the expression of androgen-responsive genes, including *PSA*. A central issue in HRPC is to understand the role of AR in this stage of disease. Would AR function be obsolete under treatment where the activating ligand was depleted? Several mechanisms have indicated the continual involvement of AR in HRPC (reviewed in ref. 7), including (*a*) *AR* gene amplification and overexpression; (*b*) altered ligand specificity of AR (promiscuous AR); and (*c*) activation of AR through cross-talks with other AI pathways. The precise role of AR in clinical

Authors' Affiliations: Departments of [1]Urology, [2]Molecular Cellular and Integrative Physiology, [3]Biological Chemistry, and [4]Molecular and Medical Pharmacology; [5]Crump Institute for Molecular Imaging; and [6]Jonsson Comprehensive Cancer Center, David Geffen School of Medicine, University of California, Los Angeles, Los Angeles, California; and [7]Department of Radiology and the Bio-X Program, Stanford University, Stanford, California

Received 9/28/04; revised 12/7/04; accepted 12/14/04.

Grant support: Department of Defense grant DAMD17-03-1-0095 and NIH grant R01 CA101904 (L. Wu); Department of Defense grant DAMD PC 020177 (M. Carey); NIH grant R01 CA82214 and Small Animal Imaging Resource Program grant R24 CA92865 (S.S. Gambhir); an interdisciplinary grant from Jonsson Comprehensive Cancer Center (M. Carey, L. Wu, and S.S. Gambhir); and Department of Defense Congressionally Directed Medical Reseach Program postdoctoral fellowship, PC020531 (M. Sato).

The costs of publication of this article were defrayed in part by the payment of page charges. This article must therefore be hereby marked *advertisement* in accordance with 18 U.S.C. Section 1734 solely to indicate this fact.

Requests for reprints: Lily Wu, Department of Urology, University of California, Los Angeles, 675 Charles Young Drive South, Los Angeles, CA 90095-1738. Phone: 310-794-4390; Fax: 310-825-3027; E-mail: lwu@mednet.ucla.edu.

situations is not fully understood. However, given the fact that AR expression is documented in the majority of HRPC cases (8, 9) and that PSA remains the most reliable marker for recurrent, metastatic prostate cancer (10), it is highly probable that the gene regulatory activity of AR is functional in this setting.

Several PSA or probasin promoter-based gene therapy approaches have been developed (ref. 11; reviewed in ref. 12). However, thorough investigations questioning the functionality of these AR-dependent therapeutic strategies in HRPC have not been completed. The current report uses cell-based activity measurements and *in vivo* molecular imaging to show that a highly amplified PSA promoter-derived (two-step transcriptional amplification, TSTA) system is active in HRPC models. Noninvasive bioluminescence imaging and positron emission tomography (PET) illustrate that the prostate-specific TSTA gene expression vectors exhibit robust activity in HRPC as well as androgen-dependent (AD) tumors. We project that our vector-based gene therapy coupled to molecular imaging would be a promising therapeutic option to develop for treating patients with recurrent disease.

Materials and Methods

Adenovirus constructs. AdTSTA-FL was constructed as previously described (13, 14). The AdTSTA-sr39tk was constructed with the AdEasy system (15). The head-to-head orientation of activator (BCVP2) and reporter (SR39tk) in the single plasmid was constructed by replacing FL with SR39tk in PBCVP2G5-L (16). The BCVP2G5-sr39tk fragment generated by *Not*I and *Sal*I digestion of PBCVP2G5-sr39tk was inserted into pShuttle, which was used in bacterial recombination to generate the full-length virus. The virus was grown on 293 cells, purified on a CsCl gradient, and titered by plaque formation assays on 293 monolayers. The level of replication competent adenovirus contamination in the viral stocks was evaluated by plaque formation on A549 cells. No plaque was detected at 10^8-fold higher viral stock dilution compared with assays on 293 cells.

Prostate cell lines and luciferase activity assay. The human prostate cancer cell lines LNCaP, CWR22Rv1, DU145, and PC-3 were grown in RPMI 1640 supplemented with 10% fetal bovine serum. Iscove's modified DMEM was used for LAPC-4. MDA PCa 2b line obtained from American Type Culture Collection (Manassas, VA) was grown in BRFF-HPC1 (Athena Environmental Sciences, Baltimore, MD) supplemented with 20% fetal bovine serum. For AdTSTA-FL assays, the cultured cells were plated onto 24-well plates at 5×10^4 cells per well with phenol red–free RPMI 1640 supplemented with 10% charcoal-stripped fetal bovine serum. Cells were counted and infected at 1 plaque-forming unit per cell [multiplicity of infection (MOI) = 1]. At 48 hours postinfection, the cells were harvested and lysed in radioimmunoprecipitation assay buffer [1% NP40, 0.1% sodium deoxycholate, 150 mmol/L NaCl, 50 mmol/L Tris-HCl (pH 7.5), and 1 mmol/L phenylmethylsulfonyl fluoride]. Luciferase activity was measured according to the manufacturer's instructions (Promega, Madison, WI) using a luminometer (Berthold Detection Systems, Pforzheim, Germany). Each value was normalized with protein concentration and calculated as the average of triplicate samples. The infectivity of all cell lines was assessed by quantitative PCR of internalized viral DNA and expression mediated by constitutive AdCMV-FL as previously described (14). Relative to the infectivity of LNCaP cells (designated as 1), the infectivity of all other lines are within 2-fold. The highest infectivity was in CWR22rv1 (2.0) and the lowest was in PC-3 (0.7). Due to the similarity of infectivity among the cell lines, activity results reported here were not adjusted.

Synthetic androgen methylenetrienolone (R1881; NEN Life Science Products, Boston, MA) or the antiandrogen bicalutamide (casodex) was added to experiments as indicated. To measure the androgen induction effect, we used the activity in the presence of 10 μmol/L bicalutamide as the basal level rather than in charcoal-stripped fetal bovine serum. The TSTA system is highly amplified and low level of residual androgen in charcoal-stripped fetal bovine serum can activate expression (16). For Western analysis, cell lysates were fractionated on 4% to 20% gradient acrylamide gels (Bio-Rad, Hercules, CA) and subjected to immunoblot analysis with anti-AR N-20 (Santa Cruz Biotechnologies, Santa Cruz, CA) or β-actin A5316 (Sigma, St. Louis, MO) antibodies, and visualized with HRP-labeled secondary antibody and ECL (Amersham, Piscataway, NJ).

Statistical analyses were done using the two-tailed Student's *t* test. For all analyses, $P < 0.01$ was considered statistically significant.

Preparation of tumor cell suspension. Preparation of tumor cell suspensions was done by slight modification of a published protocol (17). Briefly, tumors were harvested, minced to 1 mm^3, and then incubated in 1% Pronase solution (Roche Molecular Biochemicals, Mannheim, Germany) for 20 minutes at room temperature. After overnight incubation in PrEGM media (Cambrex, Walkersville, MD) with Fungizone, the cultured cells were disaggregated by pipetting through sterile 200 μm Cell-Sieve mesh (Biodesign Inc. of New York, Carmel, NY). Tumor cells were infected at 1 plaque forming unit per viable cell (MOI = 1) and analyzed after 48 hours. No difference in the infectivity (determined by infection with a green fluorescent protein expressing adenoviral vector) or nonspecific viral toxicity was observed between the androgen-dependent and androgen-independent LAPC-9 tumor cells.

Thymidine kinase enzyme assay. LNCaP and LAPC-4 were plated onto six-well plates at 5×10^5 cells per well and infected with AdTSTA-sr39tk at MOI = 1. R1881 (10 nmol/L) or asodex (10 μmol/L) was added to the infected cells as indicated and the cells were harvested and lysed in 0.5% NP40, 25 mmol/L NaF, 3 mmol/L β-mercaptoethanol, and 10 mmol/L Tris-HCl (pH 7.0) after 48 hours. The protein concentration of the cell lysates was determined by the detergent-compatible protein assay (Bio-Rad); 1 μg of the lysate was mixed with 3 μL Tk mix ([^{3}H]penciclovir (Movarek Biochemicals, Brea, CA), 250 mmol/L Na_2HPO_4 (pH 6.0), 25 mmol/L ATP, and 25 mmol/L Mg acetate) and incubated at 37°C for 20 minutes. Reactions were terminated by the addition of 40 μL cold water and heating at 95°C for 2 minutes. Forty microliters of mixture was blotted onto DE81 filters (Whatman, Clifton, NJ). The filters were dried and washed thrice with 4 mmol/L ammonium formate and 10 μmol/L thymidine, once in water and twice in 95% ethanol. After drying, the filters were counted by scintillation. Each value was calculated as the average of duplicate samples.

Animal experiments with optical and positron emission tomography imaging. Animal care and procedures were done in accordance with the University of California Animal Research Committee guidelines. Ten- to twelve-week-old male SCID mice obtained from Taconic Farms (Germantown, NY) were implanted s.c. with a tumor chunk (~0.2 cm diameter) coated with Matrigel (Collaborative Research, Bedford, MA) and allowed to grow to ~0.8 cm diameter (18). For the optical imaging experiments, 10^7 plaque-forming units of AdTSTA-FL were subdivided and injected intratumorally (i.t.) into three sites. *In vivo* expression was monitored sequentially using a cooled IVIS CCD camera (Xenogen, Alameda, CA). For each imaging session, the mice were anesthetized with ketamine/xylazine (4:1), given the D-luciferin substrate (200 μL of 150 mg/kg substrate in PBS) i.p., and imaged after a 20-minute incubation. Images were analyzed with IGOR-PRO Living Image Software as described (13, 19). Immunohistochemistry to detect AR expression in the tumor was done with anti-AR antibody (Upstate, Co., Charlottesville, VA) as previously described (13, 19).

For micro-PET imaging, 10^9 plaque-forming units (~30 μL) of AdTSTA-sr39tk were injected i.t. for 4 consecutive days. PET imaging was done on day 7 using ~200 μCi [^{18}F]FHBG substrate (specific activity 5-10 Ci/mmol) that was administered via the tail vein. After 1 hour of uptake time, mice were given inhalation isoflurane anesthesia, placed in a prone position, and imaged for 20 minutes in the micro-PET scanner (Concorde Microsystems, Knoxville, TN).

Images were reconstructed using a filtered back projection reconstruction algorithm. Micro–computed tomography (micro-CT; Imtek, Inc., Knoxville, TN) was done for the same animal sequentially, and images were overlapped using ASIPro VM (Concorde Microsystems).

Results

The transcriptional amplification activity in prostate cancer cell lines. We have developed several transcriptionally targeted gene expression systems based on the PSA gene regulatory regions. The method that exhibits most potent activity, tissue selectivity, and androgen regulation is termed two-step transcriptional activation. It uses an enhanced PSA promoter (20) that drives a potent GAL4VP16 synthetic activator, which in turn binds to tandem repeats of GAL4 binding sites to activate the secondary reporter or therapeutic gene. This TSTA method achieved nearly 1,000-fold augmentation of activity over the native PSA promoter and is more active than the strong viral cytomegalovirus promoter (14). Recently, we have shown that AR in hormone refractory LAPC-9 tumors is functionally active, and it binds to known sites in the PSA gene regulatory region by chromatin immunoprecipitation (13). Expanding upon this observation, the key objective of this study is to survey the activity of TSTA vectors in a wider array of HRPC models and to visualize the *in vivo* activity of the vectors by multimodal molecular imaging techniques.

The activity of the TSTA adenoviral vector (AdTSTA-FL; Fig. 1A) was first determined in two AD lines LNCaP and LAPC-4, and three HRPC lines CWR22Rv1, DU145, and PC-3. As shown in Fig. 1B, AdTSTA-FL activity was negligible in the AR-negative DU145 and PC-3 lines. In the three AR-expressing lines, the activity of AdTSTA-FL was stimulated by androgen ranging from 11.4- to 60.6-fold. When bicalutamide (10 μmol/L) was given simultaneously in the presence of synthetic androgen R1881 (10 nmol/L), a ~50% suppression of peak activity was observed (data not shown). In the presence of androgen, LNCaP cells exhibited the highest expression at 4.8 times the level of LAPC-4 and 14.4 fold-higher than CWR22Rv1.

We also investigated the activation in a fourth HRPC line, MDA PCa 2b, which interestingly expresses AR with a double mutation (L701H and T877A) that allows gene expression and growth to become glucocorticoid responsive (21). As shown in Fig. 1C, gene expression mediated by this promiscuous AR responded to both androgen and hydrocortisone. The induction was 105-fold by hydrocortisone and 144-fold by R1881. The absolute expression level in MDA PCa 2b was 4.4-fold lower than CWR22Rv1. Based on these expression data, we deduced that the PSA-based TSTA method is active in HRPC but its activity is dictated by the AR function in the cell.

Two-step transcriptional amplification activity in hormone refractory LAPC-9 tumor monitored by optical imaging. LAPC-9 and LAPC-4 are two human prostate tumors that can recapitulate the clinical scenario of HRPC (17, 18). They grow routinely in intact male mice and undergo tumor regression upon castration. However, after a substantial time delay, a hormone refractory tumor develops, mimicking the recurrence of HRPC. The activity of AdTSTA-FL was monitored by optical imaging of paired AD and hormone refractory LAPC-9 tumors from days 4 to 14 (Fig. 2A). By this real-time *in vivo* activity measurement, hormone refractory tumors supported a higher level of transgene expression than AD tumors. Immunohistochemistry analysis revealed that the AR protein was expressed in both AD and HRPC tumors, but the magnitude of expression is very heterogenous among the tumor cells (Fig. 2B).

Equivalent gene delivery into the different tumors by i.t. viral injection was difficult to achieve. Thus, we converted the paired tumors into single cell suspension to examine androgen regulation and the activity of the TSTA system more accurately. In doing so, the dosage of viral vector and androgen administered on a per cell basis can be controlled. The dispersed tumor cells were infected with AdTSTA-FL in the

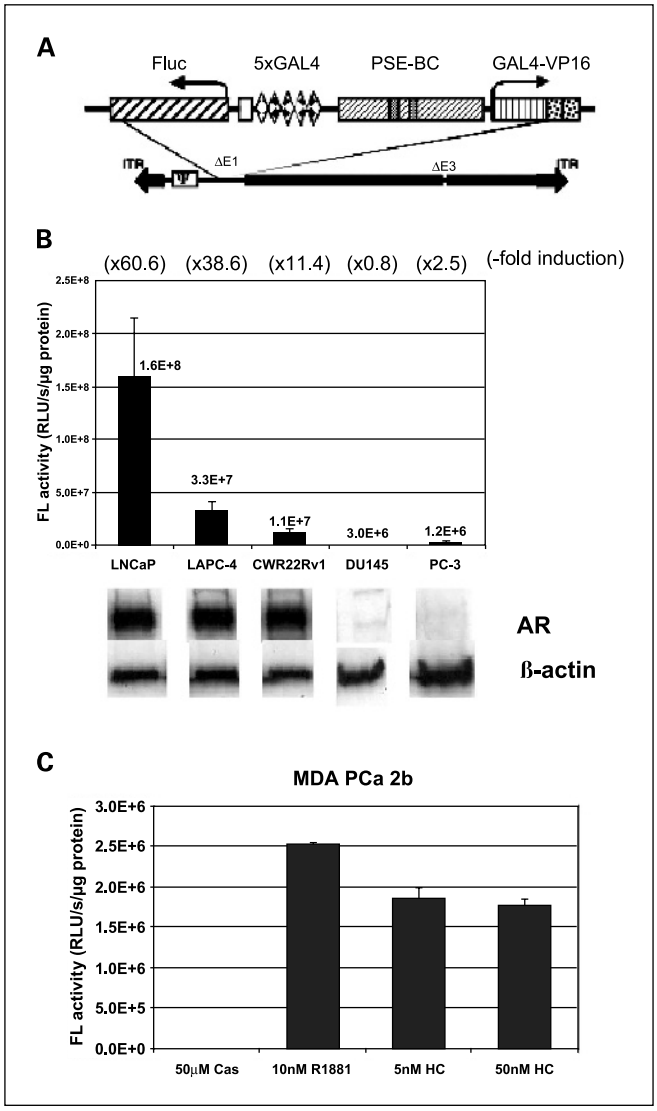

Fig. 1. The activity of AdTSTA-FL and the induction with androgen in a panel of prostate cancer cell lines. *A,* schematic representation of the AdTSTA-FL. The two TSTA components of activator (*GAL4-VP16* driven by *PSE-BC*) and reporter (*Fluc* driven by *5xGAL4*) are inserted into E1 region of recombinant adenovirus. *B,* AdTSTA-FL activity on a panel of prostate cancer cell lines. The cell lysates were harvested 2 days after infection and subjected to FL activity and Western analysis with anti-AR antibody. Fold inductions calculated by the activity ratio with 10 nmol/L R1881 over 10 μmol/L casodex are indicated at the top in parentheses. The activity difference between the AR-positive cell lines and the AR-negative lines (*DU-145* and *PC-3*) is statistically significant ($P < 0.01$). *C,* AdTSTA-FL activity in MDA PCa 2b. The cells were infected and incubated with 10 μmol/L casodex, 10 nmol/L R1881, and 5 and 50 nmol/L hydrocortisone.

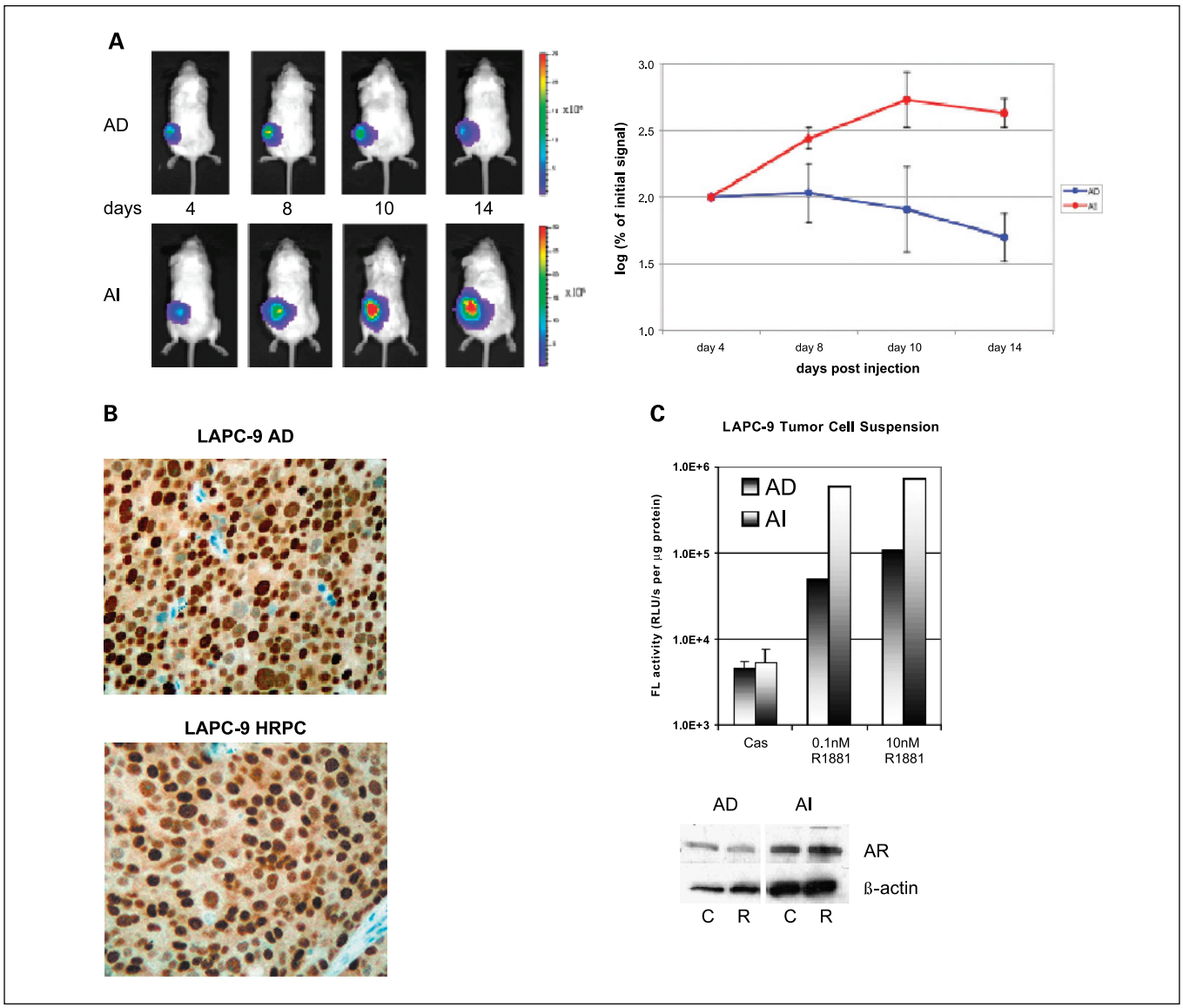

Fig. 2. AdTSTA-FL – mediated activity *in vivo*. *A,* AdTSTA-FL – mediated optical signal in LAPC-9 AD and AI (HRPC) tumors. Ten million infectious units of virus were injected i.t. and imaged by optical CCD camera on the specified day postviral injection. Common logarithms of the percentages of the signal at day 4 of AD and AI tumors are plotted in the right panel. *B,* AR protein in LAPC-9 tumors. Paraffin-fixed, thin tumor sections were stained with anti-AR antibody. *C,* AdTSTA-FL activity in tumor cell suspension prepared from LAPC-9 AD and AI (HRPC) tumors. Tumor cell suspension was infected with AdTSTA-FL at MOI = 1 and incubated in the presence of 10 μmol/L casodex or 0.1 or 10 nmol/L R1881. The cell lysates were prepared after 2 days and subjected to FL assay and AR Western blot [10 μmol/L casodex (*C*); 10 nmol/L R1881 (*R*)]. The activity difference between AI and AD cells in the presence of R1881 was statistically significant ($P < 0.01$).

presence of specified ligands. AR protein and androgen-responsive FL activity was observed in both cell populations (Fig. 2C). In close agreement with the optical imaging results in tumors, we also observed that the activity of AdTSTA-FL is 7.2-fold higher in the hormone refractory (AI) than in AD tumor cells in culture in the presence of ≥1 nmol/L concentrations of R1881.

Use of the two-step transcriptional amplification vector in positron emission tomography imaging. It is important to develop molecular imaging approaches that can be applied in clinical settings for advanced prostate cancer. To this end, we adapted our prostate-specific gene imaging to PET, a radionuclide functional imaging modality that enables three-dimensional signal localization. An adenoviral vector that expresses the herpes simplex virus thymidine kinase (*HSV-tk*) PET reporter gene under the control of TSTA was generated (Fig. 3A). An enhanced HSV-tk variant, sr39tk, was incorporated into the AdTSTA-sr39tk because this variant *tk* gene augments the uptake of radiolabeled PET tracers and improves PET imaging sensitivity by 2-fold (22). The sr39tk protein expression and enzymatic activity mediated by the vector was regulated by androgen (Fig. 3B and C).

AdTSTA-sr39tk was administered into AD and hormone refractory LAPC-4 tumors, and its activity was documented by the combined micro-PET/micro-CT. This combined imaging modality enables the precise localization of the PET signals with the anatomic information obtained from the CT scan. Using [^{18}F]FHBG as the PET substrate, robust signals were

observed in both AD and hormone refractory LAPC-4 tumors (Fig. 3D). The activity was higher in the hormone refractory tumor (0.78% injected dose/g) than in the AD tumor (0.50% injected dose/g). These results confirm that the TSTA-mediated prostate-specific gene imaging is feasible for advanced stages of tumor using the clinically relevant PET.

Discussion

Effective treatment options for recurrent prostate cancer are notably limited. Our goal has been to develop novel gene-based diagnostic and therapeutic approaches to treat advanced stages of prostate cancer. Toward this end, the well-studied PSA promoter/enhancer was utilized to achieve prostate-specific gene expression. Given that transcriptional regulation of the PSA promoter/enhancer is AR dependent, it was prudent to first verify that our PSA promoter-based expression strategy is feasible in HRPC. In this study, we showed that the highly amplified prostate-specific TSTA gene delivery vectors are indeed functional in many models of HRPC under androgen-deprived conditions.

Our data support that the presence of functional AR is necessary to activate PSA-based promoter constructs. However, other factors are likely to modulate AR activity in HRPC cells. The 14-fold range of luciferase activity observed in different models does not correlate with the level of AR expression or the status of AR mutation in the cell lines. The AR in LAPC-4 is wild type, whereas it contains the T877A mutation in LNCaP and the H874Y mutation in the ligand-binding

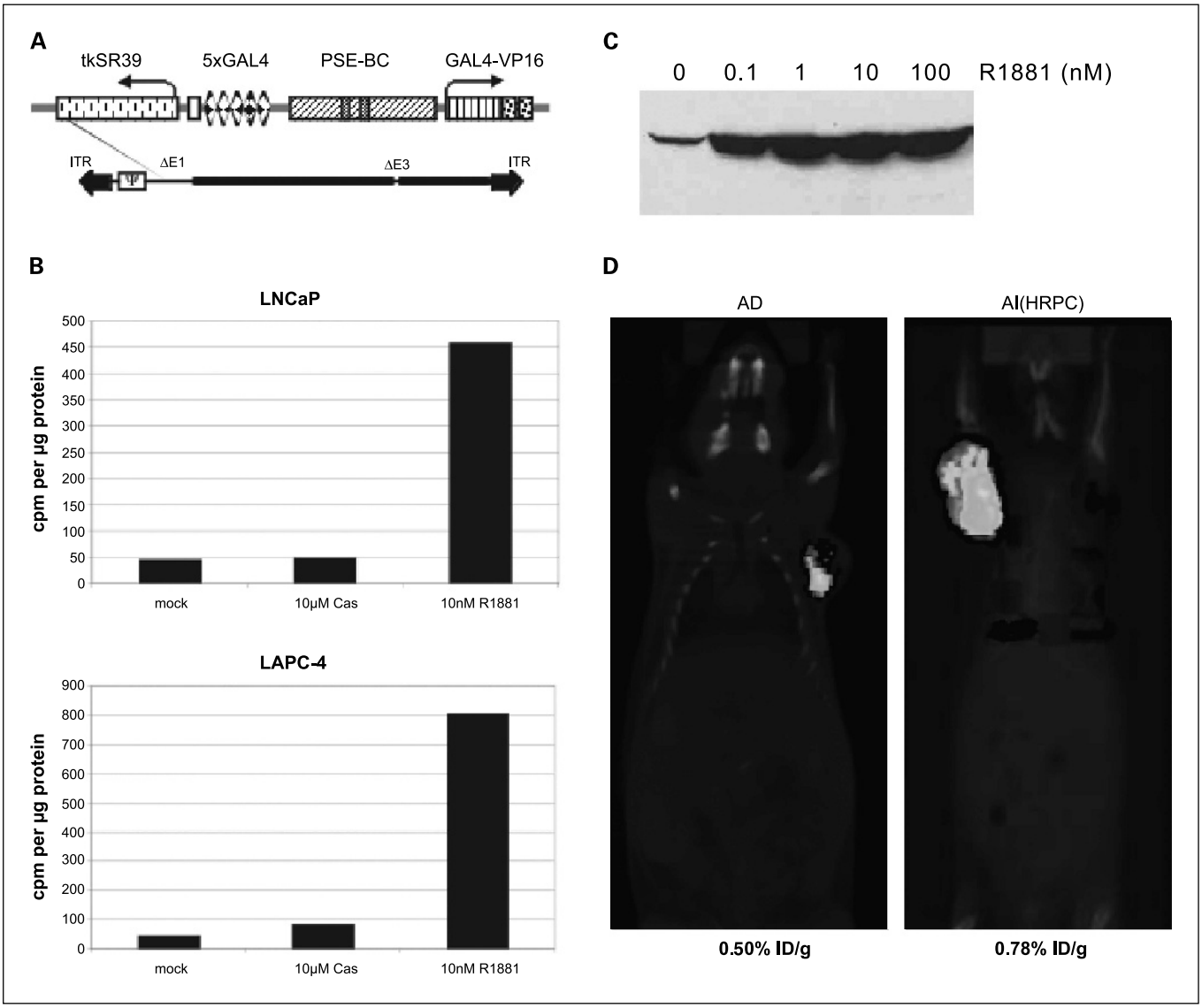

Fig. 3. The activity of AdTSTA-sr39tk and its application in micro-PET. *A,* schematic representation of the AdTSTA-sr39tk. The *sr39tk* gene is a HSV-tk variant with higher affinity for acycloguanosines. *B,* AdTSTA-sr39tk activity in AD prostate cancer cell lines LNCaP and LAPC-4. The cells were infected with AdTSTA-sr39tk at MOI = 1 and harvested 2 days later. The cell lysates were subjected to thymidine kinase enzyme assay. Phosphorylated forms of [^{3}H]penciclovir were counted and plotted after normalization with total cellular protein. *C,* androgen regulation of expression from AdTSTA-sr39tk. LNCaP cells were infected with AdTSTA-sr39tk at MOI = 5 and incubated with 0 to 100 nmol/L R1881. Cells were lysed and subjected to Western analysis using anti-HSV-tk polyclonal antibody. *D,* combined micro-PET and micro-CT of LAPC-4 AD and AI tumor. AdTSTA-sr39tk (4×10^9 infectious units) was injected to AD and AI LAPC-4 tumors. One week later, [^{18}F]FHBG injected animals were anesthetized and scanned for micro-PET and micro-CT sequentially. The signal in the tumor was measured by percentage injected dose of substrate per gram of tissue (*%ID/g*) listed below the image.

domain of CWR22Rv1. Differential activity of coactivators of the AR pathway could modulate AR function *in vivo*. Gregory et al. (23) reported elevated level of nuclear receptor coactivators, SRC1, and SRC2 in recurrent prostate cancer. Recently, Dr. Tindall's group also showed that coactivator p300 confers increased growth and progression potential in prostate cancer (24). Many other growth signaling pathways, such as IGF, Her2, or IL6, can also modulate AR-mediated expression (reviewed in ref. 7). Further investigations are needed to determine the precise AR activation mechanism in different cases of HRPC.

Both optical imaging and PET illustrated higher TSTA activity in the hormone refractory xenograft subline versus the parental AD tumor in two models. These findings endorse the idea that activation of AR function occurs despite the castrated level of androgen *in vivo*. A recent report by Chen et al. (25) showed that 3- to 5-fold elevated expression of AR is a cardinal distinguishing feature between paired AD and hormone refractory tumors. Their work also supports that AR overexpression can lead to HRPC. In fact, the two models reported here were assessed in the gene expression profiling study (25). Moreover, our results showed that the real-time assessment of AR functional activity in prostate tumors, including HRPC, can be accomplished by introducing TSTA adenoviral vectors into the tumor.

In contemplating future applications in clinical settings, we postulate that the TSTA gene expression strategy will be active in all PSA-positive prostate cancers, which include the recurrent metastatic disease. Previous histologic evaluations of clinical materials have detected AR and PSA expression in all stages of prostate cancer (8, 26, 27). Recent preliminary results (reported at Specialized Programs of Research Excellence meeting July 2004, Baltimore MD) indicated that AR expression is detected in metastatic lesions, albeit at heterogeneous level. A subtype of HRPC, the neuroendocrine prostate cancer, lacks AR and is associated with poor prognosis (28, 29). We anticipate any AR-dependent gene expression approach will be inactive in neuroendocrine tumor cells. However, solitary neuroendocrine tumors are rare as most neuroendocrine tumor cells exist in small foci interspersed within conventional AR- and PSA-positive prostate adenocarcinoma. If an AR-dependent toxic gene therapy was applied to a mixed lesion, then indirect tumoricidal effects can be transmitted to neuroendocrine tumor cells via conventional prostate cancer cells by bystander effects (12).

Linking molecular imaging to gene therapy is a favorable method to assess the performance of the intended treatment. In an earlier study, visualization of distant metastases of prostate tumor was accomplished by optical imaging mediated through the use of a modified PSA promoter-based adenoviral vector (19). Due to the inability of light energy to penetrate deep into tissues, bioluminescence imaging is not applicable in humans. Thus, to translate the above-mentioned promising findings to the clinics, the application of a high-energy clinically relevant modality, such as PET, is needed. However, the HSV-tk–based PET imaging is several orders of magnitude less sensitive than optical imaging in small animal studies (30). The nearly three-order gain in activity of TSTA over native PSA promoter is a key factor to achieve the successful PET imaging of HRPC. Because the same principles are at work in animal micro-PET as in clinical PET, this result supports the idea of an equivalent gene-based approach in clinical studies.

Many studies have shown that the *sr39tk* gene can function effectively both as a PET reporter gene as well as a toxic suicide gene (12, 31). Recently, the AdTSTA-sr39tk was applied in a "one-two punch" imaging and suicide gene therapy to treat prostate tumor.[8] Compared to a constitutive cytomegalovirus-driven vector, the prostate-targeted TSTA vector not only elicited equivalent tumoricidal effects but also dramatically reduced systemic liver toxicity. The PET imaging correlated entirely with the therapeutic outcomes. These results indicate that the TSTA methodology is a promising platform to build gene-based diagnostic and therapeutic approaches to manage HRPC.

Acknowledgments

We thank W. Ladno, J. Edwards, and Dr. D. Stout for their skillful assistance in PET/CT imaging; Baohui Zhang for technical assistance; Giri Sulur for assistance on manuscript preparation; and Drs. David Agus (Department of Molecular and Medical Pharmacology, UCLA, Los Angeles, CA) and Margaret Black (Pharmaceutical Sciences, Washington State University, Pullman, WA) for the kind gifts of CWR22Rv1 cell line and polyclonal anti-tk antibody, respectively.

[8] Johnson et al., submitted for publication.

References

1. Weir HK, Thun MJ, Hankey BF, et al. Annual report to the nation on the status of cancer, 1975-2000, featuring the uses of surveillance data for cancer prevention and control. J Natl Cancer Inst 2003;95:1276–99.
2. Dowling AJ, Tannock IF. Systemic treatment for prostate cancer. Cancer Treat Rev 1998;24:283–301.
3. Pound CR, Partin AW, Eisenberger MA, Chan DW, Pearson JD, Walsh PC. Natural history of progression after PSA elevation following radical prostatectomy. JAMA 1999;281:1591–7.
4. Roehl KA, Han M, Ramos CG, Antenor JA, Catalona WJ. Cancer progression and survival rates following anatomical radical retropubic prostatectomy in 3,478 consecutive patients: long-term results. J Urol 2004; 172:910–4.
5. Tannock IF, de Wit R, Berry WR, et al; TAX 327 Investigators. Docetaxel plus prednisone or mitoxantrone plus prednisone for advanced prostate cancer. N Engl J Med 2004;351:1502–12.
6. Gelmann EP. Molecular biology of the androgen receptor. J Clin Oncol 2002;20:3001–15.
7. Feldman BJ, Feldman D. The development of androgen-independent prostate cancer. Nat Rev Cancer 2001;1:34–45.
8. Hobisch A, Culig Z, Radmayr C, et al. Distant metastases from prostatic carcinoma express androgen receptor protein. Cancer Res 1995;55: 3068–72.
9. Magi-Galluzzi C, Xu X, Hlatky L, et al. Heterogeneity of androgen receptor content in advanced prostate cancer. Mod Pathol 1997;10:839–45.
10. Bok RA, Small EJ. Bloodborne biomolecular markers in prostate cancer development and progression. Nat Rev Cancer 2002;2:918–26.
11. DeWeese TL, van der Poel H, Li S, et al. A phase I trial of CV706, a replication-competent, PSA selective oncolytic adenovirus, for the treatment of locally recurrent prostate cancer following radiation therapy. Cancer Res 2001;61:7464–72.
12. Wu L, Sato M. Integrated, molecular engineering approaches to develop prostate cancer gene therapy. Curr Gene Ther 2003;3:452–67.
13. Zhang L, Johnson M, Le KH, et al. Interrogating androgen receptor function in recurrent prostate cancer. Cancer Res 2003;63:4552–60.
14. Sato M, Johnson M, Zhang L, et al. Optimization of adenoviral vectors to direct highly amplified prostate-specific expression for imaging and gene therapy. Mol Ther 2003;8:726–37.
15. He TC, Zhou S, da Costa LT, et al. A simplified system for generating recombinant adenoviruses. Proc Natl Acad Sci U S A 1998;95:2509–14.
16. Zhang L, Adams JY, Billick E, et al. Molecular engineering of a two-step transcription amplification (TSTA) system for transgene delivery in prostate cancer. Mol Ther 2002;5:223–32.
17. Craft N, Chhor C, Tran C, et al. Evidence for clonal outgrowth of androgen-independent prostate cancer cells from androgen-dependent tumors through a two-step process. Cancer Res 1999;59: 5030–6.
18. Klein KA, Reiter RE, Redula J, et al. Progression of metastatic human prostate cancer to androgen

independence in immunodeficient SCID mice. Nat Med 1997;3:402–8.

19. Adams JY, Johnson M, Sato M, et al. Visualization of advanced human prostate cancer lesions in living mice by a targeted gene transfer vector and optical imaging. Nat Med 2002;8:891–7.

20. Wu L, Matherly J, Smallwood A, et al. Chimeric PSA enhancers exhibit augmented activity in prostate cancer gene therapy vectors. Gene Ther 2001; 8:1416–26.

21. Zhao XY, Malloy PJ, Krishnan AV, et al. Glucocorticoids can promote androgen-independent growth of prostate cancer cells through a mutated androgen receptor. Nat Med 2000;6:703–6.

22. Gambhir SS, Bauer E, Black ME, et al. A mutant herpes simplex virus type 1 thymidine kinase reporter gene shows improved sensitivity for imaging reporter gene expression with positron emission tomography. Proc Natl Acad Sci U S A 2000;97: 2785–90.

23. Gregory CW, He B, Johnson RT, et al. A mechanism for androgen receptor-mediated prostate cancer recurrence after androgen deprivation therapy. Cancer Res 2001;61:4315–9.

24. Debes JD, Sebo TJ, Lohse CM, et al. p300 in prostate cancer proliferation and progression. Cancer Res 2003;63:7638–40.

25. Chen CD, Welsbie DS, Tran C, et al. Molecular determinants of resistance to antiandrogen therapy. Nat Med 2004;10:33–9.

26. Sweat SD, Pacelli A, Bergstralh EJ, Slezak JM, Bostwick DG. Androgen receptor expression in prostatic intraepithelial neoplasia and cancer. J Urol 1999; 161:1229–32.

27. Koivisto PA, Helin HJ. Androgen receptor gene amplification increases tissue PSA protein expression in hormone-refractory prostate carcinoma. J Pathol 1999;189:219–23.

28. Krijnen JL, Bogdanowicz JF, Seldenrijk CA, et al. The prognostic value of neuroendocrine differentiation in adenocarcinoma of the prostate in relation to progression of disease after endocrine therapy. J Urol 1997; 158:171–4.

29. di Sant'Agnese PA. Neuroendocrine differentiation in prostatic carcinoma: an update on recent developments. Ann Oncol 2001;12 Suppl 2:S135–40.

30. Ray P, Wu AM, Gambhir SS. Optical bioluminescence and positron emission tomography imaging of a novel fusion reporter gene in tumor xenografts of living mice. Cancer Res 2003;63:1160–5.

31. Pantuck AJ, Matherly J, Zisman A, et al. Optimizing prostate cancer suicide gene therapy using herpes simplex virus thymidine kinase active site variants. Hum Gene Ther 2002;13:777–89.

The EMBO Journal (2006), 1–14 | © 2006 European Molecular Biology Organization | All Rights Reserved 0261-4189/06
www.embojournal.org

THE EMBO JOURNAL

ADAMTS1 mediates the release of antiangiogenic polypeptides from TSP1 and 2

Nathan V Lee[1], Makoto Sato[2], Douglas S Annis[3], Joseph A Loo[4], Lily Wu[2], Deane F Mosher[3] and M Luisa Iruela-Arispe[1,*]

[1]Department of Molecular, Cell and Developmental Biology, Molecular Biology Institute, Jonsson Comprehensive Cancer Center, University of California, Los Angeles, CA, USA, [2]Department of Urology, Department of Molecular and Medical Pharmacology, University of California, Los Angeles, CA, USA, [3]Department of Medicine and Biomolecular Chemistry, University of Wisconsin, Madison, WI, USA and [4]Department of Biological Chemistry and Department of Chemistry and Biochemistry, University of California, Los Angeles, CA, USA

Matrix metalloproteases regulate both physiological and pathological events by processing matrix proteins and growth factors. ADAMTS1 in particular is required for normal ovulation and renal function and has been shown to modulate angiogenesis. Here we report that TSP1 and 2 are substrates of ADAMTS1. Using a combination of mass spectrometry and Edman degradation, we mapped the cleavage sites and characterized the biological relevance of these processing events. ADAMTS1 cleavage mediates the release of polypeptides from the trimeric structure of both TSP1 and 2 generating a pool of antiangiogenic fragments from matrix-bound thrombospondin. Using neo-epitope antibodies we confirmed that processing occurs during wound healing of wild-type mice. However, TSP1 proteolysis is decreased or absent in ADAMTS1 null mice; this is associated with delayed wound closure and increased angiogenic response. Finally, TSP1−/− endothelial cells revealed that the antiangiogenic response mediated by ADAMTS1 is greatly dependent on TSP1. These findings have unraveled a mechanistic explanation for the angiostatic functions attributed to ADAMTS1 and demonstrated *in vivo* processing of TSP1 under situations of tissue repair.

The EMBO Journal advance online publication, 2 November 2006; doi:10.1038/sj.emboj.7601400
Subject Categories: cell & tissue architecture; proteins
Keywords: angiogenesis; extracellular matrix; matrix metalloproteases; thrombospondin; wound healing

Introduction

Remodeling of the extracellular matrix is an essential requirement for development, repair and homeostasis of normal tissues (Mott and Werb, 2004). Among the molecules responsible for these events are the matrix metalloproteases. These constitute a major group of extracellular and membrane-bound enzymes involved in the selective digestion and processing of proteins, glycoproteins and growth factors located outside the cell (Mott and Werb, 2004; Lee *et al*, 2005b). Like many other metalloproteases, ADAMTS1 (A Disintegrin And Metalloprotease with ThrombosSpondin) is a secreted, zinc-binding enzyme broadly expressed during development and in several adult tissues (Thai and Iruela-Arispe, 2002; Lee *et al*, 2005a). However, unlike many other metalloproteases in which loss-of-function showed a minimal phenotype, genetic inactivation of ADAMTS1 results in either embryonic lethality (in about 40% of null mice) or postnatal lethality due to severe kidney dysfunction (Shindo *et al*, 2000; Mittaz *et al*, 2004; Lee *et al*, 2005a). Mice homozygous for the null allele also display multiple defects in the female reproductive tract including poor fertility and anomalies in uterine structure (Russell *et al*, 2003). In addition, mice suffer from stunted growth and showed adrenal abnormalities (Shindo *et al*, 2000). Together, these outcomes stress the relevance of ADAMTS1 during development and homeostasis of several adult organs.

Mechanistic understanding of the phenotype associated with ADAMTS1 inactivation requires a concrete knowledge of its catalytic profile, that is, biological substrates, and information of other noncatalytic functions. Towards this goal, several groups have identified: (1) substrates for ADAMTS1 that, to date, include aggrecan, versican and nidogen (Kuno *et al*, 2000; Sandy *et al*, 2001; Rodriguez-Manzaneque *et al*, 2002; Canals *et al*, 2006); (2) catalytic modifiers, such as fibulin1 (Lee *et al*, 2005a) and (3) noncatalytic function such as sequestration of VEGF to reduce signaling via this ligand (Luque *et al*, 2003).

Some of the substrates identified for ADAMTS1 have been linked to the pathologies displayed by the null mouse such as inability to ovulate due to lack of versican cleavage (Russell *et al*, 2003). Nonetheless, many of the other defects remain to be explained at a molecular level. To further expand our knowledge of substrates for ADAMTS1, we tested several potential candidates. Our strategy focused on extracellular proteins located in basement membranes, as the expression profile of ADAMTS1 includes several epithelia (kidney, lung and epidermis) and blood vessels (Thai and Iruela-Arispe, 2002; Gunther *et al*, 2005). Furthermore, basement membrane components have been shown to regulate differentiation and migration of endothelial cells during angiogenesis (Kalluri, 2003). Here we showed that TSP1, a constitutive component of epithelial and endothelial basement membrane, is cleaved by ADAMTS1.

Thrombospondins (TSPs) are a family of secreted glycoproteins broadly and highly expressed during development (Iruela-Arispe *et al*, 1993). In addition, TSPs have been associated with the regulation of several processes in the adult including angiogenesis, wound healing and collagen fibril assembly (Bornstein *et al*, 2000; Lawler, 2000, 2002; Lawler and Detmar, 2004). From all five members of the TSP

*Corresponding author. Department of Molecular, Cell and Developmental Biology, Molecular Biology Institute, UCLA, 611 Charles E. Young Drive East Boyer Hall 559, Los Angeles, CA 90095, USA.
Tel.: +1 310 794 5763; Fax: +1 310 794 5766;
E-mail: arispe@mbi.ucla.edu

Received: 5 May 2006; accepted: 26 September 2006

family, only TSP1 and 2 inhibit angiogenesis *in vitro* and *in vivo* (Lawler and Detmar, 2004). The antiangiogenic domain has been mapped to the type I (or TSR) repeats present in TSP1 and 2, a motif that is absent in TSPs 3, 4 and 5. Here we show that processing of TSP1 by ADAMTS1 releases bioactive polypeptides with antiangiogenic properties, demonstrate that this cleavage event occurs *in vivo*, and explore the biological consequences of TSP processing in mice that lack ADAMTS1.

Results

TSP1 is cleaved by ADAMTS1

To test the hypothesis that basement membrane proteins are substrates for ADAMTS1, we exposed both TSP1 and laminin to the enzyme *in vitro*. Analysis of the digestion by electrophoretic mobility under reducing conditions revealed two smaller polypeptides of 110 and 36 kDa in the TSP1 sample visible by Coomassie. In contrast, under the same conditions ADAMTS1 did not cleave laminin (Figure 1A). An assortment of several matrix proteins, including TSP1, has been previously used in ADAMTS1 enzymatic assays and indicated no cleavage (Rodriguez-Manzaneque *et al*, 2002). However, those analyses were performed using antibodies and non-reduced conditions and this prevented visualization of released fragments.

Purification of TSP1 entails thrombin-induced platelet degranulation and because thrombin is a recognized protease for TSP1 (Lawler *et al*, 1986a, b), we asked if TSP1 fragments could potentially be the result of contaminating thrombin activity. To test this, TSP1 was incubated with 2 or 5 U of thrombin. Analysis by Western immunoblot with a polyclonal anti-TSP1 antibody (GPC) confirmed that the fragment derived from ADAMTS1 cleavage, 36 kDa, was distinct from the fragment released by thrombin, 25 kDa (Figure 1B).

TSP2 is also a substrate for ADAMTS1

TSP1 and 2 share identical structural features and are 32–82% conserved in amino-acid sequence depending on the specific domain (Bornstein, 1992). Thus, we were interested in determining whether TSP2 might also be a substrate for ADAMTS1. *In vitro* digestion assays revealed that ADAMTS1 released two fragments of 42 and 30 kDa (Figure 1C).

To ensure that cleavage of both TSP1 and 2 by ADAMTS1 did not result from possible contaminating proteases, a catalytically inactive ADAMTS1 (E385A) and the ADAMTS1 C-terminal fragment (TSRs) lacking the catalytic domain were incubated with TSP1 and 2 in parallel. The inactive ADAMTS1 (E385A) and the C-terminal fragment were purified from the same cell expression system following a similar protocol. Consequently, any contaminating protease would also be present in these preparations. Both TSP1 and 2 were

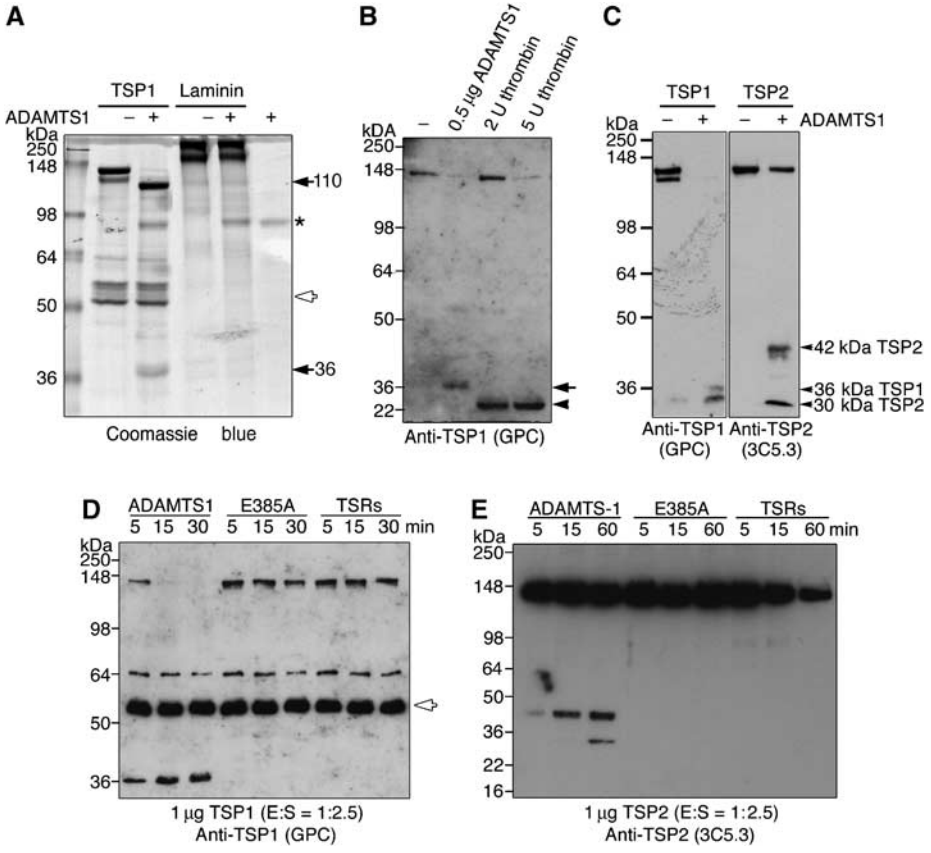

Figure 1 TSP1 and 2 are cleaved by ADAMTS1 at unique sites. (**A**) Coomassie stained gel of full-length TSP1 and Laminin incubated with ADAMTS1. Arrows indicate the 110 and 36 kDa cleavage fragments. (**B**) Western immunoblot of TSP1 incubated with ADAMTS1 or thrombin. (**C**) Western immunoblots of TSP1 and 2 incubated with ADAMTS1. (**D**) Western immunoblot of TSP1 incubated with ADAMTS1, catalytically inactive ADAMTS1 (E385A) or a truncated ADAMTS1 form that only harbors type I repeats (TSRs) for indicated times. (**E**) Western immunoblot of TSP2 incubated with ADAMTS1, catalytically inactive ADAMTS1 (E385A) or a truncated ADAMTS1 form that only harbors type I repeats (TSRs) for indicated times. Open arrow, fragment already present in preparation that is not susceptible to ADAMTS1 cleavage.

cleaved only by active ADAMTS1 (Figure 1D and E). These experiments confirmed that TSP1 and 2 cleavage resulted specifically from the catalytic activity of ADAMTS1. In addition, at an enzyme:substrate (E:S) ratio of 1:2.5, TSP1 was cleaved by ADAMTS1 in 5 min (Figure 1D). At the same ratio, TSP2 was cleaved by ADAMTS1 releasing a 42 kDa fragment in 15 min and into a second 30 kDa fragment in 1 h (Figure 1E). In certain TSP1 protein preparations, a 60 kDa fragment was already present in the starting material, but were not susceptible to ADAMTS1 (Figure 1A and D, open arrow).

To assess the cleavage efficiency of TSP1 and 2 by ADAMTS1, the proteins were incubated with varying ratios of ADAMTS1 for 1 h at 37°C. E:S ranged from 1:1 to 1:40. Within 1 h, half of the starting full-length TSP1 was processed at an E:S of 1:40 (Figure 2A). Cleavage of TSP2 by ADAMTS1 was not as effective; an E:S of 1:5 was required to cleave 30% of the starting full-length TSP2 (Figure 2B). However, proteolysis of both TSP1 and 2 was dose-dependent as more ADAMTS1 yielded increasingly more cleavage products (Figure 2A and B, arrows).

To determine if proteolysis occurs at physiological pH, TSP1 and 2 were incubated with ADAMTS1 at a pH range of 5.0 to 8.5 at an E:S of 1:20. Maximum efficiency for cleavage of TSP1 occurred at pH 6.5 to 8.5 and for TSP2 at pH 7.0 to 8.5.

TSP2 was cleaved by ADAMTS1 at two distinct sites to generate a 42 and a 30 kDa polypeptide. Kinetics experiments revealed a sequential release of these fragments (Figure 1E). In addition, increasing molar ratio of ADAMTS1 favors the generation of the 30 kDa fragment (Figure 2B). These data suggest that the initial cleavage releases the 42 kDa fragment and a second event releases the 30 kDa fragment.

Cleavage of TSP1 and 2 by ADAMTS1 is not shared by ADAMTS4

ADAMTS1 and ADAMTS4 display high sequence homology and share the substrates, aggrecan and versican (reviewed by Apte, 2004). Thus, we sought to determine whether TSP1 and 2 are also cleaved by ADAMTS4. Both TSP1 and 2 were not cleaved by ADAMTS4 compared to ADAMTS1 at the same molar concentration (Figure 3A and B). To verify that ADAMTS4 was active, aggrecan was digested with both ADAMTS1 and ADAMTS4. As expected, both were able to cleave aggrecan, although ADAMTS4 was a more effective enzyme for aggrecan than ADAMTS1 (Figure 3C). Aggrecan is cleaved by both ADAMTS1 and ADAMTS4 to 200 kDa as well as 65 kDa (Sandy *et al*, 2000; Rodriguez-Manzaneque *et al*, 2002). ADAMTS4 is more efficient at cleaving aggrecan hence majority of the product was 65 kDa in mass. In contrast, ADAMTS1 is less efficient at cleaving aggrecan yielding mainly 200 kDa fragments.

Heparin binding domains of TSP1, TSP2 and ADAMTS1 are necessary for efficient cleavage

The N-terminal domain of TSP1 and 2, as well as TSR repeats of ADAMTS1 have been shown to interact with heparin (Murphy-Ullrich *et al*, 1993; Kuno and Matsushima, 1998; Rodriguez-Manzaneque *et al*, 2000). We considered that these domains might facilitate docking and subsequent

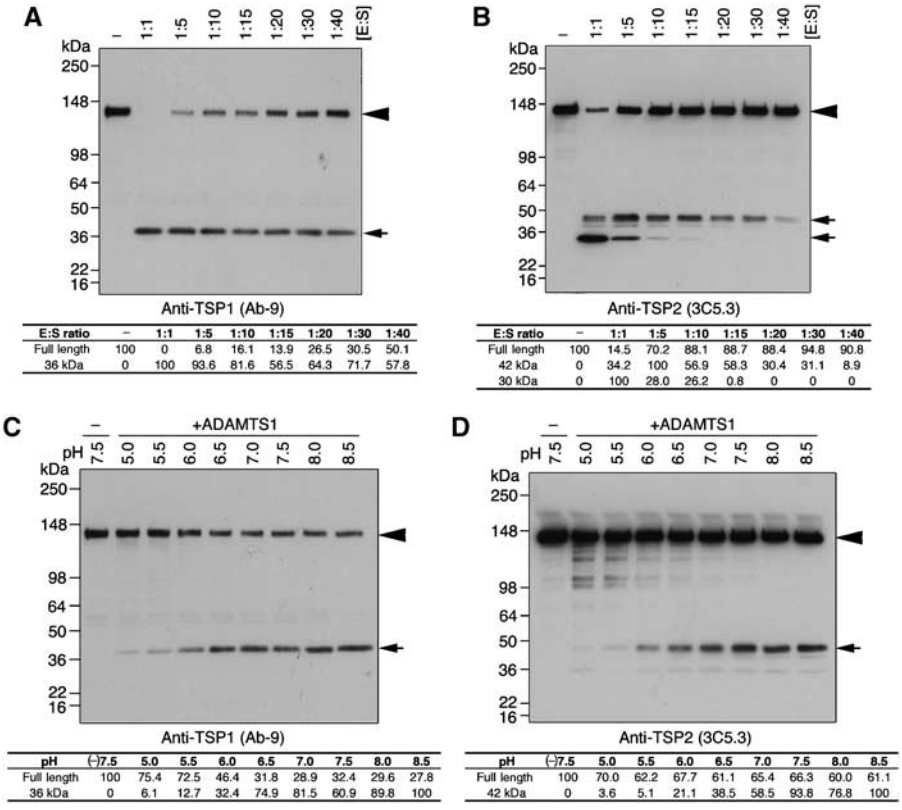

E:S ratio	–	1:1	1:5	1:10	1:15	1:20	1:30	1:40
Full length	100	0	6.8	16.1	13.9	26.5	30.5	50.1
36 kDa	0	100	93.6	81.6	56.5	64.3	71.7	57.8

E:S ratio	–	1:1	1:5	1:10	1:15	1:20	1:30	1:40
Full length	100	14.5	70.2	88.1	88.7	88.4	94.8	90.8
42 kDa	0	34.2	100	56.9	58.3	30.4	31.1	8.9
30 kDa	0	100	28.0	26.2	0.8	0	0	0

pH	(–)7.5	5.0	5.5	6.0	6.5	7.0	7.5	8.0	8.5
Full length	100	75.4	72.5	46.4	31.8	28.9	32.4	29.6	27.8
36 kDa	0	6.1	12.7	32.4	74.9	81.5	60.9	89.8	100

pH	(–)7.5	5.0	5.5	6.0	6.5	7.0	7.5	8.0	8.5
Full length	100	70.0	62.2	67.7	61.1	65.4	66.3	60.0	61.1
42 kDa	0	3.6	5.1	21.1	38.5	58.5	93.8	76.8	100

Figure 2 ADAMTS1 cleavage of TSP1 and 2 occurs in a dosage-dependent manner. (**A, B**) Western immunoblots of TSP1 and 2 incubated with ADAMTS1 for 1 h at 37°C at E:S ranging from 1:1 to 1:40. (**C, D**) Western immunoblots of TSP1 and 2 incubated with ADAMTS1 in pH ranging from 5.0 to 8.5. Arrowheads, intact TSP1 and 2; arrows, TSP1 and 2 cleavage fragments. Tables under each blot indicate densitometric quantification of the bands. Numbers are in percentile of relative intensity in relation to the darkest band in the blot.

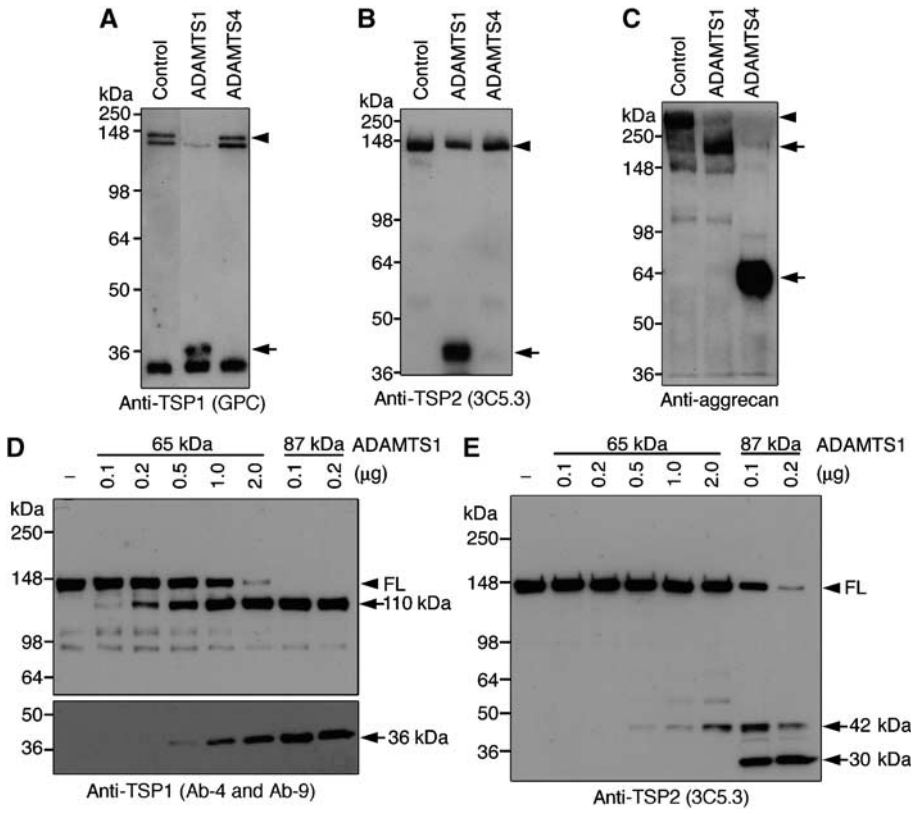

Figure 3 TSP1 and 2 are not substrates of ADAMTS4. (**A, B**), Western immunoblots of TSP1 and 2 incubated with ADAMTS1, ADAMTS4 and vehicle. (**C**) Western immunoblots of aggrecan incubated with ADAMTS1, ADAMTS4 or vehicle. (**D**, **E**) Western immunoblots of TSP1 and 2 incubated with varying amounts of 87 kDa ADAMTS1 and 65 kDa ADAMTS1, as indicated. Arrowheads, intact TSP1 and 2; arrows, TSP1 and 2 cleavage fragments.

cleavage. To test this possibility, TSP1 was incubated with the full-length active ADAMTS1 (87 kDa) and with truncated active ADAMTS1 (65 kDa), which lacks part of the spacer region and the last two TSRs, and displays lower affinity for heparin (Rodriguez-Manzaneque *et al*, 2000). The truncated form of ADAMTS1 required a higher E:S (2:1) to achieve near complete processing of intact TSP1 within 2 h in comparison to 87 kDa ADAMTS1, which completely processed intact TSP1 at an E:S of 1:10 (Figure 3D). TSP2 was also incubated with 65 and 87 kDa forms of ADAMTS1. The 65 kDa form of ADAMTS1 was rather inefficient at processing intact TSP2, as an E:S of 1:1 was required to release the 42 kDa TSP2 N-terminal fragment visible by Western blot (Figure 3E). The 87 kDa ADAMTS1 was more efficient at cleaving intact TSP2 (Figure 3E).

The reciprocal experiment was carried out by incubating truncated mutants of TSP1 and 2 lacking the heparin binding domain (delN-1 and delN-2) with ADAMTS1. In comparison to intact TSP1, which was completely processed, delN-1 was not cleaved as efficiently, as only half was processed (Figure 4B (i)). In turn, delN-2 was not cleaved by ADAMTS1 (Figure 4B (ii)). To discard concerns related to structural changes of deletion mutants, we tested another deletion mutant, NoC, which has the N-module necessary for heparin binding. Both NoC-1 and NoC-2 were cleaved by ADAMTS1 (Figure 4C (i and ii)).

To test whether heparin affects TSP1 and 2 processing, we incubated both TSP proteins with ADAMTS1 at an E:S of 1:40 in the presence of increasing amounts of heparin. TSP1 cleavage was not affected by heparin (Figure 4D (i)), similarly, the more carboxy terminal cleavage site in TSP2, which yield the 42 kDa fragment was not altered (Figure 4D (ii)). However, generation of the 30 kDa fragment was suppressed by heparin (Figure 4D (ii)). This would indicate that rather than altering enzymatic activity, heparin binds to one of the sites in TSP2 and hampers the ability of ADAMTS1 to dock and cleave within this site. Nonetheless, based on the previous findings, the heparin-binding region in TSP1 and 2 appears to function independent from heparin to facilitate processing by ADAMTS1.

Identification of cleavage sites

Analysis of with MALDI-TOF MS determined that the 36 kDa fragment corresponds to the N-terminus of TSP1 and the 110 kDa fragment corresponds to the C-terminus. Analysis repeated with LC MS yield the same result (data not shown). Because the 110 kDa fragment exposes the cleavage site at the N-terminal region, we transferred it onto PVDF membrane and performed N-terminal Edman degradation sequencing. One of the resulting peptides contained the LRRPPL sequence indicating that cleavage occurred between residues: glutamic acid 311 and leucine 312 (Figures 5A and 6A). This site is consistent with the classification of glutamyl endopeptidase attributed to ADAMTS1 based on cleavage of other substrates such as aggrecan and versican (Rodriguez-Manzaneque *et al*, 2002; Westling *et al*, 2002). Similarly, higher-molecular weight TSP2 doublets released by ADAMTS1 cleavage were also analyzed by MALDI-TOF MS and determined to corre-

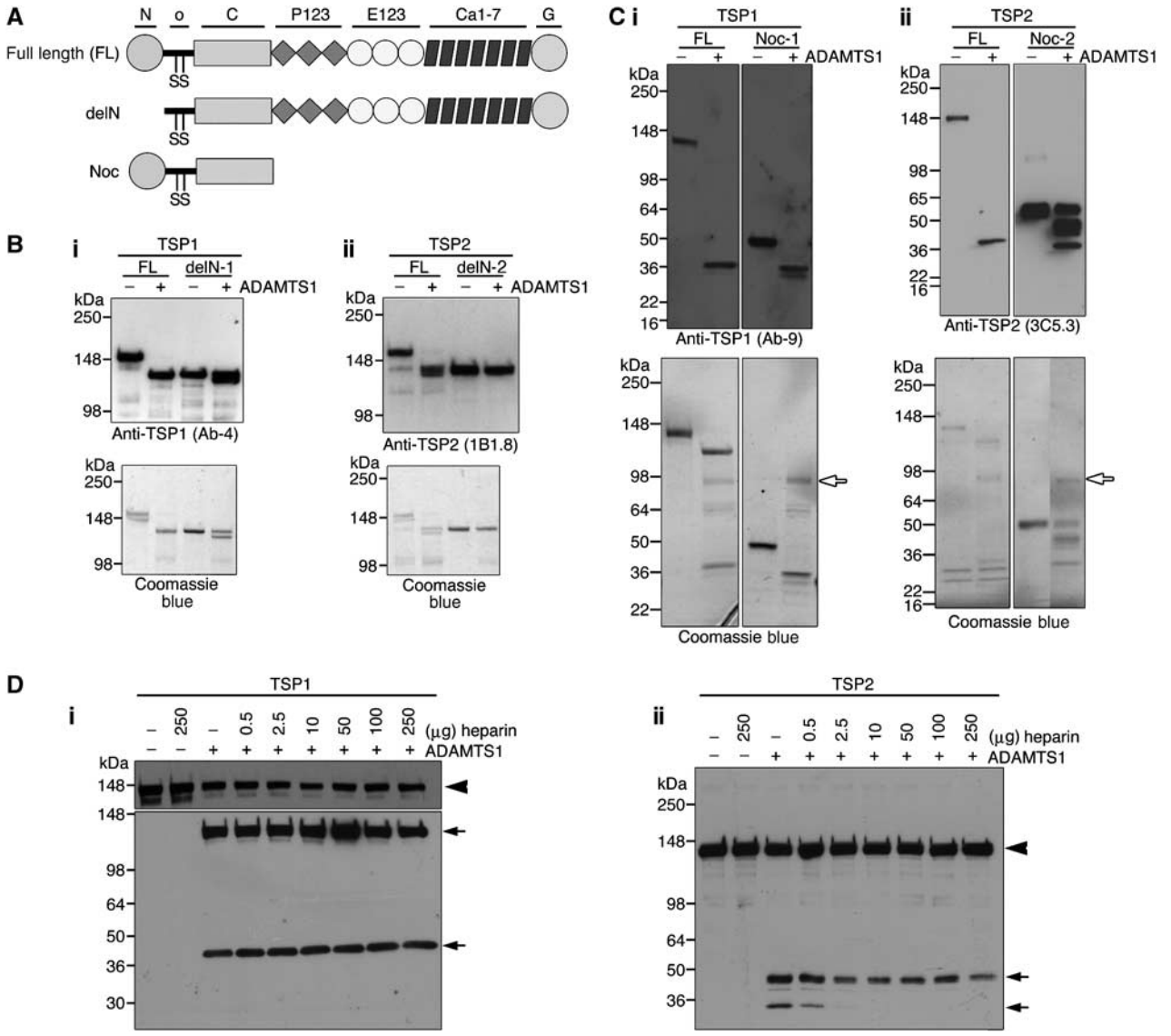

Figure 4 Heparin binding domains are important for cleavage. (**A**) schematic diagram of full-length TSP1 and 2 and deletion mutants. (**B** (i, ii), Western immunoblots and Coomassie staining of full-length TSP1 and delN-1 or TSP2 and delN-2 digested with ADAMTS1. (**C** (i, ii)), Western immunoblots and Coomassie staining of full-length TSP1 and truncated mutant NoC-1truncated or TSP2 and NoC-2 digested with ADAMTS1. Open arrows, ADAMTS1 protein. (**D** (i, ii)) TSP1 and 2 digested with ADAMTS1 in presence of increasing amounts of heparin. Arrowhead, full-length protein; arrows, cleaved fragments.

spond to the C-terminal fragment lacking the N-terminal domain (data not shown). Both fragments were transferred to PVDF, Edman sequencing resolved only the lower doublet fragment and revealed the sequence LIGGPP (Figure 5B). This indicates that one of the cleavage sites in TSP2 lies between glutamic acid 306 and leucine 307 (Figure 6A).

The second cleavage site in TSP2 remains to be determined; however, the monoclonal antibody used to detect TSP2 (3C5.3) recognizes the N-module, indicating that this cleavage is likely occur towards the N-terminal region.

Proteolytic activity of ADAMTS1 releases monomeric C-terminal peptides from TSP1 and 2

Native TSP1 and 2 exist as homotrimers linked by intermolecular disulfide bonds and the coiled-coil oligomerization domain (Engel, 2004). Additional intramolecular disulfide bonds exist within the linker region between the coiled-coil domain and the procollagen homology domain (Misenheimer *et al*, 2000). Based on the mapped cleavage site, ADAMTS1 proteolysis could have two possible outcomes: (1) release the C-terminus fragment from the N-terminus fragment; or (2) cleavage could target the disulfide bond region resulting in a nicked protein where the N-terminus remains attached to the C-terminus by disulfide bonds. To distinguish between these two possibilities, digested proteins were separated under reducing and nonreducing conditions (Figure 6B and C). The 36 kDa N-terminus fragment of TSP1 (reducing condition) was detected as a 108 kDa fragment (nonreducing) (Figure 6B), indicating that the N-terminus remained trimerized after ADAMTS1 cleavage. Since the N-terminus is the only known region required to mediate trimer formation, the 110 kDa C-terminus fragment is released in a monomeric form. Analysis of the TSP2 digestion products revealed that

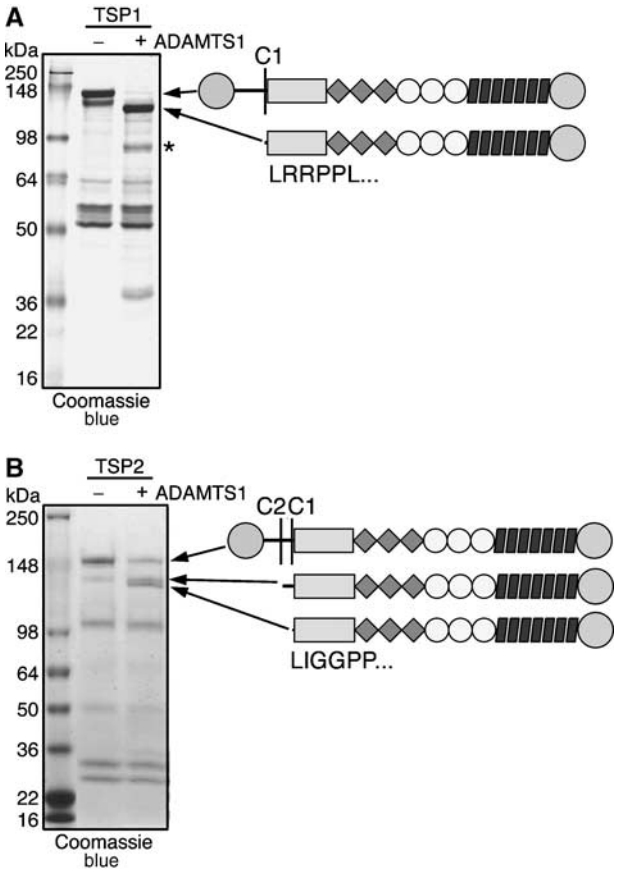

Figure 5 TSP1 and 2 cleavage sites and schematic representation of resulting fragments. (**A**) TSP1 is cleaved at one site C1 by ADAMTS1 adjacent to amino-acid sequence LRRPPL (determined by Edman degradation sequencing). (**B**) TSP2 is cleaved at two sites C1 and C2. Site C1 is adjacent to amino acids LIGGPP. Proteins were visualized with Coomassie. Asterisk in (A) represents ADAMTS1.

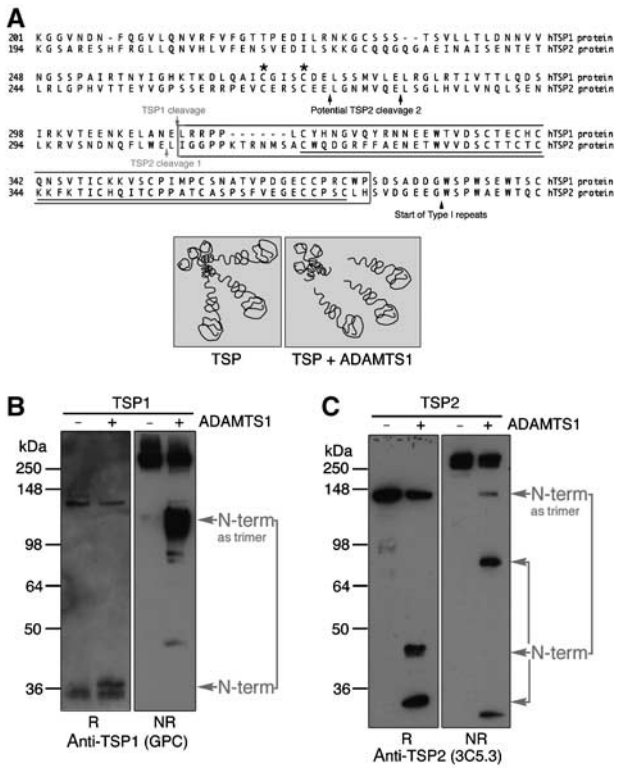

Figure 6 N-terminal fragments remain trimerized releasing the monomeric C-terminal fragments. (**A**) Sequence alignment of TSP1 and 2 including region in proximity of cleavage sites. Boxed region represents pro-collagen domain. Underlined sequence corresponds to the coiled-coil region. Asterisks denote cysteines involved in interchain disulfide bonds. Inset, schematic representation of N-terminal and C-terminal fragments in reducing (R) and nonreducing (NR) conditions. (**B, C**) Western immunoblots of TSP1 and 2 incubated with ADAMTS1 or vehicle under nonreducing and reducing conditions.

ADAMTS1 cleavage of this molecule also releases the C-terminus fragment as a monomer leaving the N-terminus in a trimeric form. Under nonreducing conditions, the 42 kDa N-terminus fragment was shifted to a 145-kDa band (Figure 6C). Trimerization of the 42 kDa would yield a complex of approximately 126 kDa in size. The discrepancy between the 142 kDa band and the expected 126 kDa band is likely due to glycosylation. In addition, the 30 kDa N-terminus fragment (reducing condition) shifted to a 90-kDa band (nonreducing condition) corresponding to a trimerized 30-kDa fragment (Figure 6C).

ADAMTS1 cleaves murine TSP1

Since murine TSP1 shares high sequence identity to the human orthologue, we assessed whether mTSP1 is also cleaved by ADAMTS1 (Figure 7B). Adenoviral constructs expressing active ADAMTS1, inactive ADAMTS1 or GFP were used to infect 293T cells. Conditioned medium (CM) was collected 24 h postinfection and was subsequently incubated with either purified hTSP1 or mTSP1 from mouse LE II cells at 37°C for 2 h. Under these conditions, mTSP1 was also cleaved by ADAMTS1 releasing a 36 kDa fragment indicating that the cleavage site was likely to be in the same region in both species (Figure 7A).

Characterization of neo-epitope antibodies

To further explore the significance of the processing events, we developed neo-epitope antibodies against the cleaved sites and the spanning region using flanking peptides, NRELVSE (#78) and LKRPPLC (#79), and the spanning TEENRELVSELKRPPL peptide (#80). All three antibodies were affinity-purified with their corresponding immunizing peptides and cross-absorbed to eliminate unwanted reactivities. We then tested their specificity against TSP1 cleaved by either thrombin or ADAMTS1. Antibody #78 specifically recognized the 36 kDa TSP1 fragment released by ADAMTS1 cleavage. Similarly, antibody #79 specifically recognized the 110 kDa TSP1 fragment. Antibody #80 recognized intact TSP1 as well as thrombin-cleaved TSP1 as the polypeptide retained the spanning region. All antibodies worked in reduced and nonreduced conditions (Figure 7C).

TSP1 is cleaved by ADAMTS1 during wound healing

It has been previously shown that ADAMTS1 is upregulated in inflammatory situations, a feature also shared by TSP1 (Agah *et al*, 2002). Thus, we investigated whether TSP1 fragments could be detected in excisional skin wound healing assays at 2-day postinjury. We made full-thickness wounds on the dorsal skin of ADAMTS1 null mice and wild-type siblings.

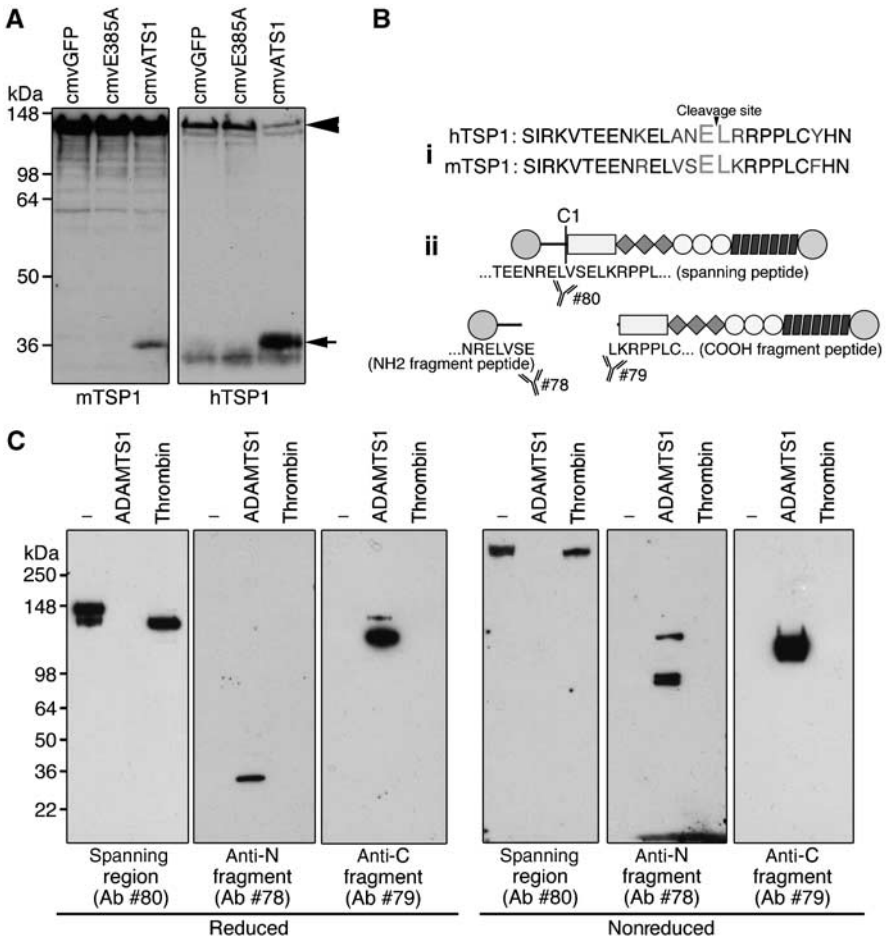

Figure 7 Characterization of TSP1 neo-epitope antibodies. (**A**) Western immunoblot of murine and human TSP1 incubated with CM from adenovirus infected cells expressing GFP (cmvGFP), inactive ADAMTS1 (cmvE385A) or full-length active ADAMTS1 (cmvATS1). (**B** (i)) Sequence alignment of human and murine TSP1 residues flanking cleavage site. (ii) Schematic diagram of TSP1 and fragments recognized by neo-epitope antibodies (78 and 79) and antibody to spanning region (80). (**C**) Western immunoblot of intact TSP1 and TSP1 fragments resulting from processing with either thrombin or ADAMTS1 under reducing and nonreducing conditions. Arrowhead, full-length TSP1; arrow, TSP1 fragment.

Intact TSP1 expression was found at the leading wound edge epithelium, fibrin clot and hair follicles in the ADAMTS1 null animals (Figure 8A (d), arrow denotes the leading edge). In comparison, less intense staining of intact TSP1 was found in the leading wound edge of the wild-type siblings (Figure 8A (a)). However, comparable levels of TSP1 protein were localized to the fibrin clot and hair follicles. In contrast, both N- and C-terminal fragments of TSP1 were present on the leading edge in the wound epithelium and hair follicles in wild-type animals (Figure 8A (b and c)). ADAMTS1 null animals displayed less intense staining of both N- and C-terminal TSP1 fragments (Figure 8A (e and f)).

ADAMTS1 has been shown to be expressed by CD11b positive cells within the clot by 1-day postinjury (Krampert *et al*, 2005). We analyzed the localization of TSP1 fragments within the clot of 2-day wounds. As expected, intact TSP1 was found in both wild-type and ADAMTS1 null clots (Figure 8A (g and j), arrows). However, the N-terminal TSP1 fragment was only found in the clot of wild-type animals (Figure 8A (h), arrows). The C-terminal fragment was not visible in either wild type or ADAMTS1 null animals. A finding that suggests that this fragment is likely soluble and short lived (Figure 8A (i and l)).

Immunoprecipitation of wound lysates using the anti-amino fragment antibody (#78) pulled down a 40 kDa species in wild-type sample, this fragment was not detected on the ADAMTS1 null sample (Figure 8B, arrow). Similarly, immunoprecipitation with the anticarboxy fragment antibody (#79) pulled down a 110-kDa fragment in the wild-type sample and to a lower degree in the ADAMTS1 null sample (Figure 8B, arrowhead). Immunoprecipitation with the anti-spanning peptide antibody (#80) was able to precipitate a 145 kDa fragment that corresponds to the intact TSP1 (Figure 8B, asterisk).

At 5-day postinjury, wounds were closed in the wild-type animals and the new epithelial layer covering the wound was thicker than the surrounding epithelia (Figure 9A (a)). In contrast, ADAMTS1 null wounds remained open with poor epithelial migration (Figure 9A (b), arrows). Evaluation of capillary density revealed more vessels in the dermis of ADAMTS1 null mice than in control littermates (Figure 9C and D).

Since ADAMTS1 null wounds exhibited greater vessel density, we explored the possibility that ADAMTS1 might release soluble TSP1 fragments from matrix-bound TSP. Cultures of human umbilical vascular endothelial cells

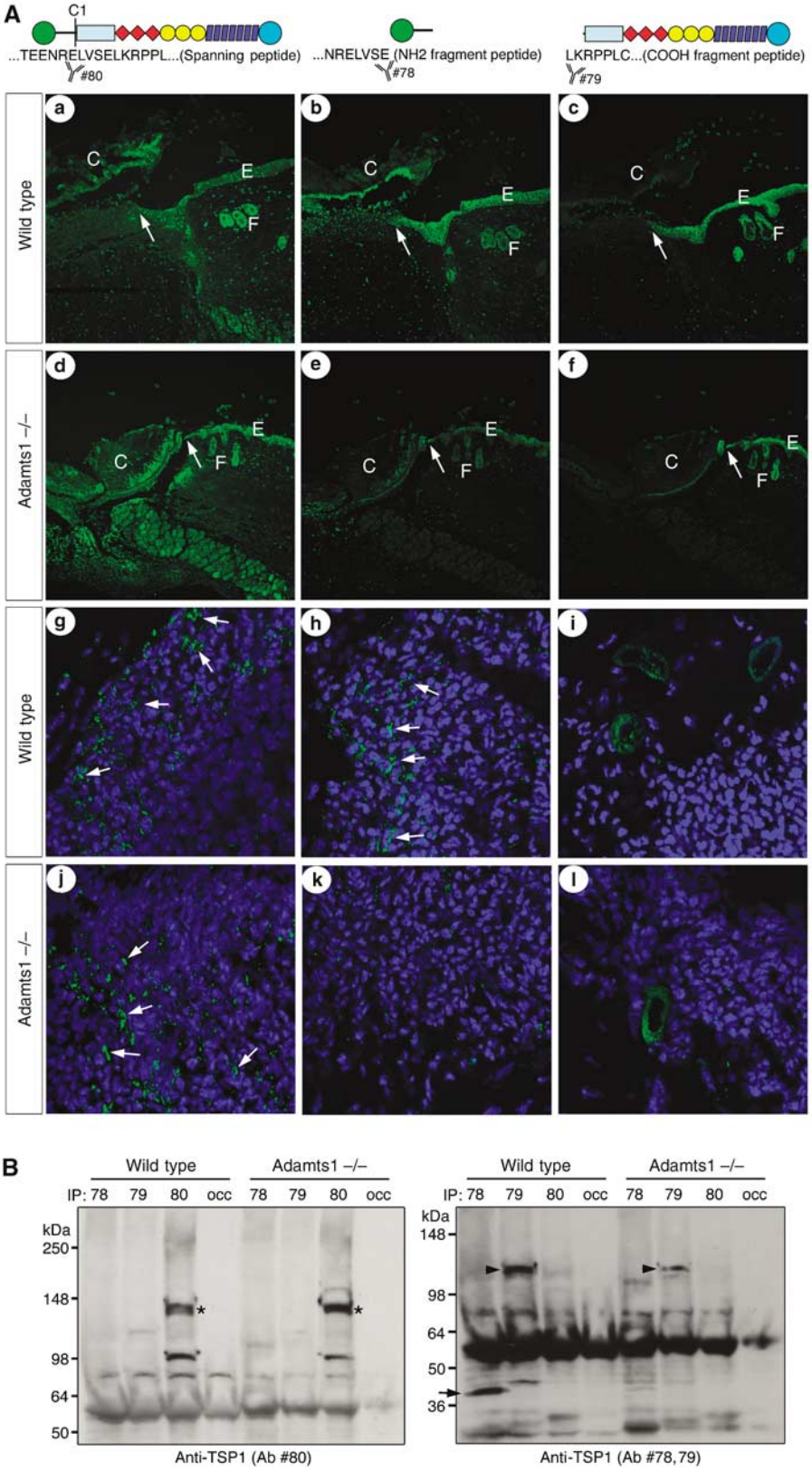

Figure 8 TSP1 cleavage by ADAMTS1 occurs during excisional wound healing. (**A**) (**a–f**) Immunohistochemical staining of intact TSP1 and TSP1 fragments in 2-day excisional wound serial sections using the spanning region antibody (#80) or neo-epitope antibodies (#78 and #79). (Arrow in a–f, invading front of epidermal cells; C: fibrin clot; E: epidermis; F: hair follicles) (A). (**g–l**), Immunohistochemical staining of intact TSP1 and fragments within fibrin clot. Arrows in (g and j), intact TSP1; arrows in (h), N-terminal TSP1 fragment. (**B**) Western immunoblot of TSP1 (intact and fragments) immunoprecipitated with anti-TSP1 antibodies (#78, 79 or 80) and anti-occludin (occ). Western immunoblot was performed using either #78, 79 or 80 (arrowhead: C-terminal TSP1 fragment; arrow: N- terminal TSP1 fragment; asterisk: intact TSP1).

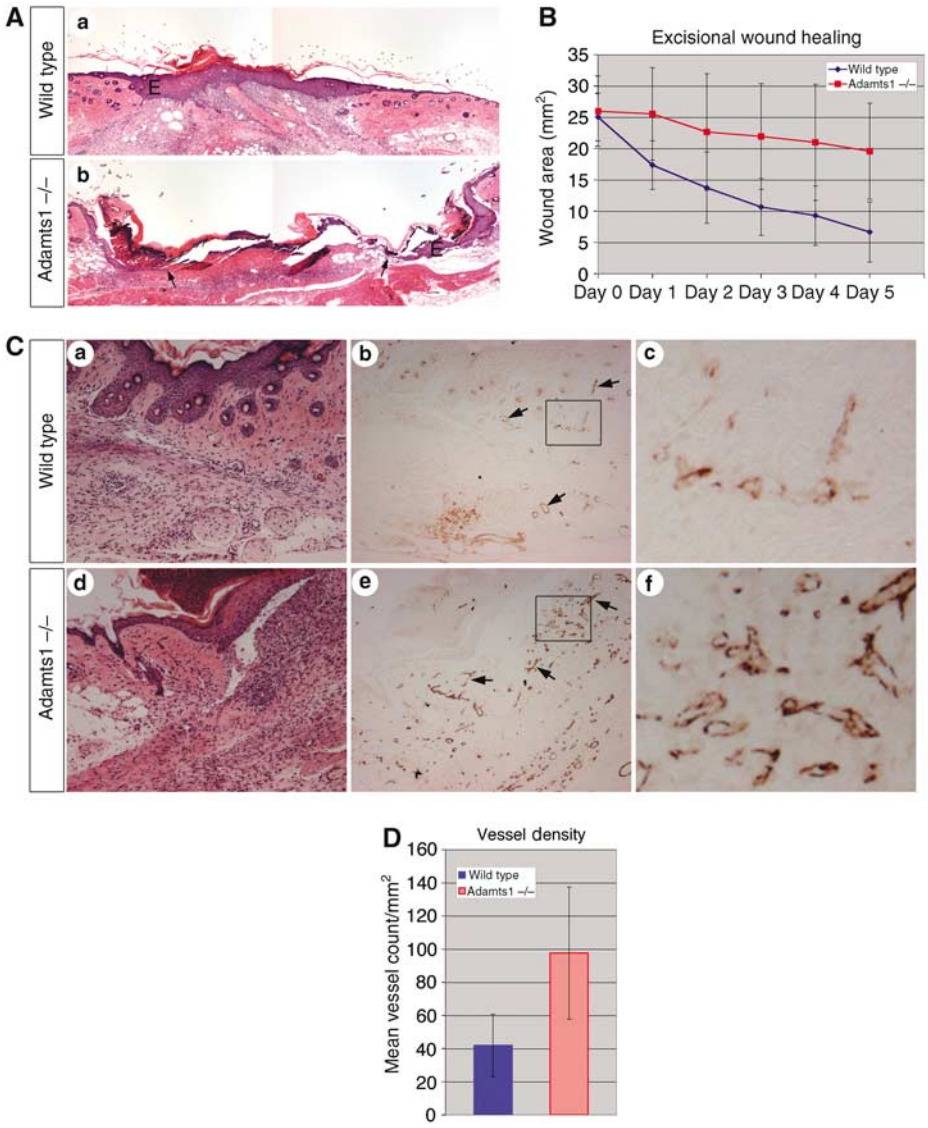

Figure 9 ADAMTS1 null animals exhibits delayed wound healing and increased angiogenesis. (**A**) Hematoxylin and eosin stained 5-day wound cross-sections of wild-type and ADAMTS1 null animals. (**B**) Excisional wound opening area quantified over 5 days in wild-type and adamts1 null animals. Difference in open wound area between wild-type and adamts1 null from day 1 onward has a *P*-value <0.005. (**C**) Hematoxylin and eosin (**a**, **d**) anti-PECAM stained (**b**, **c**, **e**, **f**) blood vessels within wound cross-sections. (c) and (f) are magnified images of boxed area in (b) and (e), respectively. (**D**) Quantification of blood vessels in wounds. Bars indicate standard error. Difference in mean vessel count between wild-type and adamts1 null has a *P*-value <0.005.

(HUVEC) were exposed to ADAMTS1 or vehicle. ADAMTS1 was able to process intact TSP1 to 110 and 36 kDa fragments, which were detected in the CM. Because *in vivo* TSP1 is frequently found incorporated in the matrix, we performed a second experiment, using matrix preparations in the absence of cells. Exposure of cell-free extracellular matrices to ADAMTS1 resulted in the processing of TSP1 and release of the 110 kDa C-terminal fragment from matrix-bound TSP1 (Figure 10A, SUP). The N-terminal fragment (Figure 10A, second panel, solid and open arrow) was found both in the supernatant, as well as bound to the matrix in the form of 36 and 25 kDa fragments (this second one, a result of further processing by thrombin).

TSP1 fragments inhibit endothelial cell proliferation

We next examined the effect of these TSP1 fragments on cell proliferation. For these experiments, we first devised a purification procedure to isolate each polypeptide from intact TSP1 (Figure 10B). Both fragments were able to suppress growth factor (FGF-2 and VEGF) induced proliferation (Figure 10C). It should be stressed that in this experimental setting, both fragments were delivered in a soluble form. In tissues, however, only the 110-kDa fragment is likely to be presented in a soluble form and provide antiproliferative signals (see Discussion).

To further explore the relationship between ADAMTS1 and TSP1 in angiogenesis, we isolated endothelial cells from TSP1 null and wild-type mice and evaluated their proliferation in response to ADAMTS1 (Figure 10F). As previously shown, exposure of endothelial cells to ADAMTS1 resulted in inhibition of FGF-2-driven endothelial cell proliferation to approximately 36%. In contrast, the absence of TSP1 significantly attenuates the inhibitory effect mediated by ADAMTS1 (Figure 10F).

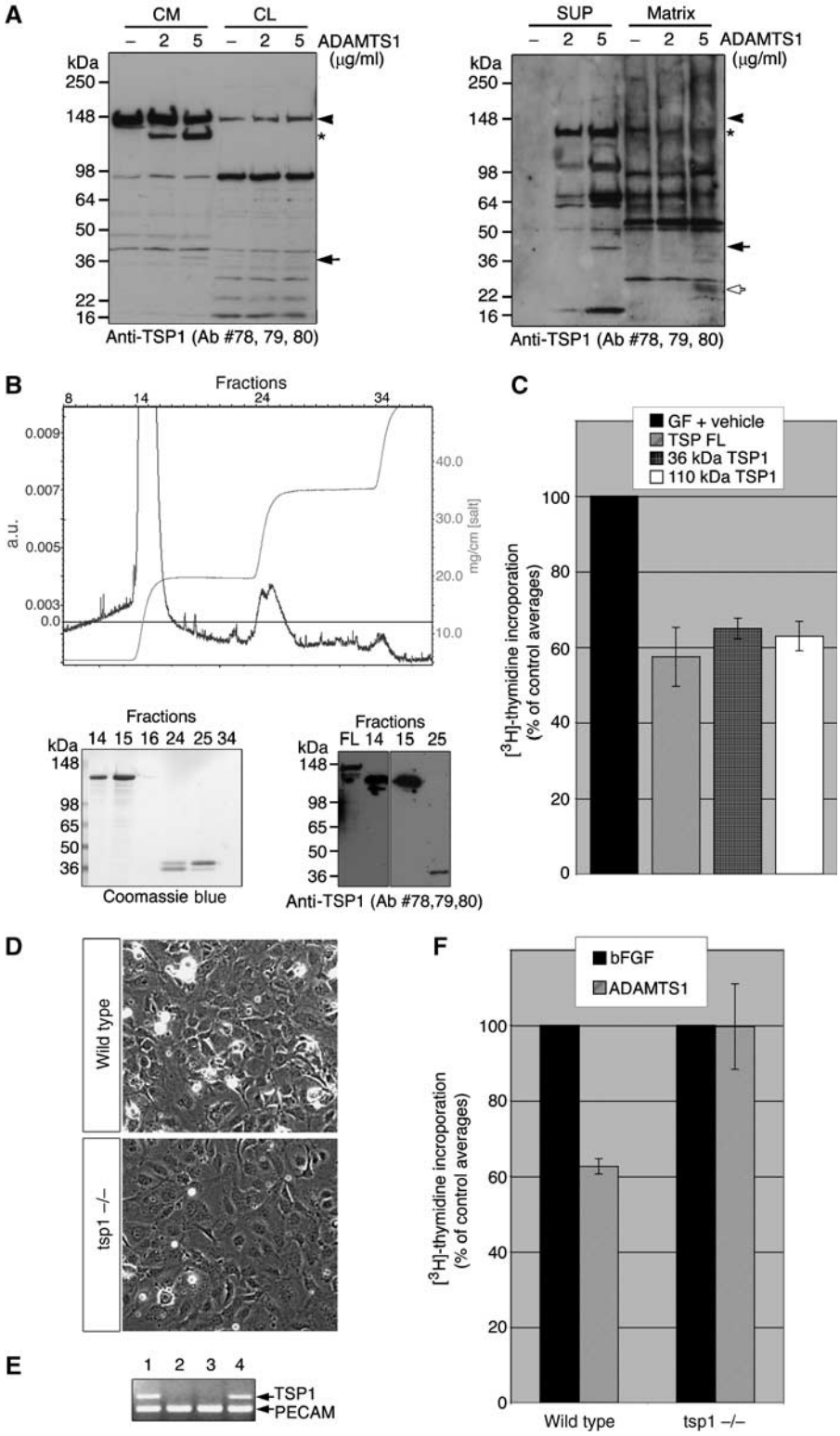

Figure 10 TSP1 fragments are released by endothelial cells and suppress proliferation. (**A**) Western immunoblots of TSP1 (intact and fragments) secreted from cells (CM), in the cell layer (CL), released from the matrix (SUP) or matrix bound (matrix) incubated with vehicle or ADAMTS1 at the indicated amounts. Arrowhead, intact TSP1; asterisk, C-term fragment; arrow, N-term fragment. (**B**) Elution chromatogram of TSP1 fragments. Elution of proteins was monitored by absorbance (a.u. on left) and conductivity is shown on the right. Fractions containing eluted proteins were separated by SDS–PAGE and visualized by Coomassie staining and Western immunoblotting with anti-TSP1 antibodies. FL, full-length TSP1 protein. (**C**) [^{3}H]thymidine incorporation in bovine aortic endothelial cells stimulated with GF (FGF-2 and VEGF) and treated with vehicle, full-length TSP1, or purified TSP1 cleavage products (36 and 110 kDa). (**D**) Phase micrograph of cultured primary mouse lung endothelial cells isolated from wild-type and tsp1 null animals at passage 3. (**E**) Representative RT–PCR from cDNA of isolated lung endothelial cells from wild-type (lanes 1 and 4) and tsp1 null animals (lanes 2 and 3). (**F**) [^{3}H]thymidine incorporation in wild-type and tsp1 null mouse lung endothelial cells stimulated with FGF-2 and treated with vehicle or ADAMTS1. [^{3}H]thymidine incorporation shown as an average percent of control.

Discussion

Proteolytic processing of matrix proteins and growth factors is a mechanism for the generation of bioactive peptides of significant biological impact. Here, we have identified TSP1 and 2 as novel substrates for ADAMTS1, a metalloprotease previously shown to inhibit angiogenesis when used at pharmacological doses *in vivo* and *in vitro* (Vazquez *et al*, 1999; Luque *et al*, 2003). Interestingly, we further demonstrate that cleavage generates a pool of TSP1 antiangiogenic polypeptides and that this mechanism is essential for most of the endothelial inhibitory activity of ADAMTS1 *in vitro*. The TSP1 fragments were also detected in wound-healing assays *in vivo*. Furthermore, the absence of ADAMTS1 was associated with delayed wound healing and enhanced vascular density; a phenotype that mirrors wound healing in TSP1 null mice (Agah *et al*, 2002; Lawler and Detmar, 2004). Together, these findings argue that the generation of antiangiogenic peptides from TSP1 is a physiologically important function of ADAMTS1.

TSP1 and 2 have been shown to be relevant endogenous inhibitors of angiogenesis (Streit *et al*, 1999; Rodriguez-Manzaneque *et al*, 2001). The effects of TSP1 on endothelial cells have been shown to occur, in some cases by direct receptor signaling (Dawson *et al*, 1997; Jimenez *et al*, 2000), and in other cases through the ability of TSP1 to interact with other extracellular proteins (Taraboletti *et al*, 1997; Iruela-Arispe *et al*, 1999). In fact, by nature of its interaction with proteoglycans, extracellular matrix molecules, proteases and growth factors, TSP1 directs the assembly of multiprotein complexes that modulate cellular function. Understanding the biological significance of TSP-ECM interactions has become a challenge for investigators in this field as the protein has the potential to impact cell function in a context-dependent manner. The generation of TSP1 null mice has demonstrated that this protein is required for the regulation of epithelial growth in the lung, lung homeostasis and wound healing (Lawler *et al*, 1998; Agah *et al*, 2002). The absence of TSP1 results in multifocal pneumonia and increased inflammatory events (Lawler *et al*, 1998). In addition, the animals display hyperplasia of pancreatic islands and show delayed wound healing (Crawford *et al*, 1998; Agah *et al*, 2002). Particularly interesting was the observation that TSP1 null animals showed a reduced litter number and increased blood vessel profiles in several organs (Crawford *et al*, 1998; Lawler *et al*, 1998).

The antiangiogenic effects of TSP1 have been well documented in several *in vivo* and *in vitro* models (Tolsma *et al*, 1993; Dawson *et al*, 1997; Taraboletti *et al*, 1997; Iruela-Arispe *et al*, 1999). More importantly, genetic manipulations that result in TSP1 overexpression using tissue-specific promoters strongly support the participation of this protein in the regulation of vascular growth and vessel diameter. In particular, two transgenic studies using the K14 promoter to drive TSP1 in the skin (Streit *et al*, 2000) and, the MMTV-promoter, to target expression to the mammary epithelium (Rodriguez-Manzaneque *et al*, 2001), support a role for this protein in the regulation of vascular morphogenesis in whole animal settings. TSP1 also modulates the size of vascular channels. These functions are also shared by TSP2, as both molecules shared the antiangiogenic domain located in the TSR repeats (Lawler and Detmar, 2004).

Cleavage of TSP1 and 2 by ADAMTS1 could modulate their functions in one of two ways: it could facilitate remodeling of matrix-associated TSP and/or release bioactive domains that might be unavailable when the protein is integrated in the matrix milieu (Nicosia and Tuszynski, 1994). The last possibility is not entirely surprising, as several studies have demonstrated activation of bioactive antiangiogenic polypeptides generated by proteolysis. Cleavage of collagen IV, XVIII and plasminogen results in the release of angiogenesis inhibitors, a function that is only gained through proteolysis (Cao *et al*, 1996; Dong *et al*, 1997; O'Reilly *et al*, 1999; Ferreras *et al*, 2000). Alternatively, cleavage of collagen IV by MMP9 unmasks a cryptic site that stimulates migration of endothelial cells and angiogenesis *in vivo* (Xu *et al*, 2001; Hangai *et al*, 2002). Thus, the nature of the cleavage could lead to potentially opposite outcomes. In the case of type IV collagen, both enhancement and suppression of angiogenesis have been demonstrated. Along the same lines, TSP1 was shown to enhance angiogenesis in some settings.

Structural information on TSP1 has been rapidly accumulating. The crystal structure of the N-terminal region has been recently resolved (Tan *et al*, 2006), as has the procollagen module (O'Leary *et al*, 2004) and the TSR (antiangiogenic repeats) (Tan *et al*, 2002). This information combined with the resolution of the last three type 3 repeats and C-terminal domain (Kvansakul *et al*, 2004) provides a comprehensive atomic information and provides a molecular image for TSP1. Together these data suggest that there is only one flexible, protease-sensitive area that lies between the N-terminal and the oligomerization domain. Indeed, our results show that the cleavage sites within TSP1 and 2 are located within the procollagen domain in proximity of the alpha helical loops and intramolecular disulfide bonds and thus dividing the molecule into two fragments: N-terminal that remains trimeric and a more soluble, monomeric, C-terminal fragment that exposes the TSR/antiangiogenic modules.

Our data have shown that the C-terminal 110 kDa fragment is as potent as intact TSP1 towards inhibiting endothelial cell proliferation and, *in vivo*, this is likely the fragment that conveys antiangiogenic effects. The state of soluble versus bound TSP1 has important biological relevance when understanding the angiostatic effects of this protein. In fact, several studies have shown that matrix-bound (insoluble) TSP1 stimulates, rather than inhibits angiogenesis (Nicosia and Tuszynski, 1994; Ferrari do Outeiro-Bernstein *et al*, 2002). Due to its multiple interactions with cells and matrix proteins, once secreted, extracellular TSP1 is incorporated in the extracellular matrix mostly by its N-terminus. The majority of integrin binding sites, as well as, calreticulin binding have been mapped to the beta strands located in the N-terminal region (Krutzsch *et al*, 1999; Calzada *et al*, 2003, 2004). Furthermore, the large majority of the protein/proteoglycan-binding motifs have been located within this N-terminal domain. Cleavage of intact matrix-bound TSP1 likely releases a soluble C-terminal monomer and leaving bound trimeric N-terminal fragments. Hence, processing by ADAMTS1 would uncover the antiangiogenic potential of matrix-bound TSP. Together these findings shed light on a long-term controversy in the field as to the pro- and antiangiogenic effects attributed to TSP1 in different experimental settings.

Finally, it is interesting to consider the similarities between the ADAMTS1 and the TSP1 null mice. Both exhibit delay in

wound healing, excessive curvature in their spines indicating osteogenic problems and poor fertility in females (Lawler *et al*, 1998; Shindo *et al*, 2000; Agah *et al*, 2002). While these mice do also exhibit nonoverlapping phenotypes, the findings here would indicate that at least in the skin the biology of these two proteins interject and are required for the normal resolution of wound healing and regulated angiogenic progression.

Materials and methods

Reagents

TSP1 was purified as previously described (Rodriguez-Manzaneque *et al*, 2001). Human TSP2 and truncated TSP1 and 2 fragments (delN-1, delN-2, NoC-1 and NoC-2) were purified as previously described (Annis *et al*, 2006). Murine TSP1 was collected from culture supernatant secreted by lung endothelial cells (LE II). TSP1 antibody GPC was raised in guinea-pig (GPC) (Rodriguez-Manzaneque *et al*, 2001). TSP1 antibodies (Ab-9, Ab-4) were purchased from Neomarkers (Fremont, CA): Ab-9 = MBC200.1 and binds the heparin binding domain; Ab-4 = A6.1 and binds to the first calcium binding loop in the calcium wire (Annis *et al*, 2006).

TSP2 antibodies 3C5.3 and 1B1.8 were raised in collaboration with the hybridoma core facility at the University of Alabama. The murine monoclonal antibodies 3C5.3 and 1B1.8 are specific for TSP2. 3C5.3 recognizes an epitope in the N-module and 1B1.8 reacts with the third properdin repeat.

Recombinant ADAMTS1 was purified as previously described (Rodriguez-Manzaneque *et al*, 2000), and dialyzed in 250 mM NaCl, 10 mM HEPES pH 7.5, 1 mM $CaCl_2$. Activity of the enzyme was assessed by proteolytic cleavage of aggrecan.

Recombinant ADAMTS1 containing a glutamic acid to alanine mutation (zinc binding mutant, catalytically inactive) and recombinant ADAMTS1 C-terminal fragment (TSRs) were isolated as previously described (Rodriguez-Manzaneque *et al*, 2002). Recombinant ADAMTS4 was purchased from (Chemicon, CA). Purified aggrecan from rat chondrosarcoma cell line was a gift from Dr John Sandy (Shriners Hosp., FL).

TSP1 fragments (36 and 110 kDa) were purified using heparin HiTrap columns (GE Healtcare Life Sciences, Piscataway, NJ).

Digestion assays

TSP1, TSP2 or laminin were incubated with 87, 65 kDa ADAMTS1 protein or vehicle, at E:S of 1:1 or indicated E:S, in a buffer containing 50 mM Tris pH 7.4, 10 mM $CaCl_2$, 80 mM NaCl for 2 h at 37°C in a maximum volume of 60 μl. Samples were resolved on 10% or 4–12% gradient (Invitrogen, Carlsbad, CA) SDS–PAGE.

Additional controls for ADAMTS1 cleavage assays included a catalytically inactive ADAMTS1 mutant (E385A), ADAMTS1 C-terminal fragment (TSRs), and ADAMTS4 (Chemicon) for indicated times.

TSP1 and 2 fragments, delN and NoC (1 μg each) were incubated with ADAMTS1 (87 kDa) for 2 h at 37°C and detected with indicated antibodies. TSP1 and 2 (2 μg) were also incubated with ADAMTS1 (50 ng) (E:S of 1:40) in the presence of heparin (Sigma) ranging from 0.5 to 250 ng for 1 h at 37°C.

Densitometric analysis of fragments was performed by scanning with a Personal Densitometer SI (Molecular Dynamics/GE Healthcare) and analyzed with ImageQuant 5.2 (Molecular Dynamics).

Aggrecan assays

Rat aggrecan (10 μg) was incubated with ADAMTS1 and ADAMTS4 (1 μg each) in 50 mM Tris pH 7.4, 10 mM $CaCl_2$, 80 mM NaCl for 2 h at 37°C. Samples were deglycosylated with Chondroitinase ABC (Sigma) in 50 mM Tris, 10 mM EDTA pH 8.0 at 37°C for 1 h prior to separation on 10% SDS–PAGE.

Digestion of murine and human TSP1 by cells infected with ADAMTS1 adenovirus

293T cells were infected with adenovirus expressing GFP (control), inactive ADAMTS1 (cmvE385A), or active ADAMTS1 (cmvATS1) at 5 MOI. Infection efficiency was assessed by visualization of GFP and estimated to be 80–85%. CM was collected after 24 h of incubation. Murine TSP1 (CM from LE II cells) and purified hTSP1 (2 μg) were incubated with CM from adenoviral infected 293T cells at 37°C for 4 h.

Mass spectrometry and N-terminal Edman degradation sequencing

TSP1 digested with ADAMTS1 was separated by 10% SDS–PAGE. Bands of interest were excised, digested with trypsin and analyzed with MALDI-TOF-MS (Applied Biosystems Voyager DE-STR mass spectrometer; Foster City, CA), and LC-MS using a nano-HPLC system (Dionex-LC Packings, Sunnyvale, CA) and a QSTAR Pulsar XL (QqTOF; Applied Biosystems, Foster City, CA) mass spectrometer equipped with a nano-electrospray interface (Protana, Denmark). TSP1 and 2 fragments were also separated by 10% tris–glycine gel electrophoresis and transferred to a PVDF membrane (BIO-RAD, Hercules, CA). After staining with Ponceau Red, the 110 kDa (TSP1) band and the 100 kDa (TSP2) doublets were excised and Edman N-terminal degradation sequencing was performed by Dr Gary Hathaway (Caltech PPMAL, Pasadena, CA).

Wound assays

Mice (2–4 month old) were anesthesized using an anesthetic vaporizer (Summit Medical, Bend, OR). The skin was shaved and sterilized. Two full-thickness excisional wounds were made on either side of the dorsal midline using 5 mm dermal punches (Krampert *et al*, 2005).

Wounds were photographed with a Sony DSC-W7 digital camera 13 cm away from the animals daily for 5 consecutive days. Open wound area was measured with ImagePro 5.0 (Media Cybernetics, Silver Spring, MD.). Statistical analysis was performed using the paired Student's *t*-test.

Wound sections were immunostained with anti-PECAM (BD Pharmingen, San Diego, CA). Images were captured from five random areas of 0.5 mm^2 per wound section at 10× and vessels counted manually. Statistical analysis was performed using the paired Student's *t*-test.

Immunohistochemistry

Paraffin-embedded skin wounds serially sectioned from the middle (5 μm thickness) were incubated with rabbit anti-TSP1 neo-epitope antibodies (#78, 79 or 80) at (20, 10 and 10 μg/ml, respectively) and subsequently incubated with anti-rabbit IgG conjugated to FITC (Sigma). Fluorescence IHC was analyzed using an MRC 1024ES confocal microscope (Carl Zeiss, Germany).

Tissue lysate preparation and immunoprecipitation

Wounds were ground up in liquid nitrogen and incubated with RIPA buffer (50 mM Tris pH 7.4, 150 mM NaCl, 1% NP-40, 0.25% sodium deoxycholate, 1 mM sodium orthovanadate, 10 mM β-glycerophosphate, 1 mM PMSF, 20 μg/ml leupeptin, 20 μg/ml aprotinin) for 3 h at 4°C. The lysate was precleared using Protein-G agarose beads (Roche, Indianapolis, IN) and 4 mg of each lysate was incubated with each anti-TSP1 neo-epitope antibodies (#78, 15 μg, #79, 10 μg and #80, 10 μg) and subsequently with protein G agarose. Bound proteins were released from beads with Laemli buffer containing β-mercaptoethanol and resolved by 4–12% gradient SDS–PAGE (Invitrogen).

Cleavage of TSP1 in cultured HUVEC cells by ADAMTS1

HUVEC (VEC, Rensselaer, NY) were then treated with ADAMTS1 or vehicle for 4 h at 37°C. CM was collected and concentrated with StrataResin (Stratagene). Bound proteins were released with Laemli containing β-mercaptoethanol and the remaining cell layer was also harvested. Both cell layer and CM fraction proteins were resolved by 4–12% gradient SDS–PAGE (Invitrogen).

Cleavage of matrix-incorporated TSP1 by ADAMTS1

HUVEC (VEC) were grown to confluency for several days. The cell layer was removed from the established matrix by incubating with cold 0.1% (w/v) sodium deoxycholate, 2 mM EDTA (Skill *et al*, 2004). The remaining matrix was treated with ADAMTS1 or vehicle in DMEM for 2 h at 37°C. Subsequently, the supernatant was collected and concentrated. The remaining matrix was solubilized with Laemli.

Isolation of mouse endothelial cells

Lungs were removed from 8 to 10 weeks old TSP1+/+ and TSP1−/− littermates. After mincing, tissue was incubated in

serum-free media containing collagenase 1 mg/ml and dispase II 2 mg/ml under constant agitation for 30 min. Suspensions were stained with anti-PECAM-PE (BD Biosciences, San Jose, CA) and CD45-FITC conjugated (BD Biosciences) for 1 h at 4°C and sorted subsequently using a FACS Star plus cell sorter (BD Biosciences).

Cell proliferation

Endothelial cells were quiesced by culturing postconfluency in DMEM with 0.2% FBS (16–24 h). Cells were then seeded onto 24-well plates in the presence of 0.2% serum, and subsequently stimulated with VEGF (200 ng/ml) (R&D Systems, Minneapolis, MN), and/or FGF-2 (R&D Systems) (4 ng/ml), and treated with vehicle, TSP1 (2.5 μg/ml), 36 kDa TSP1 (0.66 μg/ml), 110 kDa TSP1 (2 μg/ml), or ADAMTS1 (1 μg/ml) and incubated for 10–14 h followed by a 10 h pulse with 1 μCi/ml of [6–^{3}H]-thymidine (Amersham Biosciences, Piscataway, NJ). Subsequently, cells were fixed with 10% (w/v) trichloroacetic acid (Fisher Scientific), solubilized in scintillation fluid and counted with a Microbeta Trilux 1450 scintillation counter (Perkin Elmer, Wellesley, MA). Experiments were performed three independent times in triplicates and [6-^{3}H]-thymidine incorporation was represented as an average percent of control. Bovine aortic endothelial cells were used between passages 5–7. Mouse lung endothelial cells were used between passages 3–6.

Acknowledgements

We thank Jack Lawler for kindly providing purified thrombospondin and TSP1−/− mice, Liman Zhao for mouse colony husbandry, and members of the Arispe Lab for comments and discussions. The UCLA Functional Proteomics Center was established and equipped by a grant to UCLA from the WM Keck Foundation. This study was supported by funds from the National Institutes of Health (CA65624, CA77420 and HL54462). Nathan Lee was supported by the Vascular Biology Training grant at UCLA (HL69766).

References

Agah A, Kyriakides TR, Lawler J, Bornstein P (2002) The lack of thrombospondin-1 (TSP1) dictates the course of wound healing in double-TSP1/TSP2-null mice. *Am J Pathol* **161:** 831–839

Annis DS, Murphy-Ullrich JE, Mosher DF (2006) Function-blocking antithrombospondin-1 monoclonal antibodies. *J Thromb Haemost* **4:** 459–468

Apte SS (2004) A disintegrin-like and metalloprotease (reprolysin type) with thrombospondin type 1 motifs: the ADAMTS family. *Int J Biochem Cell Biol* **36:** 981–985

Bornstein P (1992) Thrombospondins: structure and regulation of expression. *FASEB J* **6:** 3290–3299

Bornstein P, Kyriakides TR, Yang Z, Armstrong LC, Birk DE (2000) Thrombospondin 2 modulates collagen fibrillogenesis and angiogenesis. *J Invest Dermatol Symp Proc* **5:** 61–66

Calzada MJ, Sipes JM, Krutzsch HC, Yurchenco PD, Annis DS, Mosher DF, Roberts DD (2003) Recognition of the N-terminal modules of thrombospondin-1 and thrombospondin-2 by alpha6beta1 integrin. *J Biol Chem* **278:** 40679–40687

Calzada MJ, Zhou L, Sipes JM, Zhang J, Krutzsch HC, Iruela-Arispe ML, Annis DS, Mosher DF, Roberts DD (2004) Alpha4beta1 integrin mediates selective endothelial cell responses to thrombospondins 1 and 2 *in vitro* and modulates angiogenesis *in vivo*. *Circ Res* **94:** 462–470

Canals F, Colome N, Ferrer C, Plaza-Calonge Mdel C, Rodriguez-Manzaneque JC (2006) Identification of substrates of the extracellular protease ADAMTS1 by DIGE proteomic analysis. *Proteomics* **6** (Suppl 1)**:** S28–S35

Cao Y, Ji RW, Davidson D, Schaller J, Marti D, Sohndel S, McCance SG, O'Reilly MS, Llinas M, Folkman J (1996) Kringle domains of human angiostatin. Characterization of the anti-proliferative activity on endothelial cells. *J Biol Chem* **271:** 29461–29467

Crawford SE, Stellmach V, Murphy-Ullrich JE, Ribeiro SM, Lawler J, Hynes RO, Boivin GP, Bouck N (1998) Thrombospondin-1 is a major activator of TGF-beta1 *in vivo*. *Cell* **93:** 1159–1170

Dawson DW, Pearce SF, Zhong R, Silverstein RL, Frazier WA, Bouck NP (1997) CD36 mediates the *in vitro* inhibitory effects of thrombospondin-1 on endothelial cells. *J Cell Biol* **138:** 707–717

Dong Z, Kumar R, Yang X, Fidler IJ (1997) Macrophage-derived metalloelastase is responsible for the generation of angiostatin in Lewis lung carcinoma. *Cell* **88:** 801–810

Engel J (2004) Role of oligomerization domains in thrombospondins and other extracellular matrix proteins. *Int J Biochem Cell Biol* **36:** 997–1004

Ferrari do Outeiro-Bernstein MA, Nunes SS, Andrade AC, Alves TR, Legrand C, Morandi V (2002) A recombinant NH(2)-terminal heparin-binding domain of the adhesive glycoprotein, thrombospondin-1, promotes endothelial tube formation and cell survival: a possible role for syndecan-4 proteoglycan. *Matrix Biol* **21:** 311–324

Ferreras M, Felbor U, Lenhard T, Olsen BR, Delaisse J (2000) Generation and degradation of human endostatin proteins by various proteinases. *FEBS Lett* **486:** 247–251

Gunther W, Skaftnesmo KO, Arnold H, Bjerkvig R, Terzis AJ (2005) Distribution patterns of the anti-angiogenic protein ADAMTS-1 during rat development. *Acta Histochem* **107:** 121–131

Hangai M, Kitaya N, Xu J, Chan CK, Kim JJ, Werb Z, Ryan SJ, Brooks PC (2002) Matrix metalloproteinase-9-dependent exposure of a cryptic migratory control site in collagen is required before retinal angiogenesis. *Am J Pathol* **161:** 1429–1437

Iruela-Arispe ML, Liska DJ, Sage EH, Bornstein P (1993) Differential expression of thrombospondin 1, 2, and 3 during murine development. *Dev Dyn* **197:** 40–56

Iruela-Arispe ML, Lombardo M, Krutzsch HC, Lawler J, Roberts DD (1999) Inhibition of angiogenesis by thrombospondin-1 is mediated by 2 independent regions within the type 1 repeats. *Circulation* **100:** 1423–1431

Jimenez B, Volpert OV, Crawford SE, Febbraio M, Silverstein RL, Bouck N (2000) Signals leading to apoptosis-dependent inhibition of neovascularization by thrombospondin-1. *Nat Med* **6:** 41–48

Kalluri R (2003) Basement membranes: structure, assembly and role in tumour angiogenesis. *Nat Rev Cancer* **3:** 422–433

Krampert M, Kuenzle S, Thai SN, Lee N, Iruela-Arispe ML, Werner S (2005) ADAMTS1 proteinase is up-regulated in wounded skin and regulates migration of fibroblasts and endothelial cells. *J Biol Chem* **280:** 23844–23852

Krutzsch HC, Choe BJ, Sipes JM, Guo N, Roberts DD (1999) Identification of an alpha(3)beta(1) integrin recognition sequence in thrombospondin-1. *J Biol Chem* **274:** 24080–24086

Kuno K, Matsushima K (1998) ADAMTS-1 protein anchors at the extracellular matrix through the thrombospondin type I motifs and its spacing region. *J Biol Chem* **273:** 13912–13917

Kuno K, Okada Y, Kawashima H, Nakamura H, Miyasaka M, Ohno H, Matsushima K (2000) ADAMTS-1 cleaves a cartilage proteoglycan, aggrecan. *FEBS Lett* **478:** 241–245

Kvansakul M, Adams JC, Hohenester E (2004) Structure of a thrombospondin C-terminal fragment reveals a novel calcium core in the type 3 repeats. *EMBO J* **23:** 1223–1233

Lawler J (2000) The functions of thrombospondin-1 and-2. *Curr Opin Cell Biol* **12:** 634–640

Lawler J (2002) Thrombospondin-1 as an endogenous inhibitor of angiogenesis and tumor growth. *J Cell Mol Med* **6:** 1–12

Lawler J, Cohen AM, Chao FC, Moriarty DJ (1986a) Thrombospondin in essential thrombocythemia. *Blood* **67:** 555–558

Lawler J, Connolly JE, Ferro P, Derick LH (1986b) Thrombin and chymotrypsin interactions with thrombospondin. *Ann NY Acad Sci* **485:** 273–287

Lawler J, Detmar M (2004) Tumor progression: the effects of thrombospondin-1 and -2. *Int J Biochem Cell Biol* **36:** 1038–1045

Lawler J, Sunday M, Thibert V, Duquette M, George EL, Rayburn H, Hynes RO (1998) Thrombospondin-1 is required for normal murine pulmonary homeostasis and its absence causes pneumonia. *J Clin Invest* **101:** 982–992

Lee NV, Rodriguez-Manzaneque JC, Thai SN, Twal WO, Luque A, Lyons KM, Argraves WS, Iruela-Arispe ML (2005a) Fibulin-1 acts

as a cofactor for the matrix metalloprotease ADAMTS-1. *J Biol Chem* **280:** 34796–34804

Lee S, Jilani SM, Nikolova GV, Carpizo D, Iruela-Arispe ML (2005b) Processing of VEGF-A by matrix metalloproteinases regulates bioavailability and vascular patterning in tumors. *J Cell Biol* **169:** 681–691

Luque A, Carpizo DR, Iruela-Arispe ML (2003) ADAMTS1/METH1 inhibits endothelial cell proliferation by direct binding and sequestration of VEGF165. *J Biol Chem* **278:** 23656–23665

Misenheimer TM, Huwiler KG, Annis DS, Mosher DF (2000) Physical characterization of the procollagen module of human thrombospondin 1 expressed in insect cells. *J Biol Chem* **275:** 40938–40945

Mittaz L, Russell DL, Wilson T, Brasted M, Tkalcevic J, Salamonsen LA, Hertzog PJ, Pritchard MA (2004) Adamts-1 is essential for the development and function of the urogenital system. *Biol Reprod* **70:** 1096–1105

Mott JD, Werb Z (2004) Regulation of matrix biology by matrix metalloproteinases. *Curr Opin Cell Biol* **16:** 558–564

Murphy-Ullrich JE, Gurusiddappa S, Frazier WA, Hook M (1993) Heparin-binding peptides from thrombospondins 1 and 2 contain focal adhesion-labilizing activity. *J Biol Chem* **268:** 26784–26789

Nicosia RF, Tuszynski GP (1994) Matrix-bound thrombospondin promotes angiogenesis *in vitro*. *J Cell Biol* **124:** 183–193

O'Leary JM, Hamilton JM, Deane CM, Valeyev NV, Sandell LJ, Downing AK (2004) Solution structure and dynamics of a prototypical chordin-like cysteine-rich repeat (von Willebrand Factor type C module) from collagen IIA. *J Biol Chem* **279:** 53857–53866

O'Reilly MS, Wiederschain D, Stetler-Stevenson WG, Folkman J, Moses MA (1999) Regulation of angiostatin production by matrix metalloproteinase-2 in a model of concomitant resistance. *J Biol Chem* **274:** 29568–29571

Rodriguez-Manzaneque JC, Lane TF, Ortega MA, Hynes RO, Lawler J, Iruela-Arispe ML (2001) Thrombospondin-1 suppresses spontaneous tumor growth and inhibits activation of matrix metalloproteinase-9 and mobilization of vascular endothelial growth factor. *Proc Natl Acad Sci USA* **98:** 12485–12490

Rodriguez-Manzaneque JC, Milchanowski AB, Dufour EK, Leduc R, Iruela-Arispe ML (2000) Characterization of METH-1/ADAMTS1 processing reveals two distinct active forms. *J Biol Chem* **275:** 33471–33479

Rodriguez-Manzaneque JC, Westling J, Thai SN, Luque A, Knauper V, Murphy G, Sandy JD, Iruela-Arispe ML (2002) ADAMTS1 cleaves aggrecan at multiple sites and is differentially inhibited by metalloproteinase inhibitors. *Biochem Biophys Res Commun* **293:** 501–508

Russell DL, Doyle KM, Ochsner SA, Sandy JD, Richards JS (2003) Processing and localization of ADAMTS-1 and proteolytic cleavage of versican during cumulus matrix expansion and ovulation. *J Biol Chem* **278:** 42330–42339

Sandy JD, Thompson V, Doege K, Verscharen C (2000) The intermediates of aggrecanase-dependent cleavage of aggrecan in rat chondrosarcoma cells treated with interleukin-1. *Biochem J* **351:** 161–166

Sandy JD, Westling J, Kenagy RD, Iruela-Arispe ML, Verscharen C, Rodriguez-Mazaneque JC, Zimmermann DR, Lemire JM, Fischer JW, Wight TN, Clowes AW (2001) Versican V1 proteolysis in human aorta *in vivo* occurs at the Glu441-Ala442 bond, a site that is cleaved by recombinant ADAMTS-1 and ADAMTS-4. *J Biol Chem* **276:** 13372–13378

Shindo T, Kurihara H, Kuno K, Yokoyama H, Wada T, Kurihara Y, Imai T, Wang Y, Ogata M, Nishimatsu H, Moriyama N, Oh-hashi Y, Morita H, Ishikawa T, Nagai R, Yazaki Y, Matsushima K (2000) ADAMTS-1: a metalloproteinase-disintegrin essential for normal growth, fertility, and organ morphology and function. *J Clin Invest* **105:** 1345–1352

Skill NJ, Johnson TS, Coutts IG, Saint RE, Fisher M, Huang L, El Nahas AM, Collighan RJ, Griffin M (2004) Inhibition of transglutaminase activity reduces extracellular matrix accumulation induced by high glucose levels in proximal tubular epithelial cells. *J Biol Chem* **279:** 47754–47762

Streit M, Riccardi L, Velasco P, Brown LF, Hawighorst T, Bornstein P, Detmar M (1999) Thrombospondin-2: a potent endogenous inhibitor of tumor growth and angiogenesis. *Proc Natl Acad Sci USA* **96:** 14888–14893

Streit M, Velasco P, Riccardi L, Spencer L, Brown LF, Janes L, Lange-Asschenfeldt B, Yano K, Hawighorst T, Iruela-Arispe L, Detmar M (2000) Thrombospondin-1 suppresses wound healing and granulation tissue formation in the skin of transgenic mice. *EMBO J* **19:** 3272–3282

Tan K, Duquette M, Liu JH, Dong Y, Zhang R, Joachimiak A, Lawler J, Wang JH (2002) Crystal structure of the TSP-1 type 1 repeats: a novel layered fold and its biological implication. *J Cell Biol* **159:** 373–382

Tan K, Duquette M, Liu JH, Zhang R, Joachimiak A, Wang JH, Lawler J (2006) The structures of the thrombospondin-1 N-terminal domain and its complex with a synthetic pentameric heparin. *Structure* **14:** 33–42

Taraboletti G, Belotti D, Borsotti P, Vergani V, Rusnati M, Presta M, Giavazzi R (1997) The 140-kilodalton antiangiogenic fragment of thrombospondin-1 binds to basic fibroblast growth factor. *Cell Growth Differ* **8:** 471–479

Thai SN, Iruela-Arispe ML (2002) Expression of ADAMTS1 during murine development. *Mech Dev* **115:** 181–185

Tolsma SS, Volpert OV, Good DJ, Frazier WA, Polverini PJ, Bouck N (1993) Peptides derived from two separate domains of the matrix protein thrombospondin-1 have anti-angiogenic activity. *J Cell Biol* **122:** 497–511

Vazquez F, Hastings G, Ortega MA, Lane TF, Oikemus S, Lombardo M, Iruela-Arispe ML (1999) METH-1, a human ortholog of ADAMTS-1, and METH-2 are members of a new family of proteins with angio-inhibitory activity. *J Biol Chem* **274:** 23349–23357

Westling J, Fosang AJ, Last K, Thompson VP, Tomkinson KN, Hebert T, McDonagh T, Collins-Racie LA, LaVallie ER, Morris EA, Sandy JD (2002) ADAMTS4 cleaves at the aggrecanase site (Glu373–Ala374) and secondarily at the matrix metalloproteinase site (Asn341–Phe342) in the aggrecan interglobular domain. *J Biol Chem* **277:** 16059–16066

Xu J, Rodriguez D, Petitclerc E, Kim JJ, Hangai M, Moon YS, Davis GE, Brooks PC, Yuen SM (2001) Proteolytic exposure of a cryptic site within collagen type IV is required for angiogenesis and tumor growth *in vivo*. *J Cell Biol* **154:** 1069–1079

Micro-PET/CT Monitoring of Herpes Thymidine Kinase Suicide Gene Therapy in a Prostate Cancer Xenograft: The Advantage of a Cell-specific Transcriptional Targeting Approach

Mai Johnson[1,*], *Makoto Sato*[1,*], *Jeremy Burton*[1], *Sanjiv S. Gambhir*[1,2], *Michael Carey*[1], *and Lily Wu*[1]

[1]University of California Los Angeles, and [2]Stanford University, USA

Abstract

Cancer gene therapy based on tissue-restricted expression of cytotoxic gene should achieve superior therapeutic index over an unrestricted method. This study compared the therapeutic effects of a highly augmented, prostate-specific gene expression method to a strong constitutive promoter-driven approach. Molecular imaging was coupled to gene therapy to ascertain real-time therapeutic activity. The imaging reporter gene (luciferase) and the cytotoxic gene (herpes simplex thymidine kinase) were delivered by adenoviral vectors injected directly into human prostate tumors grafted in SCID mice. Serial bioluminescence imaging, positron emission tomography, and computed tomography revealed restriction of gene expression to the tumors when prostate-specific vector was employed. In contrast, administration of constitutive active vector resulted in strong signals in the liver. Liver serology, tissue histology, and frail condition of animals confirmed liver toxicity suffered by the constitutive active cohorts, whereas the prostate-targeted group was unaffected. The extent of tumor killing was analyzed by apoptotic staining and human prostate marker (prostate-specific antigen). Overall, the augmented prostate-specific expression system was superior to the constitutive approach in safeguarding against systemic toxicity, while achieving effective tumor killing. Integrating noninvasive imaging into cytotoxic gene therapy will provide a useful strategy to monitor gene expression and therapeutic efficacy in future clinical protocols. *Mol Imaging* (2005) **X,** 1–10.

Keywords: Prostate cancer, molecular imaging, suicide gene therapy, targeted gene expression, systemic toxicity, two-tiered amplification, adenoviral vector.

Introduction

Prostate cancer remains the second leading cause of cancer-related mortality in men in the United States. Recurrent and disseminated disease contributes to the majority of the estimated 29,089 deaths in 2004. No effective treatment currently exists for the advanced stage of human prostate cancer [1]. Hence, limitations of current therapeutic options demand the development of more effective detection and treatment methods. Gene therapy is a promising treatment because a great variety of growth inhibitory strategies can be implemented [2–5]. When used in combination, it could also augment therapeutic effects of conventional prostate cancer treatment. In particular, cytotoxic therapy employing the herpes simplex virus type 1 thymidine kinase (HSV1-tk) gene has been widely used in both experimental and clinical settings [6,7]. Despite promising therapeutic efficacy in preclinical models, the clinical benefit of this HSV1-tk suicide gene therapy is unrealized at this time. The lack of therapeutic success could be attributed to limited specificity, modest potency, inadequate gene delivery, and inability to monitor gene expression at the targeted site [8]. In this study, we aim to address these challenges to improve upon the current status of prostate cancer gene therapy.

The use of prostate-specific promoter to express therapeutic gene is likely to be advantageous over constitutive promoters in achieving cell-specific selectivity. In support of this concept, specific gene transfer and expression in distant prostate metastatic lesions was achieved by employing a modified prostate-specific antigen (PSA) gene promoter [9]. However, the weak activity of the native PSA promoter precludes efficient gene expression in prostate cancer therapeutic applications [10]. Several methods have been used to enhance the activity of the PSA promoter. By duplicating the upstream enhancer core of the PSA promoter, a 20-fold enhancement of activity over the parental construct was achieved [11,12]. In a second method, a two-step transcriptional amplification (TSTA) strategy was employed, which boosted the activity of the native PSA enhancer/promoter over 1000-fold, exceeding the activity level of the strong cytomegalovirus immediate early (CMV) promoter [13,14]. In the two-tiered TSTA system (Figure 1A), the PSA regulatory region was employed to express the potent synthetic transcription activator,

Corresponding author: Lily Wu, University of California Los Angeles, 675 Charles Young Drive S, Los Angeles, CA 90095; e-mail: LWu@mednet.ucla.edu.
*These authors contributed equally.
Received 15 April 2005; Received in revised form 11 May 2005; Accepted 12 May 2005.

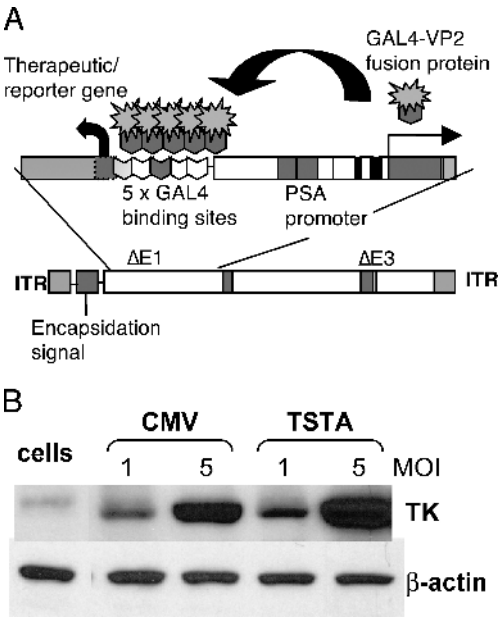

Figure 1. *Prostate-specific suicide gene therapy vector. (A) The Ad containing the TSTA system. The enhanced PSE-BC promoter drives the expression of the potent synthetic activator, composed of two herpes VP16 activation domains (aa 413–454) fused to the GAL4 DNA-binding domain (red). The GAL4-VP2 activators bind to the GAL4 binding sites, activating the expression of a therapeutic gene. These two components were inserted into an Ad5 vector. (B) The magnitude of sr39tk expression by AdTSTA-sr39tk. LNCaP cells were infected with AdCMV-sr39tk or AdTSTA-sr39tk at MOI 1 and 5. The level of sr39tk protein expression was assessed by Western blot using a polyclonal HSV1-tk antibody [15] as well as β-actin as a control.*

GAL4-VP2, which in turn activates the expression of a GAL4-responsive gene. The prostate cell specificity and androgen responsiveness activity of the PSA promoter were retained in the TSTA method [13–17].

Coupling molecular imaging approaches to gene therapy will allow real-time monitoring of in vivo gene delivery and expression [18]. Optical bioluminescent imaging based on the firefly luciferase gene has frequently been utilized to study gene expression in living animals [19–18,20,21]. Light is produced through the enzymatic interaction of luciferase with its substrate D-luciferin in the presence of magnesium and ATP [20]. The bioluminescence generated within the animal can be detected by a highly sensitive cooled charge-coupled device (CCD) camera [21,22]. This form of optical imaging is very rapid and inexpensive compared to radionuclide-based imaging. However, one advantage of radionuclide imaging is its ability to provide 3-D tomographic signals. Positron emission tomography (PET) is one such modality that has been adapted to studies in small animals, using the HSV1-tk or the enhanced sr39tk derivative as the reporter gene [18]. The sr39tk contained multiple amino acid substitutions at the active site, which greatly improved the binding affinity for guanosine analogues compared to the wild-type (WT) enzyme [23]. The use of the sr39tk gene has been demonstrated to increase the sensitivity of PET imaging by twofold over the WT HSV1-tk gene [24].

The unique enzymatic activity of HSV1-tk enables it to function both as a PET reporter gene as well as a cytotoxic suicide gene [15,24–26]. Unlike its mammalian counterpart, this HSV enzyme can efficiently phosphorylate guanosine analogues such as ganciclovir (GCV). The phosphorylation of various radioactive derivatives such as 9-(4-[^{18}F]-fluoro-3-hydroxymethylbutyl) guanine ([^{18}F]FHBG), will lead to the trapping and accumulation of the radiolabeled tracer in cells expressing HSV1-tk, which in turn can be detected and located by the PET scanner. The cytotoxic effects of HSV1-tk require the subsequent phosphorylation of the otherwise nontoxic GCV monophosphate by cellular kinases. The triphosphate derivative causes chain termination during DNA replication and can lead to chromosomal aberrations and cell death [25]. The pharmacologic dosage of GCV in cytotoxic therapy is three to four orders higher than the PET tracer dose. The sr39tk variant also exhibited stronger cytotoxicity compared to the WT enzyme [15]. The dual imaging and cytotoxic capability of the sr39tk gene is very useful in gene therapy, allowing researchers to directly monitor location, temporal representation, and magnitude of the therapeutic gene expression in vivo by noninvasive imaging.

In this study, we report the use of the bioluminescent optical CCD and micro-PET imaging to assess the effectiveness of TSTA-mediated gene therapy. Micro-PET imaging was utilized to monitor sr39tk expression by measuring the uptake of [^{18}F]FHBG in organs where the gene is expressed. More importantly, the tissue selectivity and high magnitude of the TSTA-mediated sr39tk suicide gene therapy resulted in diminished systemic side effects and effective antitumor activity in a human prostate cancer xenograft model.

Materials and Methods

Vector Design

The AdTSTA-sr39tk was constructed with the AdEasy system [27]. The head-to-head orientation of activator (BCVP2) and reporter (sr39tk) in the single plasmid was constructed by replacing FL with sr39tk in PBCVP2G5-L [13]. The BCVP2G5-sr39tk fragment generated by *Not*I and *Sal*I from PBCVP2G5-sr39tk was then ligated to pShuttle to generate pShuttleTSTA-sr39tk, which was used for the recombination with pAdEasy-1. The virus was propagated in 293 cells, purified on a CsCl gradient, and titrated by plaque assays on 293 cell monolayers.

Expression Analysis in vitro

Human prostate cancer cell line LNCaP was infected with AdCMV-sr39tk or AdTSTA-sr39tk at the multiplicity of one or five virus per cell. Cells were harvested 2 days after infection and lysed with RIPA buffer (0.1% Na deoxycholate, 0.1% SDS, 0.15M NaCl, 1mM EDTA, 10 mM Tris–HCl [pH 7.4] with protease inhibitor cocktail; Calbiochem, San Diego, CA). Equal amounts of total protein from each sample were subjected to SDS-PAGE. Following the transfer of analyzed proteins to PVDF membrane (Millipore, Bedford, MA), Western analysis was performed using polyclonal anti-HSV-tk antibody [15] and monoclonal anti-β-actin antibody [28]. Visualization was performed by BM Chemiluminescence (Roche Diagnostics, Indianapolis, IN) with HRP-conjugated respective antibodies.

Optical Imaging of Mice

Animal experiments were performed in accordance with the University of California Animal Research Committee guidelines. Ten to 12-week-old male SCID (Taconic Farms, Germantown, NY) mice were subcutaneously implanted with 0.2 cm tumor coated with matrigel. When tumors reached ~0.8 cm, the specified Ad was injected into the tumor for four consecutive days, using a 28G1/2 syringe (10 μL per site, at three different sites, and waiting 5 min between injections). Optical imaging was performed with an IVIS CCD camera (Xenogen, Alameda, CA). Mice were anesthetized with ketamine and xylazine (4:1), then given 200 μL of 15 mg/mL D-luciferin (Xenogen) intraperitoneally, and imaged 20 min after substrate administration.

Micro-PET/CT Imaging and GCV Treatment

For the therapeutic study, the specified sr39tk Ad was administered intratumorally at 1×10^9 pfu/day × 4 days (30 μL/day). On Days 8 and 22, animals were injected with 200 μCi [^{18}F]FHBG via the tail vein. Following an hour of substrate uptake, the entire animal was scanned for 20 min in a Focus micro-PET scanner (Concorde Microsystems, Knoxsville, TN) and transferred to a micro-CT scanner (MicroCAT I, Imtek, Knoxsville, TN), and imaged for 15 min at 50 keV, 325 μA, and 196 total angles of rotation in two bed positions. From Days 9 to 16, animals received intraperitoneal administration of GCV (80 mg/kg in 0.9 % saline) or saline vehicle. PET signals were quantified as the percentage of injected dose per gram (%ID/g) tissue. This %ID/g is a measure of the amount of tracer accumulated in a given area normalized to the injected amount and to the mass of the tissue examined. PET images were superimposed on CT images. All PET/CT data analyses and 3-D images were compiled using AMIDE. A total of six animals were used in each of four treatment groups. PET imaging was performed on four out of six animals in each group.

Quantitative PCR

Organs were frozen in liquid nitrogen, ground into fine powder, resuspended in 10 volumes lysis buffer (10 mM Tris–HCl pH 8.0, 5 mM EDTA pH 8.0, 200 mM NaCl, 0.2 % SDS, 100 μg/mL proteinase K), and incubated at 55°C for 3 hr. One milliliter of each lysate was treated with RNase A (50 μg/mL) for 20 min at 37°C, followed by extracting twice with phenol/chloroform/isoamyl alcohol (25:24:1). The DNA was precipitated and resuspended in TE buffer (pH 8.0). Real-time PCR was performed using the Opticon 2 Monitor (MJ Research, San Francisco, CA). The specific primers for β-actin and HSV-tk are: (β-actin: forward, 5′-TCA AGA TCA TTG CTC CTC CTG AGC-3′, reverse, 5′-TAC TCC TGC TTG CTG ATC CAC ATC-3′; HSV-TK: forward, 5′-ACA AAA AGC CAC GGA AGT CC-3′, reverse, 5′-AGT TGC GTG GTG GTG GTT T-3′). Primers for β-actin recognize an identical conserved region of the human and mouse gene. Reactions were run in triplicate, each containing 1× SYBR Green master mix (Applied Biosystems), 0.4 pmol/μL of primers and 100 ng genomic DNA in 25 μL. The amplification conditions were: 1 cycle of 2 min at 50°C and 1 cycle of 10 min at 95°C, followed by 35 cycles of 15 sec at 95°C, 30 sec at 60°C, and 30 sec at 72°C. After completion of PCR, 10 μL of the pooled triplicated reactions was run on a 2% agarose gel, resolving the 106 bp β-actin and 101 bp HSV-tk amplified fragment.

Immunohistochemical Analysis

Tumors harvested at Day 22 were fixed in 10% formalin overnight. Paraffin-embedded sections (4 μm) were deparaffinized, and stained with hematoxylin and eosin. Proliferating cells were visualized using mouse monoclonal Ki67 antibody 1:50 (Novocastra, Norwell, MA) at 4°C overnight. Color visualization of immunohistological reaction was performed with multilink antibody, streptavidin peroxidase (BioGenex, San Ramon, CA), and 3,3 diaminobenzidine (DAB) as previously described [12]. Apoptotic cells were visualized by using DeadEnd Colorimetric TUNEL System (Promega, Madison, WI), performed according to manufacturer's instructions. Samples were blinded and staining was quantified by dividing each tumor into four quadrants. Cells were then counted under ×40 magnification. Staining was recorded as a percentage of positive cells over total cells counted (average of 100 cells/field).

Liver Enzyme and PSA Assays

Blood was collected at various time points by the retro-orbital eye bleed method. Serum ALT levels were measured using GTP/ALT reagent strip with SPOTCHEM EZ system (HESKA, Fort Collins, CO). Serum PSA levels were measured in duplicates using PSA ELISA kit (American Qualex, San Clemente, CA). The relative rate of change in PSA was obtained by calculating the difference in PSA levels pre- and posttreatment divided by posttreatment.

Statistical Analysis

Statistical analyses were performed using the two-tailed Student's t test. For all analyses, $p < .05$ was considered statistically significant.

Results

Prostate-specific Gene Delivery Vector

Using the prostate-specific two-step TSTA method should be advantageous, as this method has been shown to boost the activity of a comparable one-step prostate-specific promoter by 50-fold [12,13,16]. In this study, the TSTA system was incorporated into an adenoviral vector to drive the sr39tk gene, which is designated as AdTSTA-sr39tk (Figure 1). The magnitude of sr39tk protein expression mediated by this prostate-targeted Ad was comparable to the AdCMV-sr39tk, as analyzed in LNCaP (Figure 1B) and LAPC-4 (data not shown) human prostate cancer lines. Furthermore, AdTSTA-sr39tk mediated gene expression was regulated by androgen and active in advanced AR+ androgen-independent prostate cancer cell lines and tumors [28]. The promising properties AdTSTA-sr39tk exhibited in cell culture studies lend support to assess its activities in preclinical prostate tumor models.

Imaging Transgene Expression in Prostate Tumors

To learn more about the in vivo activity of the gene therapy vectors, we applied several molecular imaging modalities, including bioluminescent imaging and micro-PET, to monitor transgene expression during treatment. The study design, as outlined in Figure 2A, was to compare the performance of the CMV versus the TSTA vectors. In the CMV group (i) of the first study, 4×10^8 infectious plaque forming units (pfu) each of the luciferase-expressing virus (AdCMV-FL) and the sr39tk-expressing virus (AdCMV-sr39tk) were coinjected into the tumor. The same viral dosage was used in the TSTA group (ii). Given that in both groups the luciferase and sr39tk are expressed from the same promoter and inserted into the same adenoviral backbone, the lucifer-

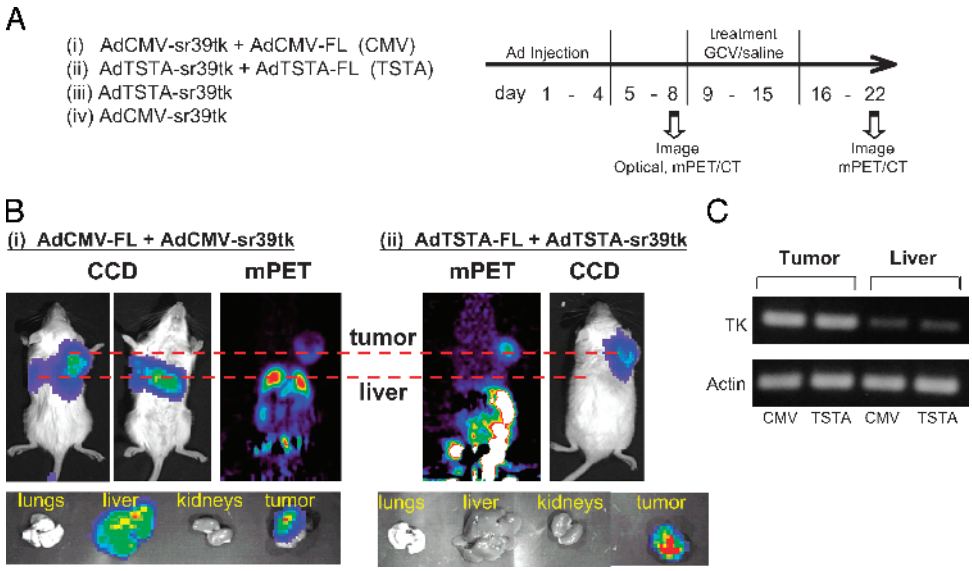

Figure 2. *Optical and PET imaging of vector mediated gene expression. (A) Therapeutic study scheme. Coinjection of the two vectors in groups i and ii in one study enables the optical FL signal to reflect the expression of sr39tk. Group iii and iv injections were performed in a second study to compare the therapeutic activity between the TSTA and the CMV vector. (B) Coinjection of the two adenoviral vectors (Ad) into LAPC-4 tumors. 4×10^8 pfu of each vector was injected and optical CCD imaging and micro-PET were performed on Day 8. Tumor and liver signals were detected in the CMV group (i), but in the TSTA group (ii) signals were limited to the tumors. Signals in the abdomen were due to the hepatobiliary and renal route of FHBG excretion. Animals were sacrificed at Day 22 and bioluminescent imaging of the isolated organs revealed the tumor-restricted expression of the TSTA vector. (C) PCR amplification of the sr39tk gene in the tumor and the liver. DNA was isolated from organs of AdCMV-sr39tk and AdTSTA-sr39tk treated animals (groups iii and iv). Real-time quantitative PCR was performed to quantify the sr39tk gene. Agarose gel resolution after completion of the 35-cycle PCR reaction revealed the presence specific HSV1-sr39tk DNA (101-bp amplified fragment) in the tumor and liver extracts. β-actin served as internal control.*

ase gene can serve as a reporter gene to reflect the expression of the sr39tk therapeutic gene. An advantage of this approach over a single vector expressing both imaging genes simultaneously is that the distribution and the gene expression profile can be verified by two independent vectors and imaging modalities. The LAPC-4 tumor was the model we examined. It is a PSA-expressing human prostate xenograft originally derived from a patient's lymph node metastases [29].

On Day 8, prominent optical signals were observed in the tumors of the CMV group (i). Strong signals emitted from the livers were consistently detected after intratumoral injection of CMV-driven vectors (Figure 2B, i). On the other hand, in the TSTA group (ii), the optical signal was confined to the tumor and the liver was devoid of signal (Figure 2B, ii). Similar to the optical analysis, micro-PET illustrated the same pattern of [^{18}F]FHBG uptake mediated by the sr39tk gene in the corresponding locations (Figure 2B).

To understand why gene expression was observed consistently in the liver of the CMV group but not in the TSTA group, real-time quantitative PCR was employed to quantify the viral distribution following intratumoral injection. The sr39tk gene delivered to the tumor relative to endogenous β-actin gene was 0.072 and 1.18 in a CMV and TSTA animal, respectively. In a CMV-treated animal, the ratio of the sr39tk gene delivered to the tumor was 452-fold higher than that in the liver. Similarly, the ratio in a TSTA-injected animal was 263-fold higher in the tumor than in the liver. The correct size of the sr39tk fragment was detected from the tumor and liver extracts (Figure 2C). These PCR data indicate that tumor-directed vector administration does not preclude gene delivery to nontargeted vital organs such as the liver. Our results would support the assumption that a tissue-specific vector provides added safety over a constitutively active vector. Imaging studies showed that the prostate-specific TSTA vector in the liver remained transcriptionally silent.

Treatment Side Effect Seen by Imaging

To compare the therapeutic activity between the CMV- and the TSTA-driven vector, a total of 4×10^9 pfu of the respective vector was injected into the LAPC-4 tumor (group iii and iv, Figure 2A). The animals were imaged by combined PET/CT on Day 8, just prior to GCV treatment (80 mg/kg for 7 days). The control groups received saline instead of GCV. All animals were re-imaged on Day 22, one week after the last day of GCV administration. At this point, no residual GCV should remain in the animal to interfere with uptake of PET substrate [^{18}F]FHBG. In the therapeutic studies, micro-CT was performed in series with the micro-PET. This combined technology enables the precise alignment of the PET signal with the anatomical location in the subject [30].

In the AdCMV-sr39tk injected group, a strong [^{18}F]FHBG PET signal was observed in the liver on Day 8 (Figure 3A). The [^{18}F]FHBG retention signal was not affected by saline treatment (2.5 ± 0.4 to 2.7 ± 0.06), but was decreased in the GCV-treated group from 3.7 ± 1.1 to 1.5 ± 0.3. The prominent [^{18}F]FHBG PET signal in the liver forecasted liver toxicity in this group. This is because the same sr39tk activity that phosphorylates [^{18}F]FHBG also functions in the first step of cytotoxic activation of GCV. After GCV treatment, a clear decrease of sr39tk-mediated PET signal in the liver was observed (Figure 3A, graph). The decrease in the functional PET signal could be attributed to the elimination of sr39tk expressing cell with GCV. No loss of PET signal was observed with saline treatment (Figure 3A, graph).

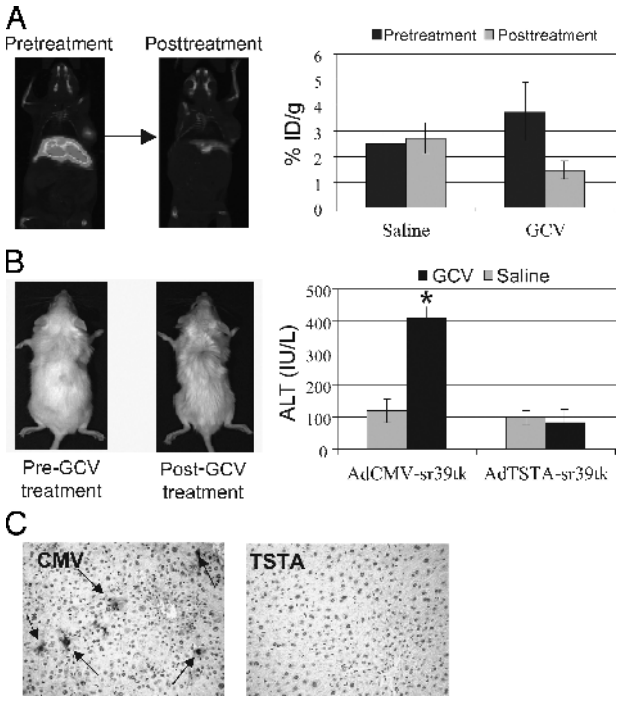

Figure 3. *Liver toxicity after GCV treatment in AdCMV-sr39tk animals. (A) Micro-PET/micro-CT of AdCMV-sr39tk treated animals. Compared to the saline treatment, GCV treatment (n = 6 per treatment group) resulted in a reduction of PET signal in the liver (PET, n = 4 per group). The graph on the right shows average [^{18}F]FHBG retention in the liver pre- and posttreatment. (B) Liver toxicity in the animals. GCV-treated mice in the CMV group were weak and disheveled. GCV treatment resulted in elevated serum ALT levels in the CMV group compared to TSTA and saline groups on Day 22. (C) Immunohistochemical analysis of the liver. Liver sections from these mice revealed significant TUNEL positive staining (arrows) indicative of apoptosis. This was not observed in the TSTA cohort.*

The extent of liver damage in the animals was assessed by several means including signs and symptoms of the animals, hepatic serology, and histology. Alanine aminotransferase (ALT) is an intracellular enzyme produced by hepatocytes that are released into the bloodstream as a result of liver cell destruction. The GCV-treated animals in the CMV group exhibited more than four times higher ALT than the saline control or TSTA groups (Figure 3B), and they appeared weak and unkempt. At the end point of the study, the average liver weight of the CMV group was 50% of the saline and TSTA-treated groups. Immunohistochemistry of the liver sections by terminal deoxynucleotidyl transferase (TdT)-mediated dUTP nick end labeling (TUNEL) revealed extensive apoptosis in the CMV GCV-treated animals (Figure 3B).

Monitoring Therapeutic Efficacy of Suicide Gene Therapy

The previous results (Figure 3) suggested that the destruction of sr39tk-expressing cells resulted in the diminution of sr39tk-mediated PET signals. Thus, we applied the radionuclide micro-PET/micro-CT to monitor the therapeutic effects of tumor cell destruction. In the AdTSTA-sr39tk-treated animals, PET signal in the tumor was significantly weakened on Day 22 compared with Day 8 (Figure 4A). Results of the entire TSTA treatment cohort showed that [^{18}F]FHBG accumulation in the tumors was 0.52 ± 0.04 %ID/g (n = 12) prior to GCV treatment on Day 8, 0.54 ± 0.09 %ID/g in the saline-treated group, and 0.33 ± 0.04 %ID/g in the GCV-treated group (n = 5) on Day 22. The GCV treatment resulted in a significant reduction of signals in the tumor (p = .026). Although adenoviral-mediated gene expression is expected to decay over time, we observed a higher magnitude of decrease (50%) in [^{18}F]FHBG retention in the GCV-treated group compared to a 20% decrease in saline-treated group from pre- to posttreatment (Figure 4A).

In the CMV treatment group, a decrease in PET signals was observed in the animal's tumor as well as in the liver following GCV treatment (Figure 3A). Three-dimensional reconstructed images of the whole animal were compiled from the PET/CT studies. The magnitude and localization of the PET signals pre- and post-GCV treatment are shown for one representative animal in the CMV and TSTA group (please refer to supplemental material for 3-D movie).

To validate the therapeutic outcome, PSA levels were examined during the course of treatment. Serum PSA, a widely used marker for the detection of prostate cancer, was applied to measure tumor load during suicide gene therapy. In this tumor model, serum PSA measurements have been shown to accurately reflect tumor volume and growth in several studies [29,31–33]. Serum PSA was sampled prior to treatment (baseline), and on Days 11 and 19 (i.e., 3 and 11 days post-GCV treatment). In the CMV group, the average baseline PSA was 21 ng/mL and increased to 26 ng/mL after GCV treatment, whereas the saline-treated group climbed to 72 ng/mL (p = .019). A similar trend was observed in the AdTSTA-sr39tk injected group. The average PSA in this cohort was 12 ng/mL at baseline and 13 ng/mL after GCV treatment compared with 46 ng/mL in saline controls (p = .018). The relative change of PSA was determined for each group (Figure 4B). The two saline-treated control groups showed continual tumor growth as is evident by the increasing PSA level, whereas tumor growth in the GCV-treated groups was halted.

Detailed histological examinations with hematoxylin and eosin (H&E) staining, proliferative marker Ki-67, and the apoptotic TUNEL staining were performed. Figure 4C shows representative tumor sections of eight different animals from the specified treatment groups. The hematoxylin dye (purple/blue) stains DNA content. Thus, the extent of purple/blue coloring in a tissue section is indicative of the extent of living cells. The overall hematoxylin staining in the unmagnified tumor sections of both saline groups was more extensive than the GCV-treated groups (Figure 4C). Moreover, the areas of proliferation that stained positive by Ki-67 were decreased in the GCV-treated tumors compared with saline controls. In contrast, the areas that did not stain for Ki-67 exhibited strong TUNEL staining. The apoptotic TUNEL staining also supports the PSA measurement that tumor growth was halted in the GCV-treated group. Quantitation of the tumor TUNEL staining revealed that an average of 67.6% tumor cells were positive in the GCV-treated versus 7.6% in the saline-treated tumor of the TSTA group. Overall, the histological assessment demonstrated that the GCV-treated tumors exhibited increased apoptosis (TUNEL staining), reduced proliferation (Ki-67 staining), and decreased living cells (hematoxylin staining). These observations therefore support that GCV treatment coupled to the sr39tk gene therapy results in effective tumor cell destruction.

Discussion

Achieving both potent and cell-selective expression could improve the therapeutic outcome of cytotoxic gene therapy of cancer. Here, we showed that the

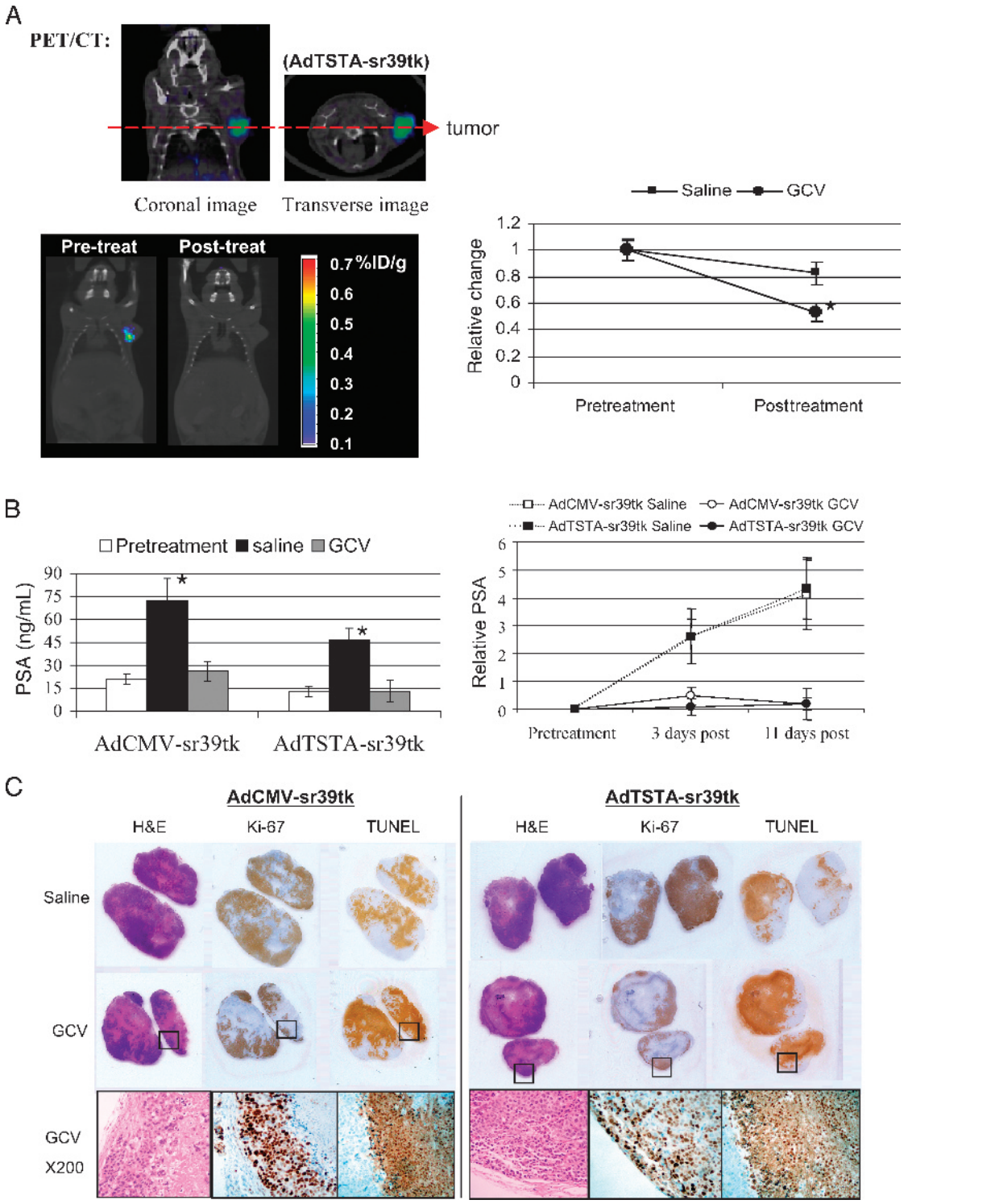

Figure 4. *Therapeutic effects of GCV treatment on the tumors. (A) PET signal in AdTSTA-sr39tk injected mice. The close-up coronal and transverse images represent a PET/CT study performed on an animal 8 days after intratumoral injection of AdTSTA-sr39tk. The lower paired images are the PET/CT results of a representative animal pre- and posttreatment with GCV. The tumor localized PET signals declined post-GCV treatment. The graph on the right shows the relative change of PET signal in the tumors of the two cohorts. The difference in the signal decay between the saline and GCV groups was significant ($p = .029$). (B) Serial PSA levels. GCV treatment in the CMV and TSTA groups resulted in a significant decrease in the serum PSA level compared with saline controls ($p = .02$). Relative change of PSA showed that the rate of the rising level was halted by GCV treatment. (C) Detailed tumor histology. Two representative tumors were shown for each condition under unmagnified objective. Consecutive thin sections were stained with hematoxylin and eosin (H & E), anti-Ki67 antibody (cell proliferation marker), and TUNEL. Comparing the lower panels of GCV-treated tumors to the upper saline controls; drug treatment resulted in decreased nucleated cells (blue staining on H&E), reduced proliferating cells (Ki-67), and elevated apoptosis (TUNEL). Higher magnification of the sections (×200) demonstrates specificity of the staining.*

adenovirus-based TSTA system can express the suicide gene in a robust, tissue-specific manner. The tissue selectivity of the TSTA method restricted the transgene expression to the LAPC-4 human prostate tumor, and thus, limited the transgene-mediated toxicity in a non-targeted organ such as the liver. The highly augmented activity of TSTA allowed the visualization of transgene expression by bioluminescent and PET imaging during treatment.

We postulated that functional gene expression activity in the tumor might provide more accurate, dynamic information on the content of living cells in a tumor than tumor size measurements. Due to its easy-to-use and rapid scan time capabilities, in vivo optical imaging has been applied frequently to interrogate tumor activities [13,14,16–22], including monitoring growth and therapy of marked tumors [22]. However, when we applied optical imaging to monitor the therapeutic effects of suicide gene therapy on renilla luciferase-labeled LAPC-4 tumors, changes in intratumoral signals were not correlated with treatment effects. Several factors could contribute to the difficulties we encountered. (i) Optical signal is known to be attenuated by hemoglobin levels, extent of tissue depth or necrotic tissue, and (ii) high, saturated signals in the xenograft tumors could make lost of signal during therapy difficult to detect. Thus, we decided to utilize PET imaging, which is a high-energy modality that is not attenuated by tissue depth, and it is applicable to human subjects. In fact, [^{18}F]FHBG was determined to be a safe tracer in healthy human volunteers [34]. Our results support the use of PET/CT to monitor the pharmacokinetic of HSV-tk suicide gene therapy in vivo.

Despite substantial tumor destruction in the suicide gene treatment, the tumor cell annihilation was incomplete at the specified end point of this study (Day 22). Potentially, a more prolonged treatment course could achieve more extensive tumoricidal effects. To ensure accuracy of gene delivery, we intentionally employed large size tumors, ~0.8cm diameter at the start of therapy. Consequently, one limiting factor likely to have contributed is the incomplete gene transduction via intratumoral viral injection. Several measures were attempted to achieve more optimal intratumoral transduction. To circumvent the high intratumoral pressure, the viral solution was administrated at a slow rate, in a small volume, divided into multiple sites and over several days. Despite these measures, the transduction rate was between 30% and 50%, which was estimated by performing flow cytometry of single-cell suspension of tumors 4 days after injection of a viral vector expressing green fluorescent protein (data not shown). Several strategies can be applied to enhance therapeutic efficacy of suicide gene therapy. The high level and specific gene expression accomplished by the TSTA method is helpful to maximize in vivo gene transduction as well as to boost the bystander effect. This bystander phenomenon, where cytotoxic effect spreads from transduced cells to neighboring nontransduced cells, is known to be augmented by increasing intercellular transfer of metabolites through gap junctions [35,36]. By combining the HSV-tk cytotoxic approach with other gene-based therapeutic targets such as anti-angiogenic or immune activation strategies, synergistic enhancement of remedial effects could be accomplished. In the context of improving efficacy of cancer treatment, gene therapy should be considered as one arm of a multiprong approach to manage cancer. Thus, it is promising that adenoviral-mediated suicide gene therapy has been shown to induce radiation sensitizing effects in tumors [37].

Another interesting finding from this and other studies [8,16,38] is that intratumoral injections of viral vectors often result in ''leakage'' into the systemic circulation, triggering transgene expression in the liver. Ongoing research in our laboratory indicates that tumor models exhibit differential viral ''leakage'' [16], and this phenomenon is likely modulated by tumor vasculature. Hence, these findings further underscore the importance of incorporating a noninvasive mean to monitor the location of toxic transgene expression in vivo, thereby obtaining the assurance that the ''on-target'' and ''off-target'' effects can be visualized. One unanticipated finding is that higher PET signal was detected in the liver of the AdCMV-sr39tk injected animal despite a much higher level of sr39tk gene delivery to the tumor (Figure 3). The possible explanations could be: (i) preferential adenoviral transduction of hepatocytes or (ii) preferential gene expression mediated by the CMV promoter in the liver or (iii) limiting PET substrate delivery to the tumor relative to the liver. We are actively investigating these possibilities.

In an attempt to improve prostate cancer gene therapy, we have coupled noninvasive imaging to a highly amplified, prostate tissue-specific gene expression system to express an enhanced cytotoxic HSV1-tk gene (sr39tk). The results demonstrated here confirm that the adenoviral vector containing prostate-specific TSTA system can achieve targeted expression in vivo. In the delivery of the potent variant sr39tk gene, effective tumor eradication with minimal systemic toxic affects was achieved. The coupling of PET imaging to this targeted suicide gene therapy will be a promising strat-

egy to develop future clinical protocols for patients with advanced stage prostate cancer.

Acknowledgments

Without the imaging technology infrastructure developed by Dr. Michael Phelps (Molecular and Medical Pharmacology, School of Medicine, UCLA) and the UCLA Crump Institute for Biological Imaging, this work could not be accomplished. We thank Waldemar Ladno, Judy Edwards, David Stout for their skillful assistance in PET/CT imaging, and Baohui Zhang for technical assistance. We deeply appreciate the guidance and shared equipment provided by Vivek Dixit (Department of Medicine, School of Medicine, UCLA) in the liver enzyme assay, and Giri Sulur for manuscript preparation. We thank Drs. Elizabeth Neufeld and Harvey Herschman for their helpful inputs. This work is supported by the California Cancer Research Program 3NI0226 (to LW), DAMD17-03-1-0095 (to LW), NIH R01 CA101904 (to LW), and an interdisciplinary seed grant from the JCCC (to MC, LW, and SSG). MS is supported by a DOD CDMRP postdoctoral fellowship (PC020531).

References

[1] Kasamon KM, Dawson NA (2004). Update on hormone-refractory prostate cancer. *Curr Opin Urol.* **14:**185–193.

[2] Stroh C, Held J, Samraj AK, Schulze-Osthoff K (2003). Specific inhibition of transcription factor NF-kappaB through intracellular protein delivery of I kappaBalpha by the Herpes virus protein VP22. *Oncogene.* **22:**5367–5373.

[3] Stacpoole PW, Owen R, Flotte TR (2003). The pyruvate dehydrogenase complex as a target for gene therapy. *Curr Gene Ther.* **3:**239–245.

[4] Herrmann F (1995). Cancer gene therapy: Principles, problems, and perspectives. *J Mol Med.* **73:**157–163.

[5] Qiao J, Doubrovin M, Sauter BV, Huang Y, Guo ZS, Balatoni J, Akhurst T, Blasberg RG, Tjuvajev JG, Chen SH, Woo SL (2002). Tumor-specific transcriptional targeting of suicide gene therapy. *Gene Ther.* **9:**168–175.

[6] Kubo H, Gardner TA, Wada Y, Koeneman KS, Gotoh A, Yang L, Kao C, Lim SD, Amin MB, Yang H, Black ME, Matsubara S, Nakagawa M, Gillenwater JY, Zhau HE, Chung LW (2003). Phase I dose escalation clinical trial of adenovirus vector carrying osteocalcin promoter-driven herpes simplex virus thymidine kinase in localized and metastatic hormone-refractory prostate cancer. *Hum Gene Ther.* **14:**227–241.

[7] Shalev M, Kadmon D, Teh BS, Butler EB, Aguilar-Cordova E, Thompson TC, Herman JR, Adler HL, Scardino PT, Miles BJ (2000). Suicide gene therapy toxicity after multiple and repeat injections in patients with localized prostate cancer. *J Urol.* **163:**1747–1750.

[8] Somia N, Verma IM (2000). Gene therapy: Trials and tribulations. *Nat Rev Genet.* **1:**91–99.

[9] Adams JY, Johnson M, Sato M, Berger F, Gambhir SS, Carey M, Iruela-Arispe ML, Wu L (2002). Visualization of advanced human prostate cancer lesions in living mice by a targeted gene transfer vector and optical imaging. *Nat Med.* **8:**891–897.

[10] Wu L, Sato M (2003). Integrated, molecular engineering approaches to develop prostate cancer gene therapy. *Curr Gene Ther.* **3:**452–467.

[11] Latham JP, Searle PF, Mautner V, James ND (2000). Prostate-specific antigen promoter/enhancer driven gene therapy for prostate cancer: Construction and testing of a tissue-specific adenovirus vector. *Cancer Res.* **60:**334–341.

[12] Wu L, Matherly J, Smallwood A, Adams JY, Billick E, Belldegrun A, Carey M (2001). Chimeric PSA enhancers exhibit augmented activity in prostate cancer gene therapy vectors. *Gene Ther.* **8:** 1416–1426.

[13] Zhang L, Adams JY, Billick E, Ilagan R, Iyer M, Le K, Smallwood A, Gambhir SS, Carey M, Wu L (2002). Molecular engineering of a two-step transcription amplification (TSTA) system for transgene delivery in prostate cancer. *Mol Ther.* **5:**223–232.

[14] Iyer M, Wu L, Carey M, Wang Y, Smallwood A, Gambhir SS (2001). Two-step transcriptional amplification as a method for imaging reporter gene expression using weak promoters. *Proc Natl Acad Sci USA.* **98:**14595–14600.

[15] Pantuck AJ, Matherly J, Zisman A, Nguyen D, Berger F, Gambhir SS, Black ME, Belldegrun A, Wu L (2002). Optimizing prostate cancer suicide gene therapy using herpes simplex virus thymidine kinase active site variants. *Hum Gene Ther.* **13:** 777–789.

[16] Sato M, Johnson M, Zhang L, Zhang B, Le K, Gambhir SS, Carey M, Wu L (2003). Optimization of adenoviral vectors to direct highly amplified prostate-specific expression for imaging and gene therapy. *Mol Ther.* **8:**726–737.

[17] Zhang L, Johnson M, Le KH, Sato M, Ilagan R, Iyer M, Gambhir SS, Wu L, Carey M (2003). Interrogating androgen receptor function in recurrent prostate cancer. *Cancer Res.* **63:** 4552–4560.

[18] Ray P, Bauer E, Iyer M, Barrio JR, Satyamurthy N, Phelps ME, Herschman HR, Gambhir SS (2001). Monitoring gene therapy with reporter gene imaging. *Semin Nucl Med.* **31:**312–320.

[19] Bhaumik S, Gambhir SS (2002). Optical imaging of Renilla luciferase reporter gene expression in living mice. *Proc Natl Acad Sci USA.* **99:**377–382.

[20] Contag PR, Olomu IN, Stevenson DK, Contag CH (1998). Bioluminescent indicators in living mammals. *Nat Med.* **4:**245–247.

[21] Wu JC, Sundaresan G, Iyer M, Gambhir SS (2001). Noninvasive optical imaging of firefly luciferase reporter gene expression in skeletal muscles of living mice. *Mol Ther.* **4:**297–306.

[22] Rehemtulla A, Stegman LD, Cardozo SJ, Gupta S, Hall DE, Contag CH, Ross BD (2000). Rapid and quantitative assessment of cancer treatment response using in vivo bioluminescence imaging. *Neoplasia.* **2:**491–495.

[23] Kokoris MS, Black ME (2002). Characterization of herpes simplex virus type 1 thymidine kinase mutants engineered for improved ganciclovir or acyclovir activity. *Protein Sci.* **11:** 2267–2272.

[24] Gambhir SS, Bauer E, Black ME, Liang Q, Kokoris MS, Barrio JR, Iyer M, Namavari M, Phelps ME, Herschman HR (2000). A mutant herpes simplex virus type 1 thymidine kinase reporter gene shows improved sensitivity for imaging reporter gene expression with positron emission tomography. *Proc Natl Acad Sci USA.* **97:**2785–2790.

[25] Nasu Y, Kusaka N, Saika T, Tsushima T, Kumon H (2000). Suicide gene therapy for urogenital cancer: Current outcome and prospects. *Mol Urol.* **4:**67–71.

[26] Wiewrodt R, Amin K, Kiefer M, Jovanovic VP, Kapoor V, Force S, Chang M, Lanuti M, Black ME, Kaiser LR, Albelda SM (2003). Adenovirus-mediated gene transfer of enhanced Herpes simplex virus thymidine kinase mutants improves prodrug-mediated tumor cell killing. *Cancer Gene Ther.* **10:**353–364.

[27] He TC, Zhou S, da Costa LT, Yu J, Kinzler KW, Vogelstein B (1998). A simplified system for generating recombinant adenoviruses. *Proc Natl Acad Sci USA.* **95:**2509–2514.

[28] Sato M, Johnson M, Zhang L, Gambhir SS, Carey M, Wu L (in press). Functionality of androgen receptor-based gene ex-

pression imaging in hormone refractory prostate cancer. *Clin Cancer Res.*

[29] Klein KA, Reiter RE, Redula J, Moradi H, Zhu XL, Brothman AR, Lamb DJ, Marcelli M, Belldegrun A, Witte ON, Sawyers CL (1997). Progression of metastatic human prostate cancer to androgen independence in immunodeficient SCID mice. *Nat Med.* **3:** 402–408.

[30] Townsend DW, Carney JP, Yap JT, Hall NC (2004). PET/CT today and tomorrow. *J Nucl Med.* **45:**4S–14S.

[31] Craft N, Chhor C, Tran C, Belldegrun A, DeKernion J, Witte ON, Said J, Reiter RE, Sawyers CL (1999). Evidence for clonal outgrowth of androgen-independent prostate cancer cells from androgen-dependent tumors through a two-step process. *Cancer Res.* **59:**5030–5036.

[32] Craft N, Shostak Y, Carey M, Sawyers CL (1999). A mechanism for hormone-independent prostate cancer through modulation of androgen receptor signaling by the HER-2/neu tyrosine kinase. *Nat Med.* **5:**280–285.

[33] Chen CD, Welsbie DS, Tran C, Baek SH, Chen R, Vessella R, Rosenfeld MG, Sawyers CL (2004). Molecular determinants of resistance to antiandrogen therapy. *Nat Med.* **10:**33–39.

[34] Yaghoubi S, Barrio JR, Dahlbom M, Iyer M, Namavari M, Satyamurthy N, Goldman R, Herschman HR, Phelps ME, Gambhir SS (2001). Human pharmacokinetic and dosimetry studies of [(^{18})F]FHBG: A reporter probe for imaging herpes simplex virus type-1 thymidine kinase reporter gene expression. *J Nucl Med.* **42:**1225–1234.

[35] Fick J, Barker FG 2nd, Dazin P, Westphale EM, Beyer EC, Israel MA (1995). The extent of heterocellular communication mediated by gap junctions is predictive of bystander tumor cytotoxicity in vitro. *Proc Natl Acad Sci USA.* **92:**11071–11075.

[36] Mesnil M, Yamasaki H (2000). Bystander effect in herpes simplex virus-thymidine kinase/ganciclovir cancer gene therapy: Role of gap-junctional intercellular communication. *Cancer Res.* **60:** 3989–3999.

[37] Rogulski KR, Zhang K, Kolozsvary A, Kim JH, Freytag SO (1997). Pronounced antitumor effects and tumor radiosensitization of double suicide gene therapy. *Clin Cancer Res.* **3:**2081–2088.

[38] Lohr F, Huang Q, Hu K, Dewhirst MW, Li CY (2001). Systemic vector leakage and transgene expression by intratumorally injected recombinant adenovirus vectors. *Clin Cancer Res.* **7:** 3625–3628.

Applications of Molecular Imaging in Cancer Gene Therapy

Meera Iyer[1,3], Makoto Sato[2], Mai Johnson[2], Sanjiv S. Gambhir[1,3,5] and Lily Wu[1,2,3,4,*]

Department of [1]Molecular and Medical Pharmacology, and [2]Urology, [3]Crump Institute for Molecular Imaging, [4]Jonsson Comprehensive Cancer Center, David Geffen School of Medicine, University of California Los Angeles and [5]Departments of Radiology and Bioengineering, the Bio-X Program, Stanford University, USA

Abstract: Gene-based therapy is a promising and flexible therapeutic approach to manage diverse types of cancer. The lack of convincing therapeutic success of current gene therapy protocols in part, can be attributed to the inability to monitor gene expression at the targeted site in the living subject. Linking molecular imaging to gene therapy will enable real-time assessment of the therapeutic process and the refinement of treatment protocols. This review will cover two common imaging modalities, positron emission tomography (PET) and bioluminescence imaging (BLI), used in pre-clinical and clinical gene therapy applications. Strategies to develop more specific and robust cancer gene therapy and imaging approaches will be discussed. Coupling PET to gene therapy of cancer has already been implemented in several clinical studies. This approach would help to improve the efficacy and safety of future gene therapy clinical trials.

Keywords: PET, BLI, gene therapy of cancer, transcriptional amplification, targeted gene expression and delivery.

INTRODUCTION

The rapid growth in cancer biology, genetics and pharmacology has led to a better understanding of the mechanisms involved in neoplastic degeneration. In parallel, significant advances have been made in establishing molecular imaging as an indispensable tool in several areas of biomedical research including gene expression imaging and evaluation of anti-cancer therapeutics. The development of non-invasive and clinically applicable techniques for gene therapy monitoring will be crucial to the understanding of disease progression and treatment. Technologies for molecular imaging are manifold; however, the three main techniques that are being used extensively include optical imaging (fluorescent and bioluminescence (BLI)), magnetic resonance imaging (MRI), and positron emission tomography (PET) imaging. Each of these technologies has its advantages and limitations; there is no one technique that fulfills all the criteria required for an ideal imaging modality. This review will discuss the two main modalities that are in use in a wide range of pre-clinical gene therapy applications, PET and BLI.

Molecular imaging as applied to the biomedical research discipline is aimed at developing novel reagents, tools and methods for studying a wide range of biological processes in living subjects in a non-invasive manner [Massoud *et al.*, 2003]. It is a multidisciplinary field, which requires expertise in image-capture technologies, cellular and molecular biology, chemistry, pharmacology, medical physics, and bioinformatics. The "molecular" basis of imaging exploits specific molecular probes to achieve image contrast that differentiate, pathological or target tissue from normal or background tissue in the subject. One particular area of research where the potential of molecular imaging continues to be realized is cancer gene therapy. The goal in cancer gene therapy is to deliver therapeutic transgenes to tumor cells either to restore the function of a damaged gene or to cause the death of the unwanted tumor. Many unanswered questions come to mind in determining the efficacy of gene delivery and expression *in vivo*. Has the gene reached its target? Is the gene product of interest being expressed in the target and if yes, how much of it is being expressed? More importantly, how long does the gene expression persist *in vivo*? Molecular imaging can provide answers to all the above questions by defining the location(s), magnitude and time-variation of gene expression in a subject.

*Address correspondence to this author at the Department of Molecular and Medical Pharmacology, and Urology, Crump Institute for Molecular Imaging, Jonsson Comprehensive Cancer Center, David Geffen School of Medicine, University of California, Los Angeles 675 Charles Young Dr S, Los Angeles, CA 90095, USA; Tel: 310-794-4390; Fax: 310-825-3027; E-mail: LWu@mednet.ucla.edu

REPORTER GENE IMAGING

There are two main strategies for imaging gene expression: direct and indirect. In direct imaging, the target (e.g., protein) is imaged directly using a probe specific for that target. One example is imaging of cell-surface antigens or epitopes using radiolabeled antibodies. Another example is the use of naturally occurring compounds, such as [^{18}F]-fluorodeoxy glucose (FDG) to image the glucose utilization in the brain, which is based on the activity of the enzyme, hexokinase. This approach was first described more than two decades ago [Reivich *et al.,* 1979]. Radiolabeled antisense oligonucleotide (RASON) probes have been used to directly image endogenous gene expression at the transcription level. RASON sequences can be synthesized complimentary to a small segment of the target mRNA or DNA sequence. Gamma camera and PET imaging of endogenous gene expression using RASONs have been reported [Dewanjee *et al.,* 1994; Tavitian *et al.,* 1998]. A major limitation of the direct imaging strategy is the need for a specific probe for each new gene product being studied. Furthermore, it requires the validation of the probe both in terms of specificity

1566-5232/05 $50.00+.00

and sensitivity, which can be very expensive and time-consuming. Alternatively, indirect imaging strategies have been developed, and validated for gene therapy application at considerably reduced costs [Haberkorn *et al.,* 2001; Sundaresan *et al.,* 2002].

Indirect imaging strategies are based on the use of reporter gene technology. In this approach, the therapeutic gene(s) are administered into the subject simultaneously with a reporter gene. The level of expression of the therapeutic gene is inferred indirectly from the level of reporter gene expression, provided the two are well correlated. The level of reporter gene expression *in vivo* is measured by reporter probe accumulation in the region of interest. The product of a reporter gene can be an enzyme that converts a reporter probe into a metabolite, which gets selectively trapped within cells carrying the reporter gene. Alternatively, the reporter gene product can be a receptor that sequesters the reporter probe. Optimal gene-reporter probe systems should meet several criteria [Massoud *et al.,* 2003]: 1) The reporter probe should accumulate only in areas where the reporter gene is expressed. 2) The reporter probe should clear from the circulation rapidly. 3) The reporter gene product should be non-immunogenic. 4) The reporter probe should not exhibit any toxicity. Many indirect imaging strategies have been developed and are widely used in radionuclide-based imaging [Tjuvajev *et al.,* 1996; Tjuvajev *et al.,* 1998; Gambhir *et al.,* 1999; Gambhir *et al.,* 2000] as well as for optical imaging [Contag *et al.,* 2000; Rehemtulla *et al.,* 2000; Wu *et al.,* 2001a; Contag *et al.,* 2002a; Contag *et al.,* 2002b; Wu *et al.,* 2002].

RADIONUCLIDE IMAGING – POSITRON EMISSION TOMOGRAPHY (PET)

The basic concept underlying radionuclide imaging techniques (PET, single photon emitted computed tomography, SPECT, planar gamma camera imaging) is the ability to image and measure the function of biological processes using positron-labeled molecules in trace quantities with minimal perturbation of the underlying tissues [Phelps, 2004]. PET registers high-energy γ-rays emitted from within the subject. Naturally occurring biological molecules can be labeled with a positron-emitting isotope that produces two gamma rays after the emission of a positron from its nucleus. The positron collides with a nearby electron to produce two high-energy gamma rays ~180° apart. These gamma rays are detected by the PET scanner and are used to construct volumetric images of the positron-emitting probe location(s) and concentrations.

The recent development of small animal PET cameras (microPET) has driven the growth of molecular imaging assays, thereby permitting rapid testing of human tumors implanted in mice. Due to the small size of laboratory animals, significantly improved resolution is required for microPET compared to the clinical PET scanners. The early prototype microPET scanner has a spatial resolution of 2^3 mm^3 [Cherry *et al.,* 2001], but the newer models offer even better resolution of 1 mm^3 [Chatziioannou *et al.,* 2001]. Reporter probes with a high specific activity are required for small animal imaging due to the need to inject smaller doses. Two categories of PET reporter systems developed are those that utilize intracellular enzyme-based approach or those associated with cell membrane receptors (Fig. **1**).

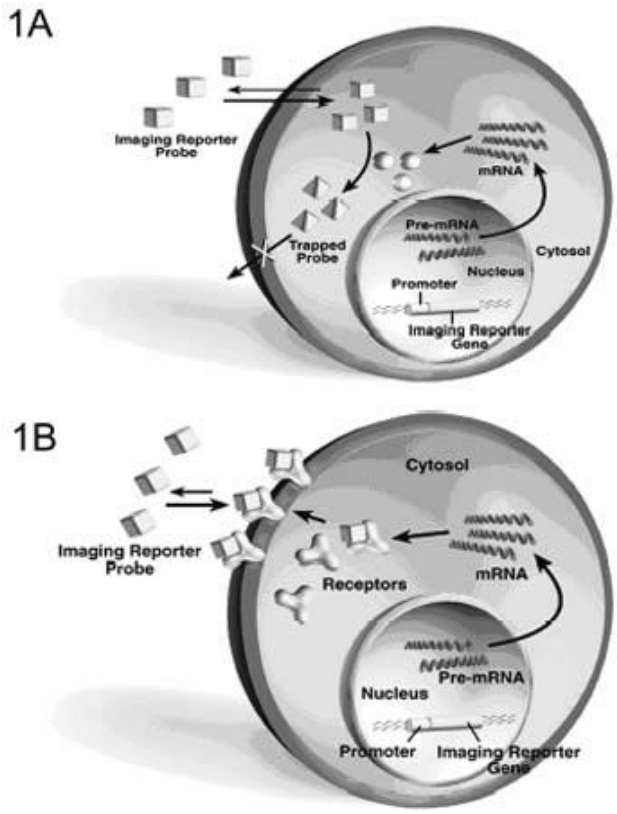

Fig. (1). A schematic diagram illustrating two different approaches for imaging reporter gene expression using PET. A reporter gene introduced into the cell can encode for (A) an enzyme (e.g., HSV1-tk) that leads to trapping of a radiolabeled probe ([^{18}F]-FPCV/[[^{18}F]-FHBG) or (B) an intracellular and/or extracellular receptor (e.g., D2R), which leads to trapping of a radiolabeled ligand ([^{18}F]-FESP). In both cases, significant trapping of the reporter probe will occur only if the reporter gene is expressed. Reproduced with permission from Sundaresan and Gambhir [Sundaresan *et al.,* 2002].

Enzyme Based Reporter Gene Imaging

The herpes simplex virus type I thymidine kinase (*HSV1-tk*) gene is currently one of the most frequently used PET reporter genes. The enzymatic activity of *HSV1-TK* is also the cornerstone of anti-viral treatment [Oliver *et al.,* 1985] and suicide gene therapy to treat cancer [Freeman *et al.,* 1996]. The viral enzyme possesses the unique ability to phosphorylate acycloguanosines, such as ganciclovir, to its monophosphorylated form. The subsequent phosphorylation of the otherwise non-toxic ganciclovir monophosphate by cellular kinases to the triphosphate derivative causes chain termination during DNA replication and cell death. In PET applications, the phosphorylation of radioactive guanine derivatives leads to the trapping and accumulation of the radiolabeled tracer in cells expressing *HSV1-tk*. The tracer level of radiolabeled probe used in PET is 3- to 4-orders lower than in cytotoxic therapy, thus, it is devoid of harmful pharmacological effects.

The enzymatic activity of *HSV1-TK* was first exploited for imaging of gene expression *in vivo* [Tjuvajev *et al.*, 1995] using radioactive iodine labeled uracil derivative 5-iodo-2'-hydroxy-1-β-D-arabinofuranosyl-5-iodouracil (FIAU) as reporter probe [Tjuvajev *et al.*, 1996]. This was followed by validation of F-18 fluorinated ganciclovir (FGCV), and penciclovir (FPCV) as probes for microPET [Gambhir *et al.*, 1998; Tjuvajev *et al.*, 1998; Gambhir *et al.*, 1999; Tjuvajev *et al.*, 1999; Gambhir *et al.*, 2000]. These PET imaging approaches enabled real-time quantification of adenoviral mediated *HSV1-tk* gene transfer to murine liver in living animals [Gambhir *et al.*, 1998]. Further optimization of the PET probe technology demonstrated that [^{18}F]-9-(4-fluoro-3-hydroxymethylbutyl)guanine (FHBG), a side chain fluorinated analog of penciclovir, was superior to FPCV and FGCV *in vivo* [Iyer *et al.*, 2001a]. Improvement in the *HSV1-tk* reporter gene was accomplished by genetic engineering of the TK protein active site to increase the affinity towards acycloguanosine analogs while decreasing the affinity for thymidine [Black *et al.*, 1996; Kokoris *et al.*, 2002], a competitor. A particular mutant, *HSV1-sr39tk*, exhibited greater than 2-fold enhanced imaging sensitivity for FHBG than the wild type *HSV1-tk* gene [Gambhir *et al.*, 2000]. Among the different gene-reporter probe combinations studied, *HSV1-sr39tk*-FHBG offered the maximum sensitivity for *in vivo* imaging of adenoviral mediated gene transfer [Min *et al.*, 2003].

Receptor Based Reporter Gene Imaging

Many imaging reporter genes encode cell surface receptors by virtue of their ability to sequester specific radiolabeled probes. These receptors include somatostatin type 2 [Hemminki *et al.*, 2002], transferrin [Moore *et al.*, 1998; Hogemann *et al.*, 2000], sodium iodide symporter [Haberkorn *et al.*, 2001; Groot-Wassink *et al.*, 2004], and dopamine 2 receptor (*D2R*) [MacLaren *et al.*, 1999]. These receptors are endogenous genes, thus, they are anticipated to be less immunogenic relative to the protein encoded by the *HSV1-tk* gene. Since its native expression profile of D2R is restricted to CNS, *D2R* has been established as a useful PET reporter gene in somatic gene transfer applications in other tissues outside of CNS [MacLaren *et al.*, 1999; Liang *et al.*, 2002]. Gene expression is measured by interaction of D2R with its ligand 3-(2'-[^{18}F]fluoroethyl) spiperone (FESP). Real-time *in vivo* PET of mice injected with a recombinant adenovirus carrying *D2R* gene demonstrated that hepatic [^{18}F] PET retention signals were directly proportional to *in vitro* measures of hepatic FESP retention, D2R ligand binding, and D2R mRNA [MacLaren *et al.*, 1999]. To create an inert PET reporter gene, the development of a truncated *D2R* gene was reported, where the signal transduction was uncoupled while maintaining affinity for FESP [Liang *et al.*, 2002].

The sodium iodide symporter (NIS) is another reporter protein that holds dual capacity to provide an imaging as well as a therapeutic function. The endogenous NIS is a 12 transmembrane domain protein expressed mainly in the thyroid, the stomach, and the salivary glands[Dai *et al.*, 1996] In the thyroid, the NIS protein transports iodide into the cytoplasm and concentrates it 20- to 40-fold, driven by the sodium gradient across the basal membrane[Filetti *et al.*, 1999]. NIS mediated radioisotope uptake has been used clinically for decades in the diagnosis and therapy of thyroid disease [Shimura *et al.*, 1997]. The cloning of its cDNA has initiated efforts to employ NIS as a tool for gene therapy [Mandell *et al.*, 1999; Spitzweg *et al.*, 2000; Cho *et al.*, 2002; Groot-Wassink *et al.*, 2002]. Recently, the applicant of NIS as an imaging reporter has been demonstrated using PET [Groot-Wassink *et al.*, 2004] or SPECT [Haberkorn, 2001]. One distinct advantage of NIS in the dual role of reporter and therapeutic gene-based applications is that the biodistribution, metabolism, and toxicity of many radiotracers are well known from decades of clinical experience. Although isotopes of iodide ($^{123/124/131}$I) are its most common substrate, NIS transports a wide range of other isotopes including ^{99m}Tc Pertechnetate, $^{188/186}$Re Perrhenate, and ^{211}At, which may be employed for many diagnostic and therapeutic purposes.

PET imaging offers several advantages over other imaging techniques. PET is quantitative and has a high spatial resolution with sensitivity ranging from 10^{-11} to 10^{-12} mole/L. A broad range of molecular imaging agents already have been approved for clinical uses with many novel agents being tested in pre-clinical models. The ability to translate data from small animal PET imaging studies to patients in the clinic is of great benefit. Moreover, rapid advances in imaging technology have now resulted in the development of fused imaging modalities, such as PET-CT [Townsend *et al.*, 2004]. The fusion modality allows researchers to understand biological information in the context of precise anatomical localization in a single imaging session.

BIOLUMINESCENCE IMAGING (BLI)

The concept of BLI is based on the emission of visible photons at specific wavelengths from energy dependent reactions catalyzed by luciferases. The luciferase proteins have been isolated from a variety of insects, marine organisms and prokaryotes [Hastings, 1996]. Firefly luciferase generates visible light through the oxidation of the enzyme-specific substrate, D-luciferin in the presence of oxygen and ATP as an energy source. During the reaction, part of the chemical energy is released as visible light (blue to yellow-green in color) with emission spectra that peaks at wavelengths of 490-620 nm. A schematic illustration of the bioluminescence concept is shown in Fig. **2**. Among the different luciferases, the luciferase from the North American firefly, *Photinus pyralis* (*fluc*) is the most commonly used bioluminescence reporter in biomedical research. It has been adapted for use in mammalian cells as an indicator of cell proliferation, gene delivery and therapeutic assessment following drug treatment [McCaffrey *et al.*, 2003].

A second luciferase validated for BLI is the renilla luciferase (*rluc*) [Bhaumik *et al.*, 2002; Bhaumik *et al.*, 2004]. *Rluc* emits blue light with a spectral peak at 480 nm [Lorenz *et al.*, 1996]. The *rluc* enzyme was isolated from the sea pansy (*Renilla reformis*), a soft coral that emits blue-green bioluminescence upon mechanical stimulation. Biochemically distinct from fluc, rluc catalyzes the oxidation of coelenterazine with a different kinetics of light production. Hence, C6 rat glioma cells marked with either *rluc* or *fluc* gene can be imaged simultaneously in the same animal

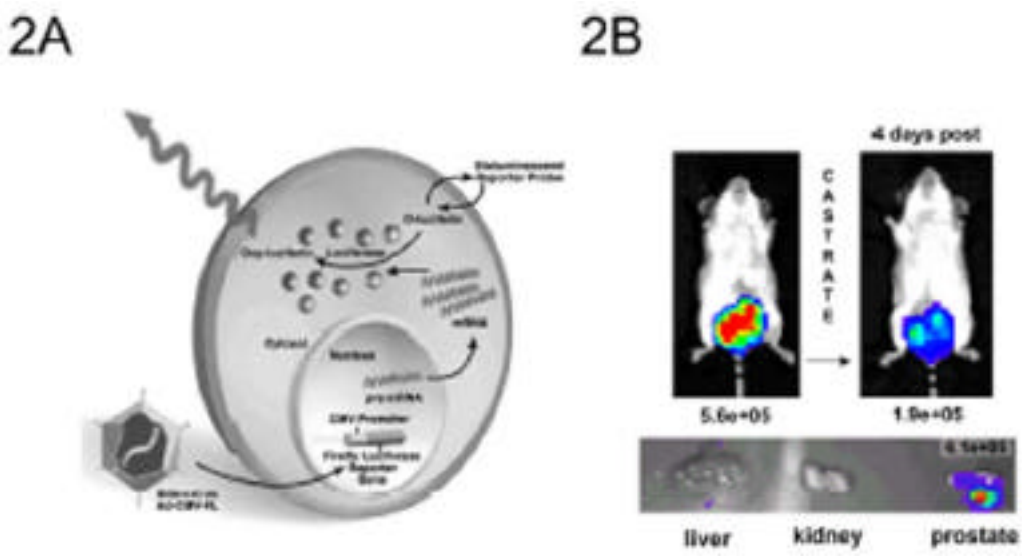

Fig. (2). Schematic representation and application of enzyme-based bioluminescence imaging. (A) D-Luciferin is a reporter probe that is acted upon by the enzyme firefly luciferase (fluc) resulting in bioluminescence via a chemiluminescent reaction under physiological conditions only within living cells carrying the *fluc* gene. Reproduced with permission from [Massoud *et al.,* 2004]. (B) Application of bioluminescence imaging to *in vivo* animal study. The FL expressed by AdTSTA-*fluc* in the same animal before and after castration. 10^7 pfu of AdTSTA-*fluc* was injected into prostate in intact SCID mouse. 31 days post injection, the animal was imaged and castrated (left panel) and reimaged at day 35 (4 days post-castration; right panel). The animal was sacrificed at 11 days post-castration and organs were isolated and imaged. The prostate gland was the predominant site of *fluc* gene expression. Numbers imply for optical activity (photons/sec/cm^2/steridan).

[Bhaumik *et al.,* 2002]. Recently, a mutant version of *rluc* has been developed that exhibits a 4-fold improvement in light output. [Loening *et al.,* 2004]. The Gaussia luciferase utilizing coelenterazine from a marine copepod has also been recently demonstrated to be suitable for mammalian gene expression imaging [Tannous *et al.,* 2005].

A critical element of the BLI technique is a sensitive detector based on cooled charge coupled device (CCD) cameras. These cameras have undergone several modifications resulting in improved sensitivity and utility. Cooled CCD cameras enable reduction of thermal noise leading to increased signal to noise ratio, while preserving the spectral sensitivity of the camera. These systems are sensitive to light across the entire visible spectrum and into near infrared wavelengths [Contag *et al.,* 2002a].

BLI enables the real-time assessment of a wide variety of gene therapy applications. For instance, the efficacy of lentiviral-mediated expression of human clotting factor IX in murine liver was verified by monitoring of the linked *fluc* marker gene [Tsui *et al.,* 2002]. In another study, a recombinant adeno-associated viral vector carrying the *fluc* gene was used to study the efficacy, safety and long-term expression of foreign genes delivered into fetuses of mice *in utero* [Lipshutz *et al.,* 2001]. Detection of light from the mice *in utero* was indicative of the substrate crossing the placental barrier. The gene expression was found to persist for up to eighteen months. Gene transfer *in vivo* using non-viral reagents can be monitored by *fluc* gene expression. Optical signals can be detected in the lungs after a single intravenous injection of cationic liposome of extruded DOTAP:cholesterol DNA complexes [Iyer *et al.,* 2002]. Intravenous delivery of transferin-targeted DNA-PEI polyplexes results in specific *fluc* gene transfer and expression in N2a tumors [Hildebrandt *et al.,* 2003].

The key advantages of BLI are that the technique is fast, costs less than the other imaging modalities, requires short acquisition times and improves the quality of the data set by allowing repetitive imaging of the same animal. More importantly, it offers a high signal to background ratio as the bioluminescence signal is detected only upon interaction of the substrate with the enzyme. However, this technique also has certain disadvantages. First, bioluminescence signals originating deep within the subject are greatly attenuated. Second, the images from the CCD camera are two-dimensional and are devoid of depth information. Work is currently underway to develop CCD cameras that enable multiple views of the same animal, which may help address this problem. And finally, the attenuation and scattering of visible light as it traverses through tissue severely hinders the use of BLI for human applications. Despite its limitations, BLI is playing a key role in gene therapy of cancer by allowing efficient, non-invasive and rapid assessment of transgene expression following vector delivery and monitoring the effects of drug therapy in pre-clinical models.

One of the biggest challenges in cancer gene therapy is to develop cancer-specific treatments. Towards this end, strategies have been employed to enhance specific viral vector transduction of cancer cells or to apply tissue- or tumor-specific promoters (TSPs) to express the therapeutic gene. The following sections will cover approaches taken to improve gene therapy of cancer and how imaging can be incorporated to enhance such applications. The schematic representation of transcriptional and transductional targeting is illustrated in Fig. **3**.

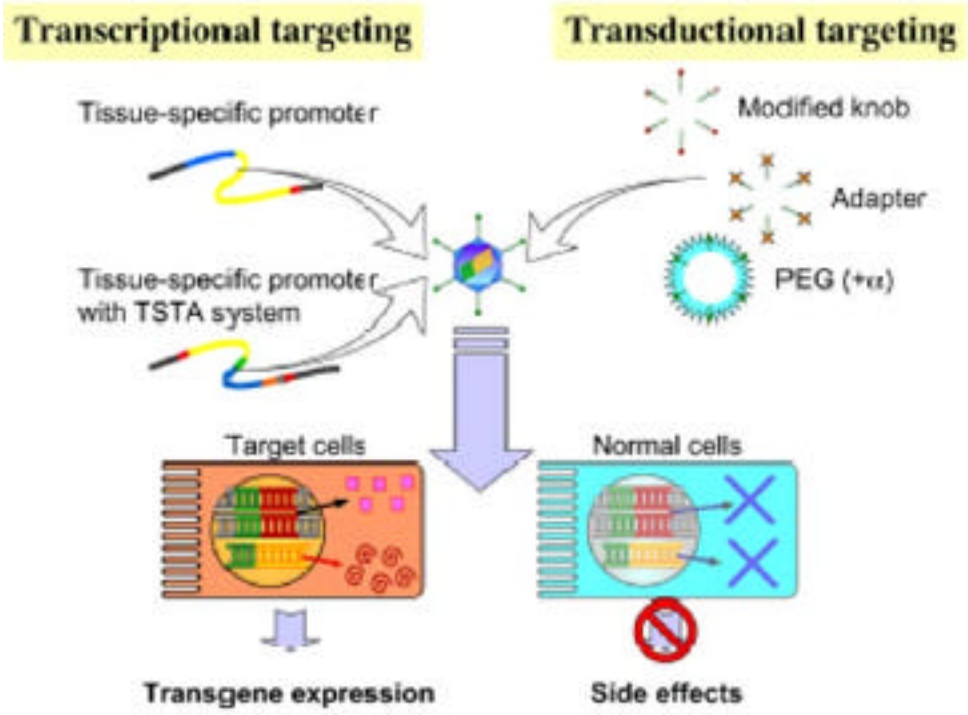

Fig. (3). Targeting strategies on cancer gene therapy. Transcriptional targeting utilizes tissue- or tumor- specific promoter to drive transgene. Robust expression is achievable with an amplification system such as TSTA system. Transductional targeting uses a variety of modifications on vector tropism like genetic modification, adapter utilization and chemical modification of the vector. Both targeting strategies aim at specific and efficient transduction of target (i.e. cancer) cells but not of normal cells to avoid unwanted side effects.

TRANSDUCTIONAL TARGETING

Transductional targeting depends on interaction between surface modified gene transfer vectors and cancer cell surface membrane proteins that the vectors specifically bind to [Mizuguchi *et al.,* 2004]. Following systemic administration, most viral gene transfer vehicles tend to accumulate in the liver. One measure of success of transductional targeting is to assess whether liver transduction is reduced. Hemminki *et al.,* inserted RGD-4C sequence into the HI loop of the fiber knob of adenovirus [Hemminki *et al.,* 2001; Hemminki *et al.,* 2002]. This modification augmented viral binding and internalization via cell surface $\alpha_v\beta_3$ and $\alpha_v\beta_5$ integrins to avert the CAR-dependent step of transduction, which is especially problematic for many CAR-deficient ovarian cancer cells. A gamma camera was used to image gene expression from the modified adenovirus. The somatostatin receptor subtype 2 and its ligand ^{99m}TC-depreotide were utilized to image the transduction of the vector, but recently available SPECT imaging can potentially provide higher resolution with quantitative information. A bispecific antibody that recognizes angiotensin-converting enzyme (ACE) of lung epithelium and the knob protein of adenovirus on its two ends was injected via tail-vein [Reynolds *et al.,* 2000]. This vector was targeted to pulmonary capillary endothelium and achieved 20-fold increase in adenovirus DNA in the lung compared to the untargeted vector.

A recent study employed dual BLI to demonstrate that a novel pseudotyped lentivirus can achieve antibody-mediated specific transduction of metastatic melanoma cells [Morizono *et al.,* 2005]. The viral envelope was substituted by a chimeric Sindbis envelope protein mutated to reduce tropism to liver and spleen, and it also contained the ZZ domain of protein A to interact with the antibody. Tumor cells were first marked by *rluc* gene and the targeted virus carried the *fluc* gene. Successful targeting of P-glycoprotein membrane antigen was demonstrated by co-localization of both luciferase signals in the tumor cells after systemic administration of the virus combined with the specific monoclonal antibody. An alternative way to follow viral distribution and transduction *in vivo* is to directly incorporate imaging protein into the virus structure. Enhanced green fluorescent protein (EGFP) was inserted into pIX, the adenovirus external capsid cement protein [Le *et al.,* 2004]. The insertions of luciferase and PET reporter protein into pIX have also been reported by Dr. David Curiel's group in the ASGT annual meeting (2005). The concept in these approaches is to monitor the reporter-fused vector directly by BLI or PET. An innovative approach to determine relevant tumor-specific antigens was reported recently [Oh *et al.,* 2004]. In this study, tissue-specific and tumor-specific expressions of endothelial cell surface proteins were mapped by proteomic approaches and successful targeted tumor eradication was achieved by antibody-mediated radioimmunotherapy.

TRANSCRIPTIONAL TARGETING

Transcriptional targeting is feasible because the tissue- or cancer-specific promoter can be activated in the targeted cancer cell in the presence of the proper subset of activators, but would remain relatively silent in the non-targeted cell.

Testing in animal models showed that specific promoters exhibit a clear advantage of reduced cytotoxicity as compared to a strong constitutive promoter such as the human cytomegalovirus (CMV) promoter currently utilized in clinical trials [Morelli *et al.,* 1999; Nettelbeck *et al.,* 2002]. A wide range of tissue-specific and tumor-selective promoters (TSPs) has been developed for gene therapy of cancer (reviewed in [Nettelbeck *et al.,* 2000; Wu *et al.,* 2003]). However, transgene expression involving the use of TSPs is generally lower than constitutive viral promoters due to their weak transcriptional activity. Hence, strategies to augment the activity of TSPs are warranted.

Several strategies have been reported to enhance the transcriptional activity of such promoters [Nettelbeck *et al.,* 2000]. Among these, a binary strategy termed two-step transcriptional amplification (TSTA, Fig. **4**) has worked well. In this approach, a specific promoter directed the potent transcription activator, GAL4-VP16, which in turn acted upon a second GAL-4-responsive reporter or therapeutic gene. This TSTA approach, based on the original "enhancer trap" methodology to study gene expression in *Drosophila melanogaster* development, can boost the activity of the prostate specific antigen (PSA) promoter over a range of up to 1000-fold [Iyer *et al.,* 2001b; Zhang *et al.,* 2002]. Optimal TSTA constructs displayed activity levels significantly higher than the CMV promoter, while maintaining prostate cell specificity and androgen responsiveness [Iyer *et al.,* 2001b; Zhang *et al.,* 2002]. Many applications of this two-tiered amplification strategy have been documented, including amplification of Mucin-1 promoter mediated expression for colon cancer [Block *et al.,* 2002], and enhancement of the carcinoembryonic antigen (CEA) promoter [Qiao *et al.,* 2002] to boost *HSV-tk* expression. Greater tumor cell killing of CEA positive breast tumor cell and accumulation of [^{131}I]-FIAU tumor signal recorded by gamma camera were documented in this latter study.

Although molecular imaging is known to be a powerful non-invasive technology to assess transgene expression *in vivo*, only a few groups have employed targeted vectors to express imaging reporter genes. Both BLI and PET technologies we have been avidly applied in the development of prostate cancer targeted gene therapy. Due to its highly specific nature, the PSA promoter has been frequently utilized in prostate cancer-targeted gene therapy approaches [Schuur *et al.,* 1996; Pang *et al.,* 1997; Rodriguez *et al.,* 1997]. When a modified PSA promoter-driven luciferase adenoviral vector was administered into mice bearing prostate tumors, it not only exhibited tissue-selective expression but it also enabled the detection of metastases in the spine and lung by BLI [Wu *et al.,* 2001b; Adams *et al.,* 2002]. The potency and specificity of the PSA promoter-based TSTA expression system was retained in an adenoviral vector [Sato *et al.,* 2003; Zhang *et al.,* 2003]. For instance, AdTSTA-*sr39tk* mediates robust and prostate-specific expression of *HSV1-sr39tk* gene. Tumor directed injection of this vector resulted in specific retention of [^{18}F] FHBG and microPET signals in the androgen-dependent human prostate tumors, as well as tumors in the advanced hormone-refractory stage [Sato *et al.,* 2005]. A lentivirus carrying the TSTA expression cassette also exhibited regulated, cell-specific and long-term expression [Iyer *et al.,* 2004].

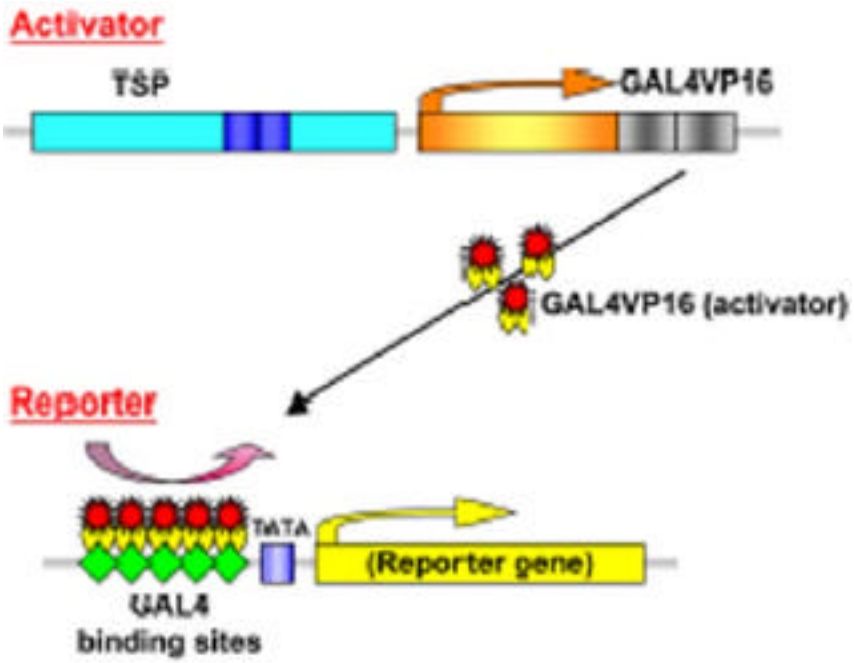

Fig. (4). Schematic representation of a TSTA system. In order to augment relatively weak tissue specific promoter (TSP), two-tiered transcriptional amplification system was developed. TSP controls GAL4VP16, a potent aritificial transactivator, which in turn binds to GAL4 binding site repeats in front of minimal promoter to regulate reporter (or therapeutic) gene. This system achieved approximately 1000-fold activity increase compared to native promoter [Zhang *et al.,* 2002].

The regulation of *GRP78* promoter was examined in human breast tumor by [^{18}F]-FHBG mPET imaging [Dong *et al.,* 2004]. The GRP78 is a stress-inducible chaperone protein that is highly expressed in tumor cells [Reddy *et al.*, 2003], and its expression is induced by photodynamic therapy, stress, and glucose starvation. [^{18}F] FHBG-PET signals were documented in breast tumors stably transduced by a retrovirus expressing *HSV-tk* driven by the *GRP78* promoter. Moreover, the signal was induced by photodynamic therapy. Epstein Barr Virus (EBV)-associated nasopharyngeal carcinoma (NPC) is defined by the presence of EBV gene products such as EBNA-1 protein in the tumor cells. An interesting NPC-specific expression strategy is to exploit EBNA-1's ability to bind to oriP regulatory sequences and induce gene expression based on these sequences [Li *et al.,* 2002]. An adenoviral vector expressing *fluc* controlled by the *oriP* sequences was able to achieve tumor-specific gene expression following systemic injection as monitored by optical imaging [Mocanu *et al.,* 2004].

Liang Q et al. took a combinatorial approach of incorporating bispecific molecule sCAR-EGF, a recombinant protein containing the soluble portion of coxsakievirus and adenovirus receptor (sCAR) fused to epidermal growth factor in addition to the COX-2 promoter for transcriptional targeting [Liang *et al.,* 2004a; Liang *et al.,* 2004b]. The sCAR moiety binds to the virus and blocks CAR-dependent adenovirus infection. The adenovirus carrying COX-2 promoter driving reporter gene and sCAR-EGF exhibited reduced transduction in the liver and preferential transduction of EGF receptor expressing cells. The improvement in gene transfer to targeted tumor was demonstrated by BLI.

LINKED GENE EXPRESSION STRATEGIES

Strategic planning of optimal gene therapy will require the simultaneous expression of multiple therapeutic genes or a combination of imaging reporter gene and a therapeutic gene. As alluded to previously, it is highly desirable to have the expression of an indirect imaging reporter gene be linked to a therapeutic gene such that the levels of therapeutic gene expression can be inferred from the levels of reporter gene expression. Several strategies to link expression of multiple genes are described in the following sections (Fig. **5**).

The bi-cistronic approach for linking two genes involves the incorporation of an internal ribosomal entry site (IRES) sequence between the two genes. Both genes are then transcribed into a single mRNA, followed by translation into two different proteins. This approach was applied to image the expression of *HSV1-sr39tk* and *D2R* reporter genes in a tumor model using microPET [Yu *et al.,* 2000]. A major limitation of this approach is the attenuated expression of the gene distal to the IRES sequence. To overcome this problem, the use of ten linked copies of the Gtx (homeodomain protein) IRES (designated as SIRES) in place of the EMCV-IRES has been described [Chappell *et al.,* 2000]. This change resulted in a significant gain in signal for the downstream *fluc* gene. Insertion of the SIRES sequence between the bioluminescence (*rluc*) and PET reporter gene also augments the PET signal mediated by the downstream genes *in vivo* [Wang *et al.,* 2005].

Another strategy to link two genes makes use of a fusion gene vector. The two genes are connected in such a way that their coding sequences are in the same reading frame generating a single protein with the characteristics of both the original proteins. This approach has been validated in several studies involving fusion reporters such as *HSV1-tk*-GFP [Doubrovin *et al.,* 2001], DHFR-*HSV1-tk* [Mayer-Kuckuk *et al.,* 2002] and DHFR-GFP [Banerjee *et al.,* 2002]. A bioluminescence-PET fusion reporter composed of *HSV1-sr39tk* and *rluc* genes can achieve successful *in vivo* imaging using dual modalities [Ray *et al.,* 2003]. This approach was further

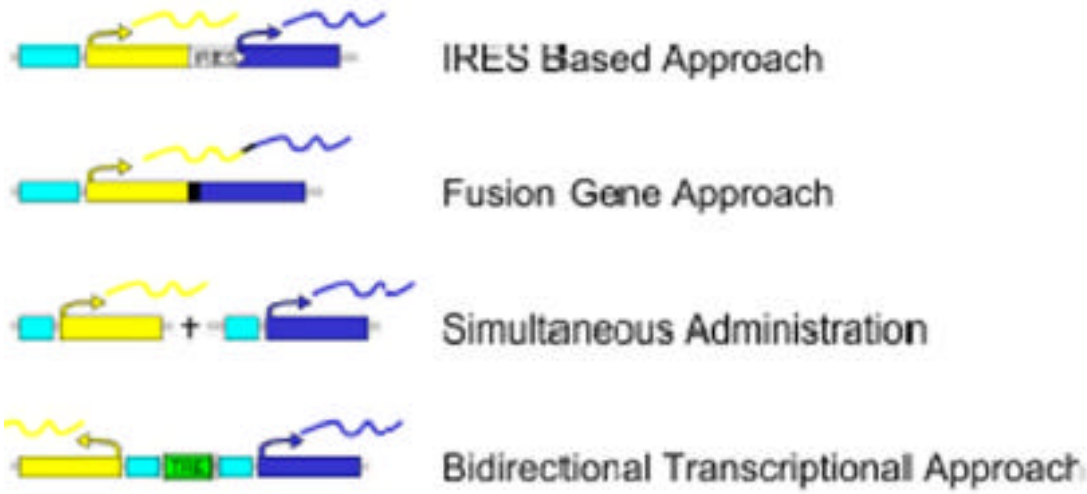

Fig. (5). Strategies to link expression of two genes in a single construct. (From the top) 1) Bi-cistronic approach to express two genes utilizes the incorporation of an internal ribosomal entry site (IRES) sequence between the two genes. 2) Fusion approach for linking two genes. Coding sequences of the two genes are connected in the same reading frame generating a single protein with a spacer. 3) Simultaneous co-administration approach. Transducing target cells with two separate vectors simultaneously. 4) Bi-directional transcriptional approach. A centrally located transcriptional regulatory element (TRE) such as tetracycline-responsive promoter elements or GAL4 binding site repeats in the TSTA system, two genes are expressed in a bi-directional manner.

extended in the development of the tri-fusion reporters carrying a fluorescent, bioluminescence and PET reporter genes [Ray *et al.,* 2004a]. A concern of the fusion approach is that the fusion protein may not yield functional activities for the individual proteins. This has been speculated to be due to the nature of the genes fused and the length of the spacer between the proteins.

A third approach to link two genes makes use of two different vectors, wherein the expression of the two genes is driven by the same promoter (CMV). The two genes are cloned into different vectors and co-administered via the tail-vein *in vivo*. The use of this approach demonstrated was for monitoring the expression of *HSV1-sr39tk* and *D2R* reporter genes using an adenoviral-mediated gene delivery vector [Yaghoubi *et al.,* 2001b]. Like other approaches, the co-vector administration approach also has a limitation associated with the delivery of multiple genes *in vivo*. Nevertheless, this strategy remains a suitable option for indirect imaging of two or more genes simultaneously.

A fourth approach to link two genes makes use of the bi-directional transcriptional strategy. The *HSV1-sr39tk* and *D2R* gene were co-expressed in a bi-directional manner with a centrally located tetracycline-responsive promoter elements. The *in vivo* expression of the two genes was highly correlated and was regulated in a dose-dependent manner by doxycycline in a tumor xenograft model [Sun *et al.,* 2001]. Recently, a novel bi-directional vector system has been described based on the TSTA strategy, which can simultaneously amplify the expression of two genes using a weak promoter (Fig. **4**, [Ray *et al.,* 2004b]). The bi-directional approach has several advantages over the other linked systems; it does not cause attenuation of either gene like the IRES based systems, and the two genes are always functionally active unlike in the fusion constructs.

MONITORING CANCER TREATMENT BY IMAGING

Besides monitoring the *in vivo* activity of the vector, molecular imaging has emerged as a useful mean to monitor cancer cells during treatment in pre-clinical models. Tumors stably expressing *fluc* implanted at subcutaneous, orthotopic or intraperitoneal sites all can be effectively imaged by optical CCD camera. In general, tumor growth is correlated with an increase of optical signal. Conversely, the cytoreductive effects of chemotherapeutic treatments manifested as signal reduction were successfully monitored in several studies [Sweeney *et al.,* 1999; Rehemtulla *et al.,* 2000; Vooijs *et al.,* 2002]. To obtain an accurate assessment of the anti-tumor effects of a retargeted conditionally replicating adenovirus (CRAd), Kanerva et al [Kanerva *et al.,* 2005] cleverly engineered both a serology marker (hCEA) and *fluc* gene into the SKOV ovarian tumor cells. In doing so, the kinetics of growth and destruction of intraperitoneal tumor cells were non-invasively monitored by both serology and BLI. Due to the limitations of BLI in significant attenuation of signals with increased tissue depth and lack of 3-D resolution, gene-based therapeutic effects on solid tumors might be more accurately assessed by MRI [Rehemtulla *et al.,* 2002; Hamstra *et al.,* 2004] or PET [Yaghoubi *et al.,* 2005].

As mentioned previously, the *HSV1-tk* gene possesses the dual capability to be a PET reporter and a suicide gene. Thus, in the setting of suicide gene therapy imaging, the *HSV1-tk* gene becomes a direct approach of monitoring the therapeutic gene [Johnson *et al.,* 2005; Yaghoubi *et al.,* 2005]. In a very recent study [Johnson *et al.,* 2005], combined [^{18}F]-FHBG PET and CT were utilized to monitor intratumoral gene transfer and therapy mediated by the prostate-specific AdTSTA-*sr39tk* or AdCMV-*sr39tk* adenoviral vectors (Fig. **6**). Loss of *sr39tk* PET signal in the tumor after GCV treatment was observed, which correlated with destruction of tumor cells. In this study, cell-specific TSTA suicide gene therapy was demonstrated to be superior to the constitutive approach in minimizing systemic liver toxicity (Fig. **6**).

Molecular imaging is a blossoming field to develop non-invasive means to visualize and interpret the internal tumor environment or signaling. For example, the dynamic process of tumor hypoxia was monitored by PET imaging employing a hypoxia-inducible promoter to control the PET reporter gene expression [Serganova *et al.,* 2004]. Gene transfer technology could be coupled to imaging to develop important diagnostic as well as therapeutic modalities. Many intracellular events are controlled by the interaction between different proteins. Extending upon the concept of yeast two-hybrid system to study protein-protein interaction, the interaction between p53 and T-antigen was exploited to create the inducible expression of *HSV1-sr39tk* PET reporter [Luker *et al.,* 2002]. An alternative approach is to split the *fluc* reporter protein into two nonfunctional halves and link each half to an interactive protein partner. Upon specific interaction between the protein partners, the two halves of the bioluminescent protein will be juxtaposed to reconstitute the optical activity [Paulmurugan *et al.,* 2002]. This strategy has been successfully applied to image homodimeric interactions [Massoud *et al.,* 2004] and drug-protein interaction [Paulmurugan *et al.,* 2004] in living mice.

The ultimate objective of reporter gene imaging is to be able to translate the findings from small animal models to clinically applicable methods. In this context, two recent clinical studies have incorporated imaging to monitor cancer gene therapy. For example, repetitive PET imaging was performed to assess a cationic liposome-mediated *HSV1-tk* suicide gene transfer into glioblastoma [Jacobs *et al.,* 2001; Reszka *et al.,* 2005]. The use of [^{18}F] FHBG probe was studied in healthy human volunteers to characterize the biodistribution and route of clearance of the reporter probe. The results showed that FHBG exhibited good pharmacokinetic properties and rapid clearance suitable for applications in patients [Yaghoubi *et al.,* 2001a]. Most interestingly, FHBG-PET can be used to monitor *HSV1-tk* gene expression in patients with hepatocellular carcinoma [Penuelas *et al.,* 2005]. Gene expression was evident in all patients who received a viral dose of 7.7×10^9 pfu or more. These findings will help support the use of the FHBG-*HSV1-sr39tk* system to directly monitor the expression of therapeutic gene in future suicide gene therapy trials.

FUTURE OUTLOOK

There is an ever-increasing knowledge of critical biological pathways in play in oncogenesis and cancer progression. Molecular imaging has become an indispensable tool in biomedical research; it provides the ability to evaluate the

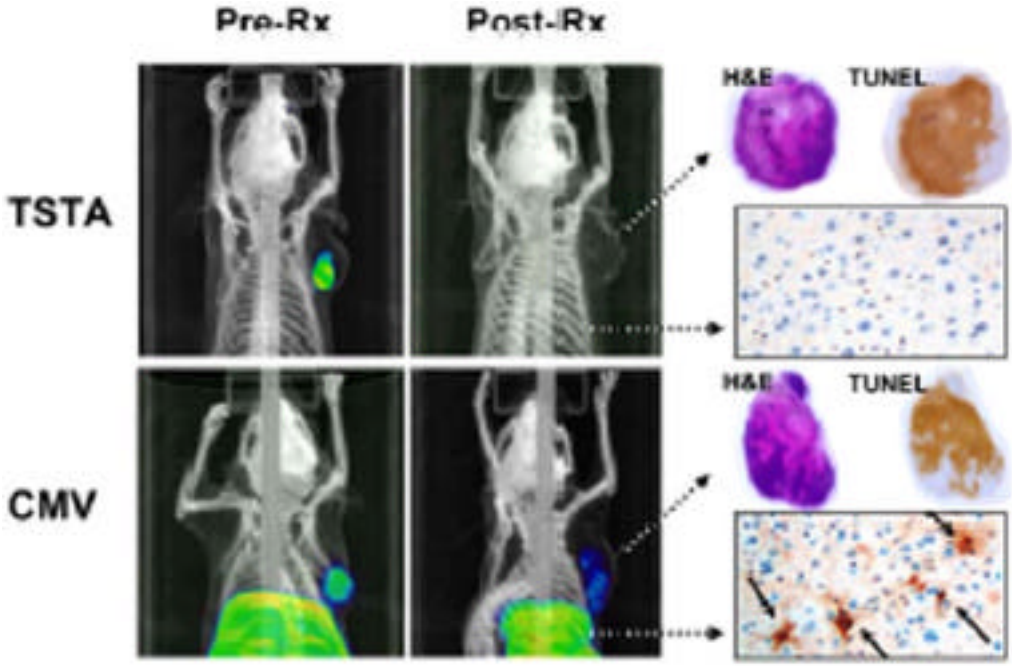

Fig. (6). MicroPET/CT imaging of suicide gene therapy. Ten to the ninth infectious units of prostate-targeted AdTSTA-sr39tk (TSTA) or constitutive active AdCMV-sr39tk (CMV) was intratumorally injected into androgen dependent LAPC-4 tumors, human prostate cancer xenografts on mice on day 0. MicroPET/CT imaging performed prior to ganciclovir (GCV) treatment on day 7 showed tumor-limited expression in the TSTA-treated animals, but the CMV-treated animal showed strong expression in the liver as well. After receiving GCV treatment, F18-FHBG PET signals at day 22 were diminished in the tumors and the liver of the CMV animals. Histology performed at the end-point (day 22) revealed extensive apoptosis (TUNEL-positive brown staining) in the tumors and the liver of the CMV-treated animals.

success or failure of gene transfer and expression in the desired tissue over time and monitor cancer progression and drug efficacy in living subjects. Imaging approaches are being used at all stages of drug discovery and development ranging from pre-clinical studies to clinical drug assessment. With continued progress in vector production and probe development, molecular imaging will provide a pragmatic hope for assessment of efficacy and safety in pre-clinical and clinical cancer gene therapy.

ACKNOWLEDGMENTS

This work is supported by Department of Defense grant DAMD17-03-1-0095 and NIH grant R01 CA101904 (L. Wu); NIH grant R01 CA82214 and Small Animal Imaging Resource Program grant R24 CA92865 (S.S. Gambhir); and Department of Defense Congressionally Directed Medical Reseach Program postdoctoral fellowship, PC020531 (M. Sato). We deeply appreciate W. Ladno, J. Edwards, and Dr. D. Stout for their skillful assistance in PET/CT imaging.

REFERENCES

Adams, J.Y., Johnson, M., Sato, M., Berger, F., Gambhir, S.S., Carey, M., Iruela-Arispe, M.L., Wu, L. (2002) Visualization of advanced human prostate cancer lesions in living mice by a targeted gene transfer vector and optical imaging. *Nat. Med.*, 8:891-7.

Banerjee, D., Mayer-Kuckuk, P., Capiaux, G., Budak-Alpdogan, T., Gorlick, R., Bertino, J.R. (2002) Novel aspects of resistance to drugs targeted to dihydrofolate reductase and thymidylate synthase. *Biochim. Biophys. Acta*, **1587**:164-73.

Bhaumik, S., Gambhir, S.S. (2002) Optical imaging of Renilla luciferase reporter gene expression in living mice. *Proc. Natl. Acad. Sci. USA*, **99**:377-82.

Bhaumik, S., Lewis, X.Z., Gambhir, S.S. (2004) Optical imaging of Renilla luciferase, synthetic Renilla luciferase, and firefly luciferase reporter gene expression in living mice. *J. Biomed. Opt.*, **9**:578-86.

Black, M.E., Newcomb, T.G., Wilson, H.M., Loeb, L.A. (1996) Creation of drug-specific herpes simplex virus type 1 thymidine kinase mutants for gene therapy. *Proc. Natl. Acad. Sci. USA*, **93**:3525-9.

Block, A., Milasinovic, D., Mueller, J., Schaefer, P., Schaefer, H., Greten, H. (2002) Amplified Muc1-specific gene expression in colon cancer cells utilizing a binary system in adenoviral vectors. *Anticancer Res.*, **22**:3285-92.

Chappell, S.A., Edelman, G.M., Mauro, V.P. (2000) A 9-nt segment of a cellular mRNA can function as an internal ribosome entry site (IRES) and when present in linked multiple copies greatly enhances IRES activity. *Proc. Natl. Acad. Sci. USA*, **97**:1536-41.

Chatziioannou, A., Tai, Y.C., Doshi, N., Cherry, S.R. (2001) Detector development for microPET II: a 1 microl resolution PET scanner for small animal imaging. *Phys. Med. Biol.*, **46**:2899-910.

Cherry, S.R., Gambhir, S.S. (2001) Use of positron emission tomography in animal research. *Ilar J.*, **42**:219-32.

Cho, J.Y., Shen, D.H., Yang, W., Williams, B., Buckwalter, T.L., La Perle, K.M., Hinkle, G., Pozderac, R., Kloos, R., Nagaraja, H.N., Barth, R.F., Jhiang, S.M. (2002) *In vivo* imaging and radioiodine therapy following sodium iodide symporter gene transfer in animal model of intracerebral gliomas. *Gene Ther.*, **9**:1139-45.

Contag, C.H., Bachmann, M.H. (2002a) Advances in *in vivo* bioluminescence imaging of gene expression. *Annu. Rev. Biomed. Eng.*, **4**:235-60.

Contag, C.H., Jenkins, D., Contag, P.R., Negrin, R.S. (2000) Use of reporter genes for optical measurements of neoplastic disease *in vivo*. *Neoplasia*, **2**:41-52.

Contag, C.H., Ross, B.D. (2002b) It's not just about anatomy: *in vivo* bioluminescence imaging as an eyepiece into biology. *J. Magn. Reson. Imaging*, **16**:378-87.

Dai, G., Levy, O., Carrasco, N. (1996) Cloning and characterization of the thyroid iodide transporter. *Nature*, **379**:458-60.

Dewanjee, M.K., Ghafouripour, A.K., Kapadvanjwala, M., Dewanjee, S., Serafini, A.N., Lopez, D.M., Sfakianakis, G.N. (1994) Noninvasive imaging of c-myc oncogene messenger RNA with indium-111-antisense probes in a mammary tumor-bearing mouse model. *J. Nucl. Med.*, **35**:1054-63.

Dong, D., Dubeau, L., Bading, J., Nguyen, K., Luna, M., Yu, H., Gazit-Bornstein, G., Gordon, E.M., Gomer, C., Hall, F.L., Gambhir, S.S., Lee, A.S. (2004) Spontaneous and controllable activation of suicide gene expression driven by the stress-inducible grp78 promoter resulting in eradication of sizable human tumors. *Hum. Gene Ther.*, **15**:553-61.

Doubrovin, M., Ponomarev, V., Beresten, T., Balatoni, J., Bornmann, W., Finn, R., Humm, J., Larson, S., Sadelain, M., Blasberg, R., Gelovani Tjuvajev, J. (2001) Imaging transcriptional regulation of p53-dependent genes with positron emission tomography *in vivo*. *Proc. Natl. Acad. Sci. USA*, **98**:9300-5.

Filetti, S., Bidart, J.M., Arturi, F., Caillou, B., Russo, D., Schlumberger, M. (1999) Sodium/iodide symporter: a key transport system in thyroid cancer cell metabolism. *Eur. J. Endocrinol.*, **141**:443-57.

Freeman, S.M., Whartenby, K.A., Freeman, J.L., Abboud, C.N., Marrogi, A.J. (1996) In situ use of suicide genes for cancer therapy. *Semin. Oncol.*, **23**:31-45.

Gambhir, S.S., Barrio, J.R., Phelps, M.E., Iyer, M., Namavari, M., Satyamurthy, N., Wu, L., Green, L.A., Bauer, E., MacLaren, D.C., Nguyen, K., Berk, A.J., Cherry, S.R., Herschman, H.R. (1999) Imaging adenoviral-directed reporter gene expression in living animals with positron emission tomography. *Proc. Natl. Acad. Sci. USA*, **96**:2333-8.

Gambhir, S.S., Barrio, J.R., Wu, L., Iyer, M., Namavari, M., Satyamurthy, N., Bauer, E., Parrish, C., MacLaren, D.C., Borghei, A.R., Green, L.A., Sharfstein, S., Berk, A.J., Cherry, S.R., Phelps, M.E., Herschman, H.R. (1998) Imaging of adenoviral-directed herpes simplex virus type 1 thymidine kinase reporter gene expression in mice with radiolabeled ganciclovir. *J. Nucl. Med.*, **39**:2003-11.

Gambhir, S.S., Bauer, E., Black, M.E., Liang, Q., Kokoris, M.S., Barrio, J.R., Iyer, M., Namavari, M., Phelps, M.E., Herschman, H.R. (2000) A mutant herpes simplex virus type 1 thymidine kinase reporter gene shows improved sensitivity for imaging reporter gene expression with positron emission tomography. *Proc. Natl. Acad. Sci. USA*, **97**:2785-90.

Groot-Wassink, T., Aboagye, E.O., Glaser, M., Lemoine, N.R., Vassaux, G. (2002) Adenovirus biodistribution and noninvasive imaging of gene expression *in vivo* by positron emission tomography using human sodium/iodide symporter as reporter gene. *Hum. Gene Ther.*, **13**:1723-35.

Groot-Wassink, T., Aboagye, E.O., Wang, Y., Lemoine, N.R., Reader, A.J., Vassaux, G. (2004) Quantitative imaging of Na/I symporter transgene expression using positron emission tomography in the living animal. *Mol. Ther.*, **9**:436-42.

Haberkorn, U. (2001) Gene therapy with sodium/iodide symporter in hepatocarcinoma. *Exp. Clin. Endocrinol. Diabetes*, **109**:60-2.

Haberkorn, U., Altmann, A. (2001) Imaging methods in gene therapy of cancer. *Curr. Gene Ther.*, **1**:163-82.

Hamstra, D.A., Lee, K.C., Tychewicz, J.M., Schepkin, V.D., Moffat, B.A., Chen, M., Dornfeld, K.J., Lawrence, T.S., Chenevert, T.L., Ross, B.D., Gelovani, J.T., Rehemtulla, A. (2004) The use of 19F spectroscopy and diffusion-weighted MRI to evaluate differences in gene-dependent enzyme prodrug therapies. *Mol. Ther.*, **10**:916-28.

Hastings, J.W. (1996) Chemistries and colors of bioluminescent reactions: a review. *Gene*, **173**:5-11.

Hemminki, A., Belousova, N., Zinn, K.R., Liu, B., Wang, M., Chaudhuri, T.R., Rogers, B.E., Buchsbaum, D.J., Siegal, G.P., Barnes, M.N., Gomez-Navarro, J., Curiel, D.T., Alvarez, R.D. (2001) An adenovirus with enhanced infectivity mediates molecular chemotherapy of ovarian cancer cells and allows imaging of gene expression. *Mol. Ther.*, **4**:223-31.

Hemminki, A., Zinn, K.R., Liu, B., Chaudhuri, T.R., Desmond, R.A., Rogers, B.E., Barnes, M.N., Alvarez, R.D., Curiel, D.T. (2002) *In vivo* molecular chemotherapy and noninvasive imaging with an infectivity-enhanced adenovirus. *J. Natl. Cancer Inst.*, **94**:741-9.

Hildebrandt, I.J., Iyer, M., Wagner, E., Gambhir, S.S. (2003) Optical imaging of transferrin targeted PEI DNA complexes in living subjects. *Gene Ther.*, **10**:758-64.

Hogemann, D., Josephson, L., Weissleder, R., Basilion, J.P. (2000) Improvement of MRI probes to allow efficient detection of gene expression. *Bioconjug. Chem.*, **11**:941-6.

Iyer, M., Barrio, J.R., Namavari, M., Bauer, E., Satyamurthy, N., Nguyen, K., Toyokuni, T., Phelps, M.E., Herschman, H.R., Gambhir, S.S. (2001a) 8-[18F]Fluoropenciclovir: an improved reporter probe for imaging HSV1-tk reporter gene expression *in vivo* using PET. *J. Nucl. Med.*, **42**:96-105.

Iyer, M., Berenji, M., Templeton, N.S., Gambhir, S.S. (2002) Noninvasive imaging of cationic lipid-mediated delivery of optical and PET reporter genes in living mice. *Mol. Ther.*, **6**:555-62.

Iyer, M., Salazar, F.B., Lewis, X., Zhang, L., Carey, M., Wu, L., Gambhir, S.S. (2004) Noninvasive imaging of enhanced prostate-specific gene expression using a two-step transcriptional amplification-based lentivirus vector. *Mol. Ther.*, **10**:545-52.

Iyer, M., Wu, L., Carey, M., Wang, Y., Smallwood, A., Gambhir, S.S. (2001b) Two-step transcriptional amplification as a method for imaging reporter gene expression using weak promoters. *Proc. Natl. Acad. Sci. USA*, **98**:14595-600.

Jacobs, A., Voges, J., Reszka, R., Lercher, M., Gossmann, A., Kracht, L., Kaestle, C., Wagner, R., Wienhard, K., Heiss, W.D. (2001) Positron-emission tomography of vector-mediated gene expression in gene therapy for gliomas. *Lancet*, **358**:727-9.

Johnson, M., Sato, M., Burton, J., Gambhir, S.S., Carey, M., Wu, L. (2005) Micro-PET/CT monitoring of herpes thymidine kinase suicide gene therapy in a prostate cancer xenograft: the advantage of a cell-specific transcriptional targeting approach. *Mol. Imaging*, **in press**.

Kanerva, A., Zinn, K.R., Peng, K.W., Ranki, T., Kangasniemi, L., Chaudhuri, T.R., Desmond, R.A., Wang, M., Takayama, K., Hakkarainen, T., Alfthan, H., Stenman, U.H., Curiel, D.T., Hemminki, A. (2005) Noninvasive dual modality *in vivo* monitoring of the persistence and potency of a tumor targeted conditionally replicating adenovirus. *Gene Ther.*, **12**:87-94.

Kokoris, M.S., Black, M.E. (2002) Characterization of herpes simplex virus type 1 thymidine kinase mutants engineered for improved ganciclovir or acyclovir activity. *Protein Sci.*, **11**:2267-72.

Le, L.P., Everts, M., Dmitriev, I.P., Davydova, J.G., Yamamoto, M., Curiel, D.T. (2004) Fluorescently labeled adenovirus with pIX-EGFP for vector detection. *Mol. Imaging*, **3**:105-16.

Li, J.H., Chia, M., Shi, W., Ngo, D., Strathdee, C.A., Huang, D., Klamut, H., Liu, F.F. (2002) Tumor-targeted gene therapy for nasopharyngeal carcinoma. *Cancer Res.*, **62**:171-8.

Liang, Q., Dmitriev, I., Kashentseva, E., Curiel, D.T., Herschman, H.R. (2004a) Noninvasive of adenovirus tumor retargeting in living subjects by a soluble adenovirus receptor-epidermal growth factor (sCAR-EGF) fusion protein. *Mol. Imaging Biol.*, **6**:385-94.

Liang, Q., Gotts, J., Satyamurthy, N., Barrio, J., Phelps, M.E., Gambhir, S.S., Herschman, H.R. (2002) Noninvasive, repetitive, quantitative measurement of gene expression from a bicistronic message by positron emission tomography, following gene transfer with adenovirus. *Mol. Ther.*, **6**:73-82.

Liang, Q., Yamamoto, M., Curiel, D.T., Herschman, H.R. (2004b) Noninvasive imaging of transcriptionally restricted transgene expression following intratumoral injection of an adenovirus in which the COX-2 promoter drives a reporter gene. *Mol. Imaging Biol.*, **6**:395-404.

Lipshutz, G.S., Gruber, C.A., Cao, Y., Hardy, J., Contag, C.H., Gaensler, K.M. (2001) In utero delivery of adeno-associated viral vectors: intraperitoneal gene transfer produces long-term expression. *Mol. Ther.*, **3**:284-92.

Loening, A.M., Wu, A.M., Gambhir, S.S. (2004) Alignment guided mutagenesis of renilla luciferase increases stability and light output. *Mol. Imaging*, **3**:237.

Lorenz, W.W., Cormier, M.J., O'Kane, D.J., Hua, D., Escher, A.A., Szalay, A.A. (1996) Expression of the Renilla reformis luciferase gene in mammalian cells. *J. Biolumin. Chemilumin.*, **11**:31-7.

Luker, G.D., Sharma, V., Pica, C.M., Dahlheimer, J.L., Li, W., Ochesky, J., Ryan, C.E., Piwnica-Worms, H., Piwnica-Worms, D. (2002) Noninvasive imaging of protein-protein interactions in living animals. *Proc. Natl. Acad. Sci. USA*, **99**:6961-6.

MacLaren, D.C., Gambhir, S.S., Satyamurthy, N., Barrio, J.R., Sharfstein, S., Toyokuni, T., Wu, L., Berk, A.J., Cherry, S.R., Phelps, M.E., Herschman, H.R. (1999) Repetitive, non-invasive imaging of the dopamine D2 receptor as a reporter gene in living animals. *Gene Ther.*, **6**:785-91.

Mandell, R.B., Mandell, L.Z., Link, C.J., Jr. (1999) Radioisotope concentrator gene therapy using the sodium/iodide symporter gene. *Cancer Res.*, **59**:661-8.

Massoud, T.F., Gambhir, S.S. (2003) Molecular imaging in living subjects: seeing fundamental biological processes in a new light. *Genes Dev.*, **17**:545-80.

Massoud, T.F., Paulmurugan, R., Gambhir, S.S. (2004) Molecular imaging of homodimeric protein-protein interactions in living subjects. *Faseb J.*, **18**:1105-7.

Mayer-Kuckuk, P., Banerjee, D., Malhotra, S., Doubrovin, M., Iwamoto, M., Akhurst, T., Balatoni, J., Bornmann, W., Finn, R., Larson, S., Fong, Y., Gelovani Tjuvajev, J., Blasberg, R., Bertino, J.R. (2002) Cells exposed to antifolates show increased cellular levels of proteins fused to dihydrofolate reductase: a method to modulate gene expression. *Proc. Natl. Acad. Sci. USA*, **99**:3400-5.

McCaffrey, A., Kay, M.A., Contag, C.H. (2003) Advancing molecular therapies through *in vivo* bioluminescent imaging. *Mol. Imaging*, **2**:75-86.

Min, J.J., Iyer, M., Gambhir, S.S. (2003) Comparison of [18F]FHBG and [14C]FIAU for imaging of HSV1-tk reporter gene expression: adenoviral infection vs stable transfection. *Eur. J. Nucl. Med. Mol. Imaging*, **30**:1547-60.

Mizuguchi, H., Hayakawa, T. (2004) Targeted adenovirus vectors. *Hum. Gene Ther.*, **15**:1034-44.

Mocanu, J.D., Moriyama, E.H., Chia, M.C., Li, J.H., Yip, K.W., Huang, D.P., Bastianutto, C., Wilson, B.C., Liu, F.F. (2004) Combined *in vivo* bioluminescence and fluorescence imaging for cancer gene therapy. *Mol. Imaging*, **3**:352-5.

Moore, A., Basilion, J.P., Chiocca, E.A., Weissleder, R. (1998) Measuring transferrin receptor gene expression by NMR imaging. *Biochim. Biophys. Acta*, **1402**:239-49.

Morelli, A.E., Larregina, A.T., Smith-Arica, J., Dewey, R.A., Southgate, T.D., Ambar, B., Fontana, A., Castro, M.G., Lowenstein, P.R. (1999) Neuronal and glial cell type-specific promoters within adenovirus recombinants restrict the expression of the apoptosis-inducing molecule Fas ligand to predetermined brain cell types, and abolish peripheral liver toxicity. *J. Gen. Virol.*, **80 (Pt 3)**:571-83.

Morizono, K., Xie, Y., Ringpis, G.E., Johnson, M., Nassanian, H., Lee, B., Wu, L., Chen, I.S. (2005) Lentiviral vector retargeting to P-glycoprotein on metastatic melanoma through intravenous injection. *Nat. Med.*, **11**:346-52.

Nettelbeck, D.M., Jerome, V., Muller, R. (2000) Gene therapy: designer promoters for tumour targeting. *Trends Genet.*, **16**:174-81.

Nettelbeck, D.M., Rivera, A.A., Balague, C., Alemany, R., Curiel, D.T. (2002) Novel oncolytic adenoviruses targeted to melanoma: specific viral replication and cytolysis by expression of E1A mutants from the tyrosinase enhancer/promoter. *Cancer Res.*, **62**:4663-70.

Oh, P., Li, Y., Yu, J., Durr, E., Krasinska, K.M., Carver, L.A., Testa, J.E., Schnitzer, J.E. (2004) Subtractive proteomic mapping of the endothelial surface in lung and solid tumours for tissue-specific therapy. *Nature*, **429**:629-35.

Oliver, S., Bubley, G., Crumpacker, C. (1985) Inhibition of HSV-transformed murine cells by nucleoside analogs, 2'-NDG and 2'-nor-cGMP: mechanisms of inhibition and reversal by exogenous nucleosides. *Virology*, **145**:84-93.

Pang, S., Dannull, J., Kaboo, R., Xie, Y., Tso, C.L., Michel, K., deKernion, J.B., Belldegrun, A.S. (1997) Identification of a positive regulatory element responsible for tissue-specific expression of prostate-specific antigen. *Cancer Res.*, **57**:495-9.

Paulmurugan, R., Massoud, T.F., Huang, J., Gambhir, S.S. (2004) Molecular imaging of drug-modulated protein-protein interactions in living subjects. *Cancer Res.*, **64**:2113-9.

Paulmurugan, R., Umezawa, Y., Gambhir, S.S. (2002) Noninvasive imaging of protein-protein interactions in living subjects by using reporter protein complementation and reconstitution strategies. *Proc. Natl. Acad. Sci. USA*, **99**:15608-13.

Penuelas, I., Mazzolini, G., Boan, J.F., Sangro, B., Marti-Climent, J., Ruiz, M., Ruiz, J., Satyamurthy, N., Qian, C., Barrio, J.R., Phelps, M.E., Richter, J.A., Gambhir, S.S., Prieto, J. (2005) Positron emission tomography imaging of adenoviral-mediated transgene expression in liver cancer patients. *Gastroenterology*, **128**:1787-95.

Phelps, M.E. 2004. Molecular Imaging and Its Biological Applications. Springer, New York.

Qiao, J., Doubrovin, M., Sauter, B.V., Huang, Y., Guo, Z.S., Balatoni, J., Akhurst, T., Blasberg, R.G., Tjuvajev, J.G., Chen, S.H., Woo, S.L. (2002) Tumor-specific transcriptional targeting of suicide gene therapy. *Gene Ther.*, **9**:168-75.

Ray, P., De, A., Min, J.J., Tsien, R.Y., Gambhir, S.S. (2004a) Imaging trifusion multimodality reporter gene expression in living subjects. *Cancer Res.*, **64**:1323-30.

Ray, P., Wu, A.M., Gambhir, S.S. (2003) Optical bioluminescence and positron emission tomography imaging of a novel fusion reporter gene in tumor xenografts of living mice. *Cancer Res.*, **63**:1160-5.

Ray, S., Paulmurugan, R., Hildebrandt, I., Iyer, M., Wu, L., Carey, M., Gambhir, S.S. (2004b) Novel bidirectional vector strategy for amplification of therapeutic and reporter gene expression. *Hum. Gene Ther.*, **15**:681-90.

Reddy, R.K., Mao, C., Baumeister, P., Austin, R.C., Kaufman, R.J., Lee, A.S. (2003) Endoplasmic reticulum chaperone protein GRP78 protects cells from apoptosis induced by topoisomerase inhibitors: role of ATP binding site in suppression of caspase-7 activation. *J. Biol. Chem.*, **278**:20915-24.

Rehemtulla, A., Hall, D.E., Stegman, L.D., Prasad, U., Chen, G., Bhojani, M.S., Chenevert, T.L., Ross, B.D. (2002) Molecular imaging of gene expression and efficacy following adenoviral-mediated brain tumor gene therapy. *Mol. Imaging*, **1**:43-55.

Rehemtulla, A., Stegman, L.D., Cardozo, S.J., Gupta, S., Hall, D.E., Contag, C.H., Ross, B.D. (2000) Rapid and quantitative assessment of cancer treatment response using *in vivo* bioluminescence imaging. *Neoplasia*, **2**:491-5.

Reivich, M., Kuhl, D.E., Wolf, A., Greenberg, J., Phelps, M.E., Ido, T., Casella, V., Fowler, J., Hoffman, E.J., Alavi, A., Som, P., Sokoloff, L. (1979) The [18F]fluorodeoxyglucose method for the measurement of local cerebral glucose utilization in man. *Circ Res*, **44**:127-37.

Reszka, R.C., Jacobs, A., Voges, J. (2005) Liposome-mediated suicide gene therapy in humans. *Methods Enzymol.*, **391**:200-8.

Reynolds, P.N., Zinn, K.R., Gavrilyuk, V.D., Balyasnikova, I.V., Rogers, B.E., Buchsbaum, D.J., Wang, M.H., Miletich, D.J., Grizzle, W.E., Douglas, J.T., Danilov, S.M., Curiel, D.T. (2000) A targetable, injectable adenoviral vector for selective gene delivery to pulmonary endothelium *in vivo*. *Mol. Ther.*, **2**:562-78.

Rodriguez, R., Schuur, E.R., Lim, H.Y., Henderson, G.A., Simons, J.W., Henderson, D.R. (1997) Prostate attenuated replication competent adenovirus (ARCA) CN706: a selective cytotoxic for prostate-specific antigen-positive prostate cancer cells. *Cancer Res.*, **57**:2559-63.

Sato, M., Johnson, M., Zhang, L., Gambhir, S.S., Carey, M., Wu, L. (2005) Functionality of androgen receptor-based gene expression imaging in hormone refractory prostate cancer. *Clin. Cancer Res.*, **11**:3743-9.

Sato, M., Johnson, M., Zhang, L., Zhang, B., Le, K., Gambhir, S.S., Carey, M., Wu, L. (2003) Optimization of adenoviral vectors to direct highly amplified prostate-specific expression for imaging and gene therapy. *Mol. Ther.*, **8**:726-37.

Schuur, E.R., Henderson, G.A., Kmetec, L.A., Miller, J.D., Lamparski, H.G., Henderson, D.R. (1996) Prostate-specific antigen expression is regulated by an upstream enhancer. *J. Biol. Chem.*, **271**:7043-51.

Serganova, I., Doubrovin, M., Vider, J., Ponomarev, V., Soghomonyan, S., Beresten, T., Ageyeva, L., Serganov, A., Cai, S., Balatoni, J., Blasberg, R., Gelovani, J. (2004) Molecular imaging of temporal dynamics and spatial heterogeneity of hypoxia-inducible factor-1 signal transduction activity in tumors in living mice. *Cancer Res.*, **64**:6101-8.

Shimura, H., Haraguchi, K., Miyazaki, A., Endo, T., Onaya, T. (1997) Iodide uptake and experimental 131I therapy in transplanted undifferentiated thyroid cancer cells expressing the Na+/I- symporter gene. *Endocrinology*, **138**:4493-6.

Spitzweg, C., O'Connor, M.K., Bergert, E.R., Tindall, D.J., Young, C.Y., Morris, J.C. (2000) Treatment of prostate cancer by radioiodine therapy after tissue-specific expression of the sodium iodide symporter. *Cancer Res.*, **60**:6526-30.

Sun, X., Annala, A.J., Yaghoubi, S.S., Barrio, J.R., Nguyen, K.N., Toyokuni, T., Satyamurthy, N., Namavari, M., Phelps, M.E., Herschman, H.R., Gambhir, S.S. (2001) Quantitative imaging of gene induction in living animals. *Gene Ther.*, **8**:1572-9.

Sundaresan, G., Gambhir, S.S. 2002. Radionuclide Imaging of Reporter Gene Expression. Pp. 799-818 *in* T. A. a. M. JC, ed. Brain Mapping: The Methods. Academic Press, San Diego.

Sweeney, T.J., Mailander, V., Tucker, A.A., Olomu, A.B., Zhang, W., Cao, Y., Negrin, R.S., Contag, C.H. (1999) Visualizing the kinetics of tumor-cell clearance in living animals. *Proc. Natl. Acad. Sci. USA*, **96**:12044-9.

Tannous, B.A., Kim, D.E., Fernandez, J.L., Weissleder, R., Breakefield, X.O. (2005) Codon-optimized Gaussia luciferase cDNA for mammalian gene expression in culture and *in vivo*. *Mol. Ther.*, **11**:435-43.

Tavitian, B., Terrazzino, S., Kuhnast, B., Marzabal, S., Stettler, O., Dolle, F., Deverre, J.R., Jobert, A., Hinnen, F., Bendriem, B., Crouzel, C., Di Giamberardino, L. (1998) *In vivo* imaging of oligonucleotides with positron emission tomography. *Nat. Med.*, **4**:467-71.

Tjuvajev, J.G., Avril, N., Oku, T., Sasajima, T., Miyagawa, T., Joshi, R., Safer, M., Beattie, B., DiResta, G., Daghighian, F., Augensen, F., Koutcher, J., Zweit, J., Humm, J., Larson, S.M., Finn, R., Blasberg, R. (1998) Imaging herpes virus thymidine kinase gene transfer and expression by positron emission tomography. *Cancer Res.*, **58**:4333-41.

Tjuvajev, J.G., Chen, S.H., Joshi, A., Joshi, R., Guo, Z.S., Balatoni, J., Ballon, D., Koutcher, J., Finn, R., Woo, S.L., Blasberg, R.G. (1999) Imaging adenoviral-mediated herpes virus thymidine kinase gene transfer and expression *in vivo*. *Cancer Res.*, **59**:5186-93.

Tjuvajev, J.G., Finn, R., Watanabe, K., Joshi, R., Oku, T., Kennedy, J., Beattie, B., Koutcher, J., Larson, S., Blasberg, R.G. (1996) Noninvasive imaging of herpes virus thymidine kinase gene transfer and expression: a potential method for monitoring clinical gene therapy. *Cancer Res.*, **56**:4087-95.

Tjuvajev, J.G., Stockhammer, G., Desai, R., Uehara, H., Watanabe, K., Gansbacher, B., Blasberg, R.G. (1995) Imaging the expression of transfected genes *in vivo*. *Cancer Res.*, **55**:6126-32.

Townsend, D.W., Carney, J.P., Yap, J.T., Hall, N.C. (2004) PET/CT today and tomorrow. *J. Nucl. Med.*, **45 Suppl 1**:4S-14S.

Tsui, L.V., Kelly, M., Zayek, N., Rojas, V., Ho, K., Ge, Y., Moskalenko, M., Mondesire, J., Davis, J., Roey, M.V., Dull, T., McArthur, J.G. (2002) Production of human clotting factor IX without toxicity in mice after vascular delivery of a lentiviral vector. *Nat. Biotechnol.*, **20**:53-7.

Vooijs, M., Jonkers, J., Lyons, S., Berns, A. (2002) Noninvasive imaging of spontaneous retinoblastoma pathway-dependent tumors in mice. *Cancer Res.*, **62**:1862-7.

Wang, Y., Iyer, M., Annala, A.J., Chappell, S., Mauro, V., Gambhir, S.S. (2005) Noninvasive monitoring of target gene expression by imaging reporter gene expression in living animals using improved bicistronic vectors. *J. Nucl. Med.*, **46**:667-74.

Wu, J.C., Inubushi, M., Sundaresan, G., Schelbert, H.R., Gambhir, S.S. (2002) Optical imaging of cardiac reporter gene expression in living rats. *Circulation*, **105**:1631-4.

Wu, J.C., Sundaresan, G., Iyer, M., Gambhir, S.S. (2001a) Noninvasive optical imaging of firefly luciferase reporter gene expression in skeletal muscles of living mice. *Mol. Ther.*, **4**:297-306.

Wu, L., Johnson, M., Sato, M. (2003) Transcriptionally targeted gene therapy to detect and treat cancer. *Trends Mol. Med.*, **9**:421-9.

Wu, L., Matherly, J., Smallwood, A., Adams, J.Y., Billick, E., Belldegrun, A., Carey, M. (2001b) Chimeric PSA enhancers exhibit augmented activity in prostate cancer gene therapy vectors. *Gene Ther.*, **8**:1416-26.

Yaghoubi, S., Barrio, J.R., Dahlbom, M., Iyer, M., Namavari, M., Satyamurthy, N., Goldman, R., Herschman, H.R., Phelps, M.E., Gambhir, S.S. (2001a) Human pharmacokinetic and dosimetry studies of [(18)F]FHBG: a reporter probe for imaging herpes simplex virus type-1 thymidine kinase reporter gene expression. *J. Nucl. Med.*, **42**:1225-34.

Yaghoubi, S.S., Barrio, J.R., Namavari, M., Satyamurthy, N., Phelps, M.E., Herschman, H.R., Gambhir, S.S. (2005) Imaging progress of herpes simplex virus type 1 thymidine kinase suicide gene therapy in living subjects with positron emission tomography. *Cancer. Gene Ther.*, **12**:329-39.

Yaghoubi, S.S., Wu, L., Liang, Q., Toyokuni, T., Barrio, J.R., Namavari, M., Satyamurthy, N., Phelps, M.E., Herschman, H.R., Gambhir, S.S. (2001b) Direct correlation between positron emission tomographic images of two reporter genes delivered by two distinct adenoviral vectors. *Gene Ther.*, **8**:1072-80.

Yu, Y., Annala, A.J., Barrio, J.R., Toyokuni, T., Satyamurthy, N., Namavari, M., Cherry, S.R., Phelps, M.E., Herschman, H.R., Gambhir, S.S. (2000) Quantification of target gene expression by imaging reporter gene expression in living animals. *Nat. Med.*, **6**:933-7.

Zhang, L., Adams, J.Y., Billick, E., Ilagan, R., Iyer, M., Le, K., Smallwood, A., Gambhir, S.S., Carey, M., Wu, L. (2002) Molecular engineering of a two-step transcription amplification (TSTA) system for transgene delivery in prostate cancer. *Mol. Ther.*, **5**:223-32.

Zhang, L., Johnson, M., Le, K.H., Sato, M., Ilagan, R., Iyer, M., Gambhir, S.S., Wu, L., Carey, M. (2003) Interrogating androgen receptor function in recurrent prostate cancer. *Cancer Res.*, **63**:4552-60.

Received: July 22, 2005 Revised: August 08, 2005 Accepted: August 10, 2005